# Modification and performance of activated carbon for $CO_2$ sequestration in pervious concrete

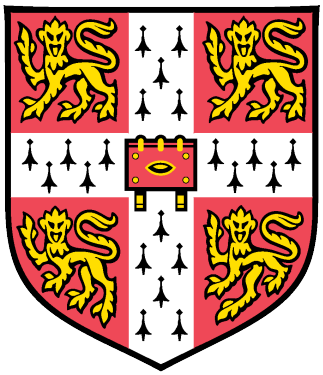

**Department of Engineering**

**University of Cambridge**

**A dissertation submitted for the degree of Doctor of Philosophy**

**Heba M. A. Hamad**

**Churchill College**

**April 2019**

*Dedicated to all my family*

## Declaration

This dissertation is the result of my own work and includes nothing which is the outcome of work done in collaboration except as declared in the Preface and specified in the text. It is not substantially the same as any that I have submitted, or, is being concurrently submitted for a degree or diploma or other qualification at the University of Cambridge or any other University or similar institution except as declared in the Preface and specified in the text. I further state that no substantial part of my dissertation has already been submitted, or, is being concurrently submitted for any such degree, diploma or other qualification at the University of Cambridge or any other University or similar institution except as declared in the Preface and specified in the text.

In accordance with the Department of Engineering guidelines, this dissertation does not exceed 65,000 words, inclusive of appendices, footnotes, tables and equations and it does not contain more than 150 figures.

Heba M. Hamad

April 2019

**Modification and performance of activated carbon for $CO_2$ sequestration in pervious concrete**

**Heba M. A. Hamad**

## Abstract

Concrete is one of the most commonly used material in the construction industry, with a global production of ~10 billion $m^3$/year. The production of Portland cement, the principal binder in most types of concrete, accounts for ~ 5–7% of global anthropogenic carbon dioxide ($CO_2$) emissions. Carbon capture and sequestration has been developed as one of several initiatives to help mitigate $CO_2$ emissions associated with cement and concrete production. Pervious concrete, a class of porous concretes, has been developed as a sustainable form of concrete that can be used for a wide range of applications. Its use is considered a 'Best Management Practice', recommended by the Environmental Protection Agency (EPA) to reduce storm water runoff, improve storm water quality and contribute to recharge of groundwater supplies. Activated carbon is a well-known adsorbent with a strong affinity for $CO_2$, and its surface chemistry can be further modified to enhance its adsorption capacity. Therefore, this research investigates optimal methods for modifying activated carbon to incorporate within Portland cement-based pervious concrete, in order to enhance its $CO_2$ sequestration capacity and improve its overall sustainability.

Two forms of activated carbon (granular and powder) were purchased from Fisher Scientific (UK) and chemically modified using different concentrations of the impregnation agents (NaOH, HCl, $CuSO_4 \cdot 5H_2O$, $NH_4OH$). The $CO_2$ adsorption capacity of the raw and the modified samples was measured using three techniques, which demonstrated that NaOH-modified samples had the highest capacity. A second round of modification was conducted to investigate whether further improvements were possible.

A two-step process of modification, first with HCl, followed by NaOH was determined to produce the highest adsorption capacity in this process. Activated carbon modified with this technique was used in three cementitious systems, which were tested in order to determine whether addition of such carbon adversely impacted important properties of the resultant materials. Modified powder activated carbon was used as a partial substitution for cement in cement pastes and pervious concrete, while modified granular activated carbon was used as a partial substitution to fine aggregate in cement mortars and pervious concrete. The investigation revealed that incorporation of small percentages of either form of modified activated carbon did not significantly alter the properties of the tested systems. Therefore, both substitutions were applied in pervious concrete to investigate the performance of modified activated carbon-pervious concrete in terms of $CO_2$ sequestration. The combined presence of the two forms of modified activated carbon had a minor effect on the compressive strength, porosity and permeability of the tested pervious concrete. Importantly, pervious concrete containing modified activated carbon had a higher $CO_2$ sequestration capacity than the control concrete. Furthermore, microstructural analysis showed that modified activated carbon-pervious concrete contained a higher content of calcite than the control concrete.

Overall, the addition of modified activated carbon to pervious concrete yielded promising results in terms of $CO_2$ sequestration. Further investigation of the long-term performance of modified activated carbon within pervious concrete systems is essential to realise the potential of this system to reduce atmospheric $CO_2$ levels and improve the sustainability of this essential construction material.

## Acknowledgment

This thesis would not have been possible without the love, guidance and support of many people. First, I would like to express my gratitude and appreciation to my supervisor Professor Abir Al-Tabbaa for her support, encouragement and kindness throughout this journey.

A sincere appreciation goes to the technical and laboratory support staff: Tim Ablett, Chris Knight, Simon Chapman, and Phil McLaren for their assistance throughout the project, and to Ahmed Al-Agha for his help in the schematic diagrams. I also extend my gratefulness to Nicola Cavaleri and Amanda Stranks for their support in proofreading this thesis. Many thanks go also to my colleagues who contributed to the vibrant atmosphere in the Environmental and Geotechnical research group, and to all my friends in Cambridge.

I would also like to gratefully thank the Islamic development Bank (IDB) and Cambridge Trust for their generous financial support during my stay here in Cambridge.

Finally, I am forever grateful to the love and faith my family has given to me. Special appreciation to my husband Ahmed for his continuous support, encouragement and patience. Thanks to my lovely children Ismail and Hamza for their endless love and countless hugs that gave me the power to continue my study. Moreover, special thanks go to my parents, my brothers and sisters for their continuous support, love and prayers.

# List of Figures

# List of Tables

## List of Abbreviations

| | |
|---|---|
| A/C | Aggregate to cement ratio |
| AC | Activated Carbon |
| BET | Brunauer-Emmett-Teller |
| C-S-H | Calcium Silicate Hydrate |
| $Ca(OH)_2$ | Calcium hydroxide |
| CaO | Calcium oxide |
| CCS | Carbon capture and storage |
| Co-CM | Control cement mortar |
| Co-con | Control pervious concrete |
| Co-CP | Control cement paste |
| $CO_2$ | Carbon dioxide |
| $CuSO_4 \cdot 5H_2O$ | Copper (II) sulfate pentahydrate |
| EPA | Environmental Protection Agency |
| FTIR | Fourier-transformed infrared spectroscopy |
| GAC | Granular activated carbon |
| HCl | Hydrochloric acid |
| M-AC | Modified activated carbon |
| M-GAC | Modified granular activated carbon |
| M-GAC-CM | Modified granular activated carbon-cement mortar |
| M-GAC-con | Modified granular activated carbon-pervious concrete |
| M-PAC | Modified powder activated carbon |
| M-PAC-con | Modified powder activated carbon-pervious concrete |
| M-PAC-CP | Modified powder activated carbon-cement paste |
| MOF | Metal-organic frameworks |
| NaOH | Sodium hydroxide |
| $NH_4OH$ | Ammonia hydroxide |
| OPC | Ordered porous carbon |
| PAC | Powder activated carbon |
| PC | Portland cement |
| SEM | Scanning Electron Microscopy |
| TGA | Thermogravimetric analysis |
| UCS | The unconfined compressive strength |
| UNFCCC | The United Nations Framework Convention on Climate Change |
| w/c | water to cement ratio |
| XRD | Powder X-ray diffraction |

# Table of Content

# 1 Introduction

## 1.1 Background

Carbon dioxide ($CO_2$) is the predominant greenhouse gas contributing to the anthropogenic climate change, in which its atmospheric concentration has increased to more than 40% when compared to the pre-industrial levels (IPCC 2013). The main human activities resulting in $CO_2$ emissions are fossil fuel combustion (e.g. coal, oil and natural gas), changes in land use (e.g. burning forests), and industrial processes (e.g. cement manufacturing) (IPCC 2013; Flower & Sanjayan 2007; Leung et al. 2014; Spigarelli & Kawatra 2013). Concrete is the most common construction material with a global production of ~10 billion $m^3$/year (Miller et al. 2016). The production of Portland cement (PC), the principal constituent of concrete, accounts for ~5–7% of total global anthropogenic $CO_2$ emissions (Harnisch et al. 2008; Fry 2013; Geng et al. 2019). The amount of $CO_2$ emitted during the manufacture of one tonne of PC is estimated at 0.85 - 1.1 tonnes (Deja et al. 2012). Moreover, the annual production of PC was around 4.3 billion tonnes in 2017 (USGS 2018), and is expected to increase to around 6 billion tonnes in 2050 (UNEP 2016). Consequently, there is a great pressure on the concrete industry to reduce the associated $CO_2$ emissions.

In response to this pressure, three main initiatives have been proposed and took place in the cement production industry. The first strategy is centred on using alternative raw materials, low energy production, and utilising the renewable energy. Moreover, it involves process innovation by addressing alternative production processes and emission control procedures. The second approach focuses on using low carbon materials, industrial by-products and wastes as partial cement replacement, while the third initiative addresses the development of new cement formulations (García-Lodeiro et al. 2013; Aranda & la Torre 2013; Konsta-Gdoutos 2013; Pacheco-Torgal & Labrincha 2013).

Regarding concrete, various approaches have been outlined to enhance its sustainability aspects. One particular approach is to investigate the concrete potential to absorb and sequester $CO_2$ from the surrounding atmosphere through a chemical reaction known as carbonation. It is a process that takes place between $CO_2$ in the atmosphere and the

alkaline materials within the concrete matrix in the presence of appropriate quantities of water. The rate of carbonation in concrete is controlled by the $CO_2$ diffusion in the concrete matrix: the higher the $CO_2$ diffusion, the higher the carbonation rate (Hewlett 2004; Taylor 1997). In spite of this potential for $CO_2$ sequestration, there are several limitations to significant carbonation, and a reduction in the carbon footprint of the conventional class of concrete. This is due to the high density and low porosity of conventional types of concrete, which control the $CO_2$ diffusion rate through the concrete matrix during carbonation. Moreover, the quantities of $CO_2$ absorbed by conventional concrete through carbonation are insignificant compared to the quantities released during concrete production.

Another approach for $CO_2$ sequestration in concrete is the implementation through utilising $CO_2$ sorbents as carbon sink materials within the concrete, which have the potential to permanently sequester large quantities of $CO_2$. Among a variety of adsorbent materials, activated carbon (AC) has a high potential to adsorb $CO_2$. AC is an extremely porous material that has been reported by many authors to have advantages over other adsorbents such as zeolites, carbon molecular sieves, silicas and metal oxides (Dantas et al. 2011; Plaza et al. 2010; Shafeeyan et al. 2014). This is due to its high thermal stability, low raw material costs, preferred adsorption kinetics and techniques resulting in easily desorption (Spigarelli & Kawatra 2013). Moreover, by tailoring its surface chemistry in a particular manner, AC can extend its sorption capacity several fold (Pevida et al. 2008; Plaza et al. 2007; Gray et al. 2004; Drage et al. 2009; Shafeeyan et al. 2010). Therefore, AC was modified in this research in an attempt to introduce basic functional groups on its surface, thereby increasing its affinity to $CO_2$.

AC has already been used within concrete mixes for certain purposes. Several researchers have examined the addition of AC to concrete to mitigate air pollutants and remove volatile organic compounds (Krou et al. 2013; Krou et al. 2015; Horgnies et al. 2012). Moreover, it has been used as a substitute for fine aggregate in cement mortars to improve their physical and mechanical properties (Justo-Reinoso et al. 2018).

While AC in concrete has been used for various purposes, no attempts have been made to investigate its applicability in concrete for sequestering $CO_2$. Therefore, the main purpose of this study is to modify AC to maximise its affinity to $CO_2$, then introduce it in two forms, powder and granular, examining its applicability to sequester $CO_2$ without a negative

impact on the fresh and hardened properties of concrete. Moreover, given the low porosity of the conventional type of concrete, a porous class known as pervious concrete, will be employed in this study. Pervious concrete has been regarded by the Environmental Protection Agency as one of the best management practices for mitigating the problem of storm water runoff (ACI 522R 2010). The fact that pervious concrete is a porous material with an interconnected network of voids enables $CO_2$ to percolate through the pervious concrete and reach as much surface area as possible.

## 1.2 Aim and Objectives

The aim of the work presented in this thesis was to develop pervious concrete that contains modified activated carbon, as a carbon sink material, in order to maximise its sustainability credentials. The objectives are:

- Produce modified activated carbon, both powder and granular forms, using different surface modification techniques to optimise the $CO_2$ uptake capacity of activated carbon.
- Study and analyse the positive and negative impacts of modified activated carbon on the fresh and hardened properties of pervious concrete.
- Investigate the efficiency of introducing modified activated carbon to the pervious concrete mixes in terms of quantification of the $CO_2$ sequestration potential and capacity.

## 1.3 Thesis Structure

This thesis comprises 6 chapters. This introduction forms Chapter 1, which sets out the background of the problem, the motivation of this research, the aim and objectives and the outline of the thesis. Chapter 2 provides the relevant literature review. This includes the high carbon footprint of concrete, mitigation strategies and $CO_2$ sequestration in cementitious materials. It also includes a comprehensive review of activated carbon, its production, properties and modification techniques. In addition, it includes a description of pervious concrete, its application, properties and the impact of different factors on these properties. Particular focus has been placed on the incorporation of AC in cement-paste systems. Chapter 3 introduces the main materials used, and the experimental techniques employed in the research work. Chapter 4 addresses the main findings and

results in terms of AC modifications. Chapter 5 investigates the effect of modified AC on three different cement-based systems, while Chapter 6 addresses the combined effect of the two forms of modified AC on pervious concrete properties along with the impact of this incorporation on the $CO_2$ sequestration. In Chapter 7, a summary of the main findings from this research work is presented followed by recommendations for future work.

# 2 Literature review

## 2.1 INTRODUCTION

This chapter presents a critical literature review of the areas relevant to the research work presented in this thesis. The chapter introduces a brief overview on cement and concrete, their production and environmental impact. This is followed by a summary of the various strategies employed to reduce these environmental impacts and in particular the carbon footprint of cement. Focus is then given to one strategy that employs carbon sequestration. An overview of carbon sequestration is then presented with a focus on carbon sequestration in cementitious systems. Activated carbon, as one of the most common materials for sequestering carbon, is then introduced and its production and properties as well as relevant sequestration studies are detailed. Pervious concrete is then introduced as an ideal candidate for optimum carbon sequestration in concrete. Finally, applications of AC in concrete are introduced with their aims and applications as well as degree of carbon sequestration where appropriate.

## 2.2 THE BIG PROBLEM – THE HIGH CARBON FOOTPRINT OF CONCRETE AND MITIGATION STRATEGIES

Carbon dioxide, the atmospheric concentrations of which has increased to more than 40% when compared to the pre-industrial levels, is the predominant greenhouse gas contributing to the anthropogenic climate change (IPCC 2013). The main human activities resulting in $CO_2$ emissions are fossil fuel combustion (e.g. coal, oil and natural gas), changes in land use (e.g. burning forests), and industrial processes (e.g. cement manufacturing) (IPCC 2013; Flower & Sanjayan 2007; Leung et al. 2014; Spigarelli & Kawatra 2013). Various approaches have been proposed to reduce human-driven $CO_2$ emissions, including reducing energy consumption and extending the deployment of existing and new technologies. Initiatives include (1) increasing the efficiency of energy conversion and utilisation, thus reducing the energy consumption, (2) increasing use of renewable energy resources producing low or zero $CO_2$ emissions, and (3) sequestering $CO_2$ emissions (WBCSD 2002; WBCSD 2012). While the first two strategies provide incremental enhancements, the third approach has the potential to attain zero emissions (WBCSD 2009b).

The production of Portland cement, the principal cementitious material in use around the world, accounts for ~5–7% of total global anthropogenic $CO_2$ emissions (Harnisch et al. 2008; Fry 2013; Geng et al. 2019). The amount of $CO_2$ emitted during the manufacture of one tonne of Portland cement (PC) is estimated at 0.85 - 1.1 tonnes (Deja et al. 2012). Concrete, the most common construction material with a global production of ~10 billion $m^3$/year (Miller et al. 2016), uses Portland cement as its main cementitious component. Global cement production has increased over 30 fold since 1950 and almost 4 fold since 1990 (Andrew 2018). Figure 2.1(a) shows world-wide cement production in 2016. Production is anticipated to reach more than 6 billion tonne/year by 2050 (Figure 2.1b) (CEMBUREAU 2017; UNEP 2016).

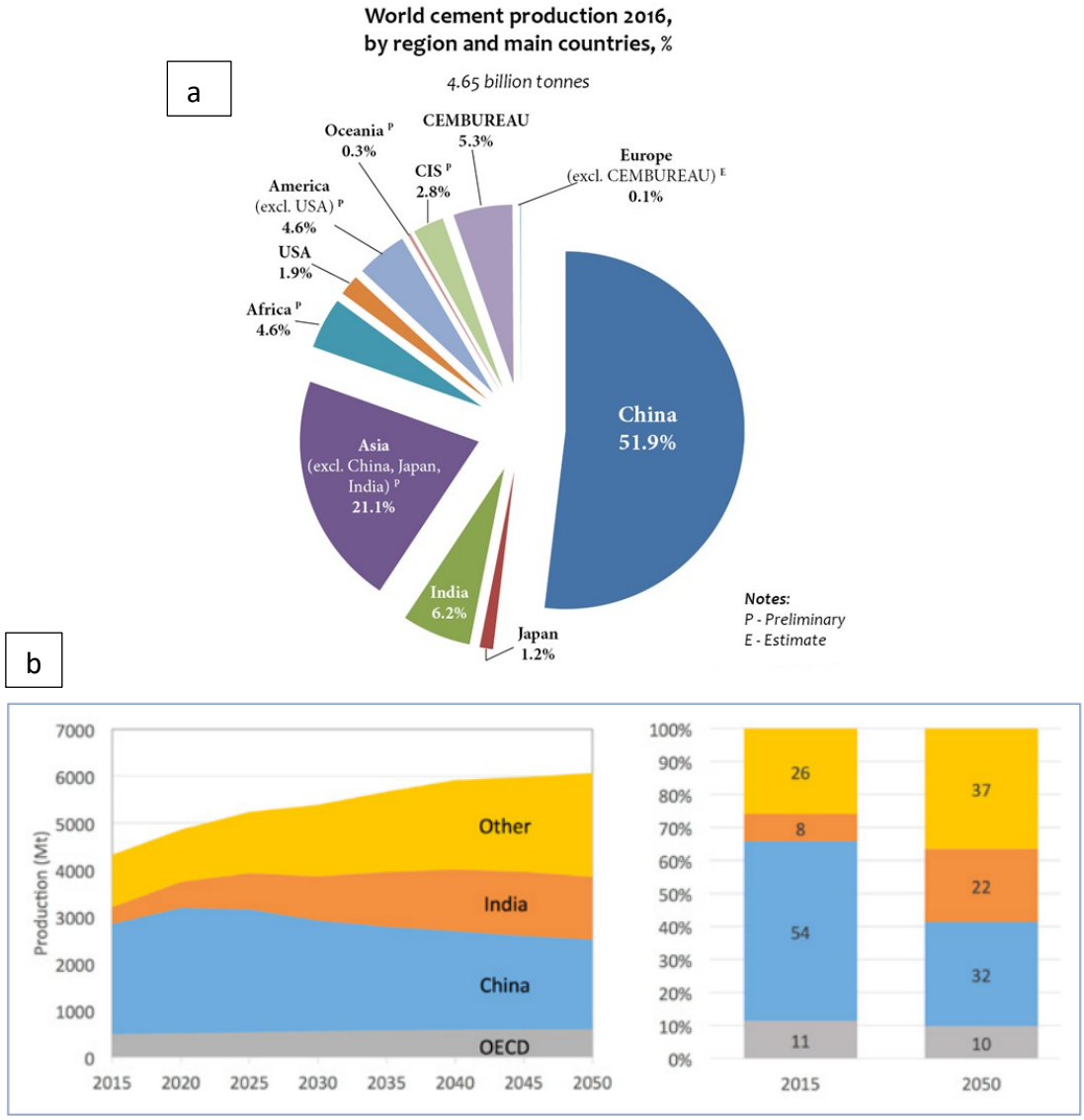


Figure 2-1: Global cement production figures (CEMBUREAU 2017; UNEP 2016) (a) World cement production in 2016 and (b) predicted global cement production until 2050.

Cement production, illustrated in Figure 2.2, requires finely crushing and milling limestone, marl or chalk (calcium carbonate) and mixing it with clay or shale before heating it in a rotary kiln to ~ 1450$^0$C. This process produces a volcanic rock-like material called clinker. After cooling, the produced clinker is mixed with mineral components such as gypsum (~ 4-5%) to control the setting time of the product. The mixture of cooled clinker and gypsum is ground into grey powder known as Portland cement (WBCSD 2002; WBCSD 2009a).

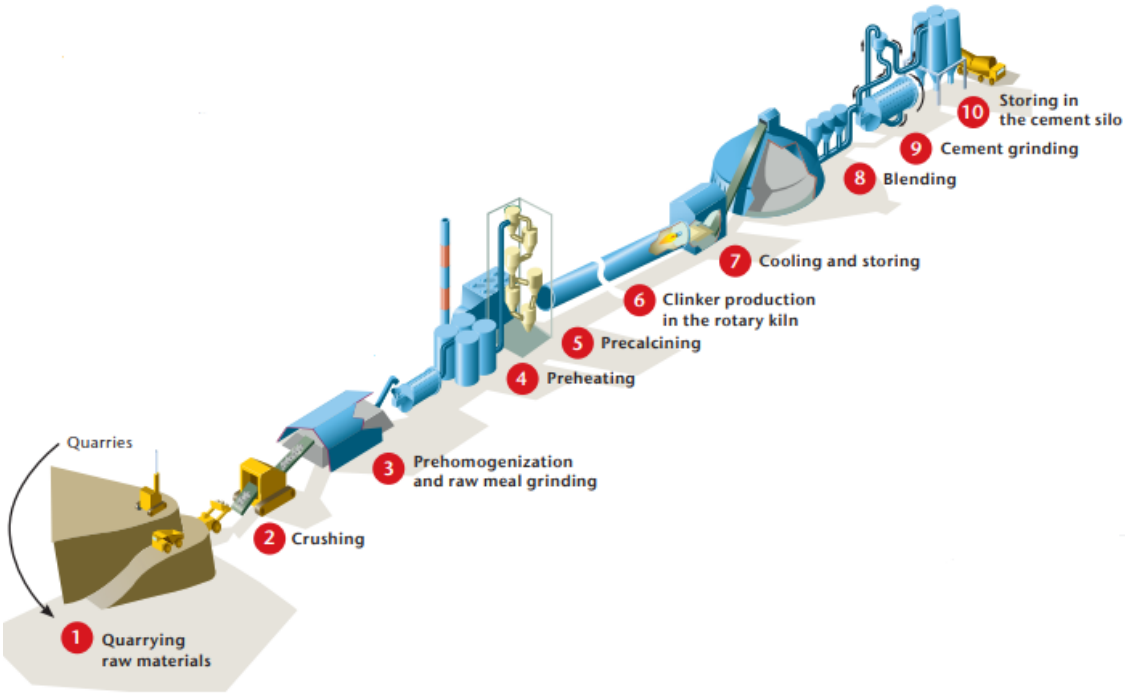


Figure 2-2: The cement production process (WBCSD 2009a)

$CO_2$ is generated during the chemical decomposition of limestone (50%), the combustion of fossil fuel (40%), transportation (5%), and from the electricity (5%) used during the manufacturing process (WBCSD 2002). Figure 2.3 shows the environmental impact of cement production in terms of the projected $CO_2$ emissions from the global cement industry to 2050, assuming no change in current practices (WBCSD 2009).

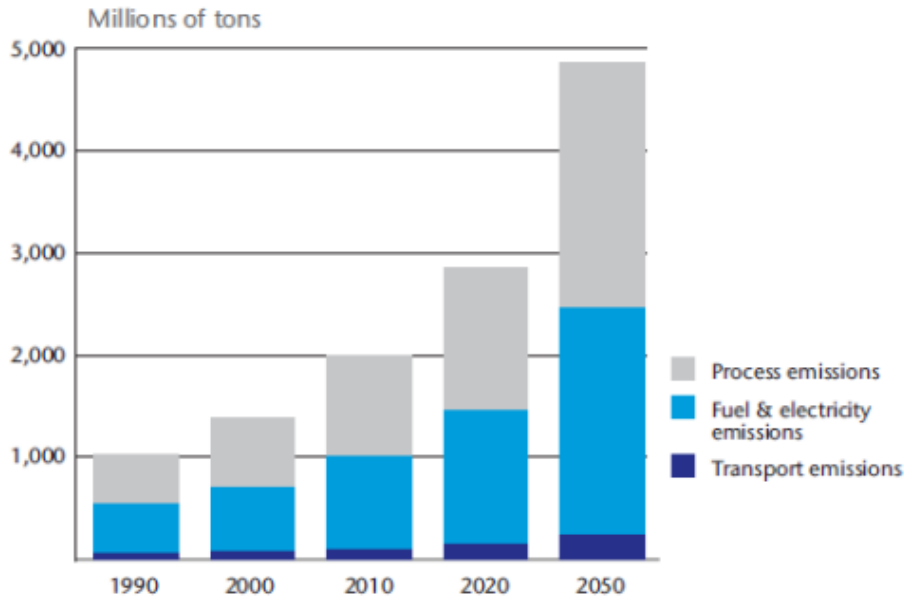


Figure 2-3: Projected $CO_2$ emissions from global cement production (WBCSD 2009a)

Considering the considerable quantity of materials quarried annually for use as aggregates, cement and other building materials, the construction industry has contributed more than any other industrial activity to the global $CO_2$ emissions (Harrison 2005). Therefore, huge pressure has been imposed on the cement industry to introduce and upscale carbon reduction initiatives.

The major sustainability issues in the cement industry include climate protection, atmospheric emissions, fuel and raw material use, and safety. A variety of approaches have been established and developed to enhance energy efficiency, support sustainable technologies in cement production and the concrete industry, and promote higher standards of environmental performance (WBCSD 2012). The main approaches include (WBCSD 2009a; Schneider et al. 2011; Unluer 2012; WBCSD 2012):

1- Improving thermal and electrical energy efficiency during clinker production by deploying state-of-the-art technologies in new cement plants.
2- Improving the efficiency of grinding systems in cement plants.
3- Reducing the extraction of raw materials through increased recycling, to mitigate the impact upon environmental quality, biodiversity, and landscape aesthetics,
4- Utilising lower-carbon fossil fuels and increasing use of alternative fuels such as discarded tyres, animals' residues, and sewage sludge and employing renewable resources at all stages of cement production,

5- Involving industrial by-products, waste products, and recycled aggregate in concrete industry to minimise further extraction of raw materials.
6- Recycling concrete waste at the end of its life and reuse it as aggregates,
7- Capturing $CO_2$ released during cement production and storing it securely.

In spite of all the aforementioned approaches, the concrete industry has not yet achieved sustainability and needs further innovation to address issues around social responsibility, environmental management and economic growth as illustrated in Figure 2.4.

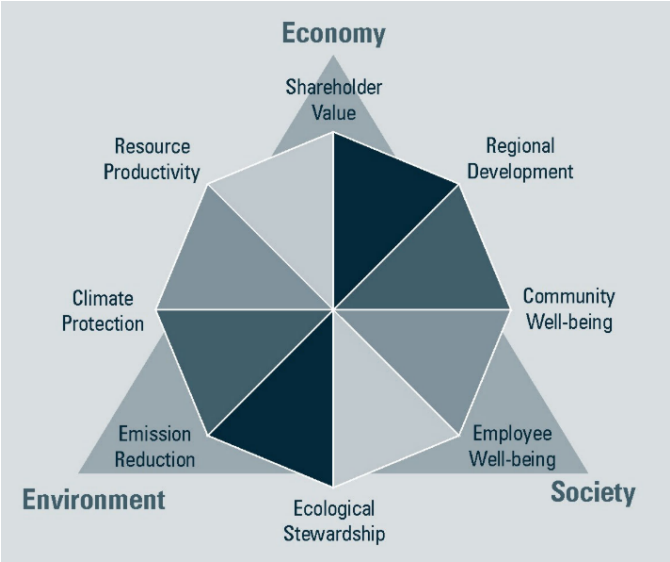


Figure 2-4: The major issues in achieving sustainable production in the cement industry (WBCSD 2002)

## 2.3 CARBON CAPTURE AND STORAGE

A range of relatively new and potentially promising technologies for carbon capture storage (CCS) exist within the cement sector to help mitigate climate change. However, they are currently unsuitable for existing cement plants due to technical and economic barriers (Schneider et al. 2011; WBCSD 2009a; Andrew 2018). $CO_2$ is captured as it is released during fossil combustion and limestone calcination and compressed to a liquid for permanent storage underground. Of the currently available capture technologies, some are more likely to be relevant to the cement industry than others (WBCSD 2009a; Schneider et al. 2011). CCS also requires the cement plant to be located close to a disposal or sales point, as $CO_2$ transport is expensive (WBCSD 2002). Some of the CCS technologies currently available are:

Post-combustion technologies: These technologies do not require fundamental changes in the clinker burning process, and therefore can be adapted to new and existing cement plants. In post-combustion systems, $CO_2$ is separated from other exhaust gases by adding an additional unit to the tail-end of the clinker process (Gerbelová et al. 2017). $CO_2$ is extracted using one of several technologies, the most common of which are: Chemical absorption, fixed-site carrier membrane technology, and mineral adsorption (Hägg et al. 2017).

Oxy-fuel technology: This is an appealing but a challenging option for existing plants because it requires an air separation plant to be established within the cement plants. The technology involves separating oxygen from air for use in combustion instead of air. Consequently, the concentration of $CO_2$ in flue gas is increased significantly (to more than 80%), which eases carbon capture after simple purification process (Schneider et al. 2011; Dubois et al. 2017). This technology has been demonstrated in a recent comparative techno-economic study as the CCS technology with the highest energy efficiency and economic indicator (Gardarsdottir et al. 2019; Cloete et al. 2019).

Photosynthesis of algae: The key principal consists of exposing the flue gas from cement kilns to algae through a reactor vessel. Algal cells absorb and fix $CO_2$ producing lipids, carbohydrates, and other value-added products, which can be harvested and used as a fuel in the cement plant. 100 tons of algal biomass can fix approximately 183 tons of carbon. This methodology allows a $CO_2$ capture and fuel production simultaneously. However, current research has demonstrated some limitations of these reactors (Schneider et al. 2011; Chisti 2008; Ghosh & Kiran 2017).

All the aforementioned methodologies focus on technologies for capturing, but not storing carbon dioxide. However, CCS involves both capturing the $CO_2$ and transporting it to the place of sequestration for storage. $CO_2$ can be sequestered in a range of underground geologic formations that meet the key requirements. These include sufficient capacity to sequester enormous quantity of $CO_2$, long-term stability, and low environmental impact (Naik & Kumar 2010). However, recent studies have reported adverse environmental effects, in addition to the high financial cost and low economic feasibility at some sites of geologic sequestration (Shao, Mirza, et al. 2006; Shao, Zhou, et al. 2006; Jang et al. 2016). That illustrates the need for new sequestration technologies. $CO_2$ sequestration in cement-based material, as discussed in the following section, may be a potential strategy.

## 2.4 CARBON SEQUESTRATION IN CEMENTITIOUS SYSTEMS

The United Nations Framework Convention on Climate Change (UNFCCC) defines a greenhouse gas "sink" as "any process, activity or mechanism which removes a greenhouse gas, an aerosol or a precursor of a greenhouse gas from the atmosphere" (UN 1992). Therefore, this section addresses the potential of concrete carbonation to act as such a $CO_2$ sink to remove $CO_2$ from the atmosphere.

Carbonation of concrete (illustrated schematically in Figure 2.5) occurs when atmospheric $CO_2$ diffuses into the concrete and dissolves in the pore solution of cement paste. This produces $CO_3^{2-}$ ions, which reacts with $Ca^{2+}$ from the alkaline components of concrete, to form $CaCO_3$ (Taylor 1997). The carbonation reaction decreases the pH of the carbonated concrete, from very alkaline values greater than pH12 to values around pH 8 (Hewlett 2004; Taylor 1997). As illustrated in Figure 2.5, the reaction proceeds at the exposed surfaces and spreads inwards. The rate, at which the carbonation takes place in cement-based systems, is a complex function of several variables including w/c ratio, cement content, porosity, compaction and curing period (Hewlett 2004; Talukdar et al. 2012; Chi et al. 2002; Moreno 2013; Possan et al. 2017; Phung et al. 2015).

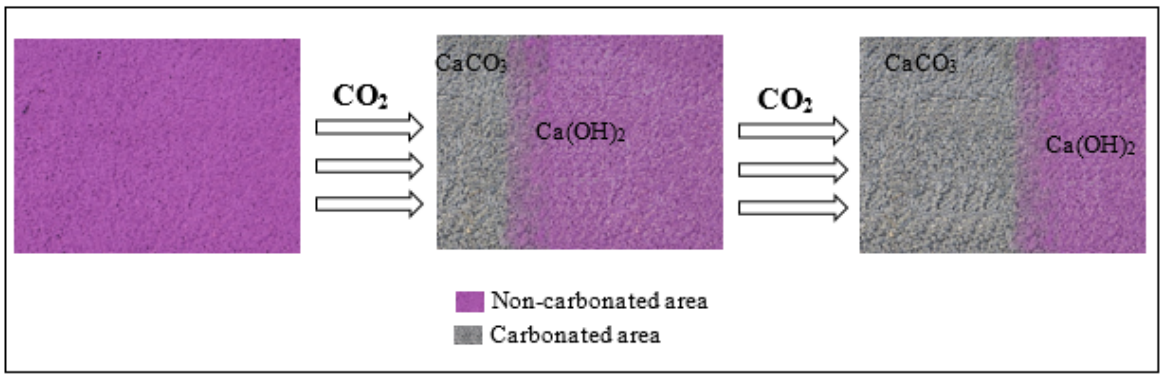


Figure 2-5: Carbonation process in concrete

Determining the extent of concrete carbonation has been an essential initial step in seminal studies for quantifying the $CO_2$ that could be re-adsorbed in concrete through carbonation. While the majority of the studies have experimentally measured the carbonation depth in concrete using phenolphthalein as a carbonation indicator, several studies were based on the theoretical content of Calcium oxide (CaO) or/and Calcium hydroxide $Ca(OH)_2$ in the cement used to estimate the maximum possible degree of carbonation.

$CO_2$ principally reacts with $Ca^{2+}$ from Calcium hydroxide $Ca(OH)_2$ to produce $CaCO_3$ and water, thus lowering the alkalinity of concrete and decalcifying (dissolution of Ca ions) all the cement hydration products (Taylor 1997). $CO_2$ reacts with $Ca^{2+}$ from Calcium Silicate Hydrate (C-S-H) (Sevelsted & Skibsted 2015; Villain et al. 2007; Groves et al. 1991; Morales-Florez et al. 2012; Rezagholilou et al. 2017), the main hydration products responsible for concrete strength, resulting in the degradation of the concrete. In a typical cement composition, CaO constitutes around 65% of cement (Taylor 1997). Several studies have built their carbonation models based on this figure with an assumption that during carbonation, all the CaO in the $Ca(OH)_2$ and a high fraction of the CaO in the C-S-H carbonate. This resulted in high estimations of the potential $CO_2$ absorption by cementitious materials during their life span (Pade & Guimaraes 2007; Lagerblad 2005; Jacobsen & Jahren 2001; Naik & Kumar 2010; Galan et al. 2010). While this assumption is theoretically valid, in practice $Ca(OH)_2$ is consumed much quicker than the CaO in C-S-H during carbonation (Lagerblad 2005). Therefore, under ambient atmospheric concentrations of $CO_2$, the carbonation process takes place mainly with $Ca(OH)_2$.

In spite of the potential of concrete carbonation for $CO_2$ sequestration, there are several limitations to significant carbonation and a $CO_2$ sequestration, thus a reduction in the carbon footprint of cement in the conventional class of concrete. This is due to the high density and low porosity of conventional types of concrete, which control the $CO_2$ diffusion rate through the concrete matrix during carbonation. This limits the carbonation process to the external surfaces of the concrete structure. In addition, the precipitated carbonates block the pores further reducing the $CO_2$ diffusion into the cementitious matrix. Given the limitations of natural carbonation of conventional concrete, a range of different approaches have been attempted to achieve significant $CO_2$ sequestration in concrete. These include accelerated carbonation curing, adding $CO_2$ to concrete mixing water, and storing $CO_2$ in concrete in stable forms of carbonates (Ashraf 2016).

One alternative approach for $CO_2$ sequestration in concrete is the implementation through utilising $CO_2$ sorbents as carbon sink materials within the concrete. A variety of sorbents have been tested for $CO_2$ capture from large anthropogenic point sources. These include activated carbon, zeolites, silica materials and metal organic frameworks (Lee & Park 2014; Choi et al. 2009). The incorporation of a carbon sorbent material inside the concrete matrix has the potential to permanently sequester large quantities of $CO_2$. The

next section introduces a brief overview on most common sorbent materials, their production, advantages and disadvantages. This is followed by a critical review on one of the most common sorbents: activated carbon.

## 2.5 $CO_2$ SORBENT MATERIALS

This section presents overview on $CO_2$ capturing adsorbents. The major commercially available adsorbents at present are zeolites, ordered mesoporous silica, metal-organic frameworks, and carbonaceous adsorbents such as activated carbon. Each adsorbent has a different pore structure and surface functional groups. The ideal adsorbent for $CO_2$ capture should meet several requirements including (1) low-cost raw materials, (2) high $CO_2$ adsorption capacity, (3) high $CO_2$ selectivity, (4) fast kinetics and (5) low heat capacity (Choi et al. 2009; Lee & Park 2014; Yu 2012). In the following paragraphs, an overview on some of the most common adsorbents is presented with a summary of various advantages and disadvantages in $CO_2$ capturing process.

Zeolites are naturally occurring microporous crystalline aluminosilicate minerals, which can also be prepared in the laboratory (Lee & Park 2014; Wang et al. 2011). They have a three dimensional crystal structure built from aluminium, oxygen, and silicon, with alkali or alkaline-Earth metals (Wang et al. 2011). Their pore structure is formed from networks of interconnected channels where gas molecules are adsorbed. They have been extensively utilised in gas separation and purification, where their adsorption efficiencies are a function of pore size, charge density and chemical composition of cations (Yu 2012). Given their relatively low cost, zeolites have been widely investigated for $CO_2$ capture because of their molecular sieving effect. Moreover, zeolites have strong dipole–quadrupole interactions between $CO_2$ and the alkali-metal cations in their frameworks (Choi et al. 2009). To enhance its $CO_2$ capacity, a number of studies investigated the potential of altering zeolites composition (the Si/Al ratio) or/and the exchange with alkali and alkaline-earth cations in the pore structure (Sayari et al. 2011). In spite of the enhancement that can be achieved by these approaches, several drawbacks remain. These include (1) the low $CO_2/N_2$ selectivity, resulting in low $CO_2$ adsorption capacity, (2) the high hydrophilic behaviour, which negatively affects the $CO_2$ adsorption in the presence of water (3) the high temperature during $CO_2$ desorption (above 300$^oC$), (Lee & Park 2014). Various researchers have reported that many classes of zeolites achieved a $CO_2$ capture capacity of up to 25 wt% at room temperature when using a 100% $CO_2$

concentration (Beltrao-Nunes et al. 2019; Kodasma et al. 2019; Lin et al. 2017; Zhang et al. 2017).

Metal-organic frameworks (MOFs) are an emerging class of crystalline solids that consist of three-dimensional organic–inorganic combination networks formed by multiple metal–ligand bonds (Choi et al. 2009; Lee & Park 2014; Modak & Jana 2019; Sahu et al. 2013). They usually have large surface area, (typically from 1000 to 10000 $m^2/g$), which has attracted interest in their use as molecular sieves and adsorbents (Olajire 2018). They exhibit exceptional selectivity and large adsorption capacities, particularity for $H_2$, $CH_4$, and adsorption of some toxic gases (Qin et al. 2014; Sahu et al. 2013; Dutta 2014). Given their controllable pore sizes and excellent surface area, MOFs are strong candidates for $CO_2$ adsorption. Previous studies showed that MOFs have high $CO_2$ uptake capacity at high pressures (Wang et al. 2011). Moreover, MOFs exhibited a high selectivity in separating $CO_2$ from binary gas mixtures, as a result of their inherent characteristic in governing the rate of diffusion of gasses through their pore structure (Lee & Park 2014). However, most of MOFs have poor $CO_2$ adsorption performance at low $CO_2$ pressure (Yu 2012) and it is not possible to retain the structure of MOFs when removing the molecules from the pores. Furthermore, the synthetic process is both very complex and expensive (Lee & Park 2014; Wang et al. 2011).

Carbonaceous adsorbents such as activated carbon, activated carbon fibres, carbon nanotubes, ordered porous carbons and graphene have been widely investigated for $CO_2$ capture (Lee & Park 2014). They have high thermal stabilities and remarkable electrical and heat conductivities. They have been used for $CO_2$ capture due to their (1) wide availability, (2) low cost, (3) high surface area and large pore volume, (4) low sensitivity to moisture, and (5) low adsorption/desorption temperature. Moreover, they can be used for $CO_2$ capture at atmospheric pressure. However, they have exhibited low $CO_2$ uptake at high temperature (Bilalis et al. 2014; Pinto et al. 2013; Choi et al. 2009). Therefore, extensive research has been conducted to enhance the $CO_2$ adsorption capacity of carbonaceous adsorbents by improving the pore structure and surface area, and by increasing the alkalinity of the surface chemistry (Lee & Park 2014). Here is an overview on two of the common carbonaceous adsorbents: ordered porous carbons and graphene, while the next section focuses on activated carbon.

Ordered porous carbon (OPC) is a type of solids with exceptional properties, making them useful for a wide range of applications such as gas storage, catalysis and as electrodes.

(Zhang et al. 2007; Joo et al. 2001; Hsueh et al. 2013). They can be prepared using various approaches such as direct synthesis by organic-organic self-assembly, and nano-casting using silica-based materials as hard templates (Lee & Park 2014; Yu 2012; Ghimbeu et al. 2014). OPCs are promising candidates for $CO_2$ adsorption because of their high surface areas, large pore volumes, high chemical stability, flexibility in altering the pore size, and possibility of surface modification (TANG et al. 2013; Wei et al. 2013). In spite of these advantages, pristine-OPCs provide poor $CO_2$ adsorption performance in both capacity and selectivity, which necessitates surface modification and pore size control to enhance the $CO_2$ adsorption (Lee & Park 2014).

Graphene, a new member of the carbon-based materials, is a promising nano-platform consisting of a single sheet of carbon atoms arranged in a honeycomb lattice formation (Ekhlasi et al. 2018; Wang et al. 2013). Graphene has attracted increasing interest in its properties since the first studies of its synthesis in 2004 (Zhou et al. 2019; Ali et al. 2019). Graphene has exceptional characteristics such as high thermal conductivity, high specific area, and strong Young's modulus (Ekhlasi et al. 2018). As a result of these features, it has been employed in various applications such as gases isolation, recovery of solvents, elimination of organic pollutants and gas storage (Chen et al. 2019; Smith et al. 2019; Ren et al. 2018). However, the principal drawback of graphene, that limits its application, is its tendency to form irreversible agglomerates if the sheets are not well separated from each other (Wang et al. 2013).

## 2.6 ACTIVATED CARBON

### 2.6.1 Introduction

Activated carbon (AC) is an extremely porous carbonaceous material that has been used effectively for many decades in adsorption processes. AC can be defined as a simple form of graphite with amorphous complex structure that is composed primarily of carbon atoms. The internal pore structure, created by the disordered layers of carbon atoms, includes cracks, nooks, and crevices of molecular dimensions (Sircar et al. 1996; Hassler 1951). Figure 2.6 illustrates SEM images of various AC samples, showing the variations in the pores structure depending on the starting material and the preparation techniques. Activated carbon (active carbon or activated charcoal) can be prepared from a wide range of starting materials such as biomass, coal and industrial by-products (Sircar et al. 1996; Hassler 1951). Coconut shell (Rashidi et al. 2014; Jain et al. 2013; Ello et al. 2013), almond shell (González et al. 2013), coffee residue (Plaza et al. 2012), nut shell (Bae & Su 2013), cotton stalks (Xiong et al. 2013) and olive stone (Plaza et al. 2014) have been used to prepare AC via a physical activation process. Wood (Ava Heidari et al. 2014), palm stone (Vargas et al. 2013), rice husk (Boonpoke et al. 2013), peanut shell (Deng et al. 2015), sunflower seeds (Deng et al. 2015), pine nut shell (Deng et al. 2014) and sludge (Al-Qodah & Shawabkah 2009) are examples of starting materials that have been chemically activated to prepare AC.

AC has various applications in purifying air, solutions, soil and many chemical products (Hassler 1951). Its adsorption capacity is a function of its textural properties and surface chemistry. Due to its wide availability, relatively low cost, low energy penalty to regenerate, high surface area and the ease with which its surface chemistry can be modified, AC is a promising material for $CO_2$ sequestration (Sevilla et al. 2011).

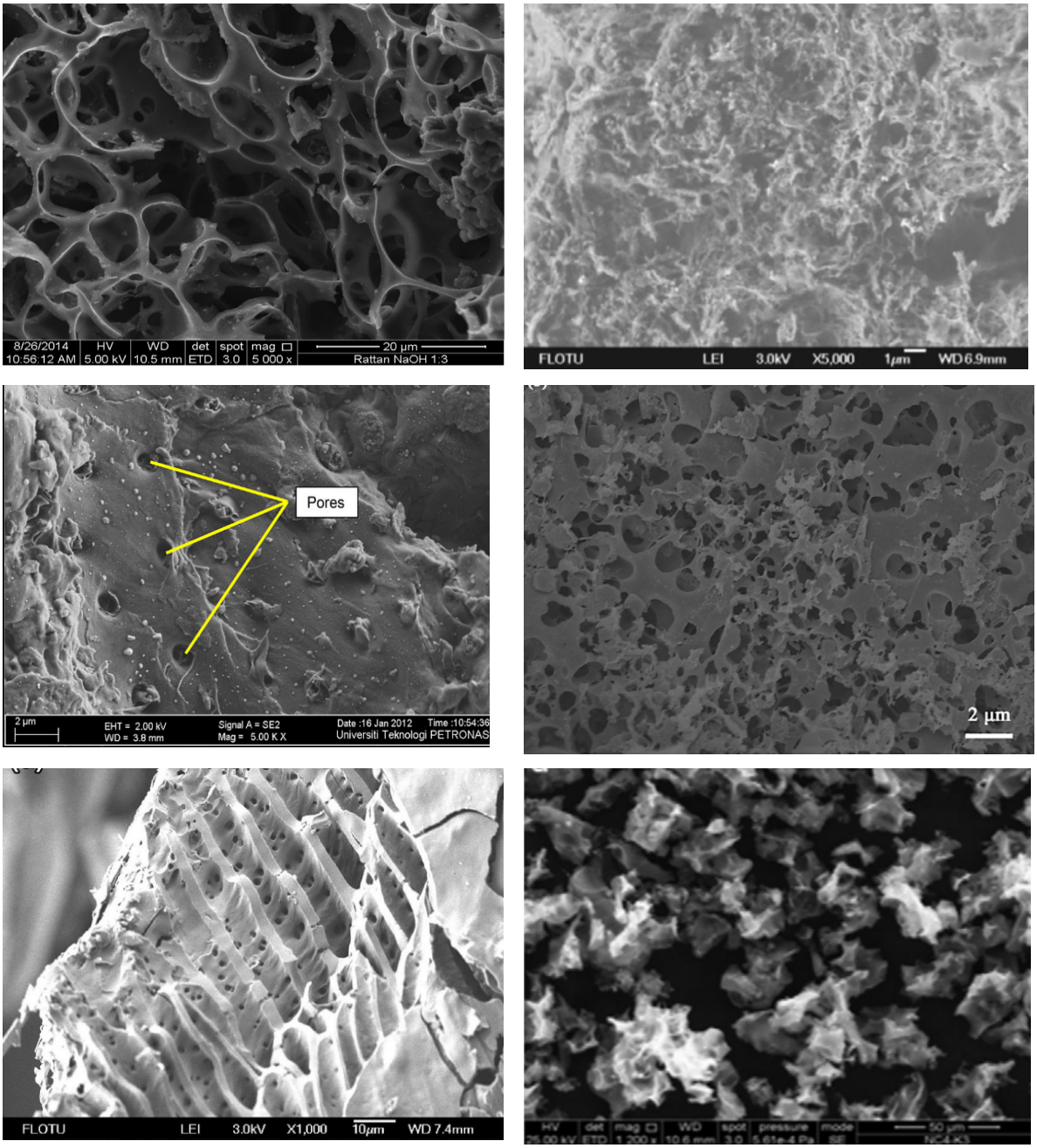


Figure 2-6: SEM of activated carbon from different starting materials (M. A. Islam et al. 2017; Rashidi et al. 2014; Deng et al. 2015; Plaza et al. 2012)

### 2.6.2 Preparation of activated carbon

There are two main steps in producing activated carbon: carbonization and activation. In carbonization, raw materials are heated in the absence of oxygen at a temperature around 800°C to remove the non-carbon elements. Following carbonization, further development of the internal pore structure is achieved by either thermal oxidation (physical activation) or chemical oxidation (activation using chemicals). Physical

activation involves activating the carbonised material using specific gases like $O_2$, $CO_2$, steam or air usually at a temperature range of 400 – 900°C. By; contrast, chemical activation is conducted by impregnating the starting material in chemical agents such as $ZnCl_2$, KOH or $H_2SO_4$ at a lower temperature, thus reducing the energy cost in AC synthesis (Lua & Yang 2004). Although chemical activation uses corrosive chemical agents, it has many advantages compared to physical activation. For example, it requires a lower temperature, produces more AC in a shorter activation time and yields a higher surface area (Wang & Kaskel 2012). Table 2.1 and Table 2.2 show a few selected articles in which the physical properties of AC differ according to the starting material and the preparation conditions.

### 2.6.3 Physical properties

The physical structure of AC plays a considerable role in its adsorption properties and performance. The textural structure of AC is a function of different factors including base material and preparation method. Therefore, changing the activation conditions or/and the starting material used to prepare AC results in a different pore structure (Chen et al. 2013; Snoeyink & Weber 1966). A few researchers have produced AC via physical activation as shown in Table 2.1 compared to Table 2.2 where the studies focused on the production using chemical activation.

The physical properties of AC can be classified into two main categories; BET surface area and pore size distribution. The surface area of AC (expressed in $m^2/g$) is usually measured using the Brunauer-Emmett-Teller (BET) method, which employs nitrogen adsorption at different pressures below the temperature of liquid nitrogen (77 K). A higher surface area results in more available adsorptive sites for the adsorption process. Pore size distribution is another useful tool to understand AC performance in adsorbing different types of molecules.

Pores in AC have numerous sizes & shapes. According to the International Union of Pure and Applied Chemistry (IUPAC), pores are classified into three types according to their size: Micropores (diameter less than 20 nm), Mesopores (diameter 20-200 nm) and Macropores (200 nm & above). Figure. 2.7 illustrates a schematic representation of a pore network of AC. While Micropores are the main contributor to the surface area, Mesopores and Macropores serve as an entrance to micropores (Dali et al. 2012). Surface area

determines the extent of the internal space available for adsorbing target adsorbates, while both size and the distribution of pores define the adsorptive properties of ACs. For example, large adsorbate molecules are not trapped by small pore size, and small molecules may not be retained in large pores (Ahmedna et al. 2004).

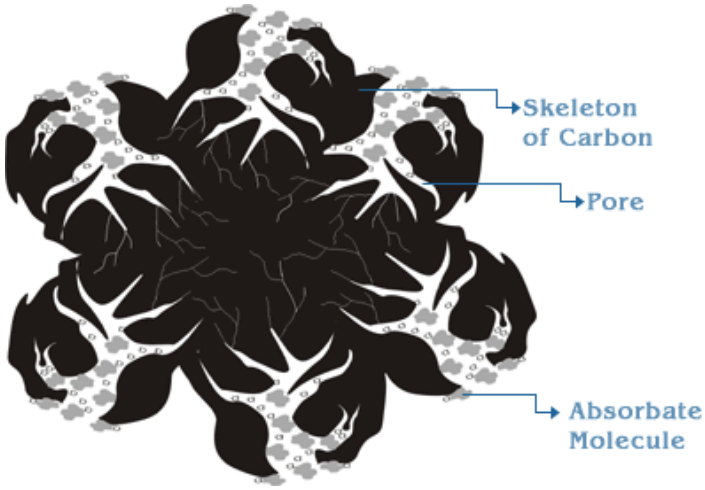


Figure 2-7: Schematic representation of pores network of AC (Birbas 2011)

The pore structure of AC is highly influenced by the starting material. Savova et al. have studied the impact of lignin and cellulose content on pore development. They found that materials with a greater content of lignin such as grape seeds and cherry stones develop AC with a macro-porous structure, while raw materials with a higher content of cellulose, for example apricot stones and almond shells, yield AC with a mainly microporous structure (Savova et al. 2001).

The pore volume and surface area of AC give an indication of the material's suitability for adsorbing certain adsorbates. It has been reported that when both the pores and the adsorbates have comparable diameters, adsorbates do not escape the adsorbent adsorption sites (Wilcox et al. 2014). In terms of $CO_2$ sequestration at atmospheric conditions, the molecular size of $CO_2$ is around 0.33 nm. Thus, only pores which are less than 1.0 nm have been reported to be effective for $CO_2$ capture because they contribute to the retention of $CO_2$ in the pore wall (Cazorla-Amorós et al. 1996; Chen et al. 2013). However, a pore with a smaller width (close to 0.33) demonstrates inefficiency in $CO_2$ uptake. Deng and his group has demonstrated that the volume of micropores in the range of 0.33–0.44 nm has a linear relationship with the adsorbed amounts of $CO_2$ at 298 K and

0.15 bar, indicating that this pore size is responsible for $CO_2$ adsorption (Deng et al. 2015). A similar trend has been found by many researchers proving that the fraction of micropore volume in AC structures is the principal contributor to $CO_2$ adsorption (Martín et al. 2011; Drage et al. 2009; Hao et al. 2010; Zhu et al. 2014). Consequently, appropriate operating carbonization and activation conditions in preparing AC should be explored in order to synthesize a high ultra-microporous carbon material (Rashidi & Yusup 2016).

In addition to the surface area and pore volume, there are other important parameters that govern the adsorption rate of AC. These includes the ambient temperature and adsorbate gas concentration (Hassler 1951). The increased pressure of the adsorbate gas leads to a higher $CO_2$ quantity being adsorbed on the surface of AC. The majority of adsorption studies have demonstrated that at a constant temperature, the higher the pressure applied to the adsorption system, the greater the amount adsorbed. Srenscek-Nazzal and his group modified a commercial AC using different solutions of KOH, $ZnCl_2$, $K_2CO_3$ for the purpose of $CO_2$ adsorption (Sreńscek-Nazzal et al. 2016). The sorption measurements were performed using the Sieverts apparatus (Hiden Isochem IMI). The adsorption isotherms at 40° C are shown in Figure 2.8. It is obvious that the higher the pressure applied, the higher the adsorption capacity of AC.

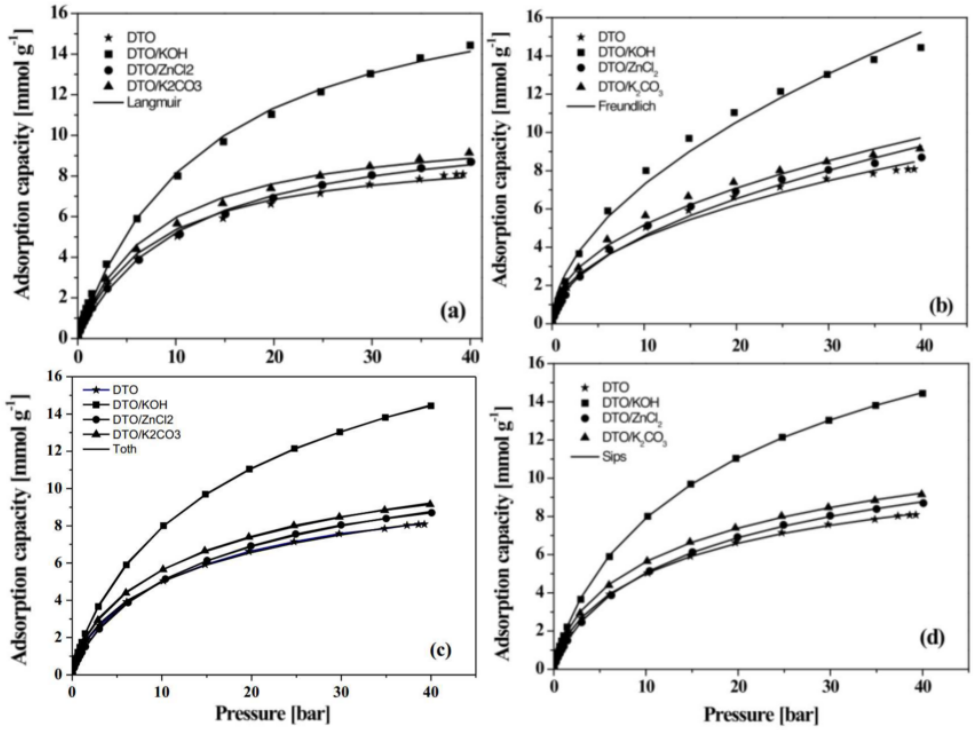


Figure 2-8: Curve fitting with (a) Langmuir, (b) Fre- undlich, (c) Toth and (d) Sips models of $CO_2$ adsorption isotherms onto ACs (Sreńscek-Nazzal et al. 2016)

In terms of temperature, at a constant pressure, the amount of physical adsorption decreases when the temperature rises. However, for chemical adsorption, this amount initially increases with increased temperature to initiate the reaction. Then it starts to decline as the latter continues to increase (Hassler 1951). A study by Shafeeyan examined the effect of temperature on $CO_2$ adsorption under fixed pressure (Shafeeyan et al. 2011). The results showed that the capture capacity of AC at 105°C is about 2–3 times lower than that at 30°C. They explained this decrease at a higher temperature by the exothermic character of physisorption, where both the molecule diffusion rate and the surface adsorption energy increase with increasing temperature (Shafeeyan et al. 2011). In addition, Lin and his group investigated the $CO_2$ adsorption performance at elevated temperatures of 25, 50, 70 and 95° C as shown in Figure 2.9 where the $CO_2$ uptake decreases significantly with increasing adsorption temperature (Lin et al. 2014). They explained this behaviour as the molecular kinetic energy of $CO_2$ rising with increasing temperature.

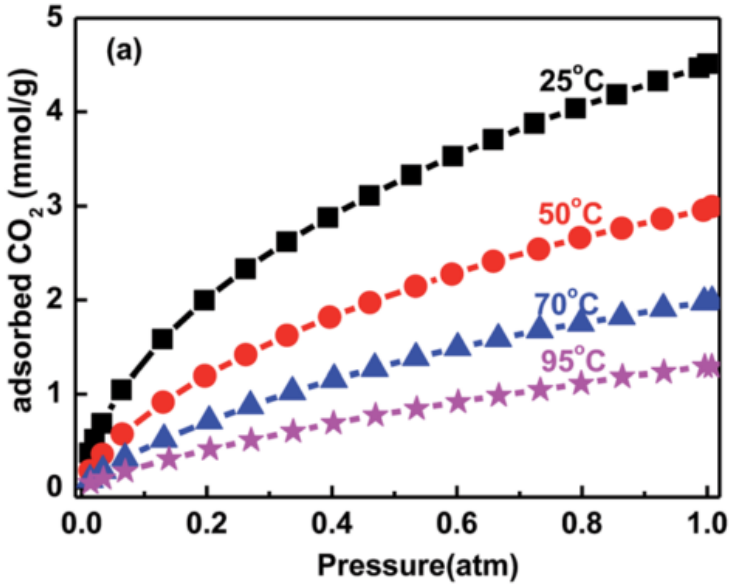


Figure 2-9: the impact of elevated temperature on $CO_2$ adsorption (Lin et al. 2014)

Maroto-Valer and his co-worker studied the effect of adsorption temperature on $CO_2$ capture capacities (Maroto-Valer et al. 2005). They noticed that the adsorption capacity declined rapidly with increasing adsorption temperature as shown in Figure 2.10, and they explained this as typical behaviour for a physical adsorption process. In addition, they clarified that both surface adsorption energy and molecule diffusion rate increase with increasing temperature, resulting in the instability of the adsorbed gas on the

surface of the AC, which leads to the desorption of adsorbed $CO_2$ molecules. Similar trends have been reported for different types of AC adsorbents at higher temperatures (Plaza et al. 2007; Drage et al. 2007; Drage et al. 2009).

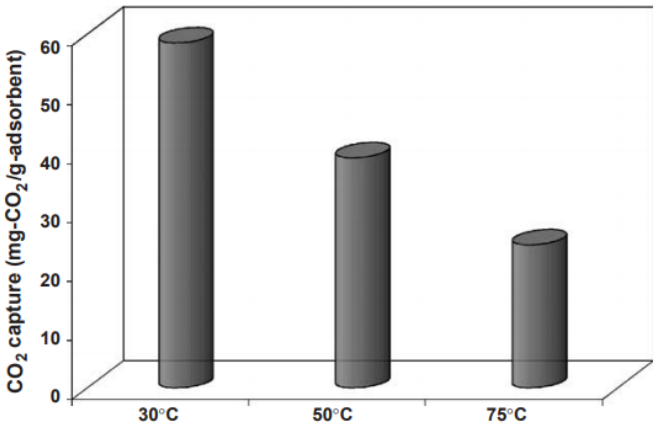


Figure 2-10: $CO_2$ adsorption capacities of the AC as a function of the adsorption temperature (Maroto-Valer et al. 2005)

Table 2-1: Comparison of the physical properties of AC produced from different starting materials by physical activation

| Starting Material | Carbonization conditions | | | Activation conditions | | | Physical properties | | Reference |
|---|---|---|---|---|---|---|---|---|---|
| | Atm | T (°C ) | t (h) | Atm | T (C ) | Time (h) | Avg D pores nm | $S_{BET}$ $m^2/g$ | |
| Coconut shell | $CO_2$ | 800 | 1 | $CO_2$ | | | 1.63 | 370 | (Rashidi et al. 2014) |
| spent coffee grounds | $N_2$ | 600 | 1 | $CO_2$ | 700 | | 2.1 | 84 | (Plaza et al. 2012) |
| Coconut shell | $N_2$ | | | $CO_2$ | 800 | 3.5 | 0.83 | 1327 | (Ello et al. 2013) |
| Olive stones | $CO_2$ | | | $CO_2$ | | 6 | 1.28 | 1215 | (González et al. 2013) |
| Macadamia nut shell | $N_2$ | 700 | 1 | $CO_2$ | 900 | 1 | | 633 | (Bae & Su 2013) |
| Paper mill sewage sludge | | 300 | 1 | steam | 850 | 0.67 | 1.178 | 280 | (W. Li et al. 2011) |
| Paper mill sewage sludge | | 300 | 1 | steam | 850 | 0.67 | | 130 | (W. H. Li et al. 2011) |
| sewage sludge | $N_2$ | 450 | 1 | air | 275 | 4 | | 105 | (Méndez et al. 2005) |
| Beer lees waste | $N_2$ | 800 | 0.25 | $CO_2$ | 950 | 0.5 | 3.18 | 972 | (Wakizaka et al. 2016) |
| Tectona Grandis sawdust. | $N_2$ | 600 | 1 | $CO_2$ | 800 | 1 | 1.67 | 404 | (Cansado et al. 2018) |
| Oak wood waste | $N_2$ | 450 | | $CO_2$ | 700 | 1 | | 92 | (Zhang et al. 2004) |
| Peltogyne wood | $CH_4$ | 580 | | $CO_2$ | 700 | | 0.70 | 580 | (Vartapetyan et al. 2005) |
| Fir wood | steam | 450 | 1.5 | steam | 900 | 7 | 2.9 | 1016 | (Wu et al. 2005) |
| Teak sawdust | steam | 600 | 1 | steam | 750 | 1 | | 611 | (Ismadji et al. 2005) |
| walnut tree wood | air | 800 | 2 | air | 550 | 2 | 2.81 | 407 | (G´ et al. 2005) |
| Eucalyptus wood | $N_2$ | 400 | 1 | $CO_2$ | 900 | 1 | 2.15 | 1491 | (Yuvarat Ngernyen 2006) |
| Wattle wood | $N_2$ | 400 | 1 | $CO_2$ | 800 | 5 | 2017 | 1032 | (Yuvarat Ngernyen 2006) |

Table 2-2: Comparison of the physical properties of AC produced from different starting materials by chemical activation

| Starting Material | Carbonization conditions | | | Activation conditions | | | Physical properties | | Reference |
|---|---|---|---|---|---|---|---|---|---|
| | Atm | T ($^oC$ ) | t (h) | Chemical | ratio | t (h) | Avg D pores nm | $S_{BET}$ $m^2/g$ | |
| pine nut shell | | 800 | 1.5 | KOH | 2:1 | | 0.33-0.82 | 370 | (Deng et al. 2014) |
| Rice Husk | $N_2$ | 500 | 1 | $ZnCl_2$ | 1:1 | 1 | 0.8 | 927 | (Boonpoke et al. 2013) |
| eucalyptus wood | | 450 | | $H_3PO_4$ | 2:1 | | 1.21 | 1889 | (Ava Heidari et al. 2014) |
| coconut shells | | | | $ZnCl_2$ | | | 2.6 | 533 | (Jain et al. 2013) |
| sunflower seed shell | | 700 | 1.5 | KOH | 1.25:1 | 48 | | 1,790 | (Deng et al. 2015) |
| paulownia sawdust | | 250 | 2 | KOH | 6:1 | 1 | | 2435 | (Zhu et al. 2014) |
| Sewage sludge and discarded tyres | $N_2$ | 650 | 0.5 | $ZnCl_2$ | 1:1 | 48 | | 472 | (Rozada et al. 2005) |
| sewage sludge | $N_2$ | 625 | 0.5 | $H_2SO_4$ | 1:1 | 48 | | 390 | (Rozada et al. 2003) |
| aerobically digested sludge | $N_2$ | 700 | 0.5 | $H_2SO_4$ | 1:1 | 48 | 2.3 | 253 | (Martin et al. 2003) |
| biological Sludge | $N_2$ | 500 | 0.5 | $ZnCl_2$ | | 24 | 2.45 | 737 | (Hsiu-Mei et al. 2009) |
| Anaerobic sludge materials | | 800 | 2 | $ZnCl_2$ | | 2 | 0.34 | 202 | (Athalathil et al. 2013) |
| dewatered surplus sludge | $N_2$ | 450 | 0.5 | $ZnCl_2$ | | 24 | 10-30 | 120 | (Liu et al. 2010) |
| Sewage Sludge | $N_2$ | 650 | 1 | $H_2SO_4$ | | 24 | 5.21 | 408 | (Zhang et al. 2005) |
| activated sludge | steam | 600 | 1 | KOH | 1:2.5 | 24 | 5.62 | 381.6 | (Wang et al. 2008) |
| sewage sludge | | 500 | 1 | KOH | 1:1 | | | 135 | (Kaçan & Kütahyali 2012) |
| rice husk | air | 475 | 0.5 | $K_2CO_3$ | 1:4 | 24 | 3.54 | 1260 | (Satayeva et al. 2018) |
| endocarp of babassu coconut | $N_2$ | 700 | | $H_3PO_4$ | 1:1 | 12 | | 1300 | (Lopes et al. 2017) |
| Chestnut wood | $N_2$ | 450 | 4 | $H_3PO_4$ | | 36 | 2.57 | 777 | (Díaz-Díez et al. 2004) |
| Tectona grandis sawdust | $N_2$ | 500 | 1 | $ZnCl_2$ | 2:1 | 1 | | 440 | (Mohanty et al. 2005) |
| Pine dust | $N_2$ | | 1 | $ZnCl_2$ | 1:1 | | 2.22 | 1390 | (Akmil-Başar et al. 2005) |
| Rubber wood | | 400 | 1 | $H_3PO_4$ | | 1 | | 954 | (Kumar et al. 2005) |
| Fir wood | $N_2$ | 300 | 1 | KOH | 0.75:1 | 2 | | 1255 | (Khezami & Capart 2005) |
| Chesnut wood | | | | $H_3PO_4$ | 1:3 | 2 | | 503 | (Gómez-Serrano et al. 2005) |
| Oak wood | $N_2$ | 450 | 2 | $H_3PO_4$ | | 2 | | 1066 | (G´ et al. 2008) |
| Prosopis ruscifolia wood | | 450 | 0.5 | $H_3PO_4$ | | | | | (Celis et al. 2009) |

| | | | | | | | | | |
|---|---|---|---|---|---|---|---|---|---|
| China fir | | 475 | 1.5 | $H_3PO_4$ | | 0.5 | | 1043 | (Zuo 2010) |
| Poplar wood | | 900 | 1 | $Na_2CO_3$ | 1:3 | | | 1579 | (Is & ¸ılUzun 2010) |
| Poplar wood | | 900 | 1 | $K_2CO_3$ | 1:3 | | | 1596 | (Is & ¸ılUzun 2010) |
| Raw corncob materials | | 400 | 1.5 | $Na_2CO_3$ | 1.5:1 | | 3.072 | 1097 | (Vu et al. 2018) |
| Tamarind wood | | 450 | 2 | $ZnCl_2$ | 1:1 | 1 | 5.3 | 1322 | (Sahu et al. 2010) |
| Eucalyptus camaldulensis wood | | 450 | 1 | $H_3PO_4$ | 1.5:1 | | 2.083 | 1875 | (Aghdas Heidari et al. 2014) |
| Eucalyptus camaldulensis wood | | 450 | 1 | $H_3PO_4$ | 2:1 | | 2.495 2.9 | 1889 | (Aghdas Heidari et al. 2014) |
| Eucalyptus camaldulensis wood | | 450 | 1 | $H_3PO_4$ | 2.5:1 | | 2.083 | 2117 | (Aghdas Heidari et al. 2014) |
| Eucalyptus camaldulensis wood | | 500 | 1 | $ZnCl_2$ | 0.75:1 | | 1.73 | 1275 | (Aghdas Heidari et al. 2014) |
| Eucalyptus camaldulensis wood | | 500 | 1 | $ZnCl_2$ | 1.5:1 | | 2.01 | 2108 | (Aghdas Heidari et al. 2014) |
| Eucalyptus camaldulensis wood | | 500 | 1 | $ZnCl_2$ | 2.5:1 | | 2.64 | 1794 | (Aghdas Heidari et al. 2014) |
| Eucalyptus camaldulensis wood | | 900 | 1 | KOH | 3.5:1 | | 1.966 | 2595 | (Aghdas Heidari et al. 2014) |

### 2.6.4 Chemical properties

The chemical nature of the AC surface plays a significant role in determining its adsorptive properties. The chemical properties of ACs are principally defined by surface chemical heterogeneity, which is related to the presence of heteroatoms, i.e., atoms present in a carbon structure that are not carbon, such as oxygen, nitrogen, hydrogen, sulfur, and phosphorus. The nature of the starting materials and the parameters of the activation process determine the type and quantity of these elements (Shafeeyan et al. 2010). Surface functional groups (which are a combination of these heteroatoms) determine the acidic or basic character of the AC surface (Shafeeyan et al. 2010). Among these heteroatoms, oxygen is the most important and commonly occurs in the form of carboxylic, lactone, phenol, carbonyl, pyrone, chromene, quinone, and ether groups (Boehm et al. 1964; Mattson & Mark 1971). Oxygen-containing functional groups (also denoted as surface oxides) can be classified into three classes according to their chemical properties: acidic, basic, neutral (Shafeeyan et al. 2010). Figure. 2.11 illustrates the main acidic and basic functional groups on the edges of AC.

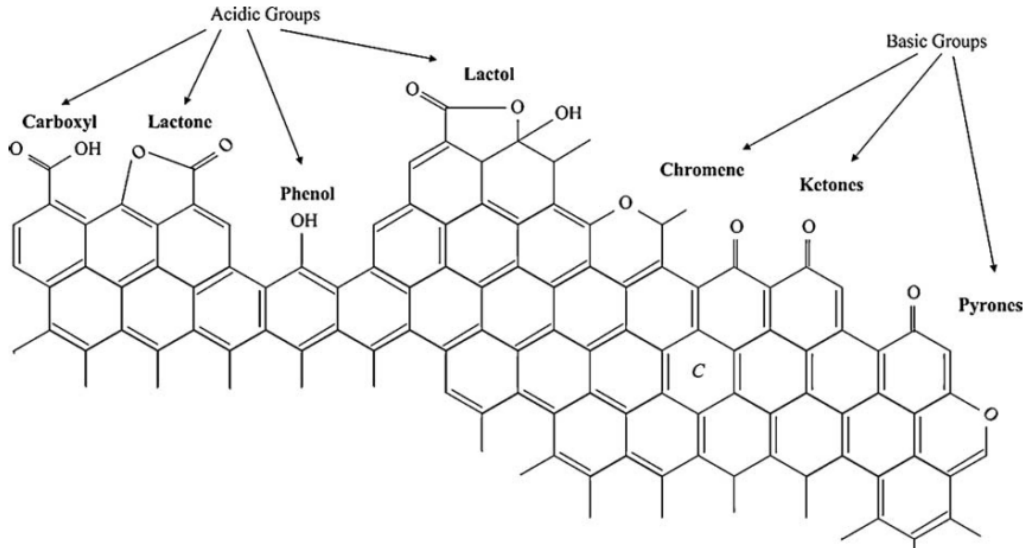


Figure 2-11: Acidic and basic surface functional groups on a carbon basal plane (Montes-Morán et al. 2004)

AC acquires an acidic nature when exposed to gases (such as oxygen, air and steam) between 200 and 700 °C or to oxidants such as $H_2O_2$, $HNO_3$, or $HNO_3$ and $H_2SO_4$ acid mixtures in aqueous solutions (McGuire & Suffet 1983; Li et al. 2002; Boehm 2002). Examples of acidic functional groups are carboxylic acid or carboxylic anhydride, lactone, and phenolic hydroxyl (Shafeeyan et al. 2010).

The basic character of AC is associated with both the basic surface functional groups (such as nitrogen containing groups) and the delocalized π electrons of graphene layers. It has been demonstrated that introducing nitrogen functional groups into the carbon surface increases the basicity of the AC surface (Pevida et al. 2008; Plaza et al. 2010; Plaza et al. 2007; Drage et al. 2009). Possible structures of the nitrogen functionalities include the amide group, imide group, lactame group, pyrrolic group, and pyridinic group (Montes-Morán et al. 2004; Shafeeyan et al. 2010; Menéndez et al. 1996)

As mentioned above, the chemical nature of the AC surface influences its adsorption behaviour. In general, AC with acidic surface chemical properties has a strong affinity to basic gas adsorption such as ammonia while AC with basic surface chemical properties is suitable for acidic gas adsorption such as sulphur dioxide and carbon dioxide (Ioannidou & Zabaniotou 2007).

### 2.6.5 Surface modification of Activated carbon

Although structural properties of ACs are effective in their adsorptive capacity, modifying their surface chemistry could potentially enhance the adsorption process, leading to viable innovative applications (Hosseini et al. 2015). Improvements of these adsorptive properties can be chemically or physically achieved. Some of the well-established techniques include heat treatment, impregnation with specific compounds, microwave, plasma and ozone treatment. During these treatments, the types and the amounts of the functional groups are changed (Caglayan & Aksoylu 2013; Shafeeyan et al. 2010; Yong et al. 2002). Given the acidic character of $CO_2$, it is recognised that introducing basic nitrogen functional groups increases the basicity of AC, thus, increasing its affinity to $CO_2$. General approaches have been proposed involving neutralizing the acidic surface groups or replacing them with proper basic ones (Shafeeyan et al. 2010; Shen et al. 2008). Several methodologies have been adapted by different researchers, and some of the most common are heat treatment in an inert gas, gaseous ammonia treatment, impregnation with amine-containing compounds, and metal earth salt treatment (Shafeeyan et al. 2010; Shen et al. 2008). The following sections review some relevant treatment techniques for $CO_2$ capture.

### 2.6.5.1 Heat treatment

High temperature (>700°C) heat treatment under oxidant gases has been used to increase oxygen-containing functional groups on the surface of AC, thus increasing its acidity. However, heating under inert gas removes most of these functionalities. This thermal treatment approach has been intensively used to offer the AC a basic surface (Shafeeyan et al. 2010; Shen et al. 2008; Dastgheib & Karanfil 2004).

The thermal treatment of AC in an inert atmosphere creates unsaturated surfaces because of the decomposition of acidic groups. Strongly acidic functionalities (such as carboxylic, anhydrides and lactones) decompose at lower temperatures, while weakly acidic functionalities (such as carbonyl, phenol and quinone) decompose at higher temperatures (Shafeeyan et al. 2010). Figure 2.12 shows some surface oxygen containing groups on carbon and their decomposition temperature.

In addition, heat treatment in hydrogen or in an inert atmosphere (nitrogen or helium) increases carbon hydrophobicity by removing hydrophilic surface functionalities (Menéndez et al. 1996; Siriwardane et al. 2001). Hydrogen is more favourable than other inert gases as it stabilizes the surface of the heated AC by forming C-H bonds (Menéndez et al. 1996; Dastgheib & Karanfil 2004)

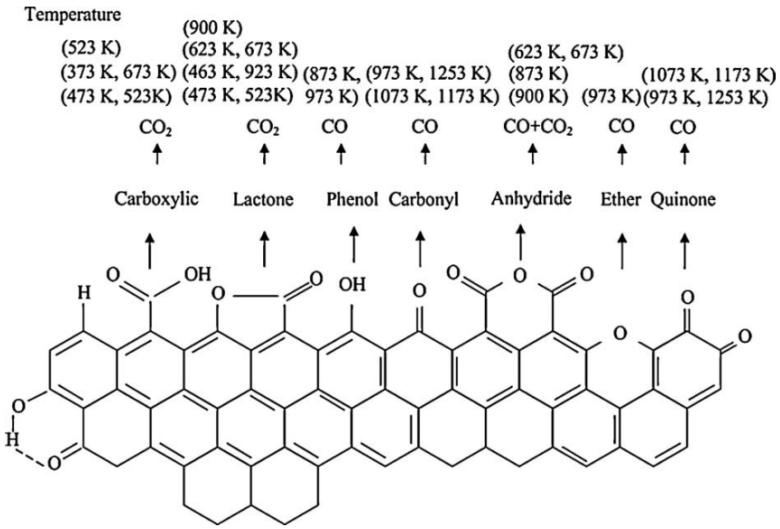


Figure 2-12: Surface oxygen containing groups on carbon and their decomposition (Shafeeyan et al. 2010)

Several researchers have confirmed that the breakdown of oxygen functional groups at high temperatures increases the basicity of the carbon surface. Dastgheib and Karanfil investigated granular AC and AC fibres in hydrogen flow at 900°C. The results showed

that the permanent removal of some oxygen functionalities had a significant impact on decreasing the overall surface acidity of AC (Dastgheib & Karanfil 2004). A similar conclusion was drawn by Dastgheib and his group who studied the influence of different treatment techniques on granular AC samples including heat treatment under helium or hydrogen (Dastgheib et al. 2004). There was a considerable increase in the basicity of the heated sample surface. Similarly, Pereira and his co-workers modified Norit ROX AC in nitrogen flow at 700°C (Pereira et al. 2003). The thermally treated samples indicated that $CO_2$ releasing groups (carboxylic, anhydrides and lactones) were almost completely removed and only a small number of CO releasing groups at higher temperatures remained, which could be assigned to some basic groups such as carbonyls, pyrone and chromene type structures. In the same way, Muniz and his group examined AC fibres in nitrogen flow at 600 and 800° C, and the findings suggested that thermal treatment at a high temperature (i.e. 800°C) is a simple method to increase the basicity of the AC surface (Muñiz et al. 1998). All the previous studies concluded that heating AC in an inert atmosphere increases its basicity, hence, its affinity toward acidic compounds.

#### 2.6.5.2 Ammonia treatment

Literature reveals the development of ammonia modification as a significant approach to increase the adsorption affinity of AC toward $CO_2$. With these modifications, nitrogen functionalities are introduced into AC offering it a basic surface.

During the reaction of AC with ammonia ($NH_3$) at high temperatures, ammonia decomposes to free radicals such as $NH_2$, NH, atomic hydrogen and nitrogen. These free radicals react with the AC to form nitrogen-containing functional groups as shown in Figure 2.13 (Bota & Abotsi 1994; Stöhr et al. 1991).

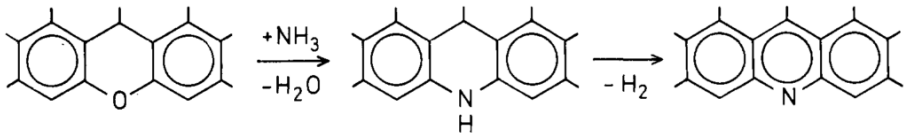


Figure 2-13: Reaction scheme for conversion of chemisorbed oxygen into imine and pyridine in the reaction with ammonia (Stöhr et al. 1991)

On the AC surface, the reaction of ammonia with carboxylic acid sites forms ammonium salts that through dehydration reaction lead to amides and nitriles as shown in equation 2.1. In addition, the substitution of OH groups can easily result in Amine groups on the surface of carbon as shown in equation 2.2 (Stöhr et al. 1991).

$$—COO^-NH_4^+ \xrightarrow{-H_2O} —CO—NH_2 \xrightarrow{-H_2O} —C\equiv N.$$ Equation 2.1

$$—OH + NH_3 \longrightarrow —NH_2 + H_2O.$$ Equation 2.2

Several authors have studied the thermal treatment of carbons in an ammonia atmosphere. Drage and his group examined the effect of heat treatment with gaseous ammonia on different types of AC. A remarkable increase in the surface area of about 30% was noticed. The best-modified sample gained new basic functional groups that increased the $CO_2$ capture capacity from 91 to 111 mg $CO_2$/g AC (Drage et al. 2009). A similar gain in surface area was reported by Shafeeyan via heat treatment under ammonia, yielding an approximate increase of 14 % in the surface area and a more than 30% increase in the $CO_2$ capture capacity (Shafeeyan et al. 2011). They also investigated the effect of prior oxidation before amination on AC samples using hot air as an oxidant. They noticed that the pre-oxidized samples had the best $CO_2$ capture capacity at an adsorption temperature of 105 $^oC$ while the just-aminated samples adsorbed more $CO_2$ at room temperature. Other oxidant reagents have been used by different researchers for exploring the impact of oxidation on the AC samples. Adelodun and his co-workers investigated Hydrogen Peroxide $H_2O_2$ as an oxidant on a coconut shell-based AC before amination with gaseous ammonia (Adelodun et al. 2013). The best modified samples demonstrated a slight surface area increase from 1221 to 1253 $m^2$/g but resulted in a 23% higher $CO_2$ capture capacity compared to the original sample. Table 2.3 shows a comparison of adsorption capacity of modified AC with ammonia from few selected articles at different treatment and adsorption temperatures.

Table 2-3: Comparison of $CO_2$ adsorption capacity of ammonia treated ACs

| Adsorbent | Treatment Temp C | Adsorption Temp C | Adsorption capacity mg/g AC | Reference |
|---|---|---|---|---|
| Commercial AC | 400 | 26 | 75 | (Przepiórski et al. 2004) |
| Commercial GAC | 800 | 30 | 73 | (Shafeeyan et al. 2011) |
| Biomass residue AC | 400 | 25 | 96 | (Plaza et al. 2009) |
| Wood-based GAC | 800 | 25 | 83 | (Pevida et al. 2008) |
| Eucalyptus wood AC | 800 | 30 | 141 | (Ava Heidari et al. 2014) |

### 2.6.5.3 Sodium Hydroxide treatment

Previous studies show that treatment with alkaline chemical materials increases the basicity of the AC surface and provides more active functional sites for $CO_2$, thus enhancing the adsorption of carbon dioxide. More specifically, researchers have investigated the impact of hydroxides on the modification of AC; however, there are only few studies on modification with NaOH (Zhi & Liu 2016; Perrin et al. 2004). Tan and his group modified coconut shell-based AC with different strengths of aqueous solutions of NaOH for predetermined soaking times. Figure 2.14 shows an SEM image of the sample that had the highest $CO_2$ adsorption capacity after a modification with 32% NaOH concentration for 3 hrs. The capacity significantly increased from 17 to 27 mg/g AC although the value of the BET surface area and micropore area decreased drastically compared to the unmodified AC (from 787.65 to 378.23 $m^2/g$). They attributed this decline to the structural changes of the AC due to the entrapment of NaOH in the micropore area, which reduced the ultimate surface area during modification (Tan et al. 2014). The same conclusion was reported by Caglayan & Aksoylu who explained this behaviour as Na sites agglomerated on the AC surface leading to a small surface area but better adsorption capacities (Caglayan & Aksoylu 2013). The same drop in surface area but to different degrees due to NaOH modification was documented by Shim and his group (Shim et al. 2001). They also explained the decrease due to the blocking of narrow pores by the surface complexes introduced by Sodium hydroxide.

Figure 2.14 exhibits that when applying 32% NaOH modification with a 3 h dwelling time the surface structure changes and shows highly cracked surfaces with a recognizably different pore size, indicating the suitability of $CO_2$ adsorption into these pores (Tan et al. 2014). Similarly, Vu and his co-workers investigated the modification of raw corncob based AC with NaOH (Vu et al. 2018). The AC was treated with 0.3 M NaOH and stirred for 24 hrs at 30$^oC$. The resulting modified AC had a high surface area of 1097$m^2/g$. The SEM figure of the modified sample is shown in Figure 2.15. The two figures of SEM for the aforementioned groups show that the starting material and activation conditions of AC have the most important impact on the surface structure. Although the two materials were modified using NaOH, the final morphological structure looks completely different. In addition, the FTIR spectra for both ACs (Figure 2.16) before and after NaOH

modification are different for the same reasons (the variations in the starting materials and the activation conditions).

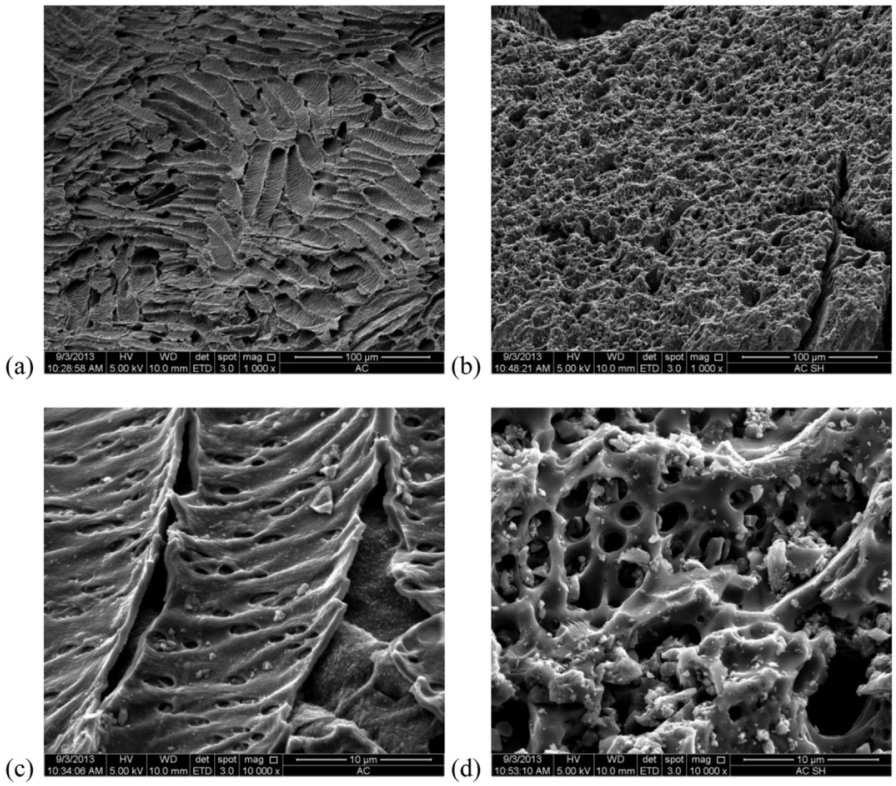


Figure 2-14: (a) and (c) Raw AC , (b) and (d) NaOH-modified AC (Tan et al. 2014)

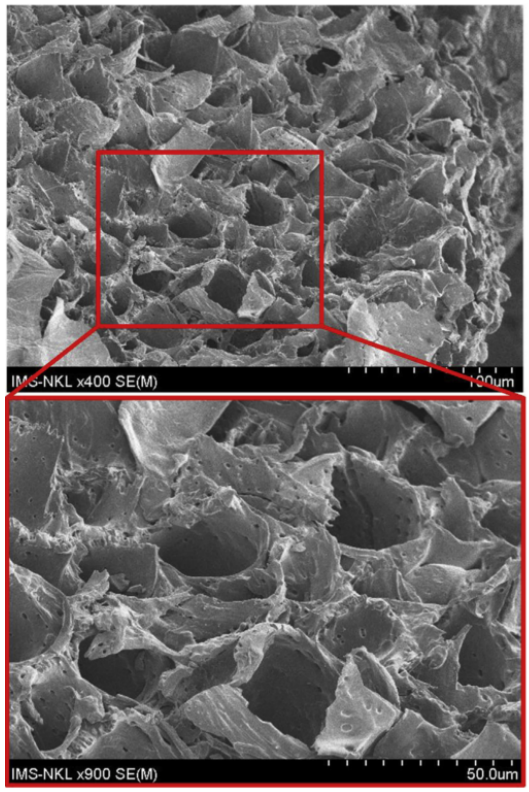


Figure 2-15: SEM image of the NaOH treated AC (Vu et al. 2018)

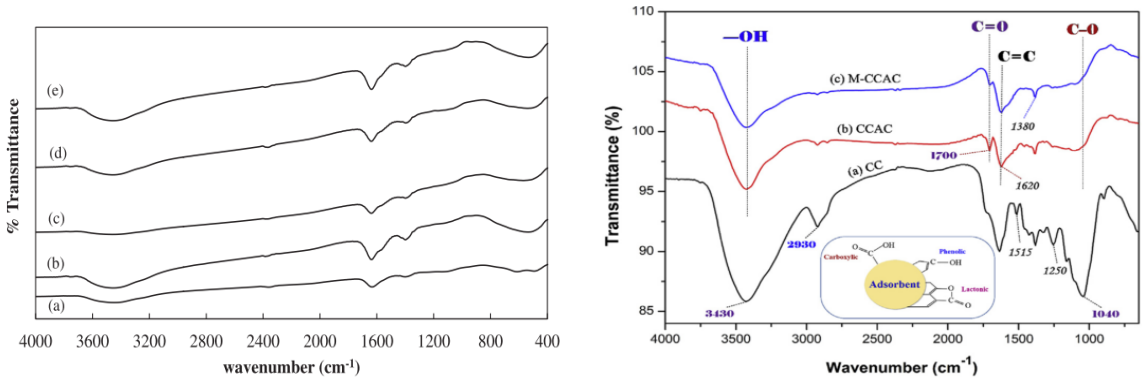


Figure 2-16: FTIR before and after NaOH modification (a) (Tan et al. 2014) , (b) (Vu et al. 2018)

### 2.6.5.4 Acid treatment

Several researchers have studied the effect of acid treatment on improving the $CO_2$ adsorption capacity of AC. Gęsikiewicz-Puchalska and his group modified three types of commercial AC by Hydrochloric acid and Nitric acid for 1 h at room temperature. They claimed that acid treatment of ACs led to the removal of mineral matter content, which boosted the $CO_2$ adsorption capacity as shown in Figure 2.17. While the surface area of the modified ACs increased slightly for two types of AC and decreased slightly for the

third type with acid treatments, $CO_2$ adsorption was significantly higher compared to the unmodified sample. They concluded that acid treatment reduces but not completely removes mineral matter content as some compounds (such as $SiO_2$ and $CaSO_4$) are not soluble in acids (Gesikiewicz-Puchalska et al. 2017).

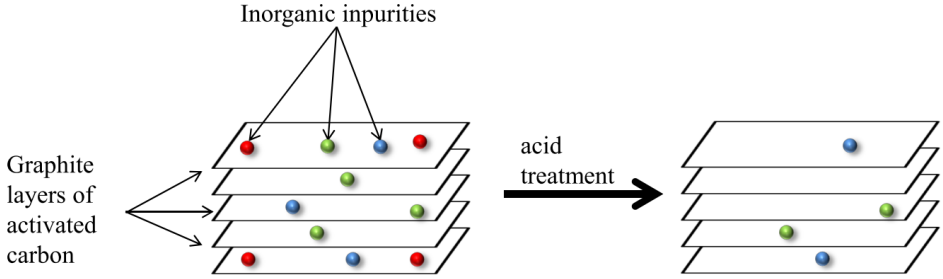


Figure 2-17: Acid treatment removes the inorganic impurities (Gesikiewicz-Puchalska et al. 2017)

This conclusion contradicts the results of another study which investigated the same acid treatments but under different conditions. Caglayana and Aksoylu treated Norit AC in a multi-step treatment starting with washing with 2 N HCl solution for 12 h under reflux, washing with distilled water under reflux for 6 h, oxidizing in 5N $HNO_3$ solution for 3 h and finally washing with boiling distilled water until the pH of the solution was 5.5. (Caglayan & Aksoylu 2013). Both the surface area and $CO_2$ mass uptake for the treated AC at 1 bar and at room temperature significantly decreased.

This could be attributed to the change in the surface chemistry of the modified AC as shown in Figure 2.18 compared to the unmodified AC. The Figure confirms the presence of surface oxygen groups such as carboxylic groups, lactones, phenols, ethers and anhydrides as a result of acid treatment at different places in the spectral regional 800-4000 $cm^{-1}$. The new incorporated oxygen functional groups diminished the affinity of AC to $CO_2$, thus decreasing the $CO_2$ adsorption capacity.

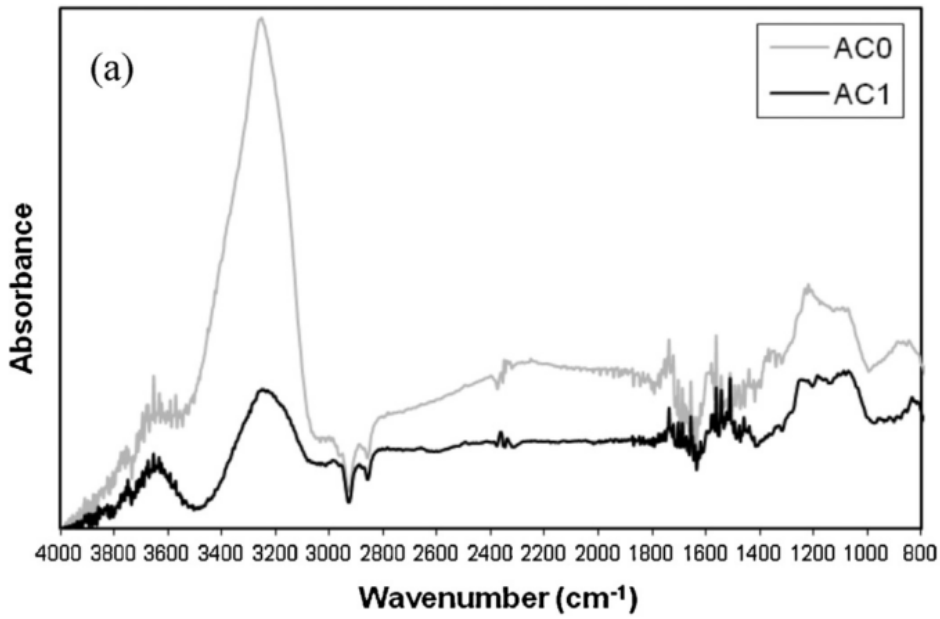


Figure 2-18: FTIR after HCl treatment (Caglayan & Aksoylu 2013)

In a different approach, Zhang and his co-workers modified the surface of AC via a two-step modification process which involved the use of a sulfuric/nitric acid mixture as a nitrating agent and then iron powder as a reducing agent (Zhang et al. 2013). They reported a considerable decline in BET surface areas and total pore volumes of AC after both nitration and reduction. The samples that were modified by the strong acid mixture showed the highest decline in surface area from 2994 to 507 $m^2/g$. They stated that this decrease was due to the destructive oxidative ability of the concentrated acid mixture used in nitration, which led to the collapse of the pore structures of the AC (Zhang et al. 2013). The adsorption capacity of both nitrated and aminated samples was higher than that of the unmodified samples, highlighting the fact that the nitrogen functionalities on the surface of AC play an important role in adsorption capacity despite the pore structure and the surface area. The FTIR spectra of the modified and unmodified AC shown in Figure 2.19 demonstrates the new vibrational bands assigned to nitro functional groups in the nitrated sample and the amino groups after reduction by iron powder in acetic acid solution. They concluded that nitro groups on AC surface can be converted into amino groups by a simple reduction process, therefore giving the AC the desirable basic functionalities required for efficient $CO_2$ adsorption.

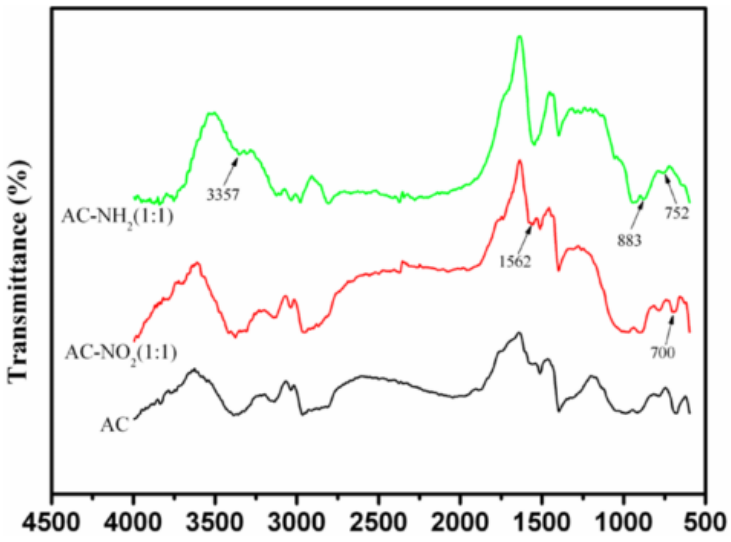


Figure 2-19: Spectra for the original AC and the modified ACs (Zhang et al. 2013)

#### 2.6.5.5 Metal salts treatment

Several researchers have investigated first–row transition metals and alkaline earth metals in the modification of AC for different purposes. Metals loading involving salts of chromium, copper, iron and zinc on AC has been successfully documented (Hosseini et al. 2015; Somy et al. 2009; Wang et al. 2006; Ghaedi et al. 2013; Yong & Mata 2001; Son et al. 2005; Tseng et al. 2003; Kim et al. 2010; Usman et al. 2012; Hu et al. 2017). For the purpose of $CO_2$ adsorption enhancement, impregnation by metal elements is a promising approach to increasing $CO_2$ uptake due to the high affinity and chemical reaction between metal oxides and $CO_2$ molecules (Rashidi & Yusup 2016). Yong and Mata reported that introducing alkaline metal or earth metal on AC produced a basic surface with a high affinity to $CO_2$, thus enhancing its adsorption (Yong & Mata 2001). For example, the presence of copper oxide on carbon materials as reported by Kim and his group showed a higher adsorption capacity to $CO_2$ compared to unmodified carbon (Kim et al. 2010). Similar behaviour was documented by Li who modified AC with copper and noticed a higher adsorption capacity after metal modification (Li et al. 2010). They explained that this increase was due to the base features of metal oxides (such as copper oxide, calcium oxide, or magnesium oxide) which indicates that they serve as electron donors and are thus electron acceptor friendly. Similarly, Somy and his group modified AC with $Cr_2O$ and

$Fe_2O_3$. In spite of the slight drop in surface area, the adsorption capacity of $CO_2$ doubled after the metal modification (Somy et al. 2009).

#### 2.6.5.6 Ammonium hydroxide treatment

Several studies have considered ammonium hydroxide for AC modification. Zhang et al modified commercial AC in different ways using an ammonia aqueous solution at 250 $^oC$. The BET surface area dropped from 2829 to 2461$m^2$/g. They attributed this decline to the collapse of the pore walls at high temperatures (Zhang et al. 2010). The results also indicated that the amounts of the basic groups on the surface of the modified ACs increased, while the amounts of the acidic groups reduced in comparison to those on the original AC. The adsorption capacity of the modified samples showed a higher value compared to the original AC increasing the $CO_2$ uptake from 2.92 to 3.22 mmol/g AC at 1 atm pressure and 25 $^oC$ temperature. In the same context, Ava Heidari and his group prepared AC from Eucalyptus camaldulensis wood residue and modified it with ammonia solution coupled with heat treatment under nitrogen gas at 400 and 800 $^oC$ (Ava Heidari et al. 2014). They reported that ammonia heat treatment of AC introduced basic nitrogen functional groups and decreased the amount of the oxygen containing functionalities. While the surface area declined at 400 $^oC$ modification, it significantly increased at 800 $^oC$, making the adsorption capacity of AC at 800 $^oC$ the highest among the examnied ACs and the 400 $^oC$ modified AC showed the least adsorption capacity. This contradicts other modification studies where surface area decline did not affect the adsorption capacity of the modified AC compared to that of the unmodified AC. Similar behaviour was noted by Vargas and his group who prepared AC from African palm stones and modified it with gaseous ammonia or ammonium hydroxide solution(Vargas et al. 2013). The surface area BET declined from 1320 to 916 $m^2$/g for the gaseous modified AC and to 785 for the aqueous ammonium modified AC. The researchers described the decrease as a result of a blockage in the carbon matrix produced by the nitrogen groups that were generated during the reaction with ammonia or ammonium hydroxide. However, this decrease in surface area had no effect on the $CO_2$ adsorption capacity. Indeed, the smallest BET area sample had the highest adsorption capacity value. The adsorption capacity almost doubled from 138 to 220 mg $CO_2$ /g AC, while the gaseous modified sample had an adsorption capacity of 170 mg/g.

### 2.6.5.7 Other treatments

In addition to the aforementioned treatments, some researchers have also used other chemicals to provide AC with a basic surface. Caglayan and Aksoylu modified Norit AC using a $O_2$ – $N_2$ mixture as a first step, and then calcinating the samples by $Na_2CO_3$. Although the surface area dropped by more than 30%, the $CO_2$ adsorption capacity increased dramatically from 3.3 to 22.7 wt% at 20 bar and from 0.75 to 8.87 wt% at 1 bar which confirms the role of chemical bonding in the adsorption process (Caglayan & Aksoylu 2013). Many researchers have reported similar area decline combined with maximizing the $CO_2$ capture capacity using different amination methodologies. Zhang and his group for example, used a mixture of Nitric and Sulfuric acids as a nitration agent to modify a petroleum coke AC, followed by a reduction and amination step by iron powder dissolved in an acetic acid. The surface area declined due to the destructive behaviour of the acids while the new fixed amine groups increased the $CO_2$ adsorption capacity from 16 to 19 mmol/g adsorbent (Zhang et al. 2013). Figure 2.20 shows the $CO_2$ capture capacity for the raw and modified samples at room temperature using the (Zhang et al. 2013) approach.

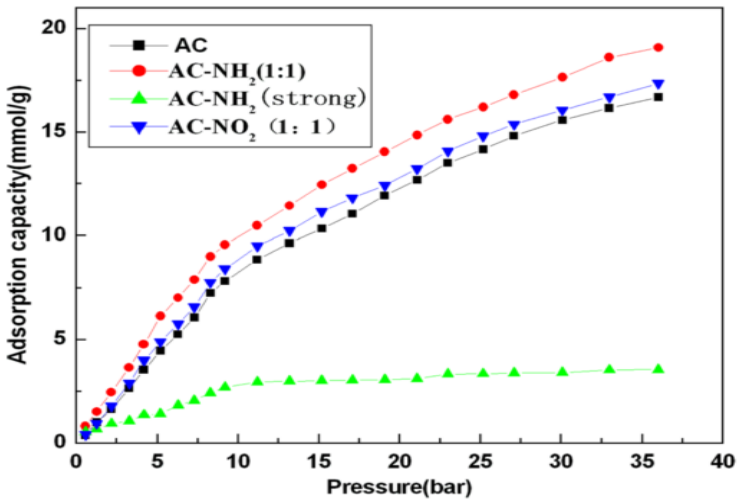


Figure 2-20: $CO_2$ capture capacity for the raw and modified AC samples (Zhang et al. 2013)

Although the majority of the modification methodologies highlighted in the literature have been effective in enhancing the adsorption capacity of $CO_2$, some have failed to increase this capacity. Plaza and his group used amine compounds dissolved in Methanol to modify Norit AC (Plaza et al. 2007). Both the surface area and the adsorption capacity showed a noticeable decline due to the impregnation technique used in the modification

process. In 2010, the same group attempted to adapt the ammoxidation approach which is a mixture of an air and gaseous ammonia to oxidize the AC samples; however, the same decline occurred in terms of both surface area and $CO_2$ capture capacity (Plaza et al. 2010). This highlights the fact that the amount of $CO_2$ adsorbed not only depends on the amount of amine incorporated into carbon, but also on the nature of the amine (Plaza et al. 2007), which justifies why some treatment approaches are more efficient in terms of $CO_2$ uptake than others.

#### 2.6.5.8 Summary of the modification techniques

Different techniques for modifying the surface of AC have been presented in the previous sections. Both heat treatment and ammonia treatment approaches require high temperature to reduce the acidity of AC, thus increasing its affinity towards $CO_2$. Employing Hydroxides such as NaOH in the modification of AC was reported to provide a remarkable increase in $CO_2$ adsorption capacity of the modified samples. Moreover, the modification was conducted in ambient temperature which means less energy-intensive process. Studies on acid treatment provided contradicted findings. While some researchers recommended acid wash for AC as a means of cleaning the surface from impurities, thus, increasing the surface area, several studies reported that acid modification can be destructive to AC structure. Modification using alkaline earth metals also demonstrated a high adsorption capacity for the modified samples. In particular, modification with copper salts was reported by many researchers as a promising technique to increase the $CO_2$ adsorption capacity. However, it was noticed that the process of modification with metals salts, reported in previous studies, included a calcination step for the modified samples at high temperature, which increases the carbon footprint of this class of modification. Modification with ammonia hydroxide also enhanced the $CO_2$ adsorption capacity by providing nitrogen functionalities, in spite of the reported decline in surface area. But similar to the earlier treatment, ammonium hydroxide was used in literature combined with high temperature of inert gas.

As this PhD work is focusing on increasing the sustainability of pervious concrete by absorbing $CO_2$ from the surrounding atmosphere, the techniques of modifying AC should follow an energy conservative approach to minimise the contribution to more $CO_2$ emissions by the process of modification. Therefore, only modification under ambient temperature will be investigated.

## 2.7 PERVIOUS CONCRETE

### 2.7.1 Definition and Applications

Pervious concrete, also known as permeable, porous and no-fines concrete, is a material that consists of cementitious material, coarse aggregate, little or no fines and water. While fine aggregate is limited in pervious concrete, coarse aggregate is kept to a narrow gradation. Typical gradation includes ASTM C33 No. 8 (9.5 - 2.36 mm), No. 67 (19.0 -4.75 mm) or No. 89 (9.5 to 1.18 mm). The term pervious concrete as defined by the ACI concrete terminology (ACI 522R 2010) is a "hydraulic cement concrete proportioned with sufficient interconnected voids that result in a highly permeable material, allowing water to readily pass". Pervious concrete is considered as one of the Best Management Practices (BMP) recommended by the Environmental Protection Agency EPA as it reduces storm water runoff, improves storm water quality and may recharge groundwater supplies (ACI 522R 2010).

Pervious concrete has been used in building construction since the middle of the nineteenth century in Europe and Australia (Francis 1965). The first reported use was in 1852 in the United Kingdom (Ghafoori & Dutta 1995a). Later in 1923, a group of 50 two-story houses were built with clinker aggregate in Edinburgh, Scotland where in the 1930s the Scottish Special Housing Association Limited accepted the use of pervious concrete for domestic buildings. This led to the use of pervious concrete in over 900 houses by 1942 (ACI 522R 2010). During the period between 1939 and 1945 (World War II), the need to develop new methods of building construction boosted the use of pervious concrete because it required less cement per unit volume compared to the conventional type of concrete and because of the availability of hard aggregate and the absence of good facing bricks (Malhotra 1976) Moreover, construction with pervious concrete before the world war was restricted to two-story buildings; however, after 1946, pervious concrete was recognised as a material for load-bearing elements in buildings up to 10 stories tall. In addition to residential buildings, pervious concrete was broadly used for public and industrial buildings especially in areas north of the Arctic Circle because of the difficulties

associated with the use of traditional building materials. These difficulties included the high cost of brick transportation, the fire hazard of timber and inadequate thermal insulation properties of concrete (Malhotra 1976). Despite this broad use of pervious concrete in Europe, its use as a building material in North America was limited because these areas did not experience the same material shortage as Europe after World War 2. Over the years, pervious concrete was used in residential construction in the UK, Spain, Germany, France, Belgium, Holland, Hungary, Russia, Venezuela, West Africa and the Middle East. In Australia and Canada, the first reported use of pervious concrete was in 1946 and 1960 respectively (ACI 522R 2010).

Pervious concrete is applied to pavement in different forms. The most frequent use is as a surface course for both parking lots and roadways. In central Florida, Utah, and New Mexico, pervious concrete was first considered as a paving material for parking lots in the 1970s to manage the massive quantities of water running off a parking lot during a storm. The high permeability rate of this concrete allows water to permeate into the ground under the pavement (Pindado et al. 1999). In addition to roadways, pervious concrete is used as a drainable base, subbase material and roadway surface. Moreover, pervious concrete shoulders are used in Europe to reduce pumping beneath concrete pavements (ACI 522R 2010).

Despite the few limitations of pervious concrete in pavement applications, mainly related to its limited use on roads experiencing heavy traffic and pavement requiring special design and construction practices, pervious concrete is advantageous for many reasons. It controls storm water runoff due to its high permeability, eliminates the need for water retention areas which increases the spaces for parking, reduces the glare on road surfaces especially at night and decreases the interaction noise between tires and the pavement (ACI).

In addition to the abovementioned applications, pervious concrete has also been used in other applications. These include greenhouses, tennis courts, noise barriers and building walls. Monahan studied the use of pervious concrete as a thermal storage system in greenhouses floors (Monahan 1981). The pervious concrete floors serve as a storage area and as a heat exchanger for the greenhouse. In addition, pervious concrete has been extensively used in the construction of tennis courts to control the ponding of water and to allow water to percolate into the ground. Moreover, pervious concrete has been used

in the construction of noise barriers and interior walls to absorb the sound and then dissipate it instead of reflecting it to another location (ACI 522R 2010).

### 2.7.2 Pervious concrete mix design

Pervious concrete requires special care to design a mix that meets the required mechanical and drainage properties. There are few publications considering approaches or methods to design pervious concrete. One practical approach is the phase-volume design which was proposed by ACI (ACI 522R 2010). In this procedure, the cement paste volume is specified first based on the required porosity. Figure 2.21 shows the relationship between the void content and paste content by volume. The design volume of each batch is calculated based on the volume of the individual ingredients and the required porosity for a specific application.

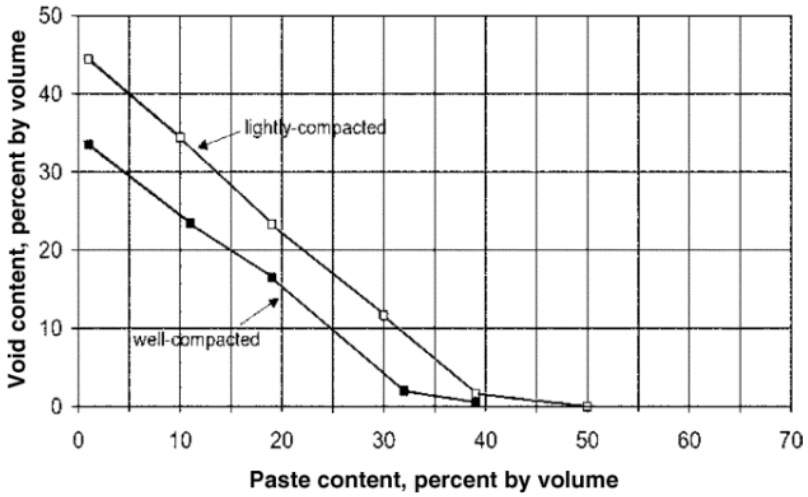


Figure 2-21: Correlation between paste and void content (ACI 522R 2010)

The procedure of the mix design is summarised in the following steps (equations 3-9):

1. The weight of aggregate under saturated surface dry condition $W_{ssd}$ is first calculated as follows:

$$W_{ssd} = \rho_{ssd} \times (\frac{b}{b_o}) \times V_{tot} \qquad \text{Equation 2.3}$$

Where:

- $\rho_{ssd}$ is the density of saturated surface dry aggregate
- $\frac{b}{b_o}$ is the dry rodded volume of coarse aggregate in a unit volume of concrete from table 2.6 for No. 8 and No. 67 aggregate.

- $V_{tot}$ = is the total batch volume

Table 2-4: Effective $b/b_o$ ratio for No. 8 and No. 67 aggregate (ACI 522R 2010)

| Percent fine aggregate | 0 | 10 | 20 |
|---|---|---|---|
| $b/b_o$ ratio for No. 8 | 0.99 | 0.93 | 0.85 |
| $b/b_o$ ratio for No. 67 | 0.99 | 0.93 | 0.86 |

2. The volume of cement paste is determined based on the required porosity as shown in Figure 2.6
3. With selected w/c ratio, the weight of cement is calculated according to the following equations:

   Paste volume $V_p$ = cement volume + water volume

   $$V_p = \frac{c}{3.15 \times 1000\ kg/m3} + \frac{w}{1000 kg/m3} \quad \text{Equation 2.4}$$

   Substituting w = (w/c)* c

   $$V_p = \frac{c}{3.15 \times 1000\ kg/m3} + \frac{\left(\frac{w}{c}\right) * c}{1000 kg/m3} \quad \text{Equation 2.5}$$

   $$c = \left[\frac{V_p}{0.315 + \frac{w}{c}}\right] \times 1000\ kg/m3 \quad \text{Equation 2.6}$$

4. The weight of water is simply calculated as w = c (w/c)
5. The total volume of solid materials is calculated as follows:

   $$V_s = V_a + V_c + V_w = \left[\frac{W_a}{G_a} + \frac{W_c}{G_c} + \frac{W_w}{G_w}\right] \quad \text{Equation 2.7}$$

6. The porosity is calculated as

   Porosity = $(V_{tot} - V_s) / V_{tot} * 100$ Equation 2.8

   Where
   - Vs is the total volume including the volume of aggregate, cement and water
   - W is the weight of the components: aggregate, cement, water
   - G is the specific gravity of the components: aggregate, cement, water
7. The total density is calculated as:

   Total density = $(W_a + W_c + W_w)/ V_{tot} * 1000$ Equation 2.9

The density and porosity are checked immediately after mixing following ASTM C1688 (2009) for fresh density and void content for the purpose of mix proportioning verification. This approach of design is simple and straight forward, however, it does not

give an indication of the water to cement ratio and doesnot consider the effect of compaction. In addition, it has a limited database of dry-rodded volume of coarse aggregate in a unit volume of concrete (No. 8 and No. 67 aggregates only).

A number of studies have since examined different design methods for pervious concrete. Yahia and Kabagire (Yahia & Kabagire 2014) proposed a novel design methodology based on the packing density of aggregate rather than the uniformity or the curvature coefficients Uc and Cc. Based on this approach, the inter-particle void index of aggregate (IPV) was determined and used a design factor to determine the optimum content of cement paste (PV) in order to generate the optimal balance between permeability and strength. The researchers examined various pervious concrete mixes in which the w/c ratio was fixed at 0.3. The findings of the study indicated that the increase in the PV/IPV ratio increased the UCS but reduced the porosity and water permeability. In addition, PV/IPV lower than 60% provided functional pervious concrete mixtures with a porosity, permeability and UCS of 19%, 1mm/s and 22 MPa respectively. Given the minimum limits of permeability and porosity (1 mm/s and 19% respectively), the functional zone was determined. Therefore, the authors suggested a PV/IPV ratio of 30-60% to obtain a good balance between the mechanical properties and the drainage requirement of pervious concrete (Yahia & Kabagire 2014).

Another study was proposed by Nguyen and his group (Nguyen et al. 2014) where an analytical approach was examined for pervious concrete proportioning based on the assumption that cement paste is required for coating the coarse aggregate in pervious concrete without clogging up the voids in the concrete mix. Therefore, the method involves three main steps: (1) determination of the aggregate volume (2) quantification of the cement paste coating layer (3) determination of the water to cement ratio. The resulting pervious concrete showed a greatly high UCS of more than 28 MPa while maintaining a large porosity of 17% and a permeability of 1 mm/sec (Nguyen et al. 2014). Both approaches optimised the composition of the pervious concrete, however, they involved complicated measurements which limit their applicability especially if a different size or type of aggregate is used. Other methodologies for pervious concrete design were proposed in previous studies such as Zouaghi method and Zheng method. Although the simplicity of the methodologies, they have several drawbacks such as (1) the relationships between the parameters are applied for local gravel (2) no

consideration for the compaction (3) a correction step is needed at the end to adjust the composition (Zheng et al. 2012; Nguyen et al. 2014).

### 2.7.3 Properties of pervious concrete

This section introduces an overview on the principal properties of pervious concrete; porosity, UCS, and water permeability. This is followed by a critical review on the effect of mix composition on these properties.

#### 2.7.3.1 Overview on pervious concrete properties

Pervious concrete is a highly porous concrete. Its porosity is a result of the interconnected network of voids and not from aggregate porosity as is the case in light weight concrete (Neithalath 2004). This porosity is the prime characteristic of pervious concrete and all other properties depend on it. Porosity, in turn, strongly depends on the cement paste volume within the mix, the water to cement ratio, the aggregate size and gradation, and the level of compaction (ACI 522R 2010). Typical porosity in pervious concrete is 15 – 35%.

The unconfined compressive strength (UCS) of pervious concrete is lower than that of conventional concrete. The range of UCS values is 3.5 MPa to 28 MPa which is suitable for a wide range of applications (ACI 522R 2010). The UCS of pervious concrete is highly affected by the mix proportion and the level of compaction during casting. There is an inverse correlation between porosity and the UCS of pervious concrete; the higher the porosity, the lower the UCS, and vice versa (Meininger 1988).

One key property of pervious concrete is the ability to permeate water through the matrix. The permeability rate of pervious concrete, sometimes known as the percolation rate, is inherently dependent on its porosity and pore structure. Meininger demonstrated that a minimum porosity of approximately 15% is required to achieve a considerable percolation rate (Meininger 1988). For a porosity of 20 to 25%, the coefficient of permeability is reported by various researchers to be approximately 0.01 m/s (ACI 522R 2010).

Several previous studies reported that the permeability of pervious concrete is directly related to its porosity (Tennis et al. 2004; Huang et al. 2010; Martin et al. 2014; N Neithalath et al. 2010). Figure 2.22 illustrates a compilation of porosity-permeability

relationships from previous studies. The general trend is that increasing porosity achieves an increase in permeability rates. However, it can be seen from the scattering of the data in the figure that representing permeability as a function of porosity alone is not adequate. Other features of the pore structure such as pore connectivity and characteristic length scale should be considered when predicting permeability (Narayanan Neithalath et al. 2010).

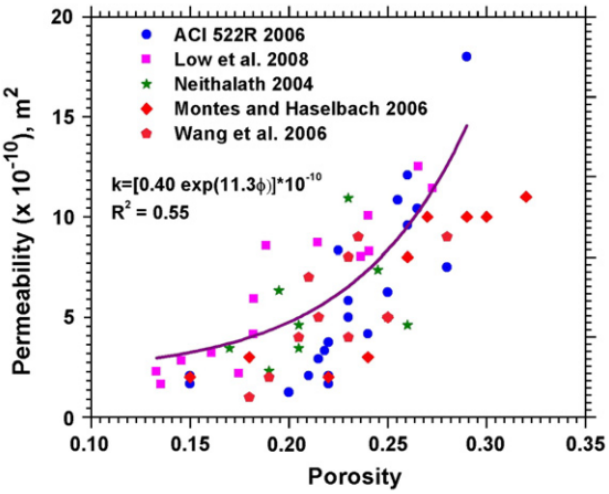


Figure 2-22: Porosity-Permeability relationships for several pervious concrete mixes (Narayanan Neithalath et al. 2010)

### 2.7.3.2 Effect of mix composition on the properties of pervious concrete

Properties of pervious concrete are highly dependent on the materials proportioning of pervious concrete mixtures. In this section, the influence of aggregate size and gradation, aggregate to cement ratio, water to cement ratio, and compaction level on the properties of pervious concrete along with past studies that investigated these effects are discussed and critically reviewed.

**Aggregate size, gradation, type and content**

The size, gradation, type of the aggregate and aggregate to cement ratio play a significant role in the mechanical and physical properties of pervious concrete (Alam & Naz 2015; Chopda & Chhattani 2015; Schaefer et al. 2006; Huang et al. 2010). Limited quantities of fine aggregate could be included in pervious concrete mixes to improve the mechanical properties but with a careful attention on its effect on concrete permeability. Fine aggregate has a pore filling effect that might block the concrete pores, thus resulting in a

decline of its permeability (Yang & Jiang 2003; Bhutta et al. 2012; Abdollahzadeh 2015). Yang and Jiange investigated the effect of fine aggregate in pervious concrete mixes with a range of 15 – 20% by mass. They concluded that using fine aggregate improved the strength of the pervious concrete; however, the cement quantity has been adjusted accordingly to meet the drainage requirements. This study further investigated the effect of coarse aggregate gradation on the UCS of pervious concrete. The results showed that the UCS increased as the aggregate size decreased as shown in Figure 2.23 (a). The authors attributed the results to the fact that a smaller aggregate size improves the strength of the interface between the aggregate and cement paste, thus, improving the UCS (Yang & Jiang 2003).

These findings were confirmed by Huang et al. who studied the impact of three types of single-sized limestone aggregates (12.5 mm, 9.5 mm, and 4.75 mm) on the properties of pervious concrete. Figure 2.23 (b) shows an increase in the UCS from 4.5 to 6.8 MPa as the size of the limestone coarse aggregate decreased from 12.5 to 4.75 mm (Huang et al. 2010) while permeability showed an acceptable value in a range of 17-19 mm/sec. The inclusion of 7% sand increased the UCS of the smaller aggregate size-mix (4.75mm) from 6.8 to 10.4 MPa.

A similar trend was reported by Bhutta et al. who utilised three sizes of crushed aggregate (13–20, 5–13 and 2.5–5 mm) to prepare high performance pervious concrete. The results showed an enhanced strength as the aggregate size decreased as shown in Figure 2.23(c), while the permeability and porosity values were in the range of 2.5-33mm/sec and 18-28% respectively (Bhutta et al. 2012).

In the same context, Maguesvari & Narasimha evaluated the influence of fine aggregate and coarse aggregate quantities on the properties of pervious concrete (Maguesvari & Narasimha 2013) using 4 different aggregate sizes, and with sand incorporation percent ranges from 0-50% of coarse aggregate. The results showed an increase in the UCS as the aggregate size decreased and as the percentage of sand inclusion increased. The permeability showed a slight increase with the increase in aggregate size as shown in Figure 2.23(d). The authors suggested that the quantity of fine aggregate that can be used in a pervious concrete mix without impacting adversely on permeability depends to a high extent on the coarse aggregate size. Table 2.5 summarises the effect of aggregate size on mechanical properties of some previous studies.

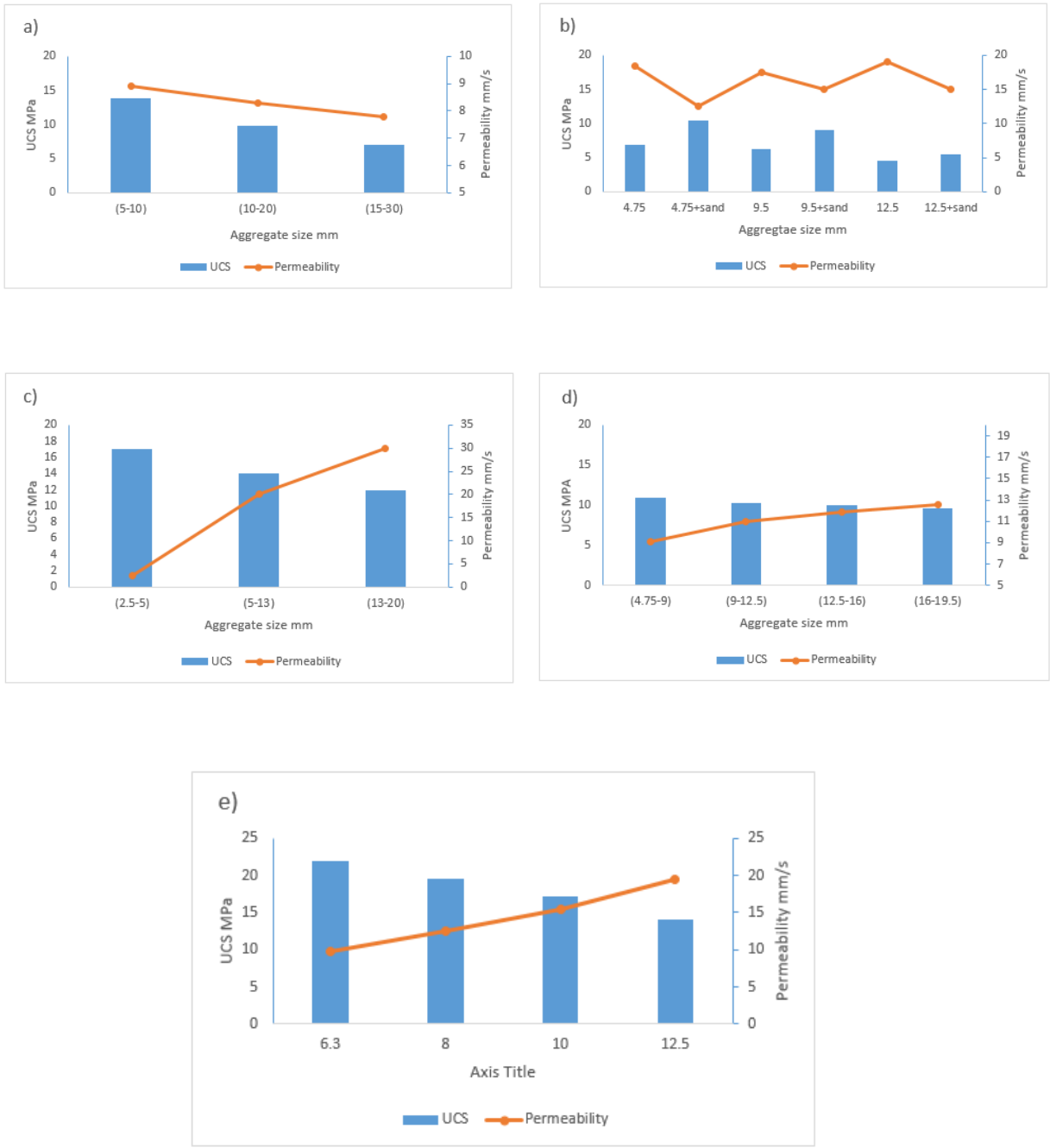


Figure 2-23: Effect of aggregate size and fine aggregate inclusion on the 28-days UCS and permeability of pervious concrete (a) (Yang & Jiang 2003) (b) (Huang et al. 2010) (c) (Bhutta et al. 2012) (d) (Maguesvari & Narasimha 2013) and (e) (Elango & Revathi 2017)

Table 2-5: Summary of the effect of aggregate size on the mechanical properties of selected previous studies.

| Reference | Aggregate size | Findings related to pervious concrete properties |
|---|---|---|
| (Yang & Jiang 2003) | 5-10 | Smaller sized aggregate can improve the UCS of the pervious concrete. However, the cement content must be adjusted accordingly. |
| | 10-20 | |
| | 15-30 | |
| (Chindaprasirt et al. 2009) | 2.5-5 | The rate of UCS decline with small aggregate size is higher than that with larger aggregate size. At the same void ratio, the UCS with large aggregate is larger than that with small aggregate. |
| | 5-13 | |
| | 13-20 | |
| (Agar-Ozbek et al. 2013) | 2-4 | The decrease in aggregate size has an increasing effect on the strength results, and a decreasing effect on porosity. |
| | 4-8 | |
| (Fu et al. 2014) | 2.4-4.8 | The UCS decreased as the aggregate size increased. Water permeability and connected porosity increased with increasing aggregate size. |
| | 4.8-6.4 | |
| | 6.4-9.5 | |
| | 9.5-12.7 | |
| (Ćosić et al. 2015) | 0-4 | The higher the aggregate size, the higher the porosity but the lower the UCS. |
| | 4-8 | |
| | 8-16 | |
| (Zhong & Wille 2016) | 1.19 | The results show the decrease in UCS with the increase of aggregate size. |
| | 2.38 | |
| | 4.75 | |
| (Yu, Sun, Wang, et al. 2019) | 2.36-4.75 | The increase of aggregate size increases the UCS rapidly at first. However, when the aggregate size is larger than 7 mm, the increase of aggregate size does not have a noticeable effect on the UCS. |
| | 4.75-6 | |
| | 6-8 | |
| | 8-9.5 | |
| (Yu, Sun, Hu, et al. 2019) | 2.36-4.75 | When the aggregate size increases, the permeability coefficient increases. |
| | 4.75-6 | |
| | 6-8 | |
| | 8-9.5 | |

Alam and Naz also investigated the impact of coarse aggregate size and fine aggregate content on the porosity and the strength of pervious concrete. They found that the higher the fine content the higher the UCS and the lower the porosity. They also found that the bigger the size of aggregate, the higher the porosity and the lower the UCS as shown in Figure 2.24 (a) (Alam & Naz 2015). Similarly, Elango and Revathi reported that an increase in aggregate size leads to an increase in porosity and decrease in the density of pervious concrete. Consequently, high density aggregate mix develops higher UCS while lower permeability and porosity as shown in Figure 2.23(e) and Figure 2.24 (b) (Elango & Revathi 2017).

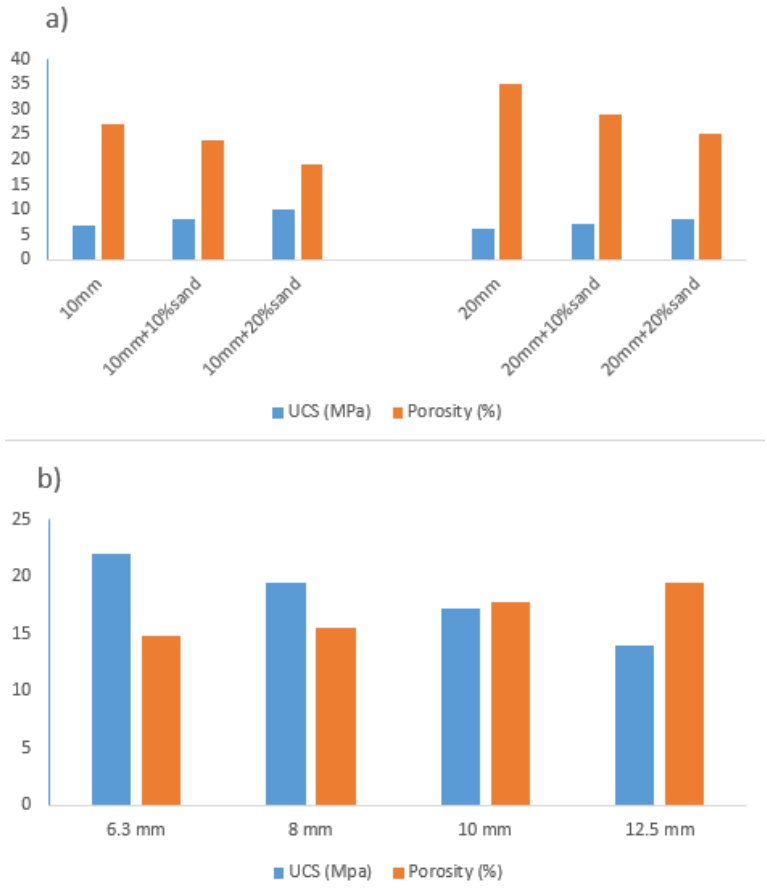


Figure 2-24: Effect of aggregate size on UCS and porosity (a) (Alam & Naz 2015), (b) (Elango & Revathi 2017)

All the aforementioned studies agree that aggregate size and gradation have a significant influence on the mechanical and physical properties of pervious concrete. Moreover, the results show that a carefully selected percentage of fine aggregate can enhance these properties. An aggregate size of 4.75 – 9 mm (No. 8 size) and 10% maximum fine aggregate can satisfy both strength and drainage requirements of pervious concrete.

In pervious concrete, aggregate to cement ratio (A/C) is another crucial factor that influences the developed properties of concrete. Generally, ratios are in the range of 4.0 to 4.5 by mass. These A/C ratios lead to aggregate contents of between about 1300 kg/m$^3$ and 1800 kg/m$^3$. Higher A/C ratios have been used in laboratory studies, but resulted in significant reductions in strength (Malhotra 1976; Tennis et al. 2004). Comprehensive research in 1976 by V.M. Malhotra investigated several factors that influence the properties of pervious concrete. One study showed that the UCS of pervious concrete highly depends on the aggregate cement ratio. The higher the aggregate cement ratio, the lower the UCS. Table 2.6 shows the influence of using different aggregate cement ratios on UCS and unit weight, while Table 2.7 shows the effect of gravel type on the UCS of pervious concrete (Malhotra 1976).

Another piece of extensive research was conducted by Nader Ghafoori in 1995 (Ghafoori & Dutta 1995b) on various aspects of pervious concrete. In one study, he investigated the parameters that affect the UCS of pervious concrete. He concluded that strength depends on the water cement ratio, the aggregate cement ratio, compaction, and curing. He also developed a chart that displays the effects of varying the aggregate cement ratio and compaction energy on UCS and permeability as shown in Figure 2.25.

Table 2-6: Effect of aggregate to cement ratio on 28-day UCS and Density (Malhotra 1976)

| Aggregate/cement ratio | Water/cement ratio | Age of test (days) | Density (kg/m$^3$) | UCS (MPa) |
|---|---|---|---|---|
| 6 | 0.38 | 3 | 2015 | 8.90 |
| | | 7 | 2008 | 11.44 |
| | | 28 | 1999 | 14.34 |
| 8 | 0.41 | 3 | 1922 | 5.86 |
| | | 7 | 1914 | 7.27 |
| | | 28 | 1912 | 9.41 |
| 10 | 0.45 | 3 | 1869 | 4.31 |
| | | 7 | 1864 | 5.38 |
| | | 28 | 1861 | 6.99 |

Table 2-7: Relationship between 28-day UCS and aggregate type (Malhotra 1976)

| Type of aggregate | Density (kg/m$^3$) | UCS (MPa) |
|---|---|---|
| Rounded quartzite gravel | 1842 | 8.62 |
| Irregular flint gravel | 1585 | 4.83 |
| Crushed limestone | 1826 | 6.89 |
| Crushed granite | 1697 | 7.58 |

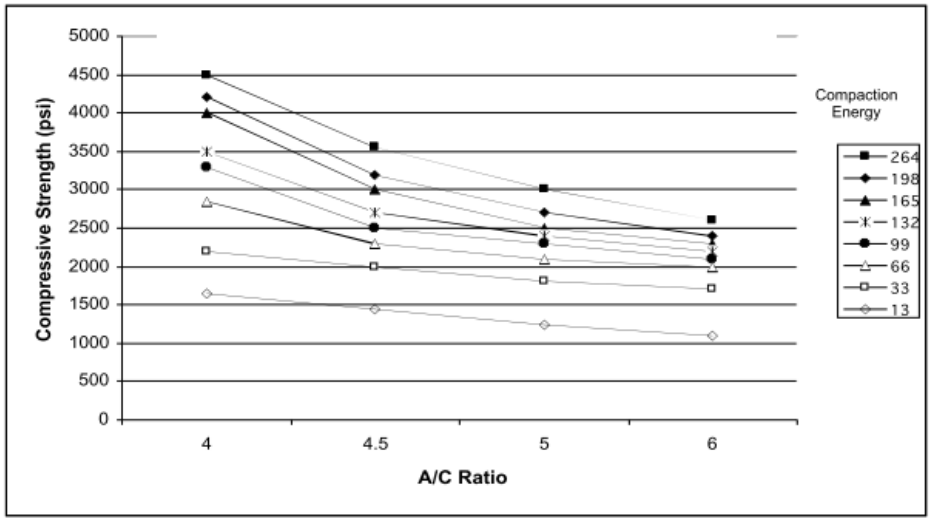

Figure 2-25: 28-day UCS vs aggregate/cement ratio (Ghafoori & Dutta 1995b)

Regarding aggregate type, the literature presents contradictory findings about incorporating recycled aggregate in pervious concrete. Zaetang and his group incorporated recycled concrete block aggregate in pervious concrete mixes. The percentages were 0%, 20%, 40%, 60%, 80%, and 100% by aggregate weight. They found that the recycled concrete aggregate increased the UCS of the pervious concrete for all the mixes except for the 100% replacement (Zaetang et al. 2016). However, Yap and his co-workers investigated recycled coarse aggregate from a demolition site using the same replacement percentage in pervious concrete, but their results showed that these mixes had lower mechanical properties compared to that of the control mix. They attributed this behaviour to the poor aggregate-cement paste bonding in recycled aggregate mixes (Yap et al. 2018). Regarding permeability, Yap found that when the percentage of replacement exceeds 40%, the rate of permeability increases drastically by 31-65% compared to the control mix.

This last finding confirms the results of Hatice Öznur Öz who investigated acidic pumice aggregate in pervious concrete. The acidic pumice replaced the crushed stone at 10%, 20%, 30%, 40% and 50%, respectively by total aggregate volume. Test results showed that incorporating pumice led to enhanced water permeability, irrespective of the replacement level. However, the compressive, splitting tensile and flexural strengths of PCs decreased with an increase in the replacement level of pumice (Öz 2018)

**Water / Cement ratio**

Water content in pervious concrete plays a significant role in the properties of fresh and hardened concrete. W/c ratio in pervious concrete is usually lower than that of conventional concrete with a tight range of about 0.27 to 0.35. The ACI report on pervious concrete (ACI 522R 2010) indicated that a higher w/c ratio increases the distance between the particles, resulting in a decline in density and strength values. It also limits the void content in the developed concrete due to the cement paste filling the pores at the base of samples. Optimum water content therefore prevents materials from crumbling due to the lack of water and prevents the loss of voids because of the extra water.

In 1988, Richard Meininger prepared different pervious concrete mixes using w/c ratios ranging from 0.27 – 0.51 but one aggregate size of 3/8" and an aggregate cement ratio equal to 6. He found the highest strength at a ratio of 0.43, while the permeability significantly decreased when the w/c ratio increased as illustrated in Table 2.8 (Meininger 1988). He then studied the relationship between UCS and w/c ratio but with different aggregate sizes and aggregate to cement ratios as shown in Figure 2.26. From the figure, it can be seen that the optimum ratio differs from 0.35 to 0.42 according to the aggregate size and content. That means the w/c ratio alone does not control the UCS and permeability. Indeed, other factors such aggregate size, A/C ratio and additives influence these properties.

Table 2-8: Relationship between strength and water content for 3/8" aggregate and A/C ratio =6 (Meininger 1988)

| w/c ratio | 28-day UCS (MPa) | Porosity % | Permeability (mm/s) |
|---|---|---|---|
| 0.51 | 9.31 | 22 | 2.12 |
| 0.47 | 9.45 | 23 | 1.69 |
| 0.43 | 10.34 | 25 | 4.23 |
| 0.39 | 9.65 | 27 | 12.7 |
| 0.35 | 8.62 | 29 | 16.93 |
| 0.31 | 6.96 | 32 | 21.59 |
| 0.27 | 5.99 | 33 | 24.98 |

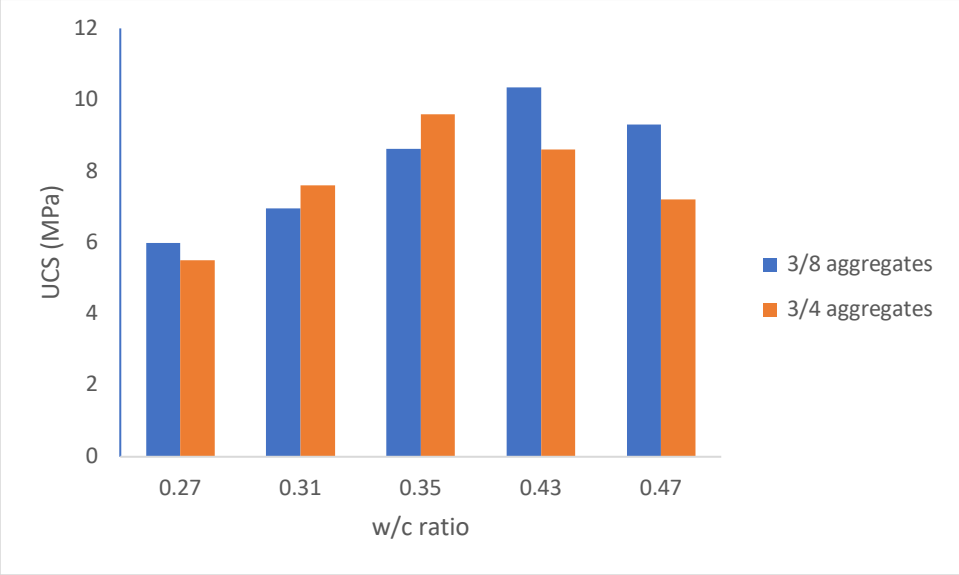


Figure 2-26: the effect of water content on 28-days UCS and permeability (Meininger 1988)

Contrasting UCS findings were reported by Ibrahim and his group. The researchers prepared 24 pervious concrete mixtures to address the effect of coarse aggregate size, w/c ratio, cement content, and coarse aggregate content on the relationships between UCS, tensile strength, porosity, and permeability (Ibrahim et al. 2014). They found that an increase in the water cement ratio from 0.3 to 0.4 led to an increase in both UCS and permeability, which contradicts the findings reported by Meininger in Figure 2.26.

From the above studies, it can be concluded that w/c ratio is not the only parameter that has a substantial effect on the UCS of pervious concrete. Aggregate to cement ratio combined with the size and gradation of aggregates play a significant role in the final properties of the pervious concrete mixes.

**Compaction methods**

The compactibility of pervious concrete is of great importance in controlling its properties. The level of compaction significantly affects the function and the characteristics of pervious concrete. A higher degree of compaction directly results in a higher value of strength in pervious concrete. This is as a result of the densification of concrete and the removal of voids, which are crucial for water permeability. Therefore, a higher level of compaction may result in a loss of permeability through the concrete, which may negatively affect the function of the pervious concrete system (Chopra et al. 2007).

Previous researchers have utilized different techniques for compaction. The most common methods have been hand compaction including rodding, hand tamping and ramming, and mechanical compaction including internal vibration and table vibration. (Chopra et al. 2007; Suleiman et al. 2006; Zhong & Wille 2016; Wu et al. 2016; Zaetang et al. 2016; Schaefer & Kevern 2011; AI-khalaf & Yousif 1986).

Short and Kinniburgh and Neville documented that rodding as a compaction technique is not recommended as it results in a high local density. Vibration on the other hand should be applied for very short periods; otherwise, the cement paste runs off (Short & Kinniburgh 1963; Neville 2011). This contradicts the findings of Malhotra who pointed out that the use of mechanical vibration is not recommended and that light rodding should be used (Malhotra 1976). Moreover, the Canadian Standard Association indicated that hand rodding in accordance with ASTM standards is more suitable for compacting pervious concrete specimens than ramming (Malhotra 1973).

Moreover, Al-khalaf and Yousif investigated the impact of different methods of compaction on the concrete properties (AI-khalaf & Yousif 1986). The methods they used were hand tamping, ramming, table vibration and internal vibration. They concluded that the optimum cement to aggregate ratio is 1:6 for all types of compaction. They also found that table vibration produced the highest UCS, while ramming developed the lowest values at all ages and cement-aggregate ratios. They also pointed out that 10 sec / layer is the optimum time for vibrating. At fewer than 10 seconds, there is a higher air void content in the mixes, resulting in lower densities and strength values. At the same time, vibrating the samples for more than 10 seconds showed a great reduction in UCS due to the instability of pervious concrete with long vibration, which resulted in the draining of cement paste away from the aggregate particles. The range of w/c ratio was 0.3- 0.35 depending on the compaction method. Vibrating table required a value of 0.3 as shown in Figure 2.27 (AI-khalaf & Yousif 1986). Finally, they emphasised that the UCS and density of pervious concrete increases when the cement content increases irrespective of the method of compaction. (AI-khalaf & Yousif 1986).

Meininger investigated the effect of the compactive effort on void content and density of a given pervious concrete mixture using eight different degrees of compaction. The unit weight values of the tested samples varied from 1680 to 1920 kg/m$^{3,}$ resulting in a significant effect on the corresponding UCS values (Meininger 1988). In the same context, Suleiman et al. produced different compaction energies during the placement of samples

by two vibrating tables with amplitudes of 0.127 mm and 0.086 mm. They reported a 11% decrease in UCS and a 5% decrease in unit weight when the vibration amplitude was reduced from 0.127 mm to 0.086 mm (Suleiman et al. 2006).

From the above studies, it can be seen that the compaction of pervious concrete is a chief factor that directly affects its properties. The choice of the compaction technique and the optimum time for vibrating should be selected carefully. Excessive compaction should be controlled as it may result in the removal of cement paste from the aggregate, leading to a failure in pervious concrete properties.

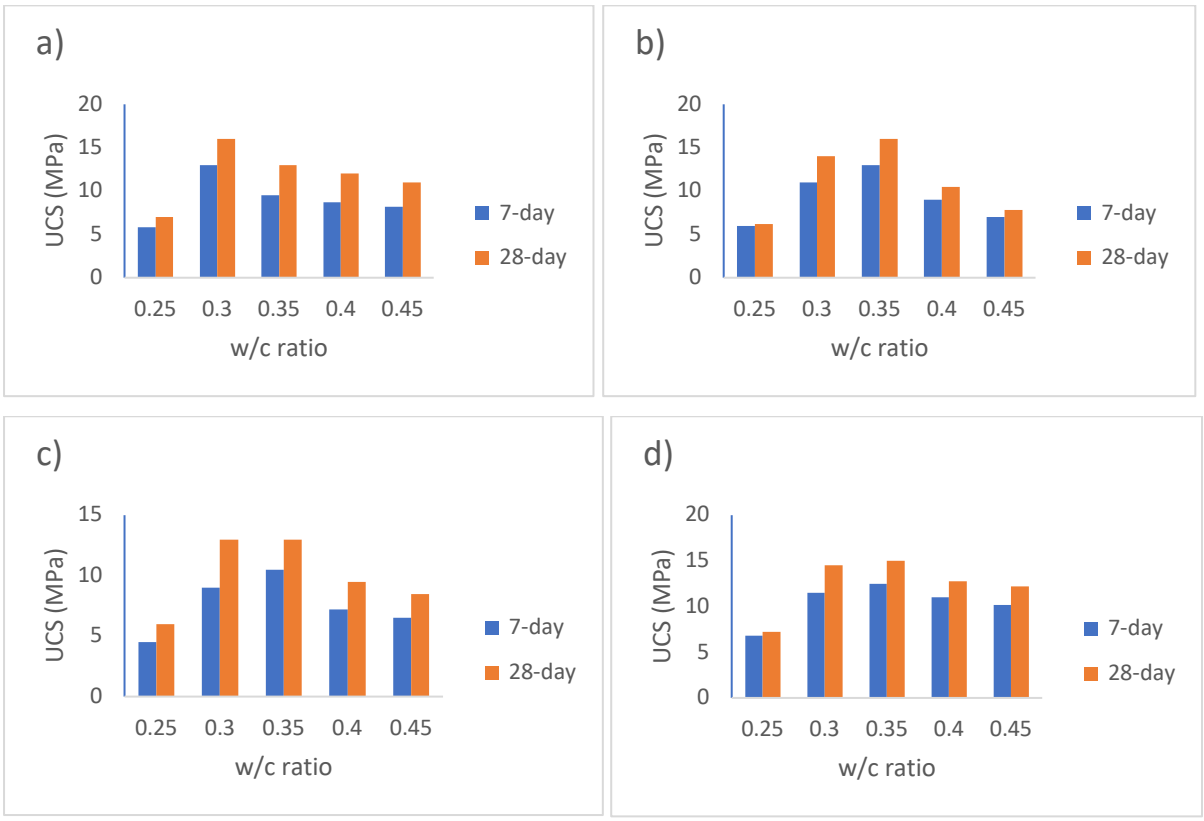


Figure 2-27: w/c vs UCS for different compaction methods (AI-khalaf & Yousif 1986) (a) vibrating table, (b) hand tamping, (c) Ramming, and (d) Internal vibrator

## 2.8 ACTIVATED CARBON IN CEMENTITIOUS MATERIALS

### 2.8.1 Introduction

Two main areas are presented and reviewed in the following sections. The first introduces the partial replacement of cement in either conventional or pervious concrete by other supplementary materials for the purpose of reducing the carbon impact of concrete. The second section deals specifically with activated carbon in concrete.

### 2.8.2 Partial replacement of cement by different materials

Although cement constitutes less than 20% of concrete by volume, it contributes to approximately 90% of the total emission of $CO_2$ from concrete production (Yang et al. 2015). This has led to intensive research in recent decades of cement, its properties and potential supplementary materials to offset a portion of cement in concrete, thus reducing its environmental impact.

A considerable number of industrial by-products have been incorporated successfully for decades within concrete to partially replace Portland cement. The most widespread and well-documented materials are fly ash, silica fume, ground granulated blast furnace slag, pumice powder and rice husk ash (Kabay et al. 2015; Divsholi et al. 2014; Chindaprasirt et al. 2007; Tošić et al. 2018; Moffatt et al. 2017; Hefni et al. 2018; Lu et al. 2018; Bhalla et al. 2018; Madani et al. 2018; Motahari Karein et al. 2017; Sanjuán et al. 2018; Verian & Behnood 2018). These materials are utilized to develop blended cement which can enhance concrete properties in addition to benefitting the environment.

For example, Aliabdo studied the possibility of using crushed waste glass obtained from containers as concrete additives. They found that a 15% replacement of cement by glass powder enhanced the concrete properties and increased the UCS by 15% compared to the control mix (Aliabdo et al. 2016). Slightly different findings were reported by Sadiqul Islam et al. who investigated waste glass powder for the same purpose. They found that the maximum replacement of cement without a negative effect on strength was 20% which improved the UCS by only 8% (G. M. S. Islam et al. 2017). This confirmed the findings of Omran and Hamou who reported that the 91-day UCS of glass-concrete increased by 7% compared to the control samples when a 20% replacement took place

(Omran & Tagnit-Hamou 2016). Higher values in UCS were observed by Kamali and Ali. The increase in strength compared to the control mixes at a late age of curing was more than 20% when a 20% of cement was replaced by an industrial by-product derived from waste glass fibre (Kamali & Ghahremaninezhad 2015).

Waste tyres have also been explored extensively for partial cement replacement (Ling & Nor 2006; Goulias DG 1998; Eldin & Senouci 1993; Siddique & Naik 2004; Thomas & Gupta 2016; Son et al. 2011; Khatib & Bayomy 1999; Holmes et al. 2014; Yung et al. 2013; Thomas et al. 2015; Thomas et al. 2014; Gesolu & Güneyisi 2011; Ganesan et al. 2013; Elchalakani 2015). Several researchers have reported a decrease in concrete workability with an increase in crumb rubber content (Holmes et al. 2014; Dong et al. 2013; Su et al. 2015; Youssf et al. 2014; Bravo & Brito 2012). Some have attributed this reduction to the reduced inter-particle friction between the rubber and other constituents (Holmes et al. 2014), while others have attributed it to the higher specific surface area and the higher water absorption of rubber particles (Su et al. 2015; Bravo & Brito 2012). Ling and Nor found that concrete paving blocks containing rubber enhanced the skid resistance but reduced the UCS (Ling & Nor 2006). This decline in UCS has been observed by numerous researchers (Ganjian et al. 2009; Gesoğlu et al. 2014a; Gesoğlu et al. 2014b; Holmes et al. 2014). The reasons behind this decrease could be attributed to the cement paste that contains the rubber particles which has a higher potential to rapidly develop cracks while loading. Another reason might be the lack of proper bonding between the cement paste and the rubber particles which can (a) lead to more cracks because of the non-uniform distribution of applied stresses, and (b) cause the rubber particles to move upwards during vibration compaction since the rubber has a lower specific gravity. This non-homogeneous concrete sample results in reduced UCS values (Ganjian et al. 2009). Holmes et al. recommended a maximum percent of replacement of 20% to avoid a significant reduction in UCS (Holmes et al. 2014).

In contrast to the abovementioned studies, numerous researchers have reported enhancements in UCS when rubber was incorporated into the concrete matrix. For instance, Dong et al. observed a significant increase in UCS when coated rubber was added to concrete (Dong et al. 2013). Similarly, Onuaguluchi and Panesar found that both the compressive and tensile strengths of concrete containing coated rubber increased (Onuaguluchi & Panesar 2014). Al-Akhras and Smadi reported a 45% increase in the UCS

after 90-days of curing when tyre rubber ash replaced 10% of the fine aggregate (Al-Akhras & Smadi 2004).

A number of other materials and by-products have been shown to enhance concrete properties when incorporated in appropriate proportions. Hen egg shell coupled with fly ash improved the strength performance and found to be cost effective (Babu & Neeraja 2017). Calcinated paper mill sludge showed a higher UCS with 10% replacement of cement (Vegas et al. 2006). Coal waste ash with a replacement percentage of up to 20% improved the UCS and the toughness of concrete pavements (Modarres et al. 2016).

In addition, agricultural waste materials have been investigated for use within concrete. Processed bamboo was reported to have the potential to produce a higher UCS of concrete. (Agarwal et al. 2014). Concrete samples containing 5% treated rice husk biochar and 5% treated bagasse biochar had a UCS of 36% and 55% higher than the control concrete, respectively, while the tensile strength demonstrated a 78% increase with a 5% treated bagasse biochar compared to the control mix (Asadi Zeidabadi et al. 2018). Palm oil fuel ash with up to 20% replacement by weight of the binder showed also a higher UCS (Sooraj VM 2013).

### 2.8.3 Activated carbon in cementitious formulations

Although carbon particles have been conventionally handled as a potential pollutant of aggregates in cementitious materials, there is an increasing interest in investigating its presence in concrete. Several researchers have claimed that a certain percentage of AC could be particularly advantageous to concrete (Justo-Reinoso et al. 2018; Asadi Zeidabadi et al. 2018; Morgan & Dumbauld 1952; Mahoutian et al. 2015; Krou et al. 2013; Krou et al. 2015).

As early as 1952, Morgan and Dumbauld recommended the use of activated charcoal as a cement additive to withstand the contamination of cement slurries with drilling muds. Such contamination prevents cementitious materials from developing early strength. The main goal of Morgan and Dumbauld research was to investigate the possibility of finding suitable additives to cement to boost its ability to resist the contamination with drilling muds. They found that the contamination could be controlled by the adsorption of the contaminants via a suitable material in the cement. After testing numerous materials, they reported that AC had the highest potential for this function. The results showed that up to 10% of AC by cement weight was adequate to develop an early strength without any negative effect on the required properties of the cement material (Morgan & Dumbauld 1952).

There have been recent attempts to incorporate AC into cementation formulations in both powdered and granular forms. Krou et al. investigated the possibility of using AC as an additive in the concrete walls of roadway tunnels and parking garages to increase the performance of these materials in reducing nitrogen oxides (Krou et al. 2013). The results showed that the small addition of AC (0.5% of cement weight) had a considerable positive effect on $NO_2$ adsorption. The reduction was 1.6 times higher than that of the control sample. Krou *et al.* concluded that the high affinity between $NO_2$ and AC explains the enhancement of the $NO_2$ reduction with AC- cement paste (Krou et al. 2013). Similarly, Horgnies *et al.* reported that introducing a small amount of activated charcoal into concrete can considerably enhance and extend $NO_2$ absorption without greatly increasing the total porosity or decreasing strength, thus suggesting that walls made of activated charcoal concrete could control the problem of $NO_2$ pollution peaks in road tunnels and parking garages (Horgnies et al. 2012). Figure 2.28 illustrates the $NO_2$ concentrations

measured at the outlet of a reactor and showing that the concrete sample containing activated charcoal (AC-C) has a much higher and more stable absorption of $NO_2$ than the reference concrete even after 20 h of exposure. On the other hand, the results show a loss in strength of 15% after 7-days of curing when 3% of a limestone aggregate was substituted with powder activated charcoal. In contrast, Resheidat et al. reported UCS gains in concrete samples when the mass ratio of powdered AC powder ranges between 2% and 10% (Resheidat et al. 2002).

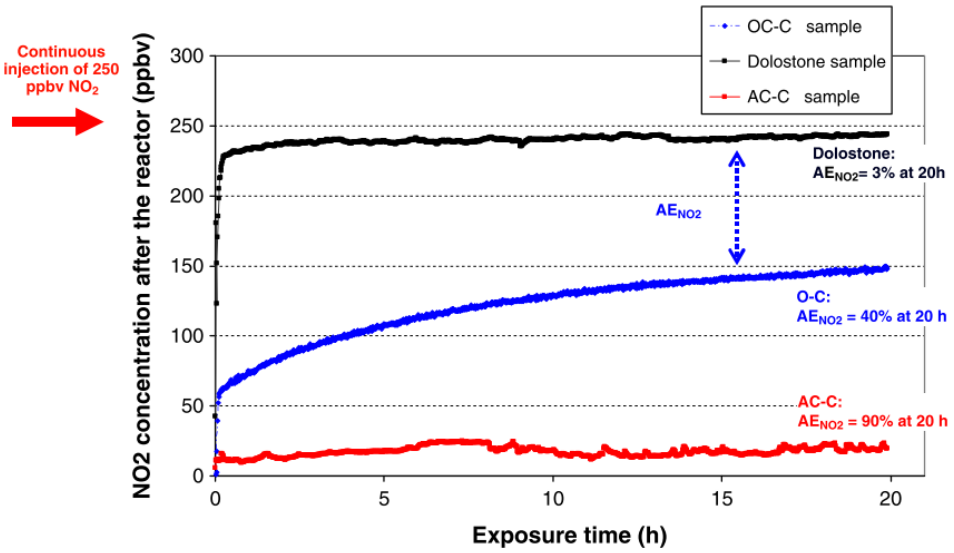


Figure 2-28: Adsorption of NO2 by dolostone, ordinary concrete and AC concrete (Horgnies et al. 2012)

Another study by Krou et al. investigated AC as an additive to cement paste for the purpose of adsorbing Volatile Organic Compounds (VOCs), namely acetaldehyde and toluene. While the results illustrated a significant abatement of toluene using the hydrated cement paste containing 0.5% AC, no significant enhancement was observed for acetaldehyde adsorption. The researchers recommended modifying the AC before incorporation into cement to increase its affinity for acetaldehyde (Krou et al. 2015).

Moreover, Ersan et al. investigated commercially available materials such as expanded clay, zeolite and granular AC for so-called microbial self-healing concrete. The study focused on the influence of these materials on the mortar setting and UCS of concrete. The UCS of cement mixtures containing 1.7% granular AC of sand mass was improved by 10% after 28-days of curing, compared to the control mix (Erşan et al. 2015).

And most recently, Justo-Reinoso et al. investigated the effect of substituting fine aggregate with similarly-sized granular AC particles on the physical and mechanical properties of cement mortars. The researchers reported that in a range of less than 2% by mass, the substitution grains can provide an increase of up to 10.6% in the UCS of mortars formulated and cured at 7, 14 and 28-day as shown in Figure 2.29 (Justo-Reinoso et al. 2018).

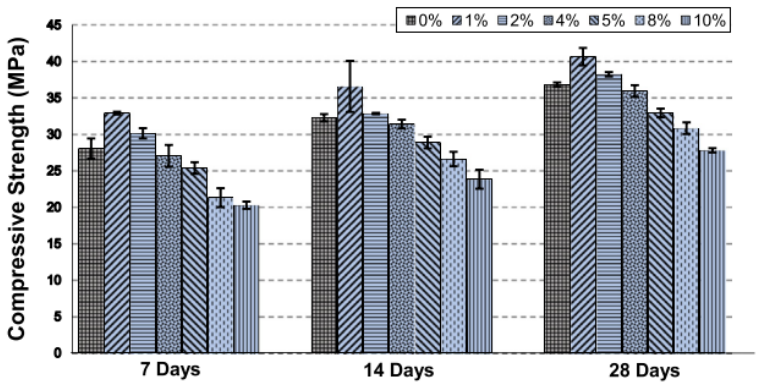


Figure 2-29: Influence of fine aggregate replacement by powdered activated carbon on UCS (Justo-Reinoso et al. 2018)

The studies presented in this chapter confirm that AC has been used within concrete for adsorbing pollutants. It has also been used to provide a high surface area to secure suitable living conditions for bacteria for self-healing purposes. However, to date, the use of AC in concrete for the purpose of carbon sequestration has not been investigated. Therefore, the primary aim of this work is to study the potential of AC in pervious concrete for $CO_2$ sequestration, along with studying the effect of this incorporation on pervious concrete properties.

### 2.8.4 Effect of unburnt carbon/ activated carbon on concrete

The adverse effect that unburnt carbon within fly ash has on concrete is well documented (Jolicoeur et al. 2009; Gao et al. 1997; Hill et al. 1997; Zhou et al. 2007; Mahoutian et al. 2015). Carbon is critical because of its negative effect on air entrainment agents in concrete. It has been reported that fly ash carbon, similar to AC, has the potential to adsorb surfactants used in air entraining agents (AEAs), thus leading to less available air

entraining agent to stabilise the air voids within concrete, resulting in a gradual loss of entrained air during handling (Jolicoeur et al. 2009).

As the concrete industry is the most significant industry for coal ash, numerous researchers have studied the influence of unburnt carbon in fly ash on concrete properties. In 1997, Gao et al. discussed the effect that this addition may have on concrete (Gao et al. 1997). A primary finding of their study is that carbon blacks interact with the AEA in concrete mixtures, thus leading to less active agents for stabilising the air bubbles. In addition, they found that the degree of the interaction of air entraining agents is highly associated with the amount of accessible hydrophobic carbonaceous surface area in the fly ash sample (Gao et al. 1997).

In the same context, Mahoutian and his co-workers investigated the effect of powdered AC (PAC) on air void properties of concrete that contains fly ash. It was reported that an increase in the PAC content in mixes containing fly ash resulted in a decrease in the fresh air void content. For 10% PAC content, the reduction in the void content was 79% compared to the control mix as shown in Figure 2.30 (Mahoutian et al. 2015).

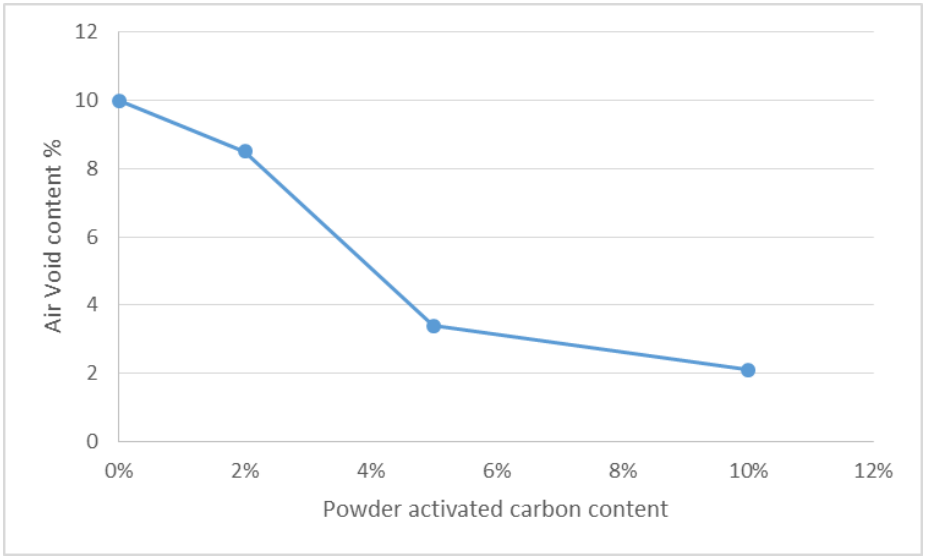


Figure 2-30: The effect of powder AC on air void content (Mahoutian et al. 2015)

Regarding UCS, an increase at all test ages was observed as revealed in Figure 2.31, when the PAC content increased. The researchers explained this finding with regard to the reduced air void content. The more PAC in the concrete, the fewer air voids developed, thus the higher UCS (Mahoutian et al. 2015).

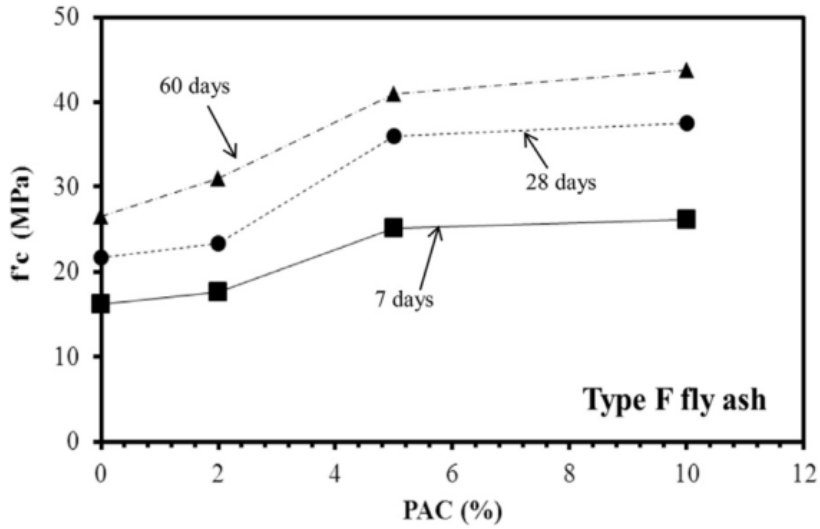

Figure 2-31: The effect of powder AC on UCS (Mahoutian et al. 2015)

These findings confirm the results of an earlier study by Jolicoeur et al. who studied the impact of the interaction between fly ash carbon and the air-entraining surfactants on the stability of air voids distributed in cement paste (Jolicoeur et al. 2009). They found that incorporation of small amounts of AC significantly increased the surfactant requirement to meet a given air content requirement. These results were attributed to the adsorption of the surfactant by the carbon particles (Jolicoeur et al. 2009).

The abovementioned studies show that the presence of AC or unburnt carbon in fly ash leads to an adsorption of the air-entraining agents which are responsible for stabilising the air voids in concrete. This adsorption results in a lower void content, reducing concrete workability and less resistance to freeze/thaw. Thus, it leads to an increase in the quantities of AEA added to the concrete mixes to meet the required concrete performance. Therefore, high carbon ash or AC is avoided whenever air void percentage is a critical characteristic (Hill et al. 1997; Gao et al. 1997). However, for pervious concrete, the void system is mainly from the pores between the aggregate particles coated with cement paste rather than from the voids in the cement paste itself. Therefore, the issue of adsorbing the air entraining agents causes less concern for pervious concrete researchers.

### 2.8.5 Powder AC as a partial replacement of Portland cement

There are almost no standards that address the allowed quantity of AC in cement-based materials. Few regulations discuss LOI (loss on ignition) as an indication of unburnt carbon in supplementary cementitious materials (SCM) such as fly ash or natural pozzolan (Tikalsky et al. 2002).

According to the American Society for Testing and Materials (ASTM), the maximum amounts of unburnt carbon in SCM are 6% and 10% for fly ash class F and natural pozzolan respectively (ASTM C618 2010). Other international standards have slightly different limits (Freeman et al. 1997; Namazirad 2012). The ASTM standards also state that class F fly ash containing up to 12.0 % LOI is allowed if either acceptable performance records or laboratory test results are provided.

Moreover, the maximum amount of fly ash as a replacement of Portland cement in cementitious materials varies according to the standards of different countries, i.e., 35% for Indian standards IS 456-2000 and 25% according to ACI 318-14 (ACI318 2014) as shown in Table 2.9.

Table 2-9: Limits on cementitious materials for concrete assigned to Exposure class F3 (ACI318 2014)

| Cementitious materials | Maximum percent of total cementitious materials by mass |
|---|---|
| Fly ash or other pozzolans conforming to ASTM C618 | 25 |
| Slag cement conforming to ASTM C989 | 50 |
| Silica fume conforming to ASTM C1240 | 10 |
| Total of fly ash or other pozzolans and silica fume | 35 |
| Total fly ash and other pozzolans slag cement and silica fume | 50 |

If fly ash partially replaces Portland cement at the maximum allowed ratio of 25%, then the allowed amount of unburnt carbon as a percent of Portland cement will be = (6% x 25%) = 1.5% of the total cementitious materials. This figure was used in this research as an indication value for selecting the percentage of AC to be incorporated in pervious concrete. Therefore, in the current study, the percentages of powder AC were chosen to be 0.5, 1 and 2% of Portland cement.

The major concerns of adding unburnt carbon (or activated carbon) to cement formulations are (1) discolouration, which is non-preferable in certain applications, and (2) the poor air entrainment performance of carbon-concrete as presented earlier (Freeman et al. 1997). In the concrete industry, fly ash with lower LOI is highly recommended for concrete applications (NTPC 2007). However, as this research study is centred on pervious concrete with no added AEA admixtures, this is not of concern in this research.

### 2.8.6 Granular AC as a partial replacement of fine aggregate

When considering granular AC as a partial replacement for fine aggregate in concrete, it is important to note that aggregates are believed to be harmful if they contain substances that react with Portland cement or negatively affect the hydration of cement or the durability of the produced concrete (Kosmatka et al. 2002). It is well-documented that incorporating excessive quantities of certain compounds such as coal, lignite or AC in aggregates affects the durability of concrete(Kosmatka et al. 2002). The existence of these impurities near the concrete surface can change the concrete surface colour. Moreover, these materials might break during mixing or absorb some of the mixing water leading to an increase in the water required for mixing (Kosmatka et al. 2002).

According to the ASTM, the maximum quantity of carbon content in aggregate is between 0.5% and 1% on a mass basis depending on the importance of the appearance of the concrete. The maximum quantity is established to be 0.5% when the appearance is a significant consideration, and 1% for other types of concrete elements (ASTM Standard C33 2003). These values were used as starting values for choosing the percentages of granular AC in the cement mortars.

# 3 Materials and experimental Procedures

## 3.1 INTRODUCTION

This chapter presents details of the materials and experimental procedures utilised in modifying, characterising and assessing activated carbon (AC) as a carbon dioxide adsorbent material to be incorporated in pervious concrete. In addition, the chapter describes the materials utilised and laboratory work performed in studying the properties of the modified activated carbon-cementitious systems as well as the effect of the incorporation of the $CO_2$ adsorbent material on pervious concrete in terms of $CO_2$ sequestration.

## 3.2 MATERIALS

The principal materials used in the cementitious mixes were Portland cement (Type CEM I), natural aggregates (sharp sand and gravel) and activated carbon in both powder and granular forms. The chemicals used in the modification process were: Sodium hydroxide, Ammonia hydroxide, Hydrochloric acid, and Copper (II) sulfate pentahydrate. The chemical and physical properties of the aforementioned materials, as provided by the suppliers, as well as those measured in the laboratory are presented below.

### 3.2.1 Portland cement

Portland cement CEMI 52.2, conforming to BS EN 197-1, supplied by Cemex, UK, was used throughout the laboratory work presented here. The chemical composition and physical properties of the cement are shown in Table 3.1 and Table 3.2 respectively.

Table 3-1: Chemical composition of Portland cement (as provided by the supplier)

| Oxides | CaO | $SiO_2$ | $Al_2O_3$ | $Fe_2O_3$ | MgO | $K_2O$ | $TiO_2$ | $SO_3$ |
|---|---|---|---|---|---|---|---|---|
| % | 63.6 | 13.9 | 10.2 | 2.7 | 0.6 | 0.9 | 0.1 | 6.9 |

Table 3-2: Physical properties of Portland cement (as provided by the supplier)

| Properties | Value |
|---|---|
| Specific surface area ($m^2/g$) | 0.3-0.4 |
| Mean size (μm) | 10-15 |
| specific gravity | 3.15 |

### 3.2.2 Aggregate

One type of aggregate, supplied by Ridgeons, Cambridge, which was used in the preparation of the pervious concrete mixes, was natural aggregate (shown in Figure 3.1) comprised of sharp sand (0-4mm, $D_{50}$=0.47) and gravel (1.18-10mm, $D_{50}$=4). The particle size distribution (PSD) of the aggregates, as shown in Figure 3.2, was determined according to ASTM C33 (ASTM C33 2010). The figure also shows the range permitted to meet the requirements of No. 8 aggregate (2.36 – 9.5mm) recommended for pervious concrete (ACI 522R 2010) as presented in section 2.7.1. Figure 3.2 shows that the coarse aggregate PSD lies within the No.8 aggregate range. While pervious concrete by definition contains no sand, recommendation by previous studies shows that up to 10% sharp sand can enhance the mechanical properties of pervious concrete without compromising the drainage requirements as discussed earlier in section 2.7.3.2. Therefore, in this study 5% of sharp sand (by mass of total solids) was incorporated in the pervious concrete mixes. The specific gravity and water adsorption of the aggregates are presented in Table 3.3.

Table 3-3: Specific gravity and adsorption properties of aggregate used (Abdollahzadeh 2015)

| Aggregate | Bulk | Effective saturated surface dry | Apparent | Adsorption% |
|---|---|---|---|---|
| Gravel | 2.45 | 2.5 | 2.62 | 1.5 |
| Sharp sand | 2.61 | 2.65 | 2.72 | 3.0 |

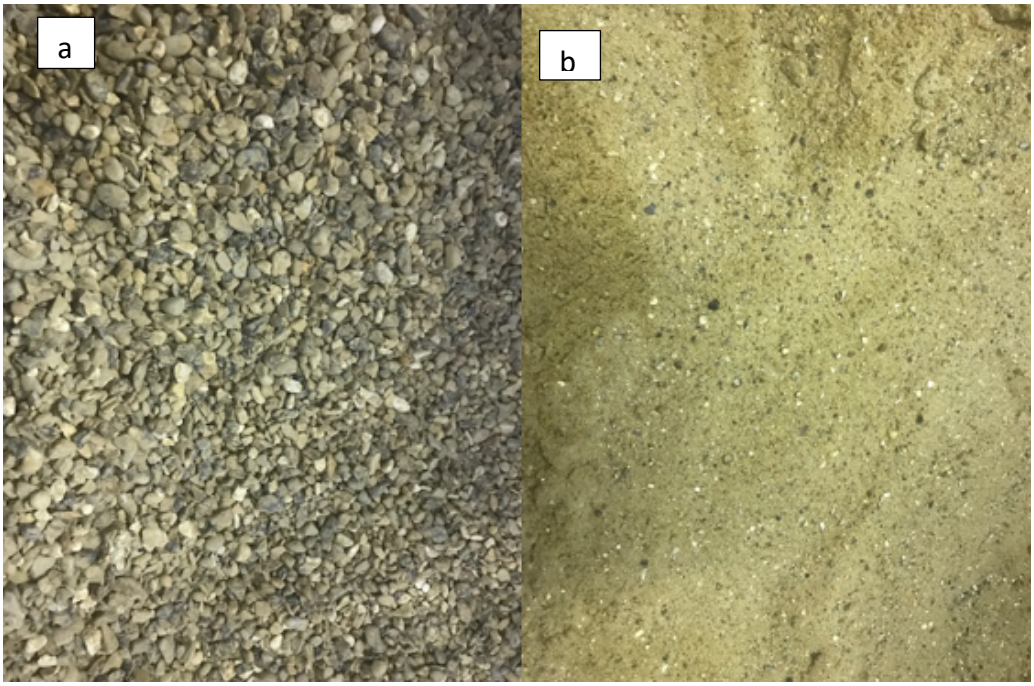


Figure 3-1: The coarse aggregates used in the study: (a) the gravel and (b) the sharp sand.

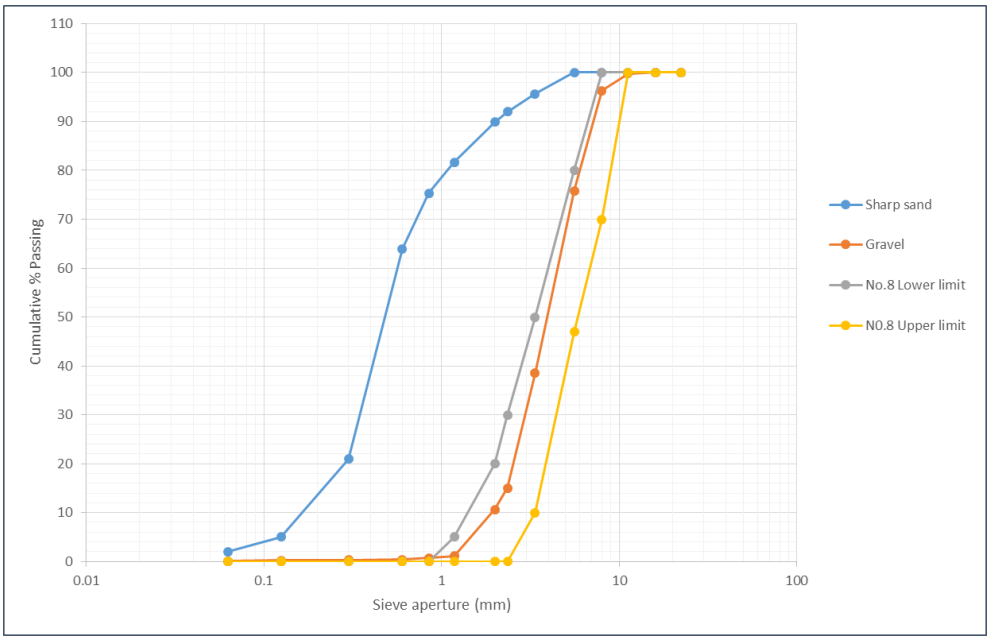


Figure 3-2: The particle size distribution for the gravel and sand used in the study and for the No. 8 aggregate limits.

### 3.2.3 Activated carbon

Two commercial activated carbons (shown in Figure 3.3), namely granular activated charcoal (GAC), (NORIT™ GAC 1240, 12-40 mesh) and powder activated carbon (PAC),

from Fisher Scientific UK, were used as starting materials. Some of the properties and specifications of powder and granular AC as provided by the supplier are listed in Table 3.4. The GAC was used as a partial replacement for fine aggregate, while the PAC was used as a partial replacement for cement.

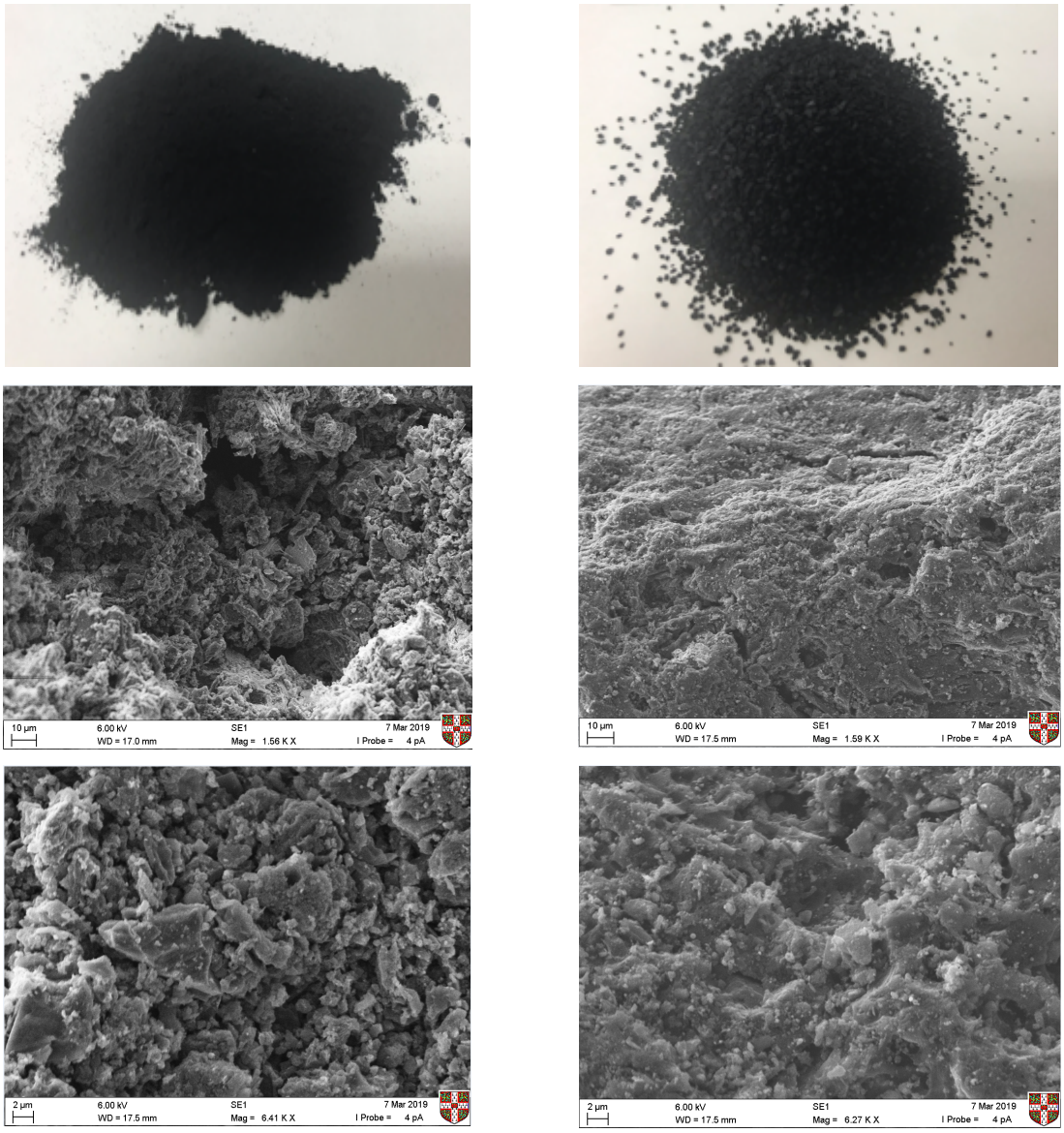


Figure 3-3: Images of the two AC used as seen by the naked eye and SEM images: Powder AC (left) and Granular AC (right)

Table 3-4: The properties and specifications of the powder and granular AC as provided by the suppliers

| Properties and specifications | Powder AC | Granular AC |
|---|---|---|
| Apparent density (g/cm$^3$) | 0.41 | 0.54 |
| Moisture (%) | 2 | - |
| Ash content (%) | 7 | 5 |
| Phenol adsorption (%) | 4.5 | - |
| Methylene blue number (%) | 14 | - |
| Internal surface area (BET) (m$^2$/g) | 800 | 1175 |
| pH | alkaline | 6-9 |
| Particle size | 77% > 10 micron | 95% > 600 micron |
| | 36% > 44 micron | 82% > 850 micron |
| | 18% > 74 micron | 44% > 1.18 mm |
| | 4% > 150 micron | |

### 3.2.4 Chemical modifying agents

Modification of the GAC was carried out using solutions of Sodium hydroxide, Ammonia hydroxide, Hydrochloric acid, and Copper (II) sulfate pentahydrate as impregnating agents. All these chemicals were purchased from Fisher Scientific UK. Some properties of these chemicals are shown in Table 3.5.

Table 3-5: Properties of the chemical modifying agents, as provided by the supplier

| **Chemical** | **Formula** | **Molar mass** | **Density** |
|---|---|---|---|
| Sodium hydroxide | NaOH | 39.997 g/mol | 2.13 g/cm$^3$ |
| Ammonia hydroxide | $NH_4OH$ | 35.04 g/mol | 0.88 g / cm$^3$ |
| Hydrochloric acid | HCl | 36.46 g/mol | 1.19 g/cm$^3$ |
| Copper (II) sulfate pentahydrate | $CuSO_4 \cdot 5H_2O$ | 249.68 g/mol | 2.286 g/cm$^3$ |

## 3.3 ACTIVATED CARBON WORK

### 3.3.1 Preparation of the modified activated carbon

#### 3.3.1.1 Stage I modification

The first stage of modification was conducted on granular AC only, while the final modification technique was applied to both granular and powder AC. The modification was carried out using different concentration solutions of the impregnation agents. For this purpose, a certain mass of AC was soaked in 100 mL of different strength aqueous solutions as shown in Table 3.6 and shaken using IKaLabortechnik shaker KS501 for a pre-determined time at room temperature and 200 rpm. The samples were then filtered and washed with deionised water until a constant solution pH is reached. The ACs were then dried in an oven at 105$^{o}$ C for 24 h. Figure 3.4 shows an example of modifying AC by solutions of copper pentahydrates. It should be mentioned that the concentrations and the soaking durations of these chemicals were selected according to the findings of relevant literature discussed in section 2.6.5.

Table 3-6: The chemical solutions used for AC modification

| **No.** | **Chemical Solution** | **Concentration** $_{wt\%}$ | **Notation** $_{concentration}$ | **Duration** |
|---|---|---|---|---|
| 1 | Sodium hydroxide | 5%, 10% and 20% | 5%, 10% and 20% | 4 hrs |
| 2 | Ammonia hydroxide | pure $NH_4OH$, 1:1 and 1:2 | 35%, 18%, 12% | 24 hrs |
| 3 | Hydrochloric acid | pure HCl, 1:1 and 1:2 | 37%, 19% and 13% | 2 hrs |
| 4 | Copper (II) sulfate pentahydrate | 5%, 10% and 20% | 5%, 10% and 20% | 72 hr |

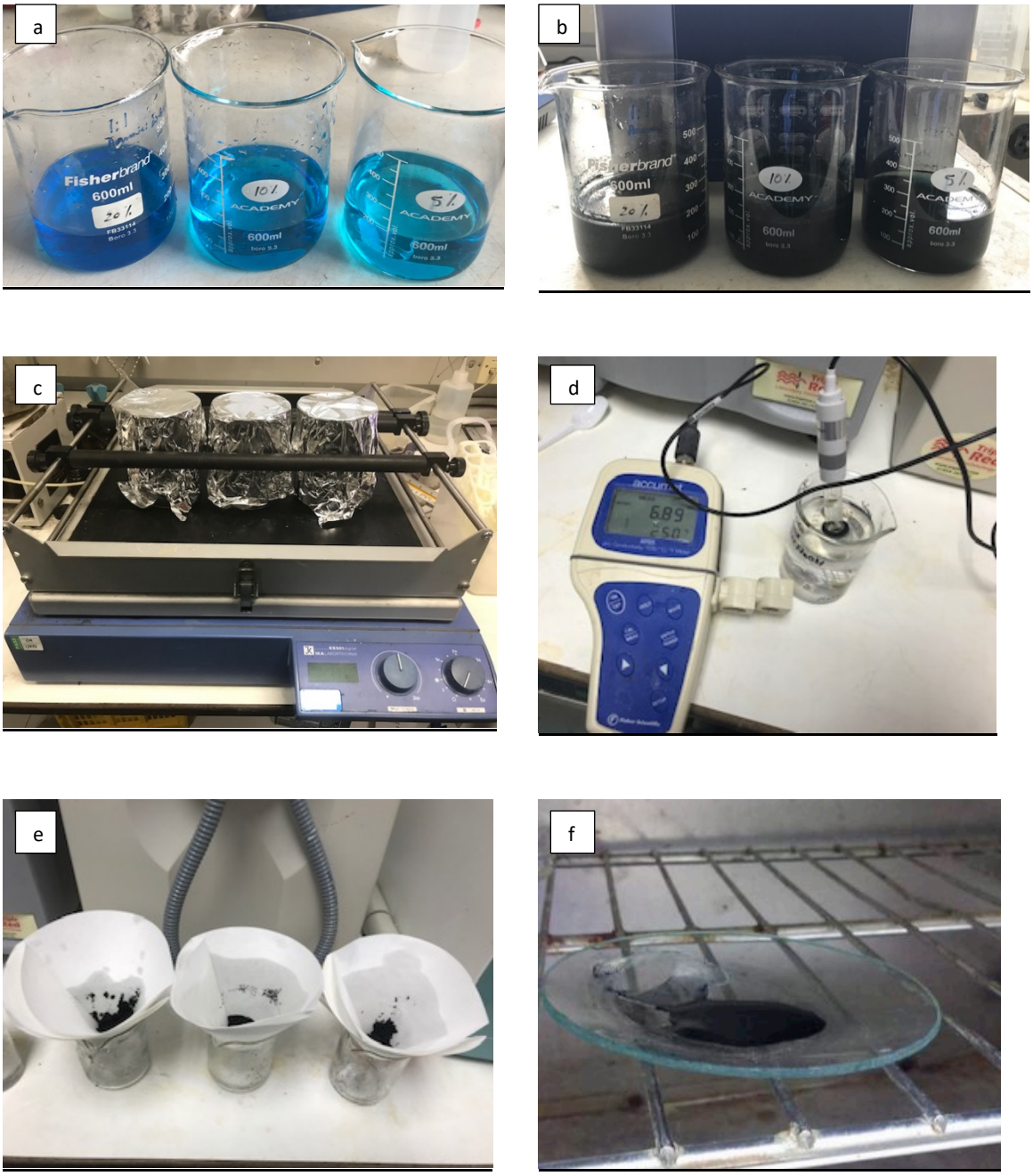


Figure 3-4: Images of the various stages of stage I modification: (a) preparing the concentrations of the impregnation agent, (b) soaking AC in the solutions, (c) shaking samples, (d) checking pH of the filtrate, (e) filtering samples and (f) drying in the oven.

#### 3.3.1.2 Stage II modification

The aim of the second round of modification was to conduct further investigations to check the possibility of maximising the $CO_2$ adsorption capacities. In this context, Copper (II) sulfate pentahydrate proved to have a slight impact on the adsorption when modified at room temperature compared to the other modifiers as will be presented in section 4.3. Therefore, it was excluded from the study, while NaOH, HCL and $NH_4OH$ underwent further investigation in the modification process according to the following pattern:

- Modification with HCL followed by modification with NaOH
- Modification with HCL followed by modification with $NH_4OH$

It should be highlighted that this two-step modification approach considered the acidic nature of carbon dioxide. Therefore, it started with a mineral acid treatment to wash the surface of the AC from any attached impurities, followed by a basic material treatment to enhance the affinity of carbon dioxide sequestration.

### 3.3.2 Quantification of the $CO_2$ adsorption of modified activated carbon

The adsorption capacity of both raw and modified activated carbon (M-AC) was evaluated using three different assessment techniques: $CO_2$ incubator, fixed bed column and TGA. The three employed techniques are believed to provide an approximate indication of the $CO_2$ adsorption capacity of the examined samples.

#### 3.3.2.1 $CO_2$ incubator environment

The first measuring technique utilised a $CO_2$ incubator (shown in Figure 3.5) as a closed space with a fixed $CO_2$ concentration inside. In the first modification stage, all AC samples were kept in the incubator in a 20% $CO_2$ concentration for a certain duration of time with regular monitoring of changes in sample weight. Samples with the highest adsorption capacities were subjected to the two-step modification process as described earlier, and then kept in three different $CO_2$ concentrations in the incubator 5%, 10% and 20% for further investigation. Changes in the samples' weight were recorded every day until the sample weight was stable.


Figure 3-5: The $CO_2$ incubator used as the first technique of measuring the $CO_2$ adsorption capacity of the AC.

#### 3.3.2.2 Fixed-bed column setup

In this setup, $CO_2$ adsorption was carried out in a fixed-bed column. The experimental setup used to measure the $CO_2$ adsorption is shown in Figure 3.6. The glass fixed-bed column was designed to be 30 cm high and its internal diameter was 1 cm. It was also equipped with a porous plate that was located at the base of the column. The inlet of the column was connected to flowmeter which is connected to a (5% $CO_2$ in air) cylinder. At the column outlet, the system was attached to a $CO_2$ sensor (SPRINTIR) purchased from (Gas Sensing Solutions Company). Some of the features of SprintiR-WF-5 sensor are listed in Table 3.7 The sensor takes 20 readings per second and measures up to 5% $CO_2$ concentration. The $CO_2$ concentration of effluent gas was continuously recorded as a function of time to generate the breakthrough curves.

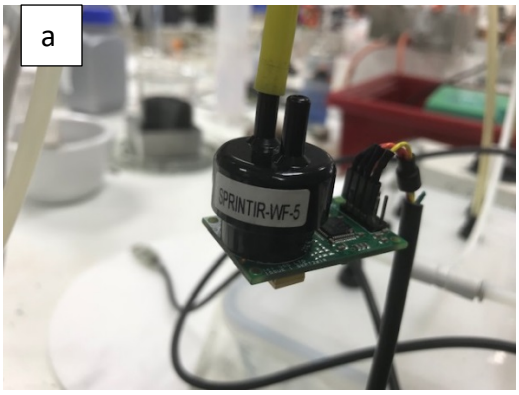



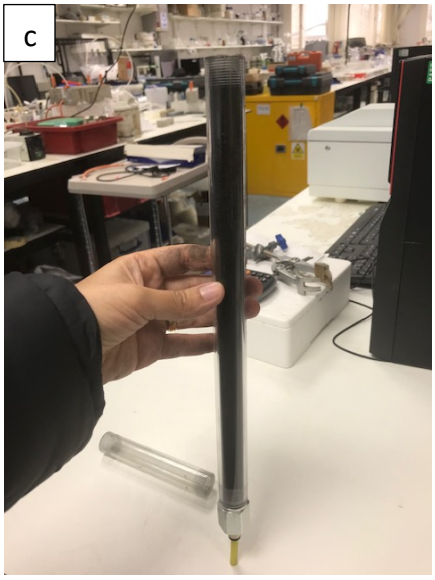


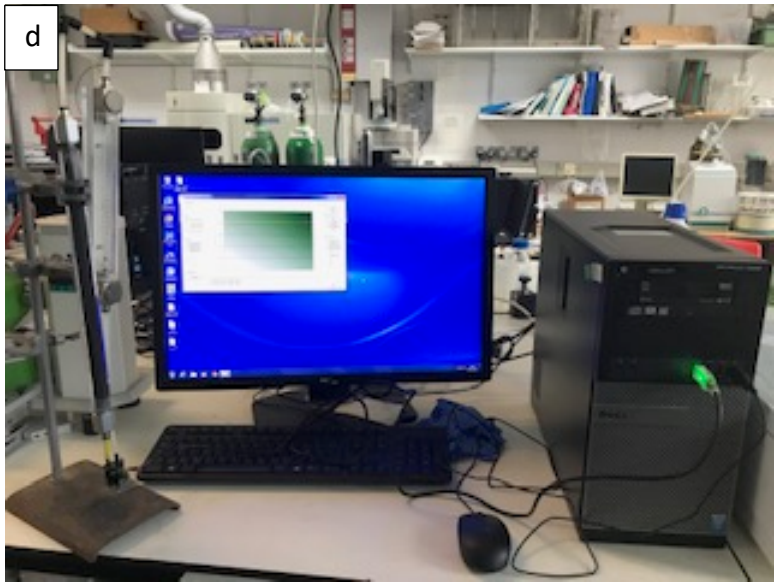


Figure 3-6: The fixed bed column setup: (a) the $CO_2$ sensor, (b) the flowmeter, (c) the 30cm columns and (d) the complete setup.

Table 3-7: The features of the SPRINTIR sensor as provided by the supplier

| Feature | Value |
|---|---|
| High speed sensing | 20 Hz |
| Low power consumption | 35 mW |
| Digital (UART) output | Yes |
| Measurement range | 0-5% concentration |
| RoHS compliant | Yes |

The $CO_2$ adsorption capacities were calculated based on the generated charts by the $CO_2$ sensor, following equation 3.1:

$$A = \int_{t_0}^{t_{end}} (\dot{C} - \dot{C}_0) dt = \frac{\dot{V}p}{RT} \int_{t_0}^{t_{end}} (x - x_0) dt \qquad \text{Equation 3.1}$$

where $A$ is the adsorption capacity (mol), $\dot{C}$ is the molar flowrate (mol/s), $\dot{V}$ is the volumetric flowrate ($m^3/s$), p is pressure (Pa), R is the gas constant (J/(mol-K)), T is the temperature (K) and x is the molar fraction.

### 3.3.2.3 Thermogravimetric analysis

Thermogravimetric analysis (TGA) is used extensively in research studies as a technique to measure with precision the change in weight corresponding to changes in temperature or/and feeding gases. TGA was conducted using PerkinElmer STA6000 instrument (shown in Figure 3.7). In this study, the increase in AC weight corresponding to exposure to $CO_2$ gas was investigated using TGA. About 10 mg of the AC was placed in a small ceramic crucible, heated up to 100°C under pure Argon flow (50$cm^3$ /min) and held isothermally for 30 min until the weight of the sample became stable. The temperature was then decreased to 25°C and the gas was switched to pure $CO_2$ at the same flow rate. The sample was held at 25°C for 1h to achieve complete saturation. The increase in weight at this stage was considered as the $CO_2$ adsorbed amount by the sample at 25°C. Figure 3.8 shows a schematic diagram of the TGA temperature with time. The weight increase during this stage was considered as the $CO_2$ capture capacity of the sample.

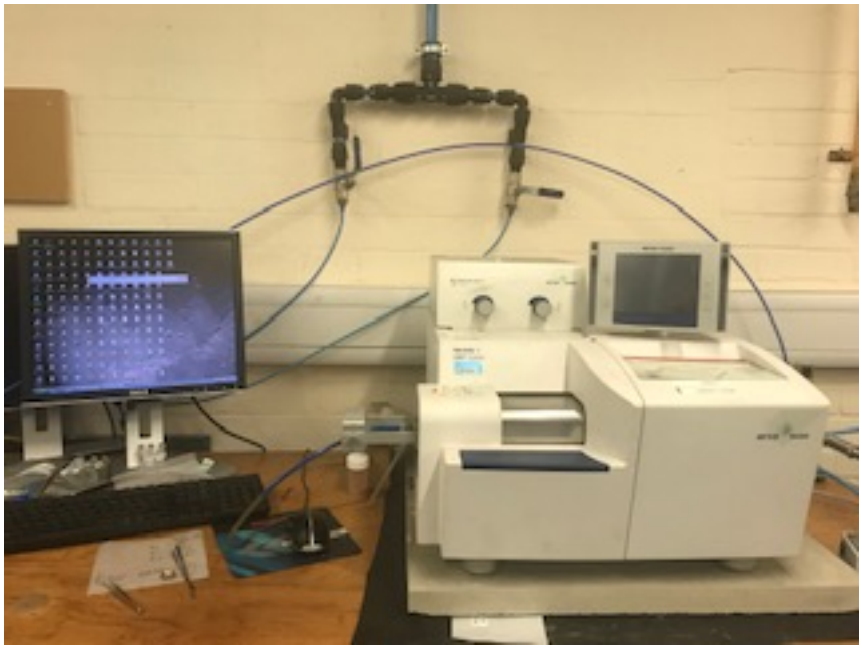

Figure 3-7: The Mettler- Toledo thermogravimetric analysis TGA used.

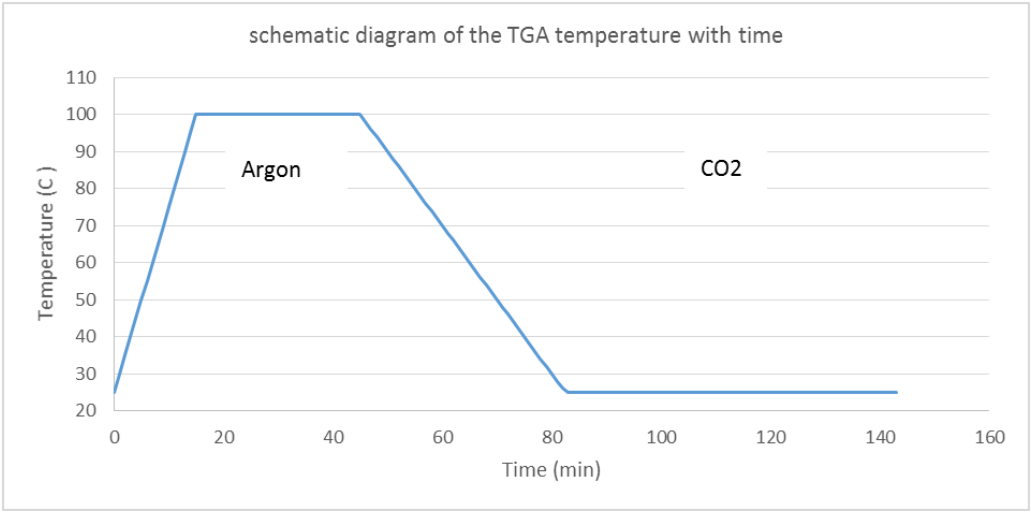


Figure 3-8: The change of temperature with time for TGA assessment technique employed in the study.

### 3.3.3 Characterisation of the modified activated carbon

#### 3.3.3.1 Texture parameters

Based on the results of the $CO_2$ adsorption capacity, selected modified AC samples were subjected to different characterisation techniques. The BET surface area, micropore

volume and average pore width of the raw and M-AC were determined by nitrogen ($N_2$) adsorption-desorption at -196$^{o}$C using an automated gas sorption system (Micromeritics ASAP 2020, USA) shown in Figure 3.9. The BET surface area is measured based on the volume of $N_2$ adsorbed to the surface of the sample at the boiling point of $N_2$ (-196°C). $N_2$ condenses at this temperature onto the surface in a monolayer. Knowing the size of $N_2$ molecules, the amount of condensed gas would be correlated to the surface area of the sample (Zhang & Luo 2018; Lowell et al. 2012).


Figure 3-9: The Micromeritics ASAP 2020 instrument used for the BET surface area measurements.

#### 3.3.3.2 Fourier-transformed infrared spectroscopy

Fourier-transformed infrared spectroscopy (FTIR) analysis investigates the presence of surface functional groups in a material based on their transmittance of infrared light at various wavelengths. FTIR analysis was performed on dry samples of raw and modified AC using Perkin Elmer FTIR Spectrometer Spectrum 100 Optica (shown in Figure 3.10) in the range of 4000cm$^{-1}$ to 450 cm$^{-1}$ at a resolution of 1 cm$^{-1}$.

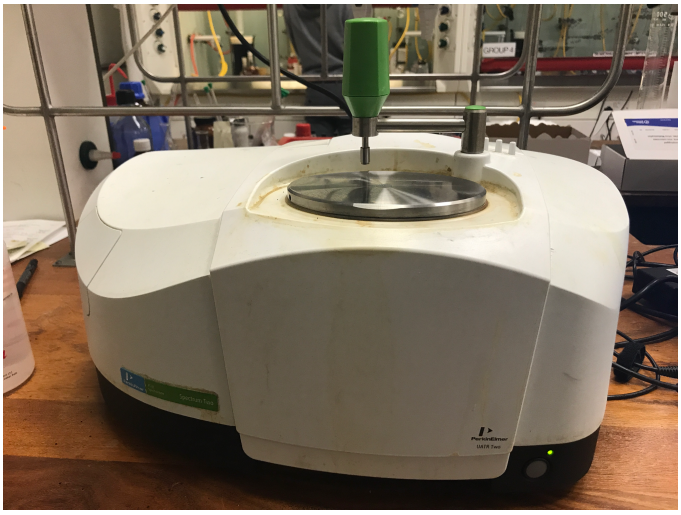

Figure 3-10: The Perkin Elmer FTIR Spectrometer used in the study.

#### 3.3.3.3 Scanning electron microscopy

Raw and selected modified AC were further investigated using Scanning Electron Microscopy (SEM) in order to determine their physical structures. A sticky double-sided conductive carbon tape was used to mount the AC samples on stubs in the SEM machine. SEM uses high powered microscopes to give an image of surface characteristics. The AC samples were examined by EVO LS 15 desktop Scanning Electron Microscope (Figure 3.11) from ZEISS Ltd.

Figure 3-11: The EVO LS 15 desktop Scanning Electron Microscope (SEM) used in the study.

## 3.4 CEMENT-BASED SYSTEMS

This section presents details of all the cement-based mixes produced, namely cement paste, cement mortars and pervious concrete. In the following sub-sections, mix composition, samples preparation and experimental procedures conducted on the three cement-based systems are presented.

### 3.4.1 Mix composition

#### 3.4.1.1 Cement pastes

In order to investigate the performance of M-PAC as a replacement of cement, 4 cement pastes (CP) were prepared. The M-PAC was incorporated as a partial cement replacement of 0.5%, 1% and 2% by weight. These percentages were selected based on the discussion presented in section 2.8.5 and 2.8.6. The notation and the percentages of the M-PAC are presented in Table 3.8.

Table 3-8: The CPs notations used in the study

| Sample | Co-CP | 0.5% M-PAC-CP | 1%M-PAC-CP | 2% M-PAC-CP |
|---|---|---|---|---|
| Powder AC % | 0 | 0.5 | 1 | 2 |

#### 3.4.1.2 Cement mortars

In order to investigate the impact of partially replacing sand with modified granular AC (M-GAC), mortar mixes were examined. Four cement mortars were prepared with a water-to-cement ratio (w/c) of 0.5 and a sand to cement ratio of 2.75:1. The M-GAC was incorporated as a partial sand replacement of 0.5%, 1% and 2% by weight. Table 3.9 illustrates the notation and percentages of M-GAC in cement mortars.

Table 3-9: The notations of the cement mortar mixes used in the study.

| Sample | Co-CM | 0.5% M-GAC-CM | 1% M-GAC-CM | 2% M-GAC-CM |
|---|---|---|---|---|
| Granular AC % | 0 | 0.5 | 1 | 2 |

#### 3.4.1.3 Pervious concrete

Various concrete mixes were prepared throughout this study. The **first group** of concrete mixes were trials to optimise the w/c ratio. Three different w/c ratios were investigated: 0.3, 0.32 and 0.35. The selection of these ratios was based on recommendations of previous studies and standards (ACI 522R 2010; Tennis et al. 2004). Mixture proportioning was determined using the phase-volume design procedure, details of which explained in section 2.7.2, as the most practical design method for pervious concrete (ACI 522R 2010; ACI 211 2002; Tennis et al. 2004; Abdollahzadeh 2015). For each trial patch, the designed porosity was fixed to 20% as a recommended value of pervious concrete porosity, and sharp sand was added with a percentage of 5% by mass. The preparation of the trial patches was conducted following the procedures presented in section 3.4.2.3. The consistency of the prepared three mixes was examined using the ball rolling method (Figure 3.12) described by Tennis (Tennis et al. 2004). The method considers the proper content of water is the content that gives the mixture a sheen without flowing off of the aggregate. Therefore, a handful of pervious concrete can be formed into a ball without crumbling or losing its void structure because of paste being flowing into the spaces between the aggregate (Tennis et al. 2004). The optimum w/c ratio was found to be 0.35. The same procedure was followed later with modified AC - pervious concrete.

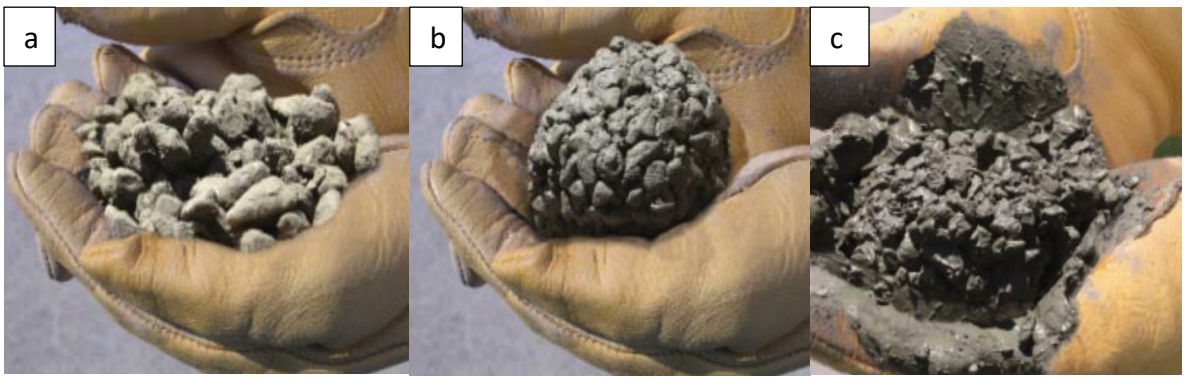


Figure 3-12: Typical pervious concrete mixes (Tennis et al. 2004) with (a) low water content, (b) acceptable water content and consistency and (c) high water content.

The aim of the **second group** of concrete mixes was to investigate the effect of incorporating different percentages of modified AC (M-GAC and M-PAC) on the concrete mixes properties as shown in Chapter 5. Trial percentages of M-AC were selected to be

0.5%, 1% and 2% to replace cement or sand by mass. Table 3.10 shows the mix composition of 6 the M-AC- pervious concrete mixes.

Table 3-10: The composition of the different AC-pervious concrete mixes used (% by mass of total solids).

| **Sample** | **Activated carbon (%)** | **Gravel (%)** | **Sand (%)** | **Cement (%)** |
|---|---|---|---|---|
| **Co-con** | **0** | **78** | **5** | **17** |
| | | | | |
| **2% M-PAC-con** | 0.34 | 78 | 5 | 16.66 |
| **1% M-PAC-con** | 0.17 | 78 | 5 | 16.83 |
| **0.5% M-PAC-con** | 0.085 | 78 | 5 | 16.915 |
| | | | | |
| **2% M-GAC-con** | 0.1 | 78 | 4.9 | 17 |
| **1% M-GAC-con** | 0.05 | 78 | 4.95 | 17 |
| **0.5% M-GAC-con** | 0.025 | 78 | 4.975 | 17 |

The **third group** of concrete mixes consisted of the 2 main mixes involved in the experiments. They were the control and the combined M-AC mix. The notations that were used for the four mixes in addition to the mix compositions by mass are included in Table 3.11.

Table 3-11: The mix composition of the four main AC-pervious concrete mixes (% by mass of total solids)

| **Mix** | **M-GAC (%)** | **M-PAC (%)** | **Gravel (%)** | **Sand (%)** | **Cement (%)** |
|---|---|---|---|---|---|
| Control concrete | 0 | 0 | 78 | 5 | 17 |
| M-AC-concrete | 0.1 | 0.34 | 78 | 4.9 | 16.66 |

### 3.4.2 Samples Preparation and curing

#### 3.4.2.1 Cement pastes

A laboratory bench-scale mixer (Kenwood 1500 W food blender), shown in Figure 3.13a was used for the preparation of cement pastes mixes. Portland cement and M-PAC were mixed by hand in the mixer stainless steel bowl, followed by one minute of dry mixing in the mixer. Water was then added, and the mixing continued for another 2 minutes, after which the mixer was stopped to scrape the unmixed materials from the sides of the

mixing bowl and the paddle. Another 2 minutes of mixing completely homogenised the cement pastes. The fresh paste was then placed into oil-wet (40mm x 40mm x 40mm) steel cube moulds as shown in figure 3.13b and compacted for 5 seconds using the vibration table. The specimens were then covered with plastic film for 24 hours before being demoulded and cured in a water tank (T= 20°C ±2°C) until the designed testing age. CPs prepared for the standard consistency test were examined directly after mixing.

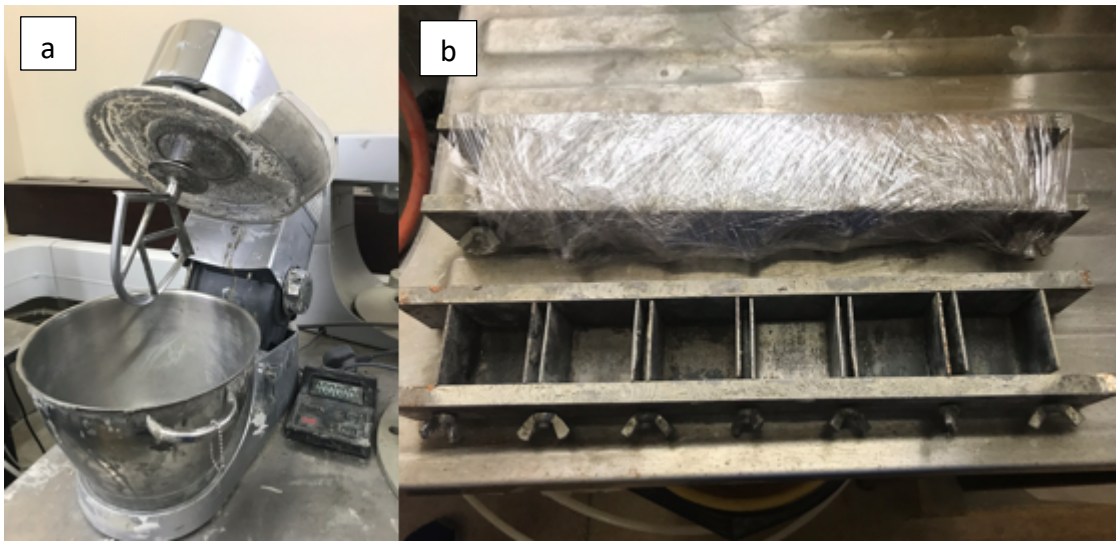


Figure 3-13: Mixer and moulds used for the cement pastes and mortar samples (a) the Kenwood bench scale mixer and (b) the steel cube moulds.

#### 3.4.2.2 Cement mortars

The preparation of cement mortars was identical to that of the cement pastes described previously, except for the sand that was added. The sand was dry-mixed with the cement and M-GAC for 2 minutes before the addition of water. For each mix, nine cube specimens (40mm x 40mm x 40mm) were prepared for UCS analysis at three ages (7, 14 and 28 days). All specimens were demoulded (as shown in Figure 3.14) after 1 day then cured in a water tank (T= 20°C ± 2°C) until the designed testing age. Another set of cement mortars mixes, prepared for investigating the flowability, were examined directly after mixing using the flow table.

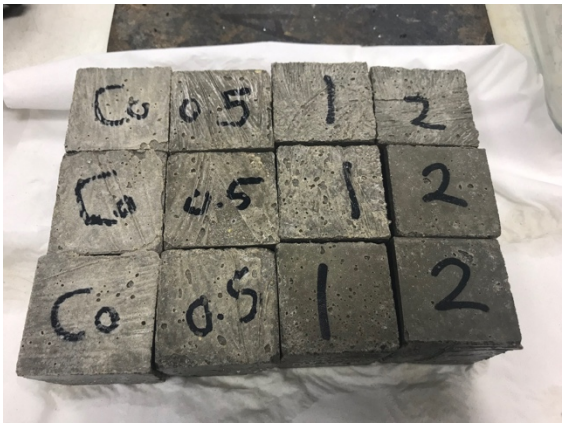


Figure 3-14: Typical cement mortars after demoulding

#### 3.4.2.3 Pervious concrete

Two different mixers were utilised in the preparation of the concrete samples according to the volume of the batch as seen in Figure 3.15 (a and b). Small volume trial mixes were prepared in the smaller 20L mixer (left), while the other 100L mixer (right) was used for preparation of larger concrete mixes. The aggregates and cement (and modified AC if applicable) were first dry mixed for ~3 minutes before water was added. Once all components were in the mixing bowl, the mixing process continued for another 3 minutes or until a homogeneous blend was obtained. During this time, the mixer was occasionally stopped to scrape unmixed materials from the sides of the mixing bowl into the mixing bowl. The produced concrete was then placed in 100 mm steel cubic moulds (Figure 3.15c) and ϕ100 mm and 200 mm height steel cylindrical moulds (Figure 3.15d) in two layers using a standard hammer. In addition, the concrete was compacted on a vibrating table for 10 seconds for better compaction, followed by levelling the top surface by a strike-off plate. The samples were covered by a plastic sheet for 24 hrs before demoulding. The samples were then cured in water until the day of the test.

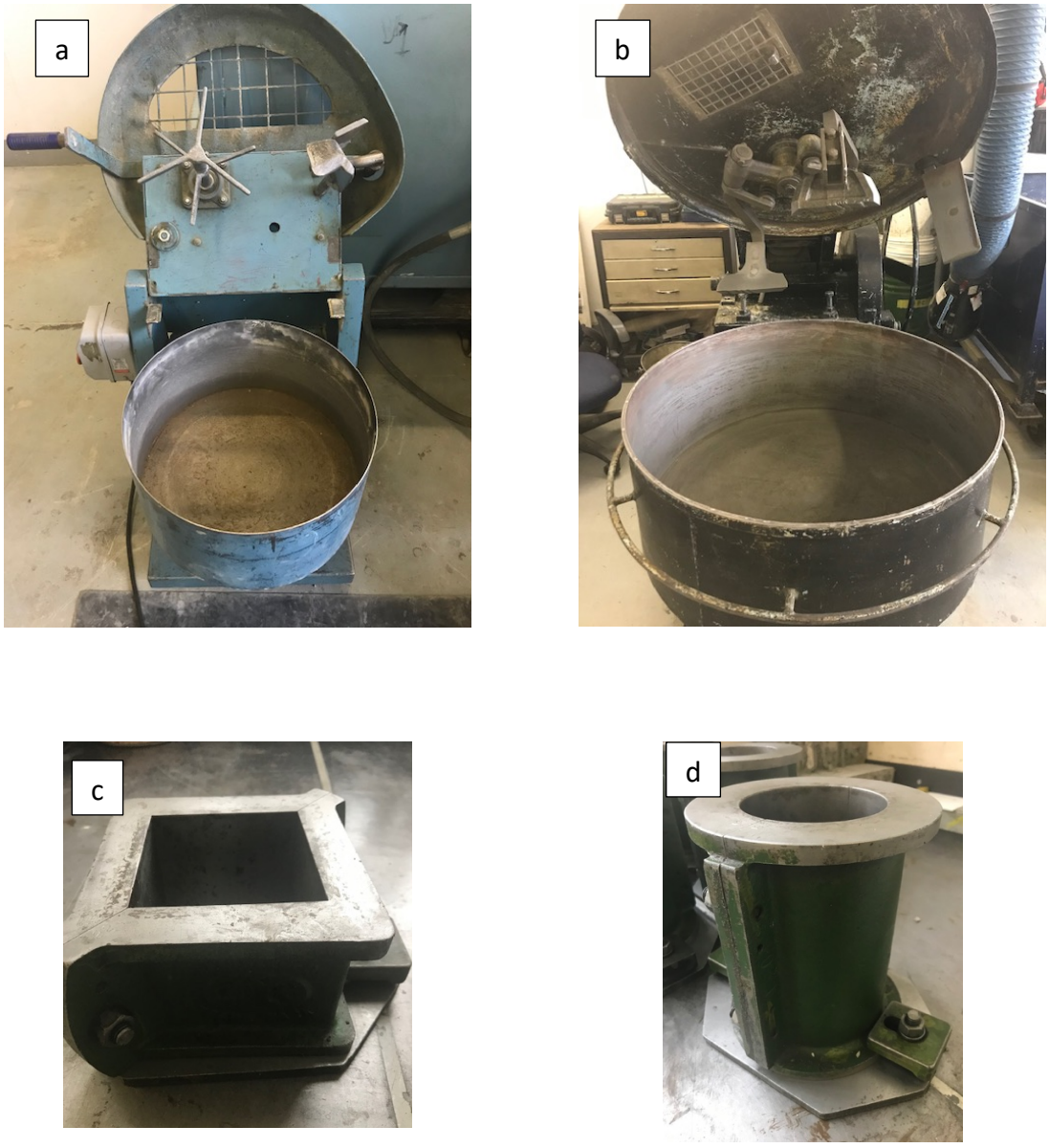


Figure 3-15: The mixers and moulds for the pervious concrete samples (a) the 20L concrete mixer, (b) the 100L concrete mixer, (c) the steel cubic mould and (d) cylindrical mould

### 3.4.3 Experimental procedure

In the following sections, the experiments that were conducted on cement pastes, cement mortars and pervious concrete samples are described. The experiments that were conducted on cement pastes were: standard consistence, Isothermal calorimetry, TGA and XRD. Cement mortars were subjected to workability (flow table) and UCS, while pervious concrete group underwent UCS, hardened density and porosity tests.

#### 3.4.3.1 Tests on cement paste

##### 3.4.3.1.1 Standard consistence

The water required for cement pastes to show a standard consistence was obtained according to BS EN 196-3 (BS-EN-196-3 2016) using a manual Vicat apparatus, shown in Figure 3.16. Vicat plunger penetration between 4 and 8 mm was acceptable according to the standards. Four series of cement pastes were prepared for this purpose with different C/W ratios. Details of w/c ratios and the corresponding penetration are illustrated in Table 5.3 in Chapter 5.

Figure 3-16: The standard consistency test used

##### 3.4.3.1.2 Isothermal calorimetry test

Isothermal calorimetry is a technique to measure the heat evolution associated with endothermic or exothermic reactions. It is used in cement-based systems to track the progression of the hydration reaction, as well as to examine the influence of mixture proportioning on early age heat evolution. In this work, it is used to examine the effect of different percentages of M-PAC on the heat of hydration of cement pastes. The instrument

used for these experiments is a Calmetrix I-Cal 2000 high precision isothermal calorimeter compliant with ASTM C1679 (ASTM-C1679 2017) (Figure 3.17). The instrument measures the heat flow required to maintain isothermal conditions, recorded in watts. These data are then normalized by the mass of the cement used to measure the changes in heat evolution in the cement. A typical rate of heat evolution of cement hydration is shown in Figure 3.18. As the heat flow rate changes, different stages of the hydration process can be identified: (I) rapid initial period, (II) induction period, (III) acceleration period, (IV) deceleration period, and (V) longer term reactions (Kirby & Biernacki 2012).

The thermostat of the calorimeter was set to 23°C. Pre-conditioning of the cement, M-PAC and water took place for 24h before hand-mixing for one minute using a plastic spoon, and then directly placing the mixture in the Calorimeter. The heat flow was then recorded for the first 48h. This time was sufficient to obtain the initial setting peak.

The peak power is calculated as the maximum power (first peak) minus the power during the induction period. The initial setting time was then calculated as the time at one-third of the peak power.

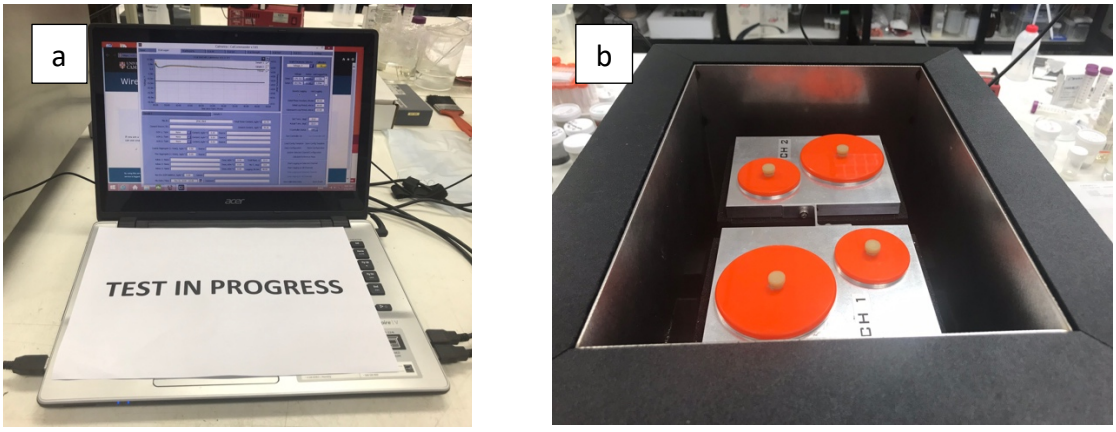


Figure 3-17: The isothermal calorimetry test set up (a) the computer software and (b) the equipment.

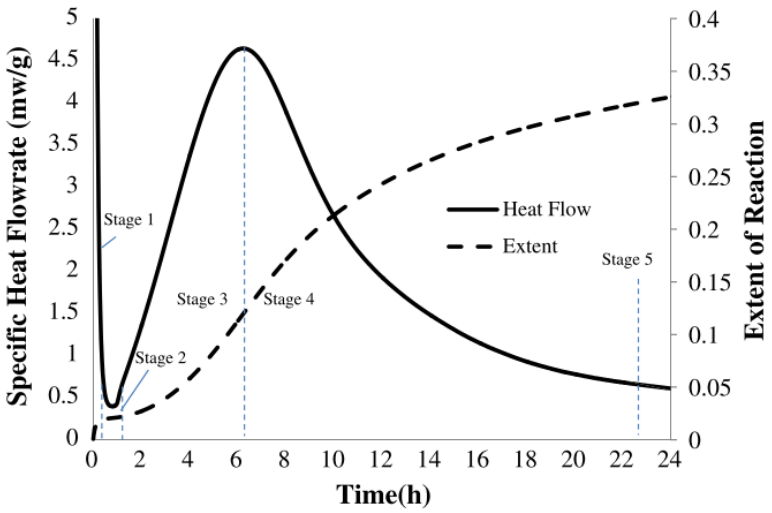


Figure 3-18: Typical rate of heat evolution curve for cement hydration (Kirby & Biernacki 2012)

#### 3.4.3.1.3 Microstructural analysis

For cement paste samples, the cubes were cut in the middle, then powder materials were extracted using a polishing machine with P80 silicon carbide abrasive paper as shown in Figure 3.19. The remained powder on the pad was collected, passed through a 75µm sieve before being tested using X-ray diffraction (XRD) and thermogravimetric analysis (TGA).

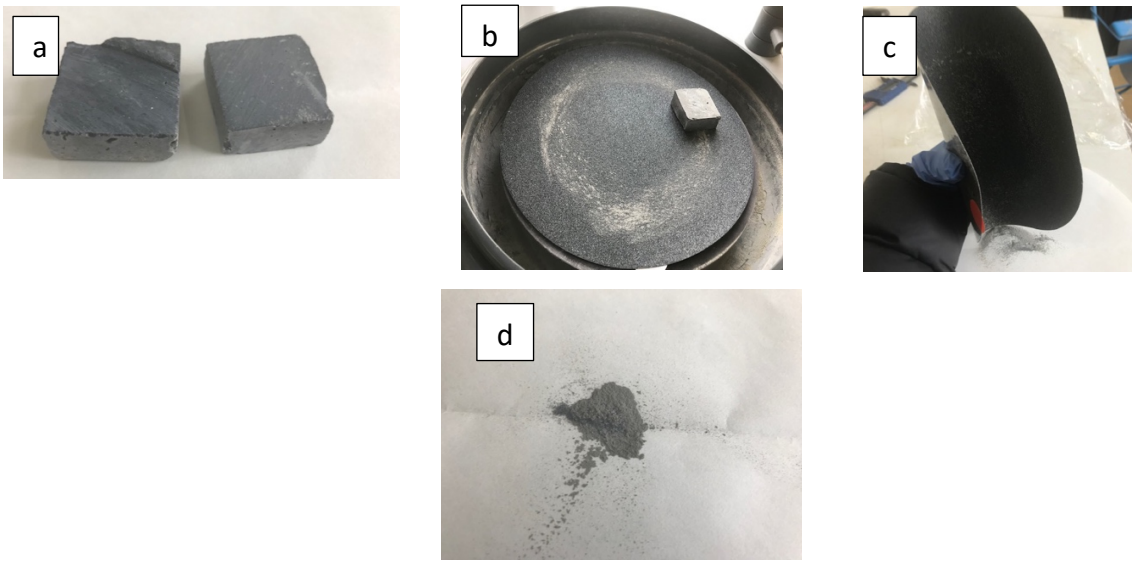


Figure 3-19: (a – d) Stages for extracting powder material for XRD and TGA analysis

### 3.4.3.2 Tests on cement mortar

#### 3.4.3.2.1 Workability

To determine the influence of adding M-GAC on the flowability and consistence characteristics of the fresh mortars, a flow table test was carried on the following BS EN 1015-3 (BS-EN-1015-3 2004). The flow table apparatus, shown in Figure 3.20a was supplied by the CONTROLS group. The mould was set centrally on the disc of the flow table before cement mortar was introduced into the mould in two layers. For a uniform filling of the mould, each layer was compacted by 10 short strokes of the tamper. Excess mortar was then removed with a palette knife and the disc was carefully cleaned of any paste or water. After 15 seconds of filling the mould, it was lifted vertically, and the disc was shaken 15 times at a constant frequency of one per second to spread out the mortar as shown in Figure 3.20b. The diameter of the paste was then measured in mm in two directions at right angles to obtain the average of the two values.

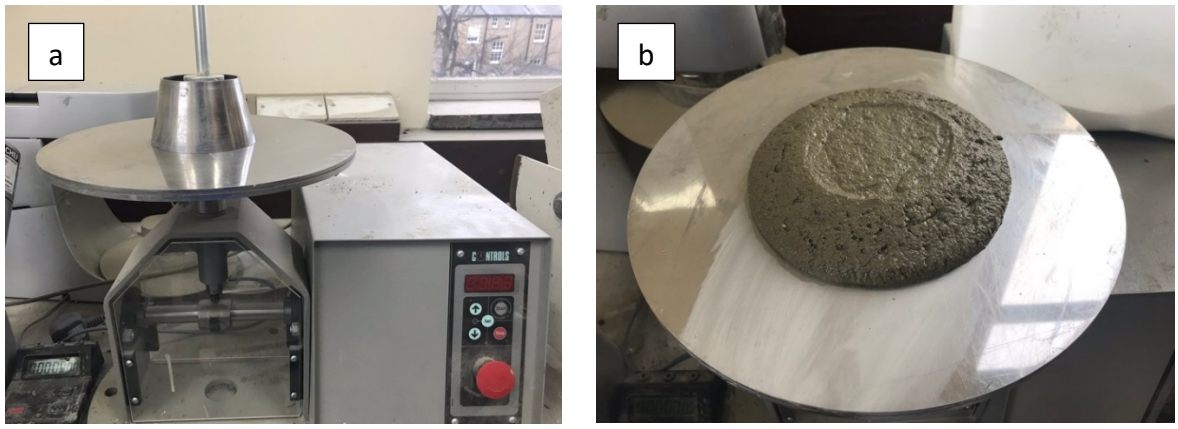


Figure 3-20: The flow table test (a) the complete set up and (b) a sample of mortar after shaking the disc 15 times

#### 3.4.3.2.2 Unconfined compressive strength

The UCS of mortar specimens was performed in accordance to BS EN 196-1. The tests were conducted in triplicate at ages of 7, 14 and 28 days and the strength reported was an average of the three specimens. The tests were conducted by a CONTROLS Advantest 9 machine (shown in Figure 3.21a) with a maximum capacity of 250 kN and at a loading rate of 2400N/s. Prior to the test, the dimensions of the cement mortars cubes were measured by digital slide callipers, and the UCS $f_c$ was calculated using equation 3.2:

$$f_c = \frac{P_{max}}{A} \qquad \text{Equation 3.2}$$

Where $P_{max}$ is the ultimate compressive failure load (kN), and A is the cross-section area of the sample tested.

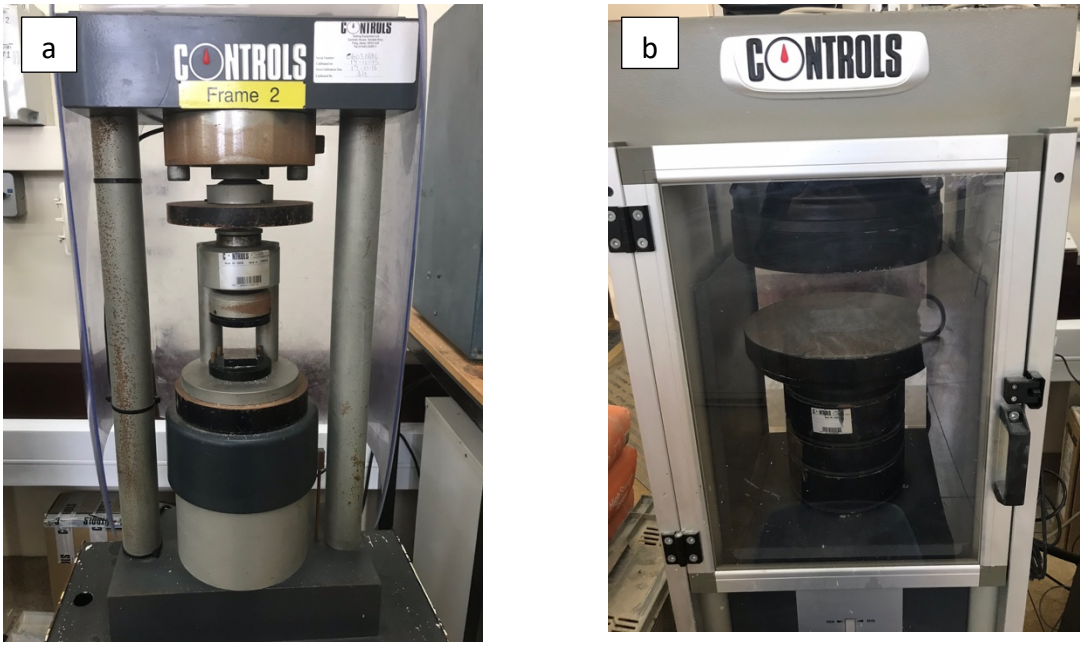


Figure 3-21: CONTROLS Advantest 9 (a) machine 2 for mortar cubes (b) machine 1 for concrete cylinders

#### 3.4.3.3 Tests on pervious concrete

##### 3.4.3.3.1 Hardened mix density and Porosity

The hardened density (equation 3.3) and the porosity (equation 3.4) of the pervious concrete samples were measured conforming to ASTM C1754 (ASTM-C1754 2015) as:

$$Density = \frac{A}{D^2 x\, L} \qquad \text{Equation 3.3}$$

$$Porosity = \left[1 - \left(\frac{A-B}{\rho_w . D^2 . L}\right)\right] x\ 100\% \qquad \text{Equation 3.4}$$

Where A is the weight of oven dried sample (g), B is the immersed weight of the sample (g), D and L are the average diameter and length of sample (cm) respectively and ρ is the density of water at the temperature of the water bath (g/cm$^3$).

#### 3.4.3.4 Unconfined compressive strength

The UCS tests were carried out according to BS EN 12390-3 (BS-EN-12690-3 2009) using a Controls Advantest 9 machine (Figure 3.21b) with a maximum capacity of 250 kN and at a loading rate of 2400N/s. The tests were conducted in triplicate.

### 3.4.3.5 Workability (Slump test)

The workability of the fresh concrete was determined according to the BS EN 12350-2 slump-flow test (BS-EN-12350-2 2009). The slump cone was filled in three equal heights following a compaction by 25 strokes of the tamping rod. The cone was then raised (as shown in Figure 3.22), and the slump was measured as the difference between the height of the mould and height of the highest point of the slumped test sample.

Figure 3-22: The slump test (left) M-AC-pervious concrete (right): control pervious concrete

### 3.4.3.6 Carbonation front by Phenolphthalein

After 28 days of water curing, the concrete samples were removed from water and stored in an ambient environment for a few days to stabilize the internal relative humidity of concrete. This step decreased the differences in the internal relative humidity among the

concrete samples before their exposure to accelerated carbonation conditions, thus minimizing the impact on the carbonation depth results (Sulapha et al. 2003). The samples were then placed in a $CO_2$ incubator until the day of the test. The $CO_2$ supply and the relative humidity inside the incubator were kept to 20% and 65% respectively.
On the day of the test, the samples were split, and the broken surfaces were sprayed with a standard solution of 1% phenolphthalein in 70% ethyl alcohol. The indicator (phenolphthalein) turned purple in the noncarbonated region with pH values above 9.2, while in the carbonated region with a pH of less than 9.2, the solution remained colourless.

#### 3.4.3.7 Water infiltration (permeability)

The water infiltration test was conducted on cylindrical concrete samples. After 7 or 28 days of water curing, the samples were removed from water for the permeability test. The coefficient of water infiltration was calculated using the method proposed by Yang and Jiang (Yang & Jiang 2003). The side surface area was covered with dental plaster while the two ends (the top and the bottom) of the surfaces of the concrete cylinders were not covered. Pyrex cylinders of 30 cm in length and 10cm in diameter with two sides opened, were placed over each concrete cylinder, and were fixed together with dental plaster as shown in Figure 3.23. After plaster drying, water was injected into the Pyrex cylinder as shown in the Figure. When the water line reached 200 mm in the Pyrex cylinder, the water tap was closed. The time taken by the water to fall a distance of ΔH was recorded using a stop watch. The water infiltration coefficient K was calculated as shown in equation 3.5:

$$K = \frac{\Delta H}{\Delta t} \qquad \text{Equation 3.5}$$

Where $\Delta t$ equals the time taken by water to fall $\Delta H$ distance.

Figure 3-23: The water permeability test

#### 3.4.3.8 Microstructural analyses

The microstructural analysis was carried out on small samples taken out of pervious concrete cylinders. After a water curing period of 7 days, the pervious concrete cylinders were sealed by dental plaster on all of the surface area expect the top and bottom ends and were then kept in a $CO_2$ incubator in a 20% $CO_2$ environment with 65% humidity until the day of test. On the day of the test, using an electrical saw, two disk samples were removed from each cylinder at 5 and 10 cm depth of the cylinder. Using a hammer, the concrete disks were crushed where the gravel was separated and the paste was ground into fine materials, and then sieved to 75μm to be analysed. The process is shown in Figure 3.24. Small pieces of the crushed material were taken off for the SEM analysis.

Figure 3-24: Extraction of powder material from pervious concrete for microstructural analysis

#### 3.4.3.8.1 Powder X-Ray diffraction (XRD)

XRD is a well-known technique that is used to provide qualitative and quantitative analyses of the crystalline phases that exist within the samples. Each crystal has its own unique diffraction pattern. XRD determines the existence of crystalline components based on their resonance in the presence of X-rays at varying incidence angles. The comparison of different diffraction patterns helps identify the chemical composition of a sample. XRD was conducted using the Siemens D500 Diffractrometer shown in Figure 3.25, in the operating conditions of Cu Kα radiation (40 kV, 40 mA); at a scan rate of 2˚/step; 2θ range from 5˚ to 50˚.


Figure 3-25: The XRD Siemens Diffractrometer used.

#### 3.4.3.8.2 Thermogravimetric analysis (TGA)

Thermogravimetric analysis (TGA) is a useful technique to characterise cementitious materials where the mass change is tracked and measured as a function of applied temperature. From TGA and DTG (first derative of TG), different cement components were identified according to their thermal characteristics.

The prepared powder samples of both the control and M-AC pervious concrete were tested using PerkinElmer STA6000 (Figure 3.26) from temperatures of 30 to 800$^{o}$ C. About 20 mg of each sample was used each time. The sample was first held for 1 min at 30$^{o}$C and then gradually increased from 30 to 800$^{o}$C by a step rate of 10$^{o}$ C / min. At the end, the sample was held for 1 min at 800$^{o}$C.

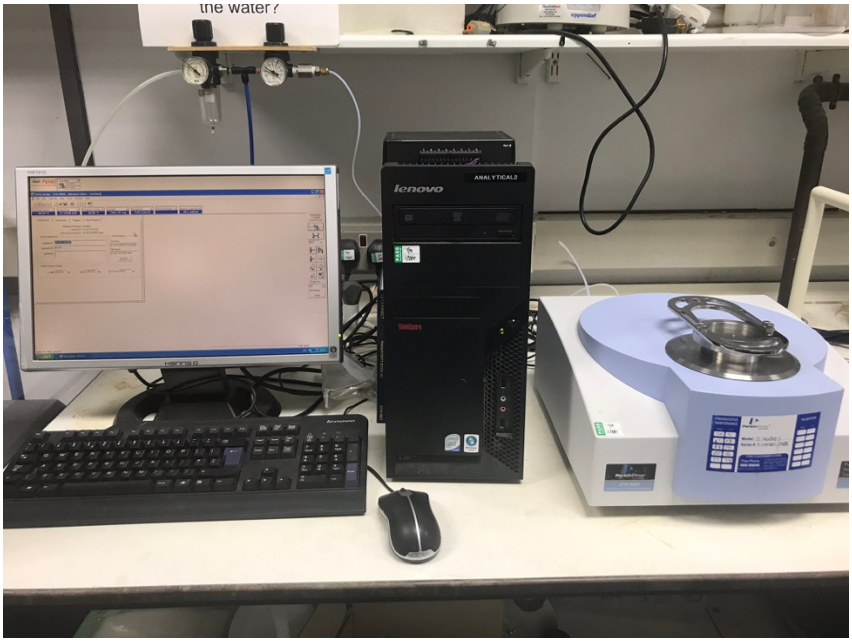


Figure 3-26: The Perkin Elmer thermogravimetric analysis TGA used.

#### 3.4.3.8.3 Scanning electron microscopy (SEM)

SEM was employed to characterise the surface morphology of the small crushed pieces extracted from pervious concrete. SEM was conducted using EVO LS 15 desktop Scanning Electron Microscope from ZEISS Ltd shown earlier in Figure 3.11.

### 3.4.3.9 $CO_2$ sequestration test

The gas flow reactor system, shown in Figure 3.27, was used to measure the $CO_2$ adsorption capacity of the control and M-AC pervious concrete samples. The system includes: a (5% $CO_2$ in air) cylinder, a (0.1 – 1.8 L/min) flowmeter, 5% $CO_2$ sensor (details provided earlier in Table 3.6), a pump, and a glass container where the examined samples are placed. The pump was used to vacuum the space surrounding the sample in the container. The $CO_2$ gas was then injected into the container via 6 holes to homogenize the flow pattern. The $CO_2$ concentration was measured continuously for 3 hrs by an automatic $CO_2$ sensor coupled with the outlet of the reactor.

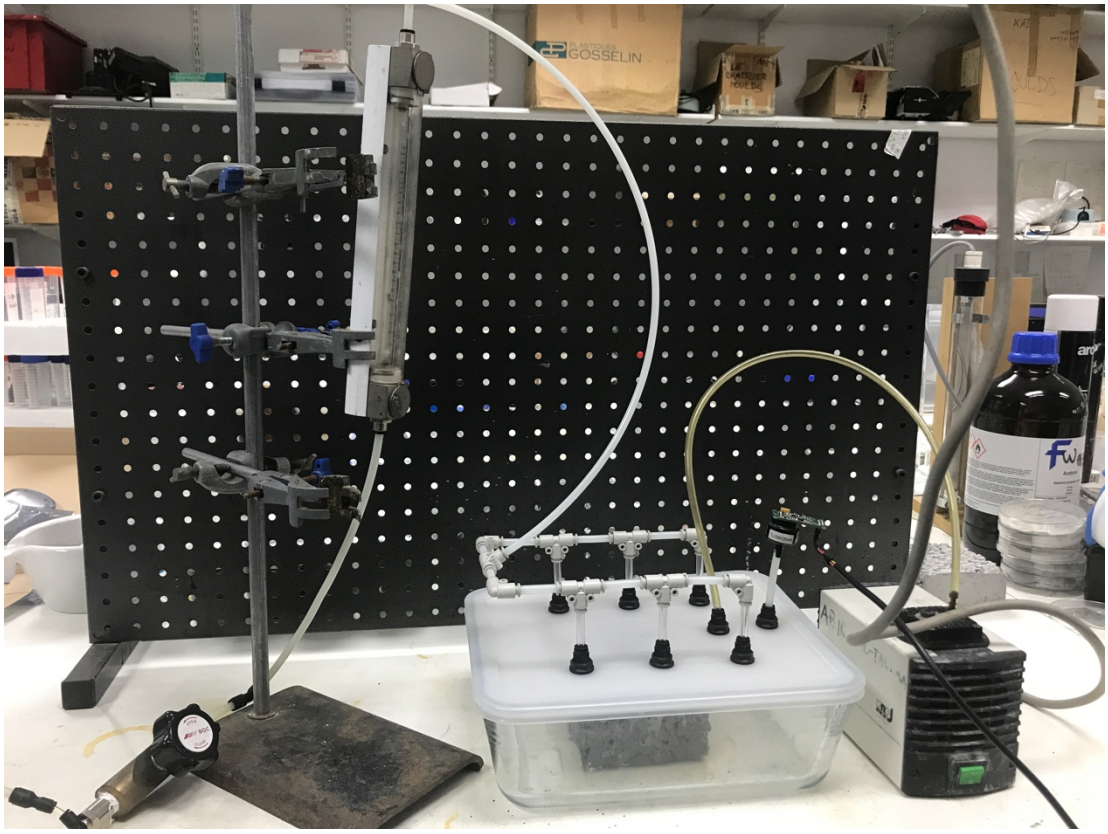


Figure 3-27: The $CO_2$ sequestration setup prepared for pervious concrete samples

# 4 Characterisation and $CO_2$ adsorption of modified activated carbon

## 4.1 INTRODUCTION

This chapter presents details of the laboratory work conducted to characterise the samples of modified ACs used and to quantify their $CO_2$ adsorption capacities. Two types of AC were used; granular and powder AC. In order to maximise their $CO_2$ adsorption capacity, a two-stage modification process was carried out on the activated carbons. The granular activated carbon (GAC) underwent a first modification stage as described in section 3.3.1.1. Physical and chemical characterisation of the first modified GAC is presented in Section 4.2, followed by a quantification of the $CO_2$ adsorption capacity of the raw and modified samples by three different measuring tools (Section 4.3). Based on the findings of the adsorption capacities of this step, the GAC underwent a second round of modification as described in Section 3.3.1.2. The results of physical-chemical characterization of the second stage modified GAC are presented and discussed in Section 4.4. The results of the measurement of the $CO_2$ adsorption capacities of the second stage modified GAC compared to the unmodified GAC are discussed in Section 4.5. Based on the results of the second modification step, an optimised modification approach was selected and applied to the powder activated carbon (PAC), and its characterisation results are presented in Section 4.6.

## 4.2 CHARACTERISATION OF THE FIRST STAGE MODIFIED GAC

It is well established that $CO_2$ adsorption is strongly dependent on the physical-chemical characteristics of the AC surface. High surface area and favourable functional groups are necessary for the $CO_2$ to be adsorbed through chemical bonds and/or physical interlock substrate. At the first stage, modification by a single impregnation agent was considered and NaOH, HCl, $NH_4OH$ and $CuSO_4$ were investigated as modifying agents in varying concentrations. Characterisation of the texture parameters and the surface chemistry of the raw and modified GACs was carried out using BET, FTIR and SEM analyses. These tests provide insights into the texture parameters and the surface chemistry of the examined samples. The results from these tests are significant in assessing the modification, as well as the subsequent $CO_2$ adsorption capacities of the modified

samples. Table 4.1 presents the modified samples that were selected for the characterisation experiments.

Table 4-1: Characterisation tests performed in raw and selected first stage modification of the granular AC

| Sample | BET | FTIR | SEM |
|---|---|---|---|
| Raw GAC | √ | √ | √ |
| 20% NaOH-GAC | √ | √ | √ |
| 10% NaOH-GAC | | | |
| 5% NaOH-GAC | | | |
| 37% HCl-GAC | √ | √ | √ |
| 19% HCl-GAC | | | |
| 13% HCl-GAC | | | |
| 35% $NH_4OH$-GAC | | √ | √ |
| 18% $NH_4OH$-GAC | | | |
| 12% $NH_4OH$-GAC | | | |
| 20% $CuSO_4$-GAC | | √ | √ |
| 10% $CuSO_4$-GAC | | | |
| 5% $CuSO_4$-GAC | | | |

### 4.2.1 Physical characterisation

The measured BET surface area, micropore area and average pore size of selected adsorbents are presented in Table 4.2. Experiments on the GAC samples were conducted in the Department of Materials Science at the University of Cambridge by a specialist technician in the BET laboratory.

Some of the results are significantly lower than the data provided by the supplier. The granular AC was supplied by Fisher Scientific-UK, where the BET surface area is 1175 $m^2/g$ as specified by the supplier. However, the measured BET surface area is 887 $m^2/g$. The variation in BET values might be attributed to (1) the extent of accuracy between the instruments used to measure the texture parameters, or (2) the differences in the operation conditions applied during the experiments.

A high percentage of the raw GAC area is micropores (604 $m^2/g$). Micropores (diameter less than 2 nm) are responsible for $CO_2$ adsorption. The molecular size of $CO_2$ is 0.33nm. It is well known that only the micropores area are effective in $CO_2$ adsorption at room temperature because they contribute to the retention of $CO_2$ in the pore wall. Pores that have sizes close to or exceeding the diameter of $CO_2$ molecules by a factor of 2-5 are employed in adsorption (Caglayan & Aksoylu 2013). As the micropores constitute around

68% of the total pore system in the raw GAC, the latter is expected to have some adsorption characteristics even before conducting any chemical modification to its surface.

Table 4-2: Texture parameters of raw and selected modified GAC

| **Sample** | **BET surface area** $m^2/g$ | **Micropore area** $m^2/g$ | **Average pore width** nm | **Pore volume** $cm^3/g$ |
|---|---|---|---|---|
| Raw GAC | 887 | 604 | 2.24 | 0.50 |
| NaOH-GAC | 805 | 587 | 2.28 | 0.45 |
| HCl-GAC | 849 | 602 | 2.24 | 0.48 |

Table 4.2 shows that the modification process using NaOH and HCl decreased the surface area of the raw AC, while maintaining virtually the same average pore width and pore volume. For NaOH, the decrease in the surface area is likely to be attributed to structural changes in the AC due to the entrapment of NaOH molecules in the micropore areas. This resulted in a reduction in the surface area of the NaOH modified GAC (Auta et al. 2013). The reduction in pore volume also supports this explanation. A similar observation was reported by (Tan et al. 2014) where the BET surface area of the 32% NaOH-modified AC decreased to almost half the area of the unmodified samples.

For the HCl modified samples, a slight reduction of 4% in the BET surface area was noticed. In this study, modification with the HCl acid was considered to be a promising step to remove any volatile or mineral matters that are attached to the surface of AC, thus allowing more space and more volume for the $CO_2$ molecules entrapment (Gęsikiewicz-Puchalska et al. 2016). However, a slight reduction in the BET surface area from 887 to 849 $m^2/g$ was observed. In spite of the possibility of being an experimental error, this slight reduction could be explained as a structural change in the pores system of GAC due to modification with this acid. A similar finding of a change in pore structure was previously reported by Zhang and his group ( 2013) who modified AC by pure sulfuric and nitric acid mixture and by a diluted acid mixture. The BET surface area was reduced in both cases but showed an extreme reduction from 2994 to 507 $m^2/g$ in the case of modification with the pure acid mixture. They attributed this reduction to a collapse of the pore structure of the GAC due to the oxidative ability of the pure acids (Zhang et al. 2013). Other previous studies reported the same decreasing BET surface area effect due to the modification of granular AC with acid (Liu et al. 2017; Tamai et al. 2006). As the area of micropores of the HCl-modified is almost the same that of the raw sample

(changed only from 604 to 602 $m^2/g$), this could indicate that the reduction in the total area was mainly in the macropores and mesopores.

### 4.2.2 FTIR analyses

To investigate the presence of functional groups on the raw and modified GAC, Fourier-transformed infrared (FTIR) spectroscopy was used. FTIR measures the transmittance of infrared light at various wave lengths, thus identifying the functional groups on the surface of the sample. As shown in Figure 4.1, the horizontal axis is the wave number ($cm^{-1}$) while the vertical axis is transmittance (%). For the first modification samples, only the highest concentration of each chemical modified GAC underwent the FTIR test. Figure 4.1 shows that the overall shape of the FTIR spectra are similar for all the examined samples. The raw GAC surprisingly did not show any bands in the range of 450 to 4000 $cm^{-1}$. The basic chemical structure of AC is relatively similar to that of graphite. The graphite crystal is composed of layers of combined hexagons held by C-C bonds. Hence AC might be considered as a disorganised form of graphite due to the presence of impurities in the AC.

No sample showed any peaks or trends at wave numbers greater than 3200 $cm^{-1}$ which indicates that no water was adsorbed by the samples. All spectra showed band characteristics of C-H groups located at the edges of the aromatics ring below 800 $cm^{-1}$. Also, all the spectra of the modified GAC showed peaks with different intensities in the region of 2360–2340 $cm^{-1}$, associated with the asymmetric stretching vibration of gaseous phase $CO_2$ (Srenscek-Nazzal et al. 2016). This implies that the modified samples had adsorbed some of the atmospheric $CO_2$ before being examined by the FTIR test.

The NaOH-modified GAC presented the most accentuated absorption bands in the FTIR spectra. The bands at 2150 to 1980 $cm^{-1}$ might be attributed to alkyne C≡C stretching vibrations (Socrates 2004). The band at 964 $cm^{-1}$ is due to O-H out-of-plane deformation vibrations which exist in carboxylic acid, while the band at 1426 $cm^{-1}$ is probably due to the in-plane O-H deformation vibration or to carboxylates (C=O) functional groups (Socrates 2004; Tan et al. 2014).

Treatment with the $NH_4OH$ caused few changes to the spectra of the raw GAC. New but weak bands related to N-containing species were observed. The presence of C–N (1061 $cm^{-1}$) and the small N–H (1400 $cm^{-1}$) bands may indicate the formation of amide (–CO–

NH–) groups during the modification of the GAC with $NH_4OH$. The small bands at 2154 and 1981 $cm^{-1}$ were assigned to nitrile groups (Shafeeyan et al. 2011). A previous study showed that modification of GAC with aqueous ammonia at room temperature did not result in noticeable changes in GAC chemistry (Przepiórski et al. 2004).

For the $CuSO_4.5H_2O$ modified GAC, the band at 1270 $cm^{-1}$ could be associated with the C-O-C asymmetric stretching vibration. The band at 973 $cm^{-1}$ can be assigned to C–H groups located at the edges of aromatic ring (Shafeeyan et al. 2011). The metal bands have appeared at lower frequencies around 750 $cm^{-1}$ (Hosseini et al. 2015b).

No pronounced band was observed in the HCl-modified sample. The small absorption band which appeared in the HCl modified sample at 1047 $cm^{-1}$ might be associated with ether C-O symmetric and asymmetric stretching vibration (-C-O-C- ring) (Al-Qodah & Shawabkah 2009). The region 450-750 $cm^{-1}$ reveal a few bands which are associated with the CH in-plane and out-of-plane aromatic ring deformation vibrations (Socrates 2004). The spectral zone in the 2900 to 2800 $cm^{-1}$ range displays bands mostly attributed to O-H (hydroxyl) groups (alcohol, phenols and carboxylic acids), while bands located at 2162 and 1981 $cm^{-1}$ are probably associated with alkyne C≡C stretching vibrations (Socrates 2004; M. A. Islam et al. 2017). Previous studies revealed that a limited amount of surface oxygen groups (e.g. no carboxylic acid groups) were introduced on the surface of AC after HCl modification.

In summary, NaOH-, $CuSO_4$- and $NH_4OH$-modified samples presented absorption bands in the FTIR spectra associated with functional groups. By contrast, the raw GAC presented no absorption bands and the HCl-modified GAC presented very little differences. The new chemical functional groups incorporated on the surface of modified samples may explain the higher adsorption capacity of these samples compared to the unmodified samples.

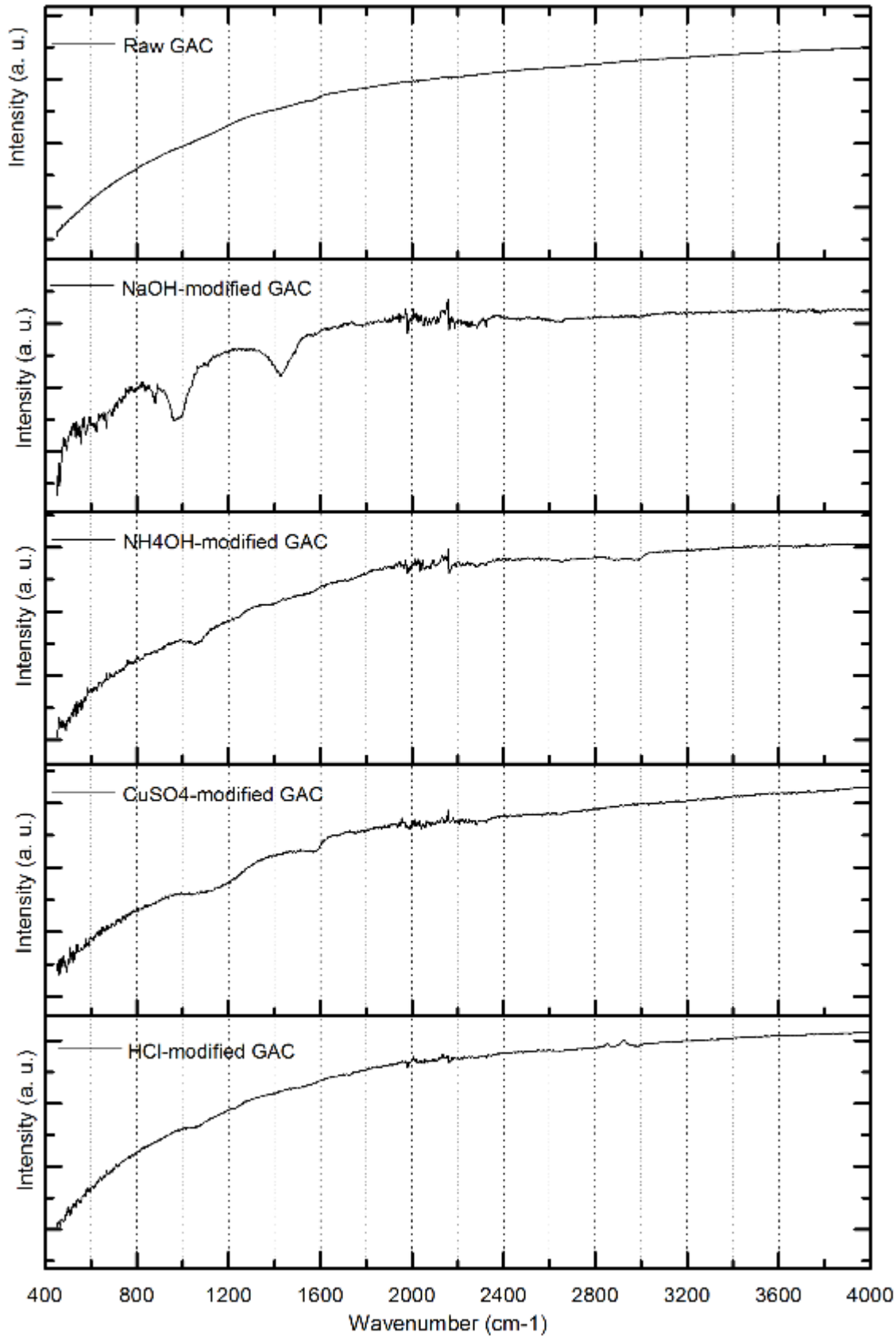


Figure 4-1: FTIR spectra for the raw and the stage one modified GACs

### 4.2.3 Scanning electron microscopy

To observe the surface physical morphology of the raw and modified GAC samples, the scanning electron microscopy (SEM) imaging was employed. Figure 4.2 show the SEM micrographs of the GAC before and after modification with NaOH, HCl, $CuSO_4$ and $NH_4OH$. It can be observed from the micrographs that the surface of raw GAC is full of cavities, showing a heterogeneous structure in terms of both size and shape. Modified GAC samples also exhibit an irregular and heterogeneous surface morphology. The SEM of GAC shows the existence of various impurities and small particles distributed on the surface, most of which disappeared after HCl modification. The surface of the NaOH modified samples show some scattered white particles which might be attributed to carbonated particles on the surface of GAC. The $NH_4OH$ and $CuSO_4$ modified samples show a much rougher surface with an increased number of pores compared to the raw GAC. Some salt particles which are scattered on the surface of $CuSO_4$ modified samples can also be seen, which might be attributed to the presence of remailing copper salts left over from the modification process. Some of these particles are trapped in the AC pores which could block the entry of other particles into these pores. SEM images reveal the cleaning effect of HCl as a modifying agent, while showing that other impregnating agents may have a blockage effect on the pore structure of AC.

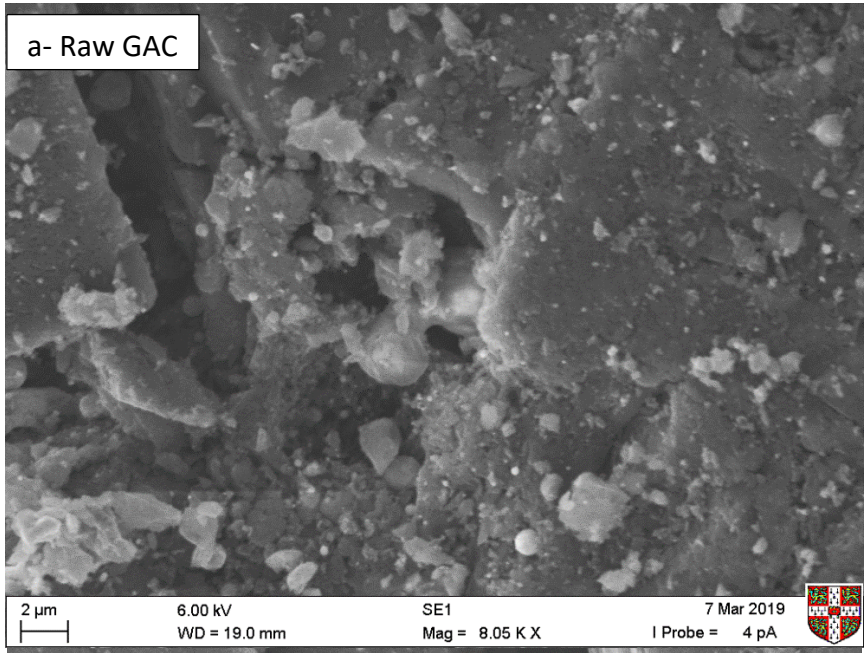
a- Raw GAC
2 µm
6.00 kV
WD = 19.0 mm
SE1
Mag = 8.05 K X
7 Mar 2019
I Probe = 4 pA

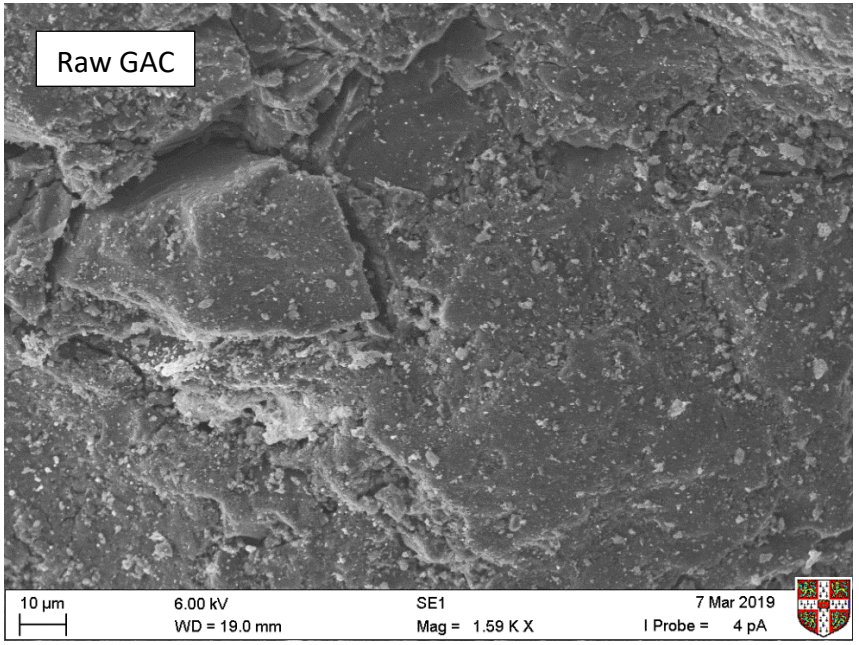
Raw GAC
10 µm
6.00 kV
WD = 19.0 mm
SE1
Mag = 1.59 K X
7 Mar 2019
I Probe = 4 pA

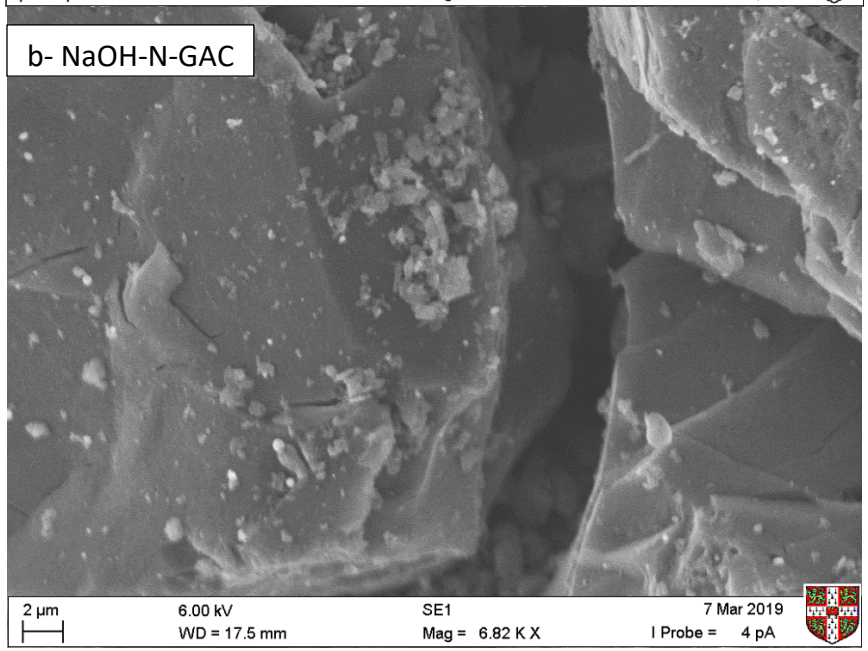
b- NaOH-N-GAC
2 µm
6.00 kV
WD = 17.5 mm
SE1
Mag = 6.82 K X
7 Mar 2019
I Probe = 4 pA

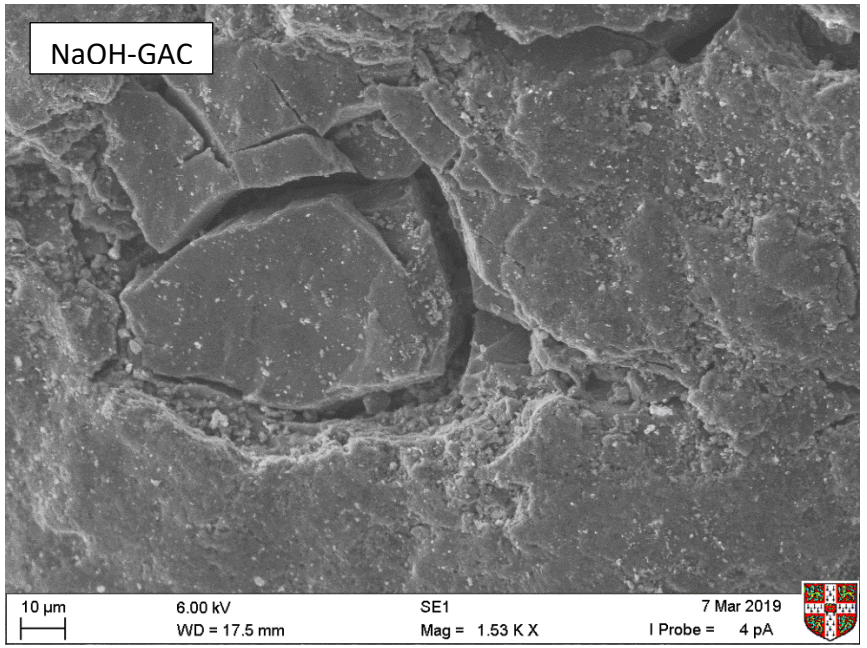
NaOH-GAC
10 µm
6.00 kV
WD = 17.5 mm
SE1
Mag = 1.53 K X
7 Mar 2019
I Probe = 4 pA

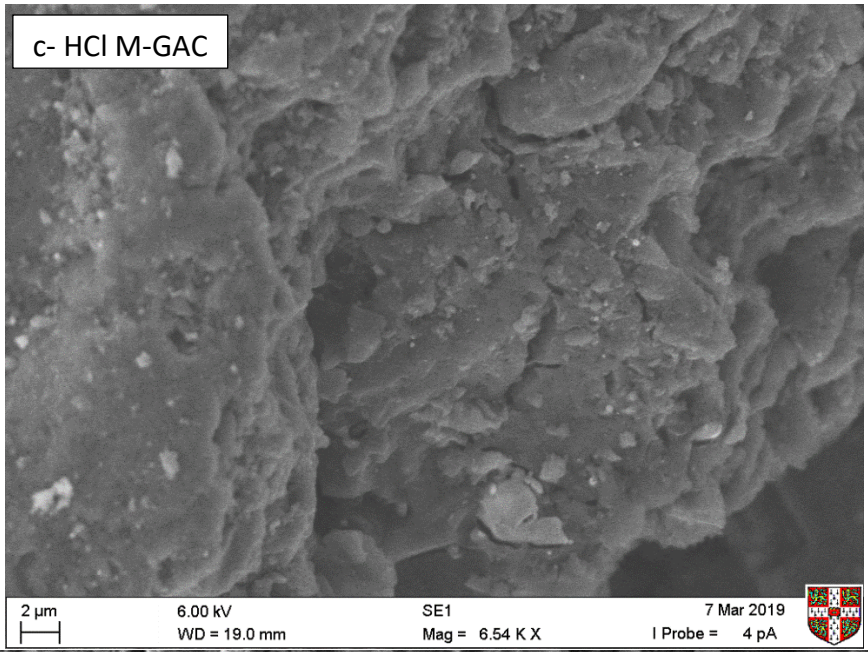
c- HCl M-GAC
2 µm
6.00 kV
WD = 19.0 mm
SE1
Mag = 6.54 K X
7 Mar 2019
I Probe = 4 pA

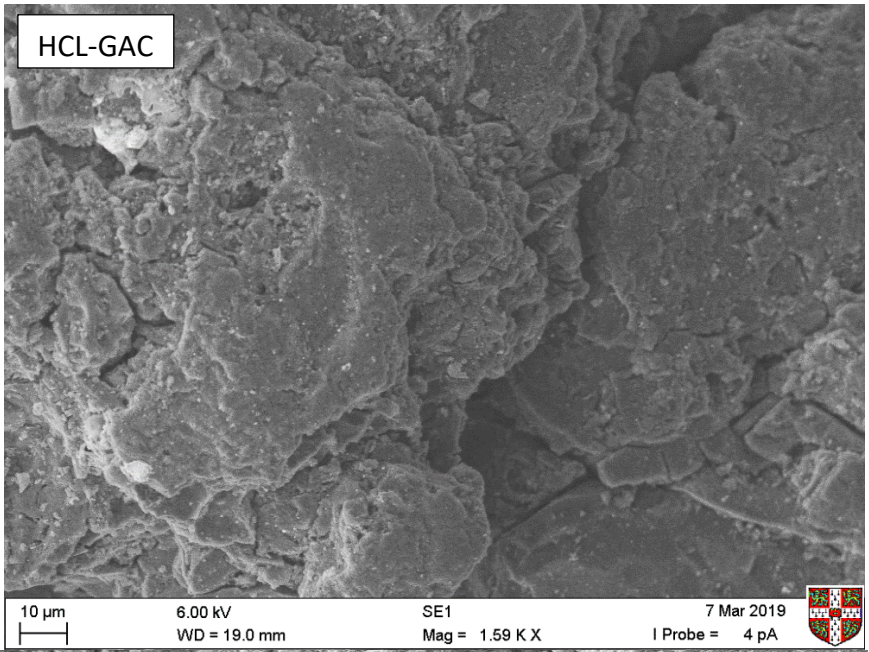
HCL-GAC
10 µm
6.00 kV
WD = 19.0 mm
SE1
Mag = 1.59 K X
7 Mar 2019
I Probe = 4 pA

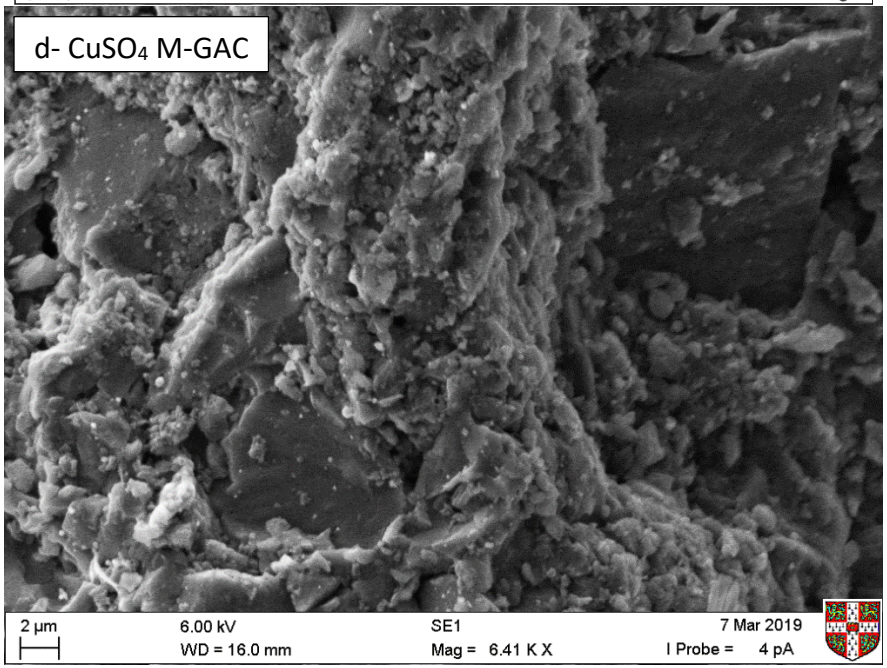
d- CuSO4 M-GAC
2 µm
6.00 kV
WD = 16.0 mm
SE1
Mag = 6.41 K X
7 Mar 2019
I Probe = 4 pA

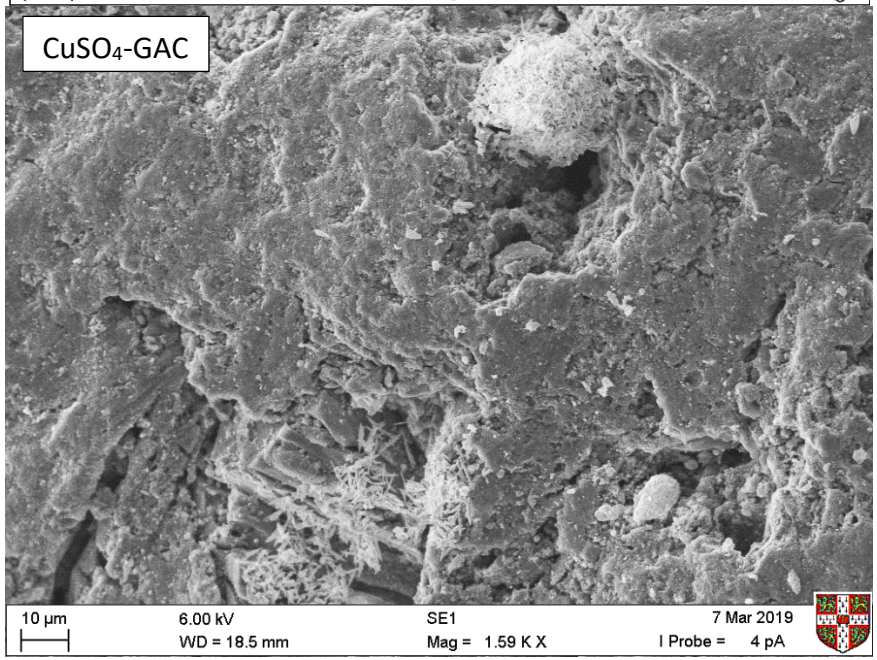
CuSO4-GAC
10 µm
6.00 kV
WD = 18.5 mm
SE1
Mag = 1.59 K X
7 Mar 2019
I Probe = 4 pA

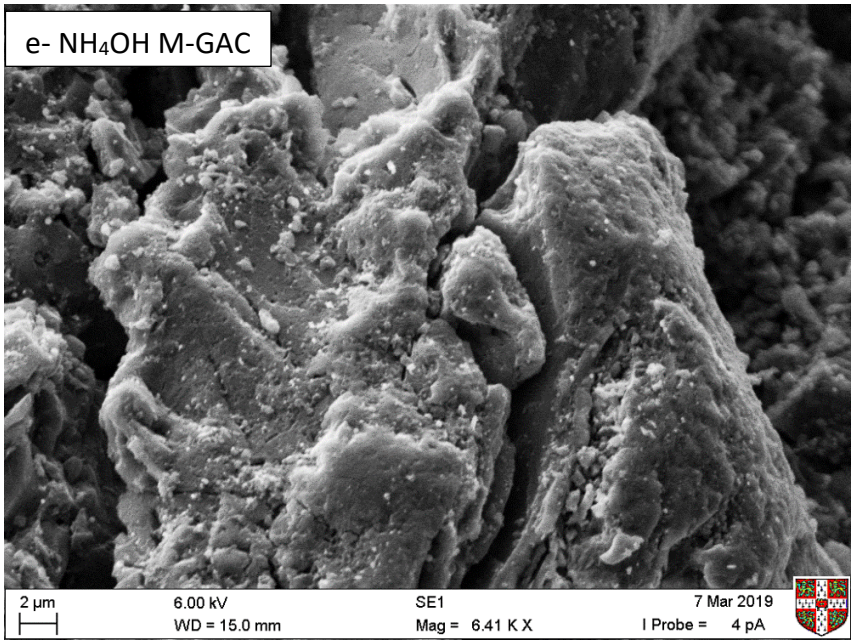


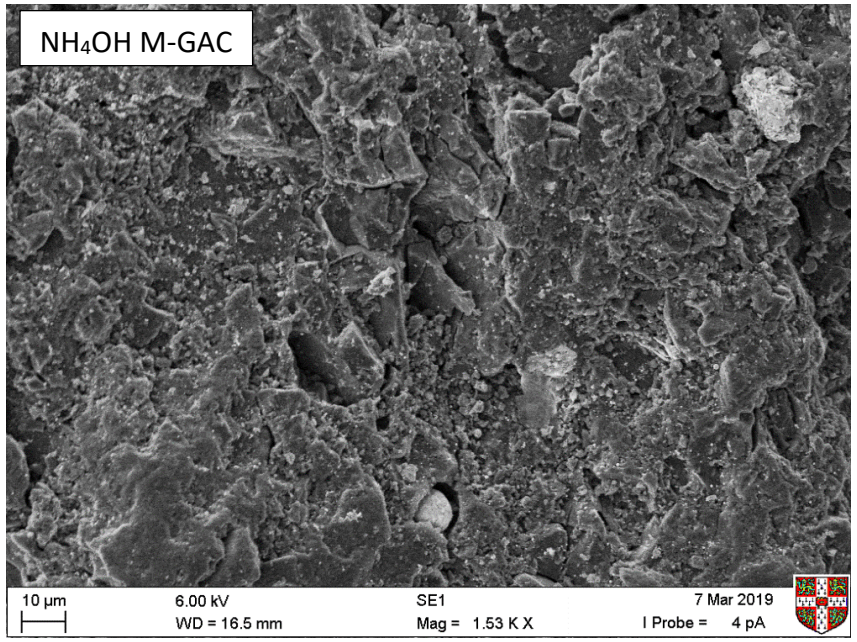


Figure 4-2: SEM images of the raw and modified GAC using two different magnifications (a) raw GAC, (b) 20%NaOH-GAC, (c) 37% HCl-GAC, (d)20%$CuSO_4$-GAC and (e) 25% $NH_4OH$-GAC

## 4.3 QUANTIFICATION OF $CO_2$ ADSORPTION CAPACITIES OF FIRST STAGE MODIFIED SAMPLES

This section focuses on the quantification of the $CO_2$ adsorption capacities of the raw and modified GAC in order to better understand the influence of the modification techniques on the surface and the chemistry of AC, and consequently on their adsorption capacities. The first stage of modification included modifying raw GAC in solutions with different concentrations of the impregnation agents, NaOH, HCl, $NH_4OH$ and $CuSO_4.5H_2O$. The details of the concentrations and the modification procedure are described in Section 3.3.1.1. Raw and modified GAC were subjected to the same assessment tools to measure their adsorption capacities of $CO_2$. To measure the adsorption capacities, three different techniques were utilised: a $CO_2$ incubator, a fixed-bed column and thermogravimetric analysis. Below are the results of the adsorption capacities from each technique.

### 4.3.1 $CO_2$ incubator environment

To measure the adsorption capacity of AC, modified and unmodified samples were kept in the $CO_2$ incubator until a constant weight was reached, as described in Section 3.3.2.1. The average change in the weight of the samples over time for the modified and raw samples, for each one of the four impregnation agents, is shown in Figure 4.3. The $CO_2$ adsorption capacity (calculated as the average of three samples) is the difference between the initial and final weight of GAC sample and is shown in Table 4.3.

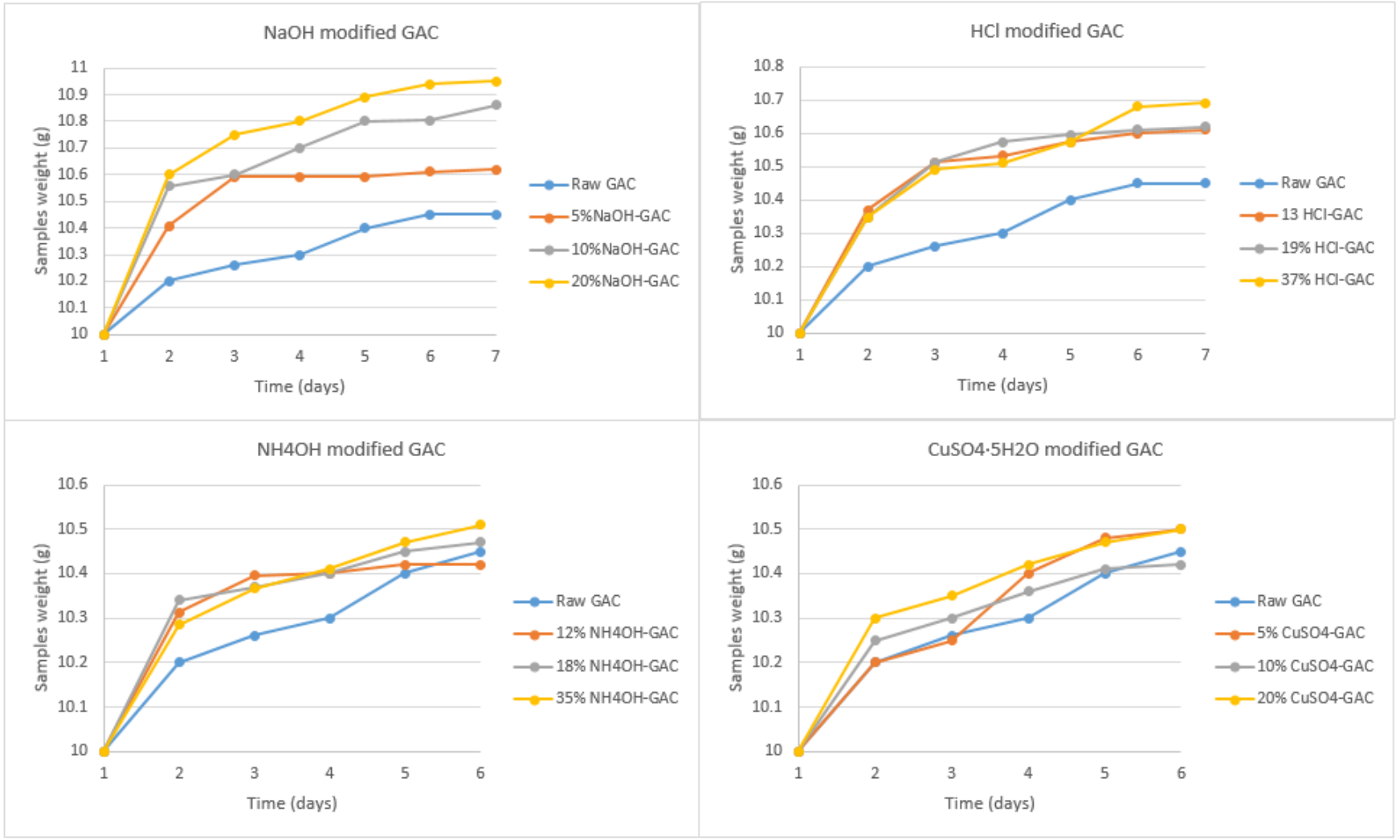


Figure 4-3: $CO_2$ adsorption capacities of raw and modified GACs using $CO_2$ incubator

Table 4-3: $CO_2$ Adsorption capacities of the raw and modified AC using $CO_2$ incubator

| Sample | Concentration | $CO_2$ adsorption capacity (mg $CO_2$/g AC) | (S D) |
|---|---|---|---|
| Raw GAC | NA | 45 | 4.1 |
| | | | |
| NaOH-GAC | 20% | 95 | 7.3 |
| | 10% | 80 | 6.1 |
| | 5% | 61 | 5.3 |
| | | | |
| HCl-GAC | 37% | 69 | 5.3 |
| | 19% | 62 | 6.4 |
| | 13% | 60 | 6.9 |
| | | | |
| $NH_4OH$-GAC | 35% | 52 | 7.5 |
| | 18% | 48 | 5.6 |
| | 12% | 42 | 6.2 |
| | | | |
| $CuSO_4$-GAC | 20% | 50 | 6.5 |
| | 10% | 42 | 3.8 |
| | 5% | 50 | 6.7 |

Overall, most of the modified AC exhibited a higher adsorption capacity than that of the raw samples. Moreover, there were significant variations in the adsorption capacities of the AC samples modified by the same impregnation agent but with different concentrations. In addition, the rate of adsorption in all examined samples was generally high on the first day of exposure to $CO_2$ gas in the $CO_2$ incubator, decreasing thereafter. The high adsorption rate could be attributed to the highly porous AC which accommodated the $CO_2$ molecules in its active sites. Over time, the adsorption rate decreased due to a reduction in the active sites, thus slowing down the adsorption process from taking place (Rashidi et al, 2013). All the examined AC samples stopped showing any increase in weight after 6 or 7 days in the $CO_2$ incubator. It was noticed that NaOH-modified AC showed the highest adsorption capacity followed by HCl modified samples. Modification with $CuSO_4.5H_2O$ had the least influence on the raw AC, increasing its $CO_2$ adsorption capacity from 45 to only 50 mg $CO_2$/g AC as shown in Table 4.3.

The adsorption capacity of GAC modified by 20% NaOH was 95 mg $CO_2$/g AC which is more than double the capacity of the unmodified GAC. From Figure 4.3, it can be seen that the 5% and 10% modified samples showed a higher adsorption rate during the first two days, followed by a lower rate for the 10% NaOH modified sample and almost no change in the weight of the 5% NaOH modified samples. In general, the three concentrations

demonstrated a higher $CO_2$ uptake compared to the unmodified AC. The reason behind this higher capacity could be the new $Na^+$ species on the surface of the AC that were incorporated through the NaOH impregnation. This increased the affinity of modified AC for $CO_2$ molecules. The sites interacted strongly with $CO_2$ gas leading to an increased adsorption capacity (Caglayan & Aksoylu 2013). Similar findings have been reported by other researchers. Tan and his colleagues have modified AC through different concentrations of NaOH (24 – 48%) and their highest $CO_2$ adsorption capacity was 27 mg/g AC (Tan et al. 2014), a lower value compared to the current results of this study.

For the HCl modified samples, the adsorption capacities slightly increased according to the acid concentration. During the first two days, the modified samples with different concentrations of HCl showed the same rate of adsorption. 19% and 13% acid-modified samples increased the $CO_2$ adsorption capacity, but the pure acid modified AC showed the highest value of 69 mg $CO_2$/g AC among the HCl-set. However, this value is lower than the adsorption capacity of HCl-modified samples reported by other researchers. Gesikiewicz and his group measured the adsorption capacity of three different types of AC modified by HCl. The values ranged from 100 to 190 mg/g AC under a pressure of 0.95 bar (Gęsikiewicz-Puchalska et al. 2016). In contrast, other studies reported a significantly lower capacity, not exceeding 10 mg $CO_2$/g AC (Caglayan & Aksoylu 2013). The great variation in results are probably due to differences in (a) the initial precursors where AC was prepared, (b) the operating conditions of modification or (3) the assessment techniques for adsorption.

The same trend was observed for the $NH_4OH$ modified AC samples. The first four days in the $CO_2$ incubator showed a high adsorption rate for the modified samples compared to the raw samples. After that, the adsorption decreased until it almost stopped on the sixth day of the experiment. The current adsorption capacity of the $NH_4OH$ modified samples ranges from 48-52 mg/g AC, significantly lower than previously reported values. Zhang and Vargas have reported 140 mg $CO_2$/g AC (Zhang et al. 2010) and 200 mg $CO_2$/g AC (Vargas et al. 2013) for $NH_4OH$ modified AC.

The adsorption capacities of $CuSO_4$ modified GAC showed some enhancement compared to the unmodified GAC. However, these values are still small in relation to the results documented in the literature (Hosseini et al. 2015; Rashidi & Yusup 2016; Kim et al. 2010). Hosseini and his group modified AC with different metals including copper. They

reported an adsorption capacity of 87 mg $CO_2$ /g AC for the 20% copper modified AC and 66 mg $CO_2$ /g AC for the raw AC. The variations in the obtained results among studies might be attributed to variations in the operating conditions (such as the temperature, flow rate, gas concentration, etc.) involved in different experiments. Another important point to highlight here is the calcination step that was typically implemented in previous studies, which was the last step for modifying AC with metals such as copper and zinc, was not followed in the current study due to the energy conservation approach which was followed.

The AC samples were tested in triplicate and the standard deviation for each capacity was calculated (as shown in the last column of Table 4.3). All the standard deviation values were within around 15% of the average capacity.

### 4.3.2 Fixed-bed column environment

The second technique used to measure the $CO_2$ adsorption capacity of AC was a fixed-bed column setup. Figure 4.4 shows the concentration readings by a $CO_2$ sensor at the outlet of the column, as described in Section 3.3.2.2. The operational conditions were: pressure = 1 bar, gas flow rate = 200 mL/min, and gas concentration = 5%. The $CO_2$ gas passed through the AC in the column, where the active sites on the AC surface adsorbed the $CO_2$ molecules rapidly until they were fully saturated. In a typical run, the gas flow was stopped when the $CO_2$ concentration at the outlet reached the saturation state.

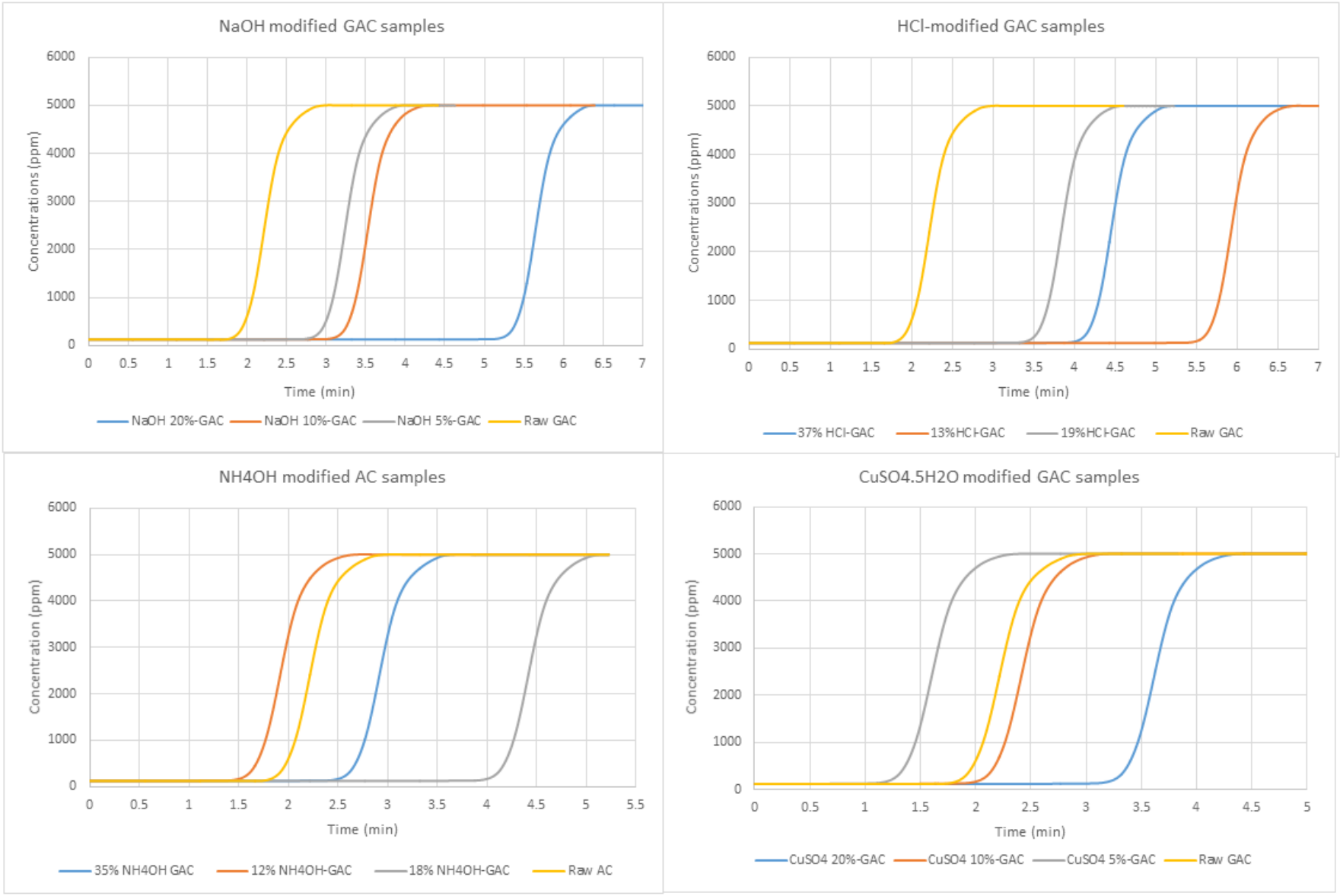


Figure 4-4: Adsorption capacity of the raw and modified GACs using fixed bed column

Based on Figure 4.4, two parameters were calculated and summarised in Table 4.4; the $CO_2$ adsorption capacity of the AC samples, and the breakthrough time which is the time required to reach the initial $CO_2$ concentration (5000ppm). This is referred to here as the time to saturation. The starting points in the curves (zero on the x-axis) represent the times when the valve was opened to allow the $CO_2$ gas to pass through the setup. The adsorption capacities were calculated following equation 3.1.

It can be seen from Figure 4.4 that the rate of adsorption gradually decreased with time until saturation was achieved. The $CO_2$ adsorption was intensive during the first few minutes. The rapid adsorption rate at the beginning can be attributed to the high surface area of AC which is responsible for interaction with the $CO_2$ molecules. Over time, the curves show a decrease in the adsorption rate due to a decrease in AC active sites that may slow down the adsorption process. In addition, due to the small volume of AC in the column in the current study, the saturation was reached in only a few minutes, compared to a previous study where the column height was 33 cm and the diameter was 2.5 cm, and the saturation was achieved at around 50 min (Hosseini et al. 2015).

Table 4-4: Time to saturation and adsorption capacity of raw and modified samples using the Fixed-bed column tool

| Sample | Concentration | Time to saturation (min) | Adsorption Capacity (mg/g) | (S D) |
|---|---|---|---|---|
| Raw-GAC | N.A. | 2.99 | 1.97 | 0.09 |
| | | | | |
| NaOH-GAC | 20% | 6.38 | 4.98 | 0.32 |
| | 10% | 4.31 | 3.1 | 0.09 |
| | 5% | 3.97 | 2.9 | 0.13 |
| | | | | |
| HCl-GAC | 37% | 5.18 | 3.9 | 0.15 |
| | 19% | 4.57 | 3.4 | 0.21 |
| | 13% | 6.69 | 5.2 | 0.18 |
| | | | | |
| $NH_4OH$-GAC | 35% | 3.65 | 2.6 | 0.21 |
| | 18% | 5.15 | 3.9 | 0.26 |
| | 12% | 2.68 | 1.7 | 0.09 |
| | | | | |
| $CuSO_4$-GAC | 20% | 4.38 | 3.2 | 0.30 |
| | 10% | 3.19 | 2.14 | 0.11 |
| | 5% | 2.37 | 1.4 | 0.08 |

In general, most of the modified samples showed a higher $CO_2$ adsorption capacity compared to the raw samples which confirms the significance of the modification process

to enhance the $CO_2$ adsorption. ACs modified with 13% HCl and 20% NaOH solutions exhibited the highest adsorption capacities of 5.2 and 4.98 mg $CO_2$/g AC respectively, compared to 1.97 mg $CO_2$/g AC associated with the raw GAC. The adsorption capacity of the 13% HCl-modified sample was just under triple the value obtained from the raw AC, which emphasises the importance of the acid treatment for a higher $CO_2$ adsorption capacity. Based on the values shown in Table 4.4, the highest $CO_2$ adsorption capacities were achieved in the samples modified by 13% HCl, 20% NaOH, 37% HCl and 18% $NH_4OH$ respectively. The other modified samples resulted in adsorption capacities that were lower than 3.5 mg $CO_2$/g AC. In particular, two modified samples (5% $CuSO_4$ and 12% $NH_4OH$) showed very small adsorption capacities of 1.4 and 1.7 mg $CO_2$/g AC which were lower than that of the raw AC. This order in the adsorption capacities by fixed-bed column was completely different from the order found in the $CO_2$ incubator. A comprehensive comparison and discussion between the capacities obtained using different tools is presented in Sections 4.3.4 and 4.8.

The results in Figure 4.4 reveal that the NaOH treatment of AC led to a significant enhancement in the $CO_2$ adsorption capacity. The value of 20% NaOH modified AC was more than double the capacity of the raw sample. The adsorption capacities of 5% and 10% NaOH modified AC were very close but still higher than that of the unmodified AC. The adsorption capacities for HCl modified samples were 5.2, 3.9 and 3.4 mg $CO_2$/g AC for (13% HCl), (37% HCl) and (19% HCl) samples respectively. $NH_4OH$ modified samples depicted an adsorption capacity that ranged from 1.7 to 3.9 mg $CO_2$/g AC, resulting in a 98% improvement of the adsorption of the raw sample by the 18% $NH_4OH$ modified sample. This result varies from that of Zhang et al. (2010) who also modified AC using $NH_4OH$. Although the adsorption capacity increased from 128 to 140 mg $CO_2$/g AC, the improvement was less than 10% (Zhang et al. 2010). It is worth highlighting that the BET surface area of the Zhang et al. (2010) raw sample was 2829 $m^2$/g compared to 887 $m^2$ /g in the current study.

The AC samples modified with $CuSO_4 \cdot 5H_2O$ solutions demonstrated the lowest adsorption capacities ranging from 1.4 to 3.2 mg/g AC. These values are significantly lower than the values documented by other researchers (Hosseini et al. 2015). Hosseini and his co-workers reported a value of 88 mg $CO_2$/g AC for 20% copper salts modified AC. Apart from their different operating conditions in their experiments (a higher gas

concentration and a lower flow rate), their fixed-bed setup was designed to desorb the AC at a high temperature before applying the $CO_2$ gas. The desorption step might have helped to increase the adsorption capacities. Overall, the adsorption capacities calculated here are significantly lower than those calculated by the $CO_2$ incubator. The probable reasons behind the small values are presented and discussed in Section 4.3.4.

One last point to consider here is the variation of the results of the same examined sample is lower than that of the $CO_2$ incubator results. Here, the standard deviation values of the adsorption capacities were within around 8% of the average which implies a higher accuracy and consistency compared to the $CO_2$ incubator environment.

### 4.3.3 Thermogravimetric analysis

The third technique used to measure the $CO_2$ adsorption capacity of the raw and modified AC samples was TGA. The analysis goal was to measure the total $CO_2$ adsorbed by AC after exposure to $CO_2$. The TGA operated for 142.5 min and the conditions are summarised in the four stages shown in Table 4.5. The samples were exposed to different temperatures and gases but at a constant flow rate of 50 $cm^3$/min.

Table 4-5: The TGA temperature-gas stages

| Stage | Time | Temperature | Rate | Gas |
|---|---|---|---|---|
| First | 15 min | 25 – 100$^o$ C | 5$^o$C/min | Argon |
| Second | 30 min | 100$^o$C | constant | |
| Third | 37.5 min | 100 – 25$^o$C | 2$^o$C/min | |
| Fourth | 60 min | 25$^o$C | constant | $CO_2$ |

Figure 4.5 and Table 4.6 present the $CO_2$ adsorption capacities of the samples at a temperature of 25$^o$C. The adsorption capacities were measured by TGA as the mass gain of the samples after exposure to $CO_2$ gas at a flow rate of 50$cm^3$/min and a concentration of 100%. Since the AC mass in the TGA crucible was variable in each run (10 ± 2 g), the graphs in Figure 4.5 were standardised for the purpose of comparison.

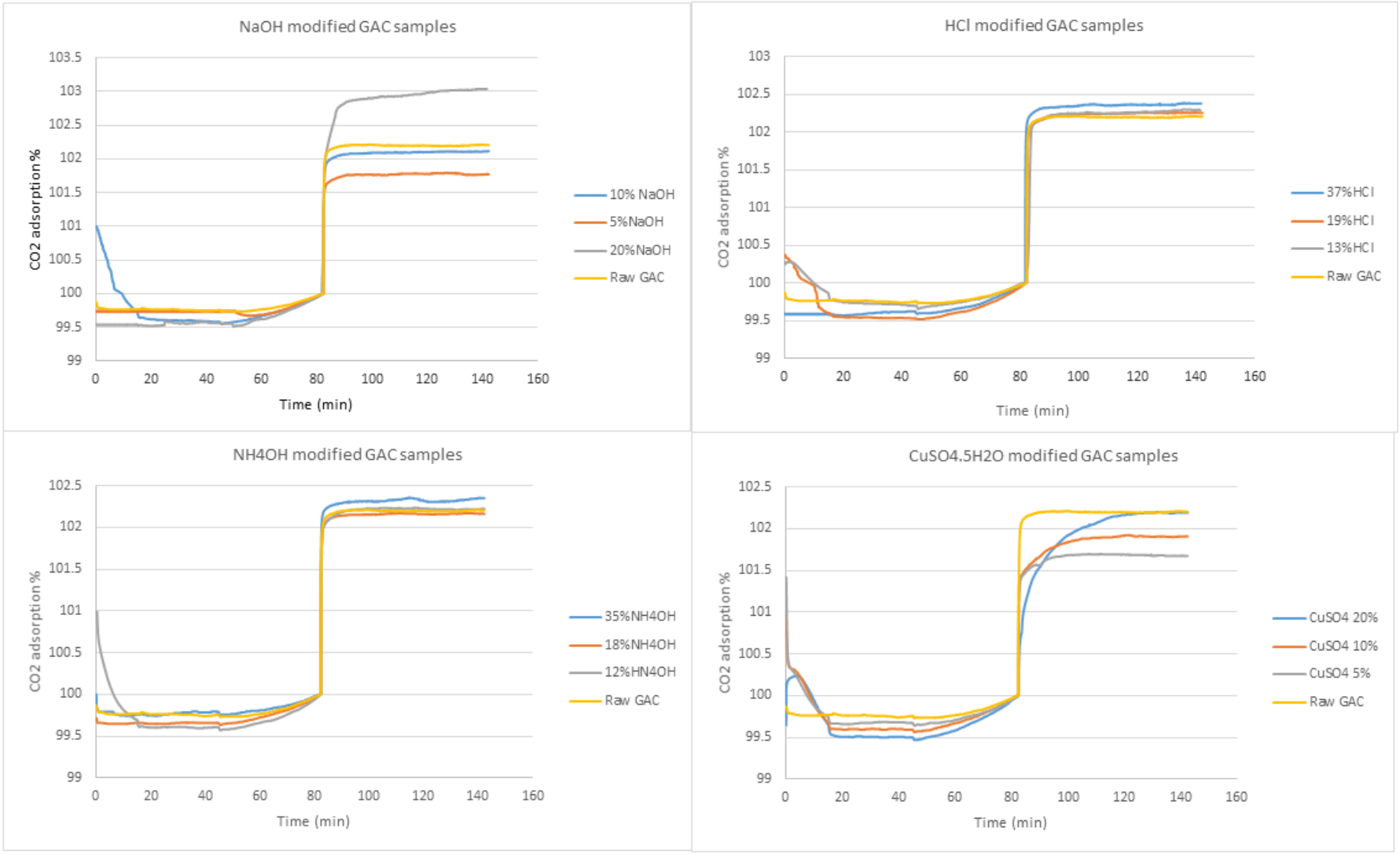


Figure 4-5: Adsorption capacities of the raw and modified GAC samples using TGA analysis

Table 4-6: $CO_2$ adsorption capacities of raw and modified samples measured by TGA

| Sample | Concentration | Adsorption Capacity (mg/g) |
|---|---|---|
| Raw-GAC | N.A. | 22.1 |
| | | |
| NaOH-GAC | 20% | 30.4 |
| | 10% | 21.2 |
| | 5% | 18 |
| | | |
| HCl-GAC | 37% | 23.9 |
| | 19% | 22.7 |
| | 13% | 23 |
| | | |
| $NH_4OH$-GAC | 35% | 23.6 |
| | 18% | 21.7 |
| | 12% | 22.4 |
| | | |
| $CuSO_4$-GAC | 20% | 22.0 |
| | 10% | 19.2 |
| | 5% | 17.0 |

The overall shape of the curves is almost the same for all AC samples. A significant rise is shown at 82.5 min in all curves. This is the moment when the gas was switched from argon to $CO_2$ where the adsorption by the AC was taking place. Due to the small volume of the samples tested by TGA, it was noticed that the adsorption was very rapid, followed by a very slight increase in the mass uptake until the end of the test. In addition, some curves were seen to show a mass drop during the first few minutes of the test. This was most probably due to water evaporation from these samples when exposed to a high temperature at the beginning. It should be confirmed here that all samples were kept in the same storage conditions, however, during the test itself, some samples were exposed to air for more time than others.

Apart from the $CuSO_4$ modified samples, most of the modified AC showed higher adsorption capacities than the raw samples. Consistent with the results of the previous techniques for measuring the adsorption capacities, 20% NaOH modified samples exhibited the highest $CO_2$ mass uptake amongst the modified AC samples. The 20% NaOH modified sample showed a capacity of around 30 mg $CO_2$/g AC, which is significantly higher than the 10% and 5% NaOH modified samples. The latter surprisingly exhibited a lower adsorption capacity than those of the raw AC sample itself. All other modified samples exhibited a capacity in the range of 17-24 mg $CO_2$/g AC.

It should be highlighted that the $CuSO_4$ modified samples showed slightly different shapes compared to other examined samples. In a typical run, the curve rose vertically due to $CO_2$ adsorption at 82.5 minutes. Then, the weight was almost constant. However, in the copper modified samples, the curve sloped upwards for a short amount of time followed by a slower adsorption rate until a constant weight was reached. The tests were repeated three times and the curves were almost the same.

The last point to address here is that the values of the adsorption capacities obtained by TGA are noticeably higher than those of the fixed-bed column. This could be attributed to the desorption step carried out by the Argon gas at 100$^{o}$C before applying the $CO_2$ gas. At an elevated temperature, any previously attached molecules are believed to be released from the active sites of AC due to molecule diffusion. This leads to instability of the adsorbed gas on the surface of AC and, consequently, molecules are released (Rashidi et al. 2013). This step was conducted here in TGA before applying the $CO_2$ gas at room temperature, which thus helped the surface of the AC to adsorb a higher quantity of $CO_2$.

### 4.3.4 Comparison and discussion on the adsorption capacity measuring techniques

Table 4.7 and Figure 4.6 display the adsorption capacities of the raw and M-GAC samples obtained by the three measuring techniques: $CO_2$ incubator, fixed-bed column and the TGA. The overall trend is that the adsorption values when using the $CO_2$ incubator are greatly higher than the other two techniques, followed by that of TGA. The adsorption capacities obtained by the fixed-bed column are the least of the three tools. The 20% NaOH M-GAC sample shows almost the highest adsorption capacities among the first-modified samples of 95, 4.98 and 30.4 mg $CO_2$/g AC for $CO_2$ incubator, fixed-bed column and TGA techniques respectively.

Table 4-7: $CO_2$ adsorption capacities of M- GAC using the three different techniques

| Sample | Concentration | $CO_2$ Incubator | Fixed-bed column | TGA |
|---|---|---|---|---|
| | | mg $CO_2$/g AC | | |
| Raw GAC | NA | 45 | 1.97 | 22.1 |
| | | | | |
| NaOH-GAC | 20% | 95 | 4.98 | 30.4 |
| | 10% | 80 | 3.1 | 21.2 |
| | 5% | 61 | 2.9 | 18 |
| | | | | |
| HCl-GAC | 37% | 69 | 3.9 | 23.9 |
| | 19% | 62 | 3.4 | 22.7 |
| | 13% | 60 | 5.2 | 23 |
| | | | | |
| $NH_4OH$-GAC | 35% | 52 | 2.6 | 23.6 |
| | 18% | 48 | 3.9 | 21.7 |
| | 12% | 42 | 1.7 | 22.3 |
| | | | | |
| $CuSO_4$-GAC | 20% | 50 | 3.2 | 22 |
| | 10% | 42 | 2.14 | 19.2 |
| | 5% | 50 | 1.4 | 17 |

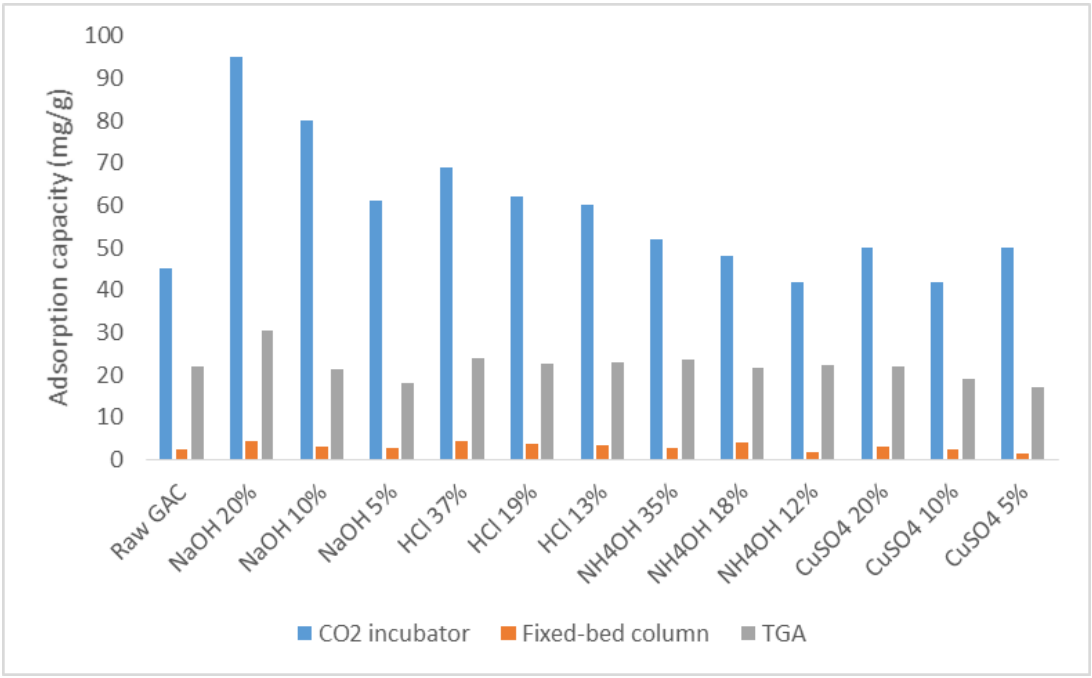


Figure 4-6: $CO_2$ adsorption capacities of M-GAC using the three different techniques

The adsorption capacities of NaOH M-GAC when using the $CO_2$ incubator are higher than other modified samples. The adsorption capacities followed the same order for all tools: 20% > 10% > 5% NaOH modified GAC. This trend was the same for the HCl modified

samples examined by using the $CO_2$ incubator and TGA, but a different order is obtained by the fixed-bed column. For $NH_4OH$ and the $CuSO_4$ modified samples, this consistency between the results was missing. For $NH_4OH$ modified set of samples, the 18% modified sample showed the highest adsorption value using the fixed-bed column while the lowest value was obtained by using the TGA among the $NH_4OH$ samples. The 5% and the 20% $CuSO_4$ modified sample showed the same adsorption value using the $CO_2$ incubator, while the 5% modified sample showed the lowest value when using the TGA and the fixed-bed column.

This inconsistency in the results between the three tools could be due to a variety of reasons. First is the accuracy of the technique itself. The $CO_2$ incubator is believed to be the least accurate method to measure the adsorption capacity because it depends on reading the change in sample weight in a large/not tightly controlled space. The AC samples were kept in the $CO_2$ incubator for a few days while recording the weight every day, until there was no significant change in the weight. The process of taking the samples from the incubator to the balance and returning them back might allow some particles to deposit on the samples from the surrounding air. These particles will change the samples weight while they are not necessarily $CO_2$ molecules. Indeed, inside the $CO_2$ incubator, there is a high probability that other particles might deposit on the AC samples when opening and closing the $CO_2$ incubator door for any reason. This also explains why the $CO_2$ incubator values are much higher than that of TGA and fixed-bed column. In the other two tools, the samples exposure to $CO_2$ gas took place in a closed space. However, both tools resulted in greatly different adsorption capacities. The reason behind this variation might be attributed to the desorption step that proceeded the $CO_2$ application in the TGA assessment tool. In that step, any previously attached particles on the surface of AC were de-attached due to the high temperature, providing more space for the coming $CO_2$ gas molecules. This step resulted in more weight increase in the measured TGA adsorption capacities than in the fixed-bed column values.

A second reason which might be behind the differences in adsorption capacities values is the different operating conditions of the three tools. These include the $CO_2$ flow rate and $CO_2$ concentration. For TGA, the applied gas was of a concentration of 100% $CO_2$, while in the fixed-bed column, the $CO_2$ gas used was 5% $CO_2$ in air. In the $CO_2$ incubator, the maximum allowed $CO_2$ concentration was 20%. The higher the gas concentration, the

higher the gas adsorption in the adsorption systems. This is because of the higher mass-transfer flux from the surrounding gas to the AC surface (Hosseini et al. 2015). In a previous study, the adsorption capacity increased from 0.58 to 4.09 mol/kg when the $CO_2$ concentration increased from 5 to 50% (Hosseini et al. 2015). In addition to concentration, the flow rate is also a crucial parameter. In TGA, the flow rate was 50 ml/min. This allowed more time for the AC to adsorb $CO_2$. In the fixed-bed column, the $CO_2$ flow rate was 200 ml/min, which might be one of the reasons behind the small adsorption capacities measured by the fixed-bed column tool. If a smaller flow rate was used in the fixed-bed column, a higher adsorption capacity would be expected as proved by a previous study. Tan et al. changed the flow rate from 120ml/min to 90 ml/min, and the adsorption capacity increased by 6.8 % from 25.38 mg/g AC to 27.1 mg/g AC (Tan et al. 2014). These reasons explained in this section are applied to all samples examined throughout this study. This includes the first modified GAC samples, the second modified GAC samples and the modified PAC samples.

Based on the findings of the first modification procedure, modification with $CuSO_4 \cdot 5H_2O$ showed to have a slight effect on $CO_2$ adsorption compared to the other modifiers when the modification took place at room temperature. Therefore, this impregnation agent was excluded from the study. Other impregnation agents (NaOH, HCL and $NH_4OH$) underwent a further investigation in the modification process to investigate the possibility of obtaining a higher adsorption capacity while modifying at room temperature.

## 4.4 CHARACTERISATION OF THE SECOND STAGE MODIFIED GAC

This section is centred on the physical and chemical characterisation of second modified GAC. The second modified samples are the samples that were subjected to two steps of modification instead of a single modification step. Based on the adsorption capacities of the first modification stage, a two-steps modification was conducted in the following pattern:

- Modification with 37% HCl followed by modification with 20% NaOH
- Modification with 37% HCl followed by modification with 35% $NH_4OH$

The second modified samples (HCl-NaOH-GAC and HCl-$NH_4$OH-GAC) were characterised using BET and FTIR. These tests provide insights into the texture parameters and the surface chemistry after exposure to two different modifying agents sequentially. The results from these tests are significant in assessing the modification, as well as the subsequent $CO_2$ adsorption capacities of the modified samples. Table 4.8 shows the second-modified samples that were subjected to the characterisation experiments.

Table 4-8: Stage one modification of GAC: Characterisation tests

| **Sample** | **BET** | **FTIR** |
|---|---|---|
| Raw-GAC | √ | √ |
| HCl-NaOH-GAC | √ | √ |
| HCl- $NH_4$OH-GAC | | √ |

### 4.4.1 Physical characterisation

The BET surface area, micropore area and average pore size of HCl-NaOH-GAC and the raw GAC are presented in Table 4.9. The BET surface area of the modified sample significantly decreased by 54% from 887 to 406 $m^2/g$, in which the micropores' area declined by 52% from 604 to 290 $m^2/g$. The micropores' area constitutes around 71% of the modified GAC sample, almost the same as the percentage for raw GAC (68%). whereas the HCl-modification almost didn't change the texture properties of GAC as presented earlier in section 4.2.1, the second step of the modification (NaOH modification) was responsible for the extensive change in the physical structure of the samples. Although the surface area of the second-modified sample is lower than half the surface area of raw GAC, its adsorption capacity, in contrast, is greatly higher, as will be presented in Section 4.5. This might be explained as follows. The HCl treatment resulted in hydroxylic groups on the surface of HCl-modified AC as shown earlier in Figure 4.1. These groups might have provided anchoring sites for the Na species upon the NaOH modification. The newly developed Na sites boosted the $CO_2$ adsorption capacity (Caglayan & Aksoylu 2013), but at the same time agglomerated on the GAC surface, leading to smaller surface area and smaller pore volume. Therefore, treatment with both HCl and NaOH played an important role in increasing the adsorption despite the decrease in the BET. HCl not only washed the surface of raw GAC from impurities and inorganic particles, but also enhance the fixation of Na species provided by the NaOH treatment on GAC surface.

Table 4-9: Texture parameters of the raw and second-modified AC

| **Sample** | **BET surface area** $m^2/g$ | **Micropore area** $m^2/g$ | **Average pore width** nm | **Pore volume** $cm^3/g$ |
|---|---|---|---|---|
| Raw GAC | 887 | 604 | 2.24 | 0.50 |
| HCl-NaOH-GAC | 406 | 290 | 2.28 | 0.23 |

### 4.4.2 FTIR analyses

Figure 4.7 displays the FTIR spectra for the raw GAC, HCl-NaOH-GAC and HCl-$NH_4OH$-GAC samples. The graphs reveal that the second modification changed the chemistry of the GAC structure, creating new functionalities on the GAC surface. Peaks characteristics of the C-H groups located at the edges of the aromatics ring below 800 $cm^{-1}$ were observed in second modified GAC samples. The small bands associated with hydroxylic groups (-OH), observed on the HCl-modified samples as shown earlier in Figure 4.1, diminished. This may confirm the bonding between -OH groups and the species provided by the second modified agents (e.g. Na or NH).

Also, both modified spectra showed peaks in the region of 2360–2340 $cm^{-1}$ which probably correspond to the physisorbed and chemisorbed atmospheric $CO_2$ in the modified samples (Murugan & Bajaj 2010; Rege & Yang 2001). This again implies that the second modified samples might have adsorbed $CO_2$ before being tested by the FTIR.
While the intensive band which appeared in both graphs, around 1400 $cm^{-1}$, might be associated with carboxylates (C=O) functional groups on the surface of HCl-NaOH GAC, or may indicate the formation of amide groups on the surface of HCl-NH4OH-GAC (Socrates 2004; Tan et al. 2014), it also might correspond to the chemisorbed $CO_2$ (Murugan & Bajaj 2010; Rege & Yang 2001).

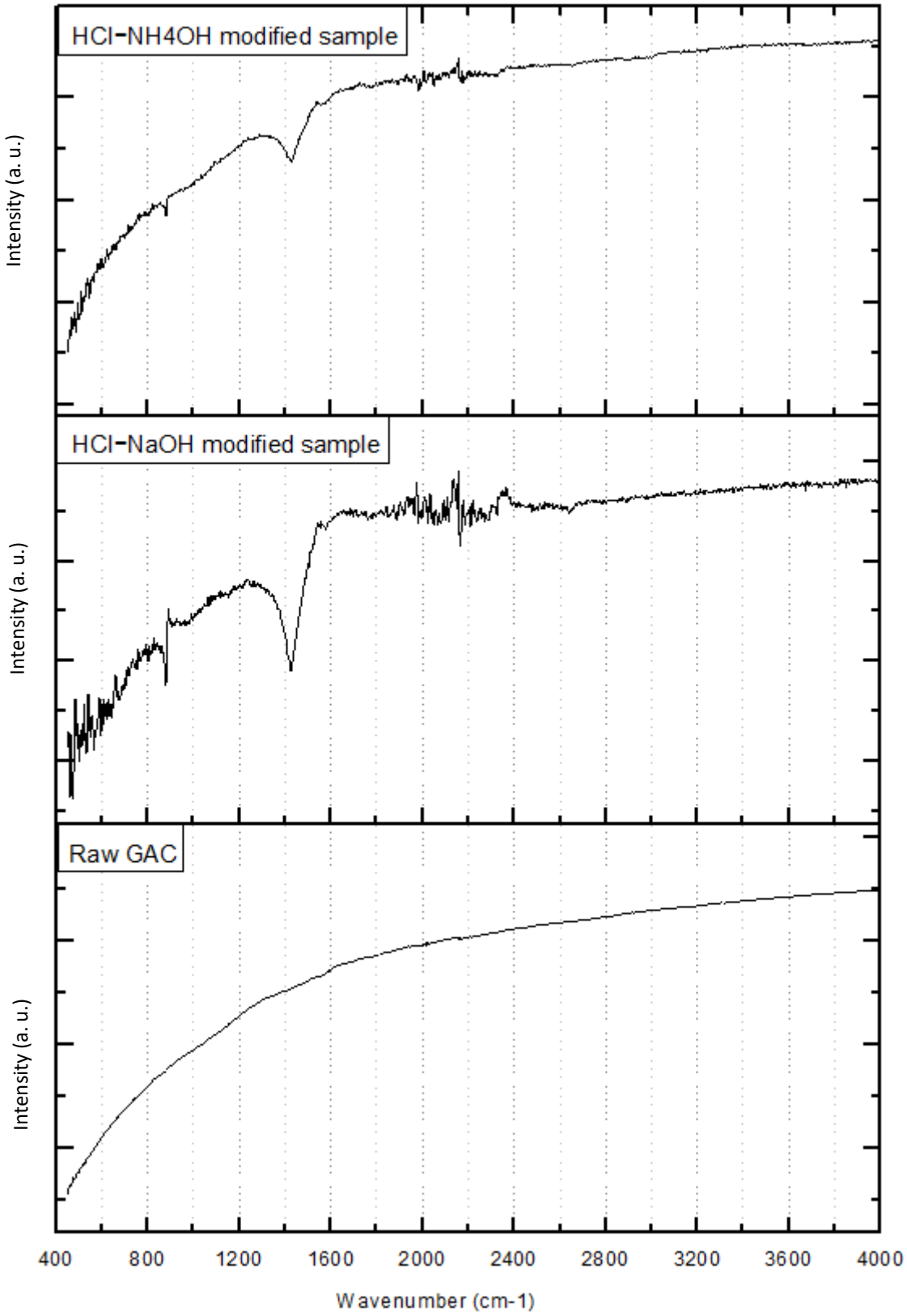


Figure 4-7: FTIR spectra for second-modified GAC samples

## 4.5 QUANTIFICATION OF $CO_2$ ADSORPTION CAPACITIES OF SECOND STAGE MODIFIED SAMPLES

In this section, the results of the $CO_2$ adsorption capacities of the second-modified GAC samples are presented and discussed. The second modification technique considered modifying the raw AC by two chemicals in a row (sequentially). The first impregnation agent was selected to enhance the surface area and the overall physical properties of the AC, while the second modifying agent was chosen to increase the alkalinity of the surface area thus increase the affinity towards $CO_2$ sequestration. The two modified GAC samples are HCl-NaOH-GAC and HCl-NH4OH-GAC. The modified samples were assessed in terms of $CO_2$ adsorption compared to the raw GAC.

### 4.5.1 $CO_2$ incubator environment

The adsorption capacities of the second-modified GACs were examined using a $CO_2$ incubator following the same procedures mentioned in the first modification stage. However, in the first stage, the samples were kept with only 20% $CO_2$ environment. Here in this stage, the experiments were conducted three different times under 3 different $CO_2$ concentrations; 5%, 10% and 20% for further investigation. Table 4.10, Figure 4.8 and Figure 4.9 show the $CO_2$ adsorption capacities of the raw and second-modified GAC samples under 5%, 10% and 20% $CO_2$ concentrations. The values in the table and the figure are the average of three examined AC samples where the standard deviation for each value is shown in brackets.

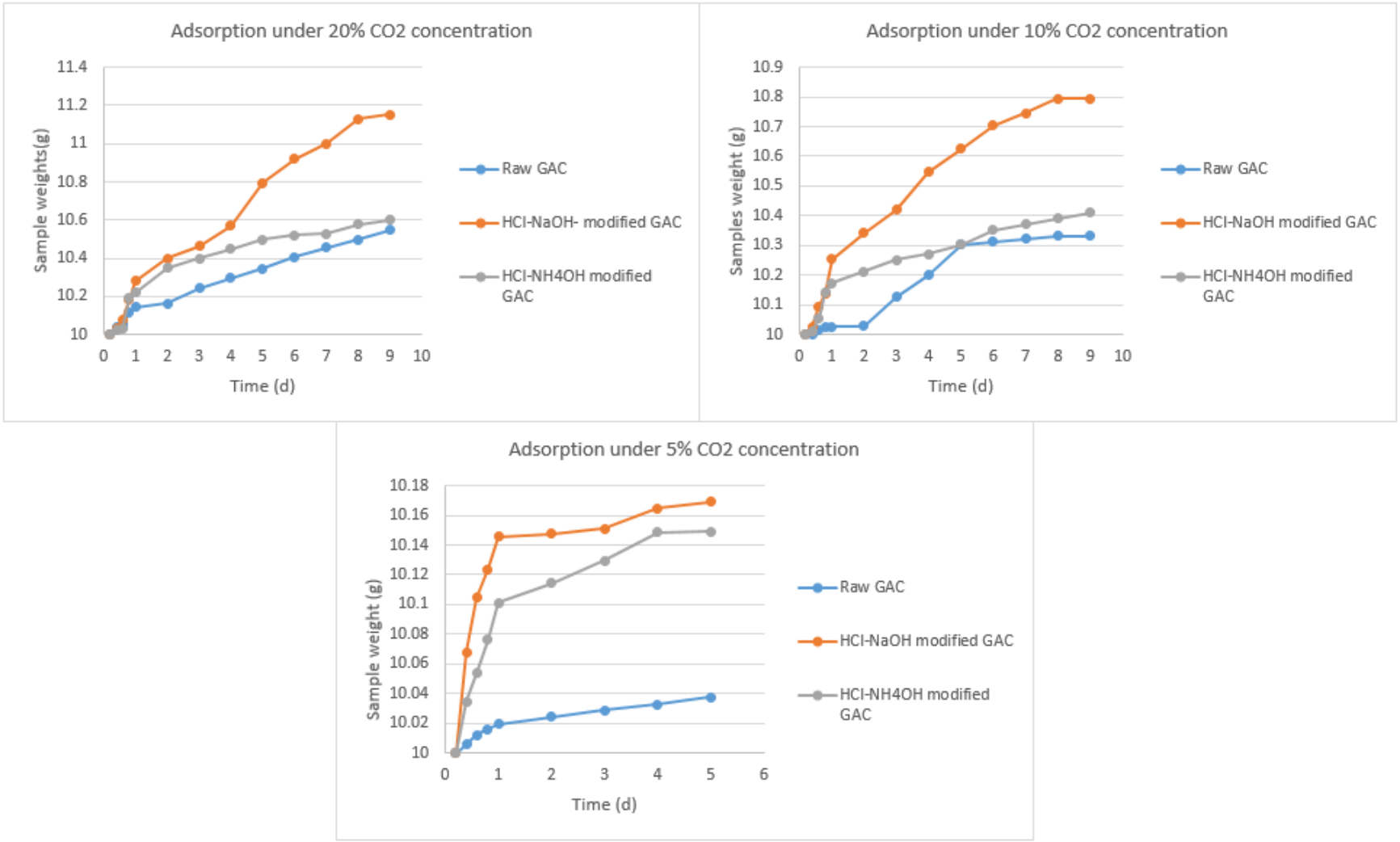


Figure 4-8: Adsorption capacity of second-modified GAC samples under 20%, 10% and 5% $CO_2$ environments

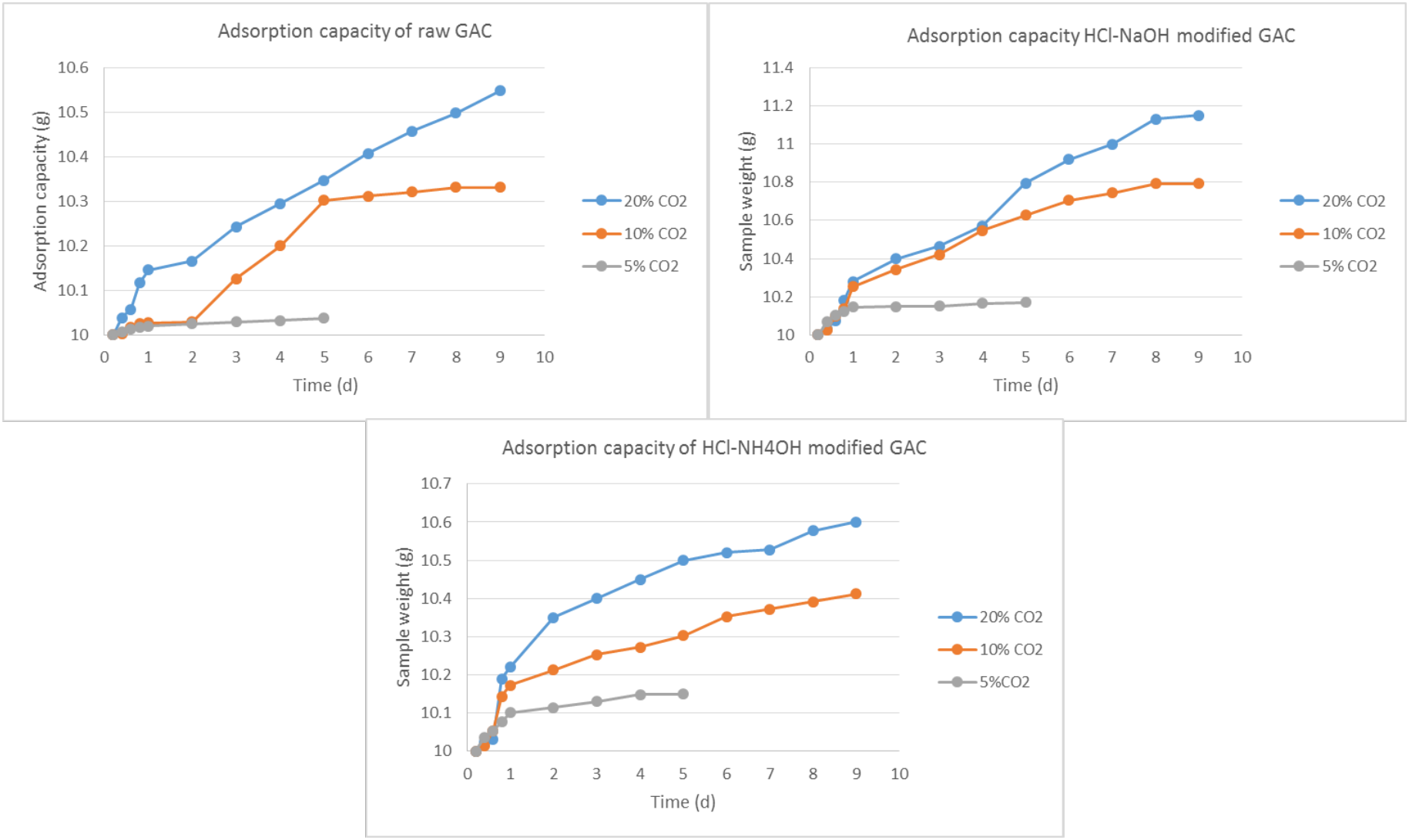


Figure 4-9: Adsorption capacities of second-modified GAC samples for each sample individually

Table 4-10: Adsorption capacities of second modified-GAC

| | Adsorption capacity (mg $CO_2$/g AC) | | |
|---|---|---|---|
| **Sample** | **20%** | **10%** | **5%** |
| Raw GAC | 55 (5.1) | 33 (4.6) | 4 (1.7) |
| HCL-NaOH-GAC | 115 (6.8) | 79 (7.1) | 17 (3.5) |
| HCl-$NH_4$OH-GAC | 60 (6.3) | 41 (4.8) | 15 (3.0) |

- Numbers in brackets are the standard deviation of three samples

While Figure 4.8 compares the three examined samples under one $CO_2$ concentration in each graph, Figure 4.9 shows the behaviour of each sample individually under different $CO_2$ surroundings. From the graphs, it can be seen that the three samples showed a higher adsorption rate when kept in a 20% $CO_2$ environment in comparison to the 10% and 5% $CO_2$ environment. This confirms the importance of the surrounding environment on adsorption. The higher the percentage of $CO_2$ in the atmosphere, the higher the amount of $CO_2$ adsorbed by the AC. This is because of the higher mass-transfer flux from the surrounding gas to the AC surface (Hosseini et al. 2015).

Another considerable point is the time it took the GAC samples in 5% $CO_2$ environment to reach the equilibrium. For the other two environments, the increase in the sample weight lasted for 9 days. However, for the 5% $CO_2$ incubator, this time was considerably shorter (5 days). The lower amount of $CO_2$ molecules surrounding the AC surface decreased the probability of high adsorption. Studies pertaining to the $CO_2$ adsorption often use highly concentrated gas as the adsorption rate is increased by ambient $CO_2$ concentration.

The adsorption capacities obtained using the $CO_2$ incubator showed a high variation from the average values as indicated by the standard deviation. The 5% $CO_2$ environment showed the highest variation of the standard deviation from the average values, which implies the unsuitability of this technique under low $CO_2$ concentration (coefficient of variation was more than 40% in raw GAC case).

Table 4.11 shows the improvement percentages of each sample relative to the raw GAC. The adsorption capacities of HCl-NaOH-GAC samples under different $CO_2$ environments show great enhancement compared to that of HCl-$NH_4$OH-GAC samples. The performance of the latter is in agreement with previous reported findings on aqueous ammonia and amines absorption, in which the processes required high pressure and a high

concentration of $CO_2$ to achieve high levels of adsorption (Plaza et al. 2010; Radosz et al. 2008; Dave et al. 2009).

Table 4-11: Adsorption capacity improvements by second-modification

| | Improvement in adsorption % | | |
|---|---|---|---|
| **Sample** | **20%** | **10%** | **5%** |
| HCl-NaOH-GAC | 109 | 139 | 325 |
| HCl-$NH_4$OH-GAC | 9 | 24 | 275 |

Another point to highlight is that raw AC was tested again in the $CO_2$ incubator along with the second-modified GAC samples to keep all the samples under the same operating conditions (concentration, humidity and temperature). The adsorption capacity was 55 mg $CO_2$/g AC in this round compared to 45 mg $CO_2$/g AC in the previous section in a 20% $CO_2$ environment. This difference in capacities reflects the inaccuracy of the $CO_2$ incubator as an assessment technique for the adsorption capacity.

### 4.5.2 Fixed-bed column environment

The fixed-bed column was used to measure the $CO_2$ adsorption capacity of the second-modified samples: (HCl-$NH_4$OH) and (HCl-NaOH) modified GAC. The same procedure was followed in this stage as was done in the single modification stage. Figure 4.10 shows the concentrations at the outlet of the fixed-bed column measured by a 5% $CO_2$ sensor. The graph of the raw GAC is not included in this Figure (as it was shown earlier in Figure 4.4), but the values for its $CO_2$ adsorption and the time to saturation are shown in Table 4.12.

The HCl-NaOH-GAC sample, as shown in the Figure 4.10 takes the longest time to reach saturation out of the whole set of the assessed samples (first and second). The corresponding adsorption capacity is 8.72 mg $CO_2$/g AC, which is more than four times the capacity of raw GAC. The adsorption capacity of the HCl-$NH_4$OH-GAC sample is 3.89 mg/g AC which is approximately double the capacity of the raw GAC. Both modified samples achieved high improvement percentages compared to the raw sample.

The higher capacity of the HCl-NaOH sample might be explained by the strong effect of HCl acid in removing any volatile material, followed by the existence of sodium molecules

on the surface of the NaOH-HCl modified sample. The adsorption capacity of the HCl-$NH_4OH$ modified sample is almost the same as the adsorption capacity of the 13% $NH_4OH$ modified samples in the first modification stage. This implies that the second modification by HCl-$NH_4OH$ did not benefit the GAC as was expected.

Table 4-12: Adsorption capacity and time to saturation for second-modification by fixed-bed column

| Sample | Time to saturation (min) | Adsorption Capacity (mg/g) | Improvement in adsorption (%) |
|---|---|---|---|
| Raw-GAC | 2.99 | 1.97 (0.09) | - |
| HCl-NaOH-GAC | 10.68 | 8.72 (0.55) | 343 |
| HCl-$NH_4OH$-GAC | 5.20 | 3.89 (0.32) | 97 |

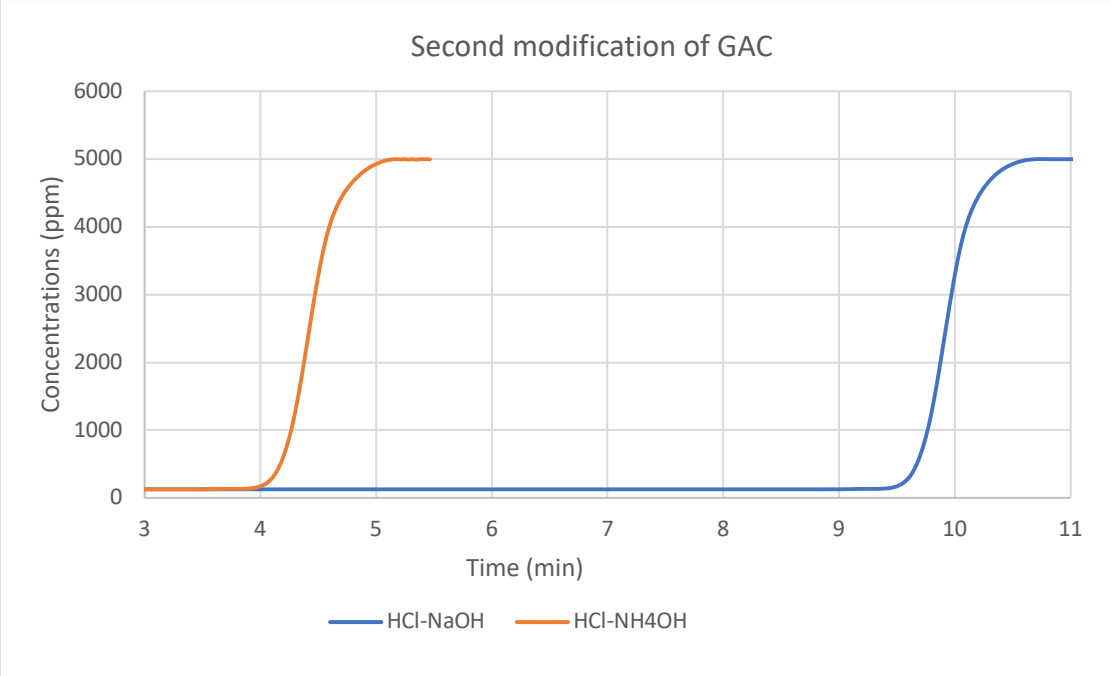


Figure 4-10: Adsorption capacities of second-modified GAC by $CO_2$ sensor

### 4.5.3 Thermogravimetric analysis

The third technique to measure the $CO_2$ adsorption capacity of the second-modified GAC was the TGA. Figure 4.11 shows the change in the samples' weight with time. As illustrated earlier, the argon gas was applied in the first 82.5 min, after which it was switched to $CO_2$. The adsorption capacities of unmodified AC, HCl-$NH_4OH$-GAC and the HCl-NaOH-GAC samples along with the improvement percentages compared to raw GAC adsorption are presented in Table 4.13.

The HCl-NaOH-GAC samples exhibited a higher adsorption capacity compared to raw GAC with an improvement in adsorption of 123%. In contrast, the adsorption capacity of the HCl-$NH_4OH$-GAC was almost the same as the unmodified samples. This is consistent with the results of the $CO_2$ incubator presented in the previous section. Moreover, the shape of the HCl-NaOH curve is noticeably different from the typical curve shape obtained from the TGA. In a typical run, the sudden rise in the curve at 82.5 min was followed by a relatively constant weight until the end of the experiment. In contrast, the HCl-NaOH-GAC sample provided an increasing curve after 82.5 min. The test was repeated three times, but the resulting curves were the same. The higher adsorption capacity of HCl-NaOH obtained by TGA is in agreement with the capacity demonstrated by the fixed-bed column.

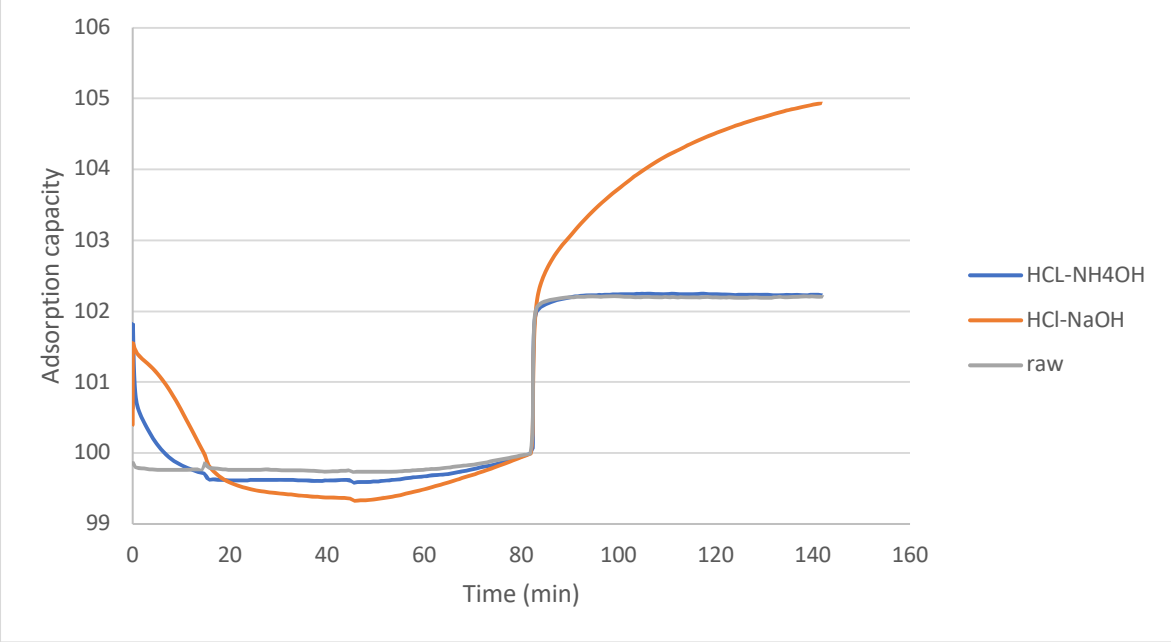


Figure 4-11: adsorption capacities of second-modified samples by TGA

Table 4-13: Adsorption capacities and adsorption percentage for second modified samples by TGA

| Sample | Adsorption Capacity (mg/g) | Improvement in adsorption (%) |
|---|---|---|
| Raw-GAC | 22.1 | - |
| HCl-NaOH-GAC | 49.4 (3.1) | 123.5 |
| HCl-$NH_4OH$-GAC | 22.5 | 1.8 |

Based on the findings of the $CO_2$ adsorption capacities of M-GAC samples, the second modification by HCl followed by NaOH demonstrated the highest $CO_2$ adsorption capacity which ranks it as the best modification technique among the examined approaches in

terms of $CO_2$ adsorption. Therefore, the powder activated carbon (PAC) directly underwent the same technique of modification in order to maximise its $CO_2$ adsorption capacity.

### 4.5.4 Comparison of the adsorption capacities by different measuring techniques

Table 4.14 and Figure 4.12 show the adsorption capacity of raw and second modified GAC obtained by the three techniques to measure the $CO_2$ adsorption capacity.

Table 4-14: $CO_2$ adsorption capacities of modified GAC by the three different techniques

| Modifying Agent | $CO_2$ Incubator | Fixed-bed column | TGA |
|---|---|---|---|
| | mg $CO_2$/g AC | | |
| Raw GAC | 55 | 1.97 | 22.1 |
| HCl-NaOH-GAC | 115 | 8.72 | 49.4 |
| HCl-$NH_4$OH-GAC | 60 | 3.89 | 22.5 |

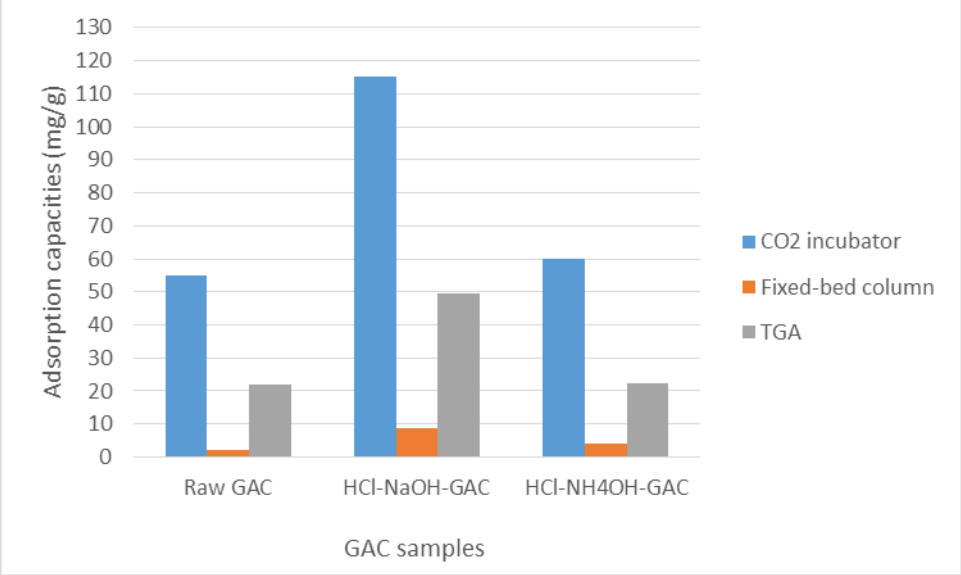


Figure 4-12: Adsorption capacities of second-modified GACs by the three techniques

Similar to adsorption capacities of the first modified GAC samples, the values obtained by the $CO_2$ incubator were greatly higher than those measured by the fixed-bed column and the TGA techniques. HCl-NaOH modified GAC demonstrated higher adsorption capacity values among the three techniques of measurement. The HCl-$NH_4$OH modified sample showed a slight increase in the adsorption capacity compared to the raw GAC, however, compared to the results of the $NH_4$OH modified sample presented earlier, in the first modification stage, there is almost no enhancement in the $CO_2$ capacity.

Two-step modification using HCl and NaOH exhibited a better approach in terms of $CO_2$ adsorption than the single modification approach. This is because of the HCl effect on the GAC surface, which included a reduction in the impurities in the pore systems of GAC. Moreover, it provided hydroxylic groups working as anchoring sites for the next treatment of NaOH. The Na species, anchored on the surface of the HCl-GAC, increased the $CO_2$ adsorption capacity to a higher extent.

Based on the findings of the adsorption capacities and the enhancement in the adsorption which ranged, depending on the assessment techniques, from 100% to more than 300% in the HCl-NaOH modification, this approach will be applied to the powder AC, and will be presented in the next section.

## 4.6 CHARACTERISATION OF MODIFIED POWDER ACTIVATED CARBON

This section addresses the chemical and physical characterisation of the modified powder activated carbon (PAC) in comparison to the raw PAC. The modification technique that achieved the highest $CO_2$ adsorption capacity for the GAC was applied directly to PAC without repeating the whole process of modification.

Characterisation of raw and modified PAC was carried out using BET, FTIR and SEM to investigate the effect of modification on PAC. Although the same modification technique was applied on both GAC and PAC, variations in the initial precursor of the AC or the preparation and activation approaches may change the responses of both GAC and PAC to modification. Therefore, these tests would provide a better understanding on a microstructural level to the modified PAC. Table 4.15 shows the modified samples that were subjected to the characterisation experiments.

Table 4-15: Stage one modification of PAC: Characterisation tests

| **Sample** | **BET** | **FTIR** | **SEM** |
|---|---|---|---|
| Raw PAC | √ | √ | √ |
| HCl-NaOH-PAC | √ | √ | √ |

### 4.6.1 Physical characterisation

The measured BET surface area, micropore area and average pore size of raw and modified PAC are presented in Table 4.16. The texture parameters experiment of these two samples was conducted in the Department of Materials Science-University of Cambridge.

Table 4-16: Texture parameters of raw and some modified AC

| **Sample** | **BET surface area** $m^2/g$ | **Micropore area** $m^2/g$ | **Average pore width** nm | **Pore volume** $cm^3/g$ |
|---|---|---|---|---|
| Raw PAC | 632 | - | 3.06 | 0.48 |
| HCl-NaOH-PAC | 112 | - | 3.85 | 0.11 |

The surface area of the HCl-NaOH-PAC is 112 $m^2/g$, with a severe reduction of more than 80% from the raw PAC area. Moreover, the measured BET surface area was 632 $m^2/g$ compared to 800 $m^2/g$, provided by the supplier. There was no provided information about the micropore area of both samples. The reduction in BET area in PAC samples was more intensive than that of GAC samples. This could be explained by the variation in the average pore width between the GAC and PAC samples, where PAC has a higher average pore width than GAC (3.06 compared to 2.28). The wider pores may allow for accumulation and trapping of a higher quantity of Na species in PAC than in GAC upon NaOH treatment. This resulted in a development of a lower surface area in the modified PAC samples combined with creating wider pores in the surface structure.

### 4.6.2 FTIR analyses

Figure 4.13 displays the FTIR spectra for raw and modified PAC samples. The spectra show some changes in the FTIR of the modified PAC compared to that of raw PAC, indicating that the modification with HCl and NaOH incorporated new functionalities on the surface of the modified PAC. The FTIR spectra shown in Figure 4.13 is very similar to the modified GAC samples shown in Figure 4.7, but the effect here is less intensive.

The samples show a small characteristic aromatic C=C peak at approximately 1590 $cm^{-1}$, as well as out of plane aromatic –CH peaks at lower than 800 $cm^{-1}$ (Tan et al. 2016; Wang et al. 2015). The distinct strong peak at around 1400 $cm^{-1}$ might be attributed to the

presence of some carboxylates (C=O) (Tan et al. 2014), or it may correspond to the chemisorbed $CO_2$ on the modified PAC (Murugan & Bajaj 2010; Rege & Yang 2001).

The variations in the FTIR spectra between raw and modified PAC, might be the reason behind the higher $CO_2$ adsorption capacity of the modified PAC samples compared to the unmodified one, as will presented in Section 4.7. This implies that the $CO_2$ adsorption on AC was mostly chemical adsorption.

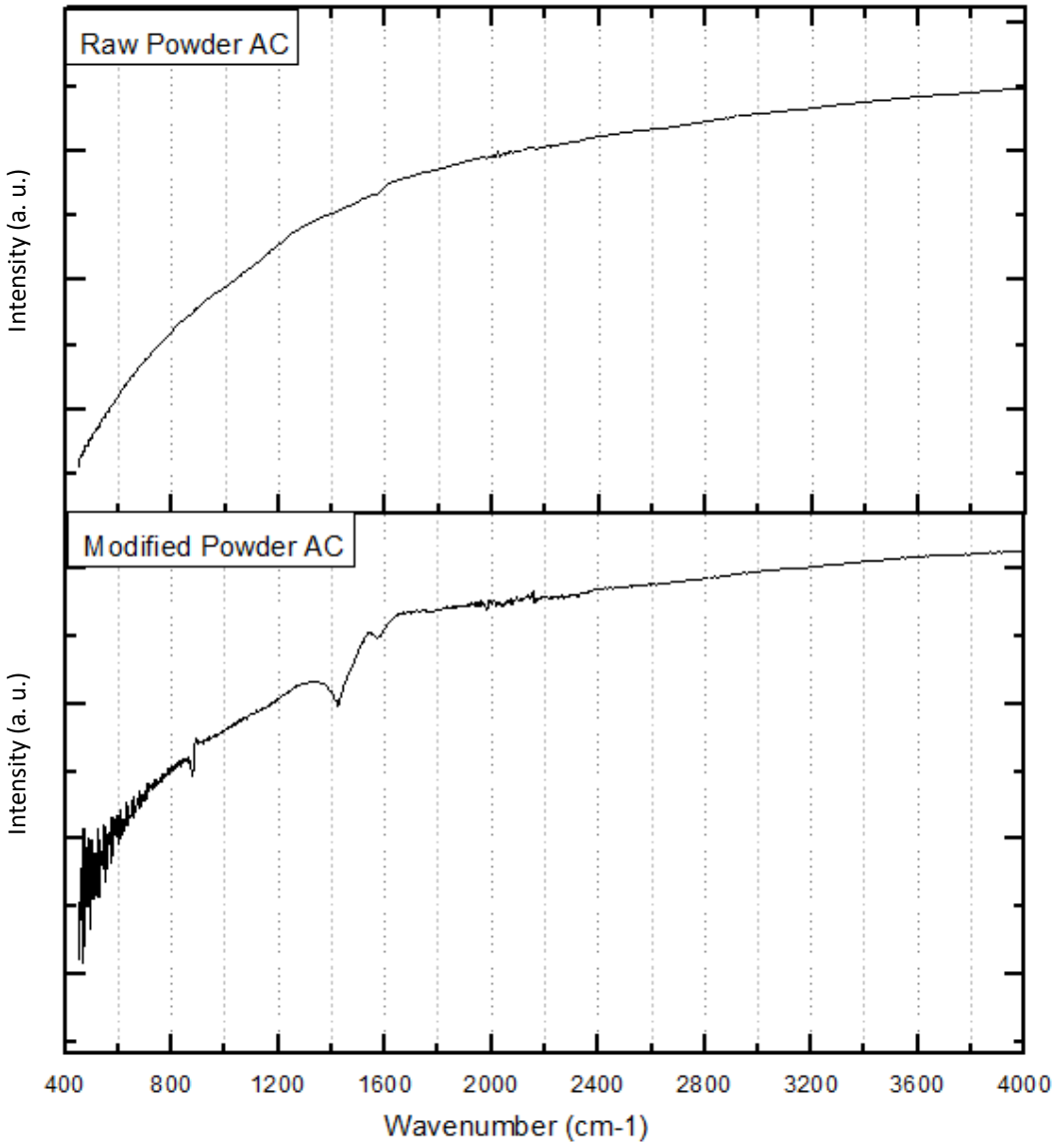


Figure 4-13: FTIR spectra of the raw and modified PAC

### 4.6.3 SEM

Figure 4.14 shows the SEM images of the raw and modified PAC. The morphological structure demonstrates the intensively rich porous structure of PAC before and after applying the modification. Both samples show highly cracked surfaces with distinct pore size. Modified PAC shows agglomeration of white particles that might be attributed to carbonated species due to residual NaOH after the treatment.

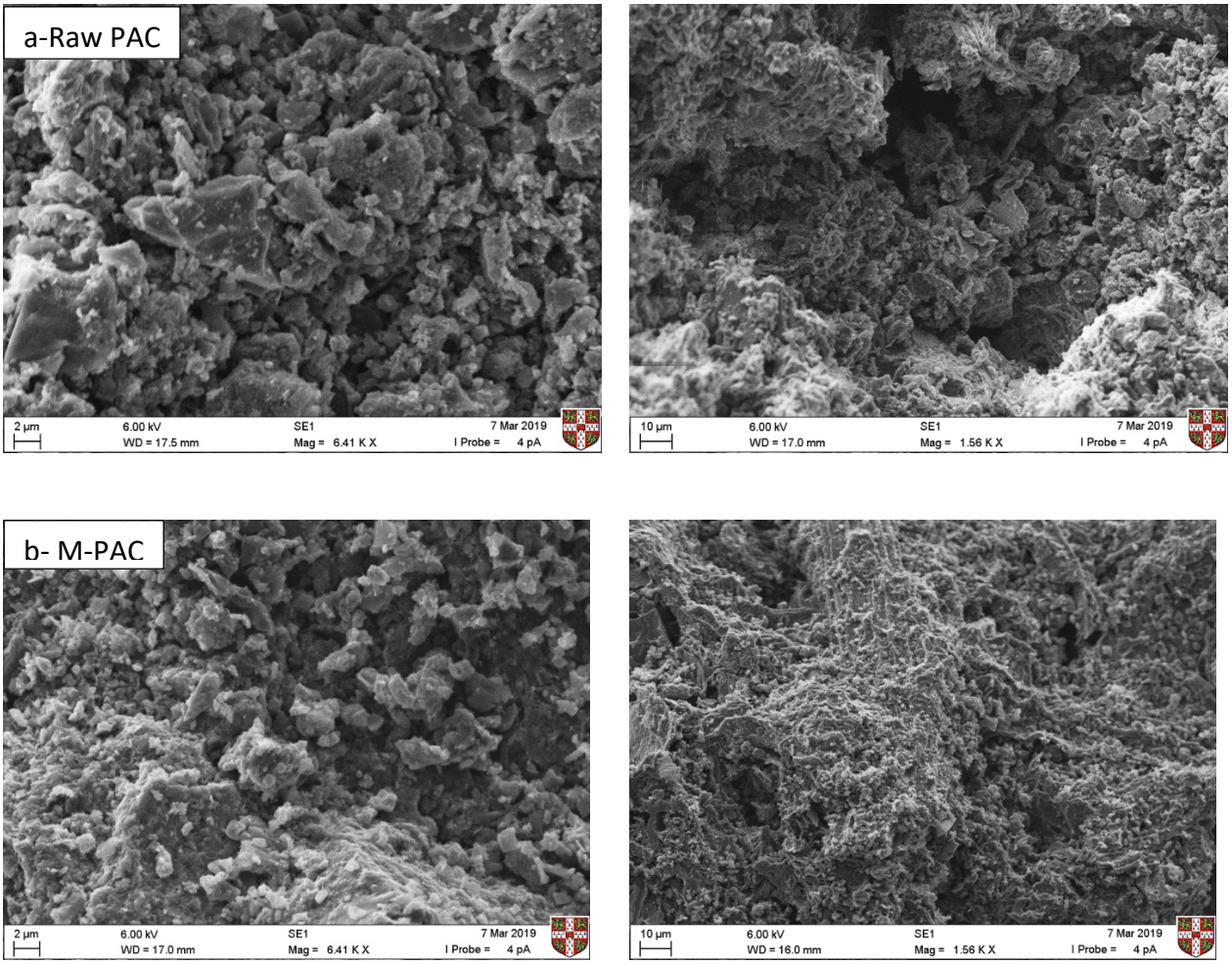


Figure 4-14: SEM images of (a) the raw and (b) modified PAC using two stage magnification

## 4.7 QUANTIFICATION OF $CO_2$ ADSORPTION CAPACITIES OF MODIFIED PAC

### 4.7.1 $CO_2$ incubator environment

The raw and modified PAC was kept in the $CO_2$ incubator for 7 days. The change in the samples weight with time for the modified samples compared to the raw PAC is shown in Figure 4.15. The adsorption capacities (calculated as the difference between the initial and final weight of the AC sample after a certain duration of time) are shown in Table 4.17.

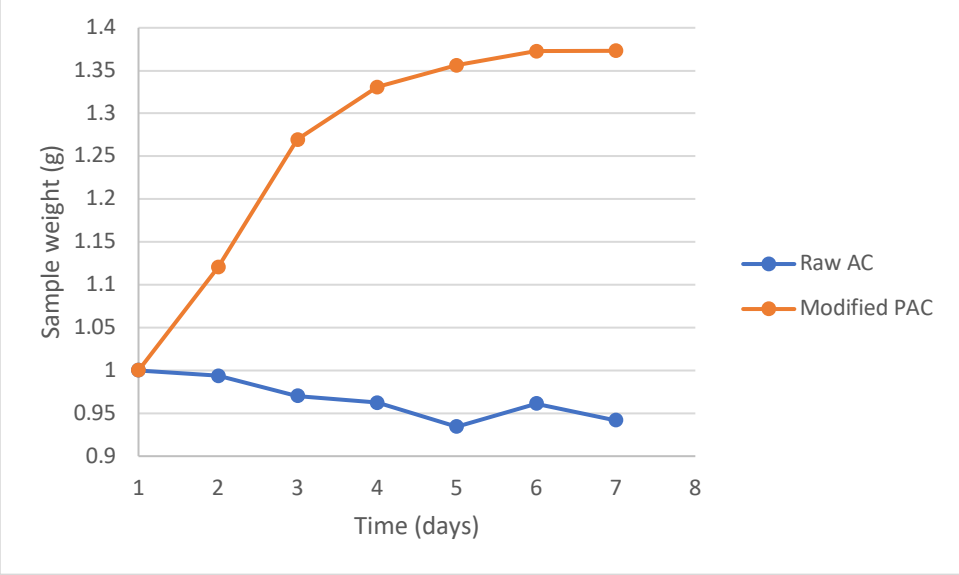


Figure 4-15: Adsorption capacity of raw and modified AC using a $CO_2$ incubator

Table 4-17: $CO_2$ adsorption capacity of raw and modified AC using a $CO_2$ incubator

| Sample | Adsorption (mg $CO_2$/g AC) |
|---|---|
| Raw PAC | -58 (9.3) |
| M-PAC | 373 (15.2) |

- Values in brackets are the standard deviation of three samples

The loss of weight for the raw material could be explained as a release of the very light powder of the AC samples either during taking the samples out of the incubator for taking records of the weight or while they were in the $CO_2$ incubator. The HCl-NaOH modified PAC gained a significant amount of weight, mostly during the first two days. This was followed by a lower rate of increase with time until almost no change in the weight after 6 days in the $CO_2$ incubator. All the $CO_2$ incubator tests were performed in triplicate, and all the raw PAC samples showed a mass loss with time.

### 4.7.2 Fixed-bed column environment

The fixed-bed column was used to assess the $CO_2$ adsorption capacity of the raw and modified PAC samples. Figure 4.16 and Table 4.18 show the concentrations at the outlet of the fixed-bed column for the raw and modified PAC samples.

The adsorption capacities of PAC are significantly higher than that of GAC. While raw GAC demonstrated an adsorption capacity of 1.97, the raw PAC samples showed a capacity of 17.18 mg $CO_2$/g PAC, and the modified PAC showed a capacity of 24.17 mg $CO_2$/g PAC.

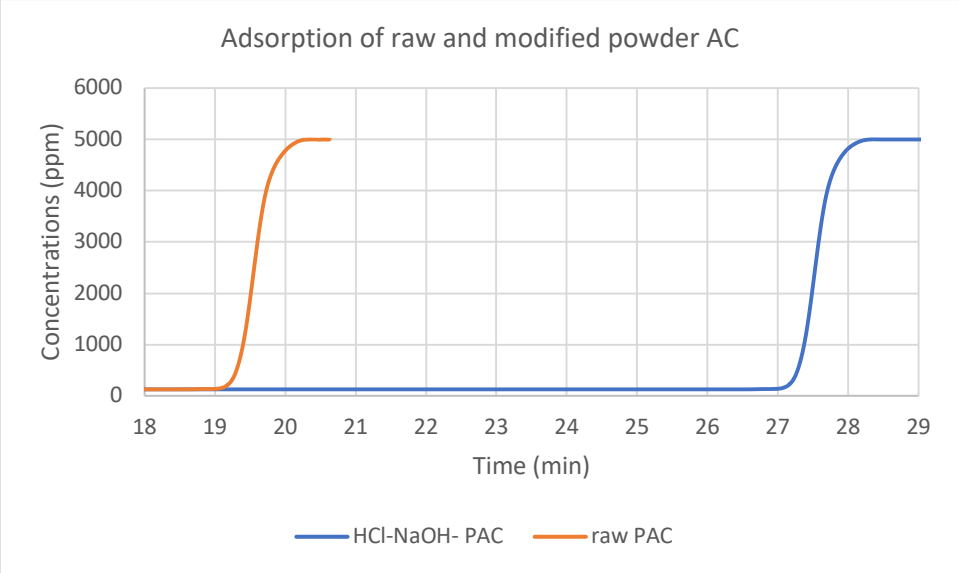


Figure 4-16: Adsorption capacity of raw and modified PAC using fixed-bed column

Table 4-18: $CO_2$ adsorption capacity of raw and modified PAC using fixed-bed column

| Sample | Adsorption (mg $CO_2$/g AC) | Improvement percentage % |
|---|---|---|
| Raw APC | 17.18 (1.5) | - |
| M-PAC | 24.17 (2.6) | 40.7 |

### 4.7.3 Thermogravimetric analysis

TGA was used to measure the $CO_2$ adsorption capacity of both raw and PAC. Figure 4.17 and Table 4.19 show the change in mass and the adsorption capacities respectively.

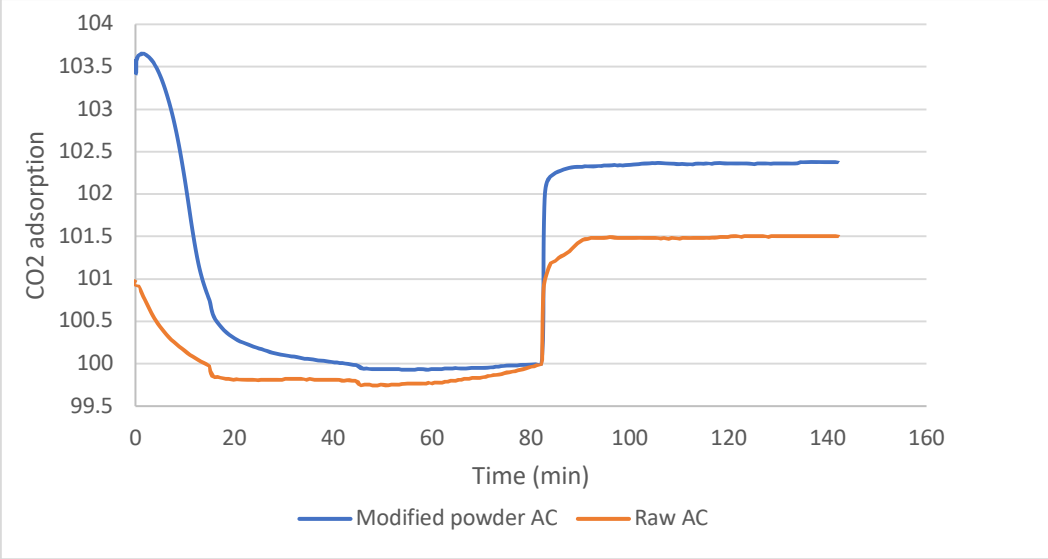


Figure 4-17: Adsorption capacity of the raw and modified powder AC using TGA

The modified PAC sample showed a higher adsorption capacity of around 58% compared to the raw sample. This value is relatively close to the improvement achieved using the fixed-bed column tool, but greatly different from the very high value measured using the $CO_2$ incubator technique. In addition, the adsorption capacity of the modified PAC is noticeably lower than that of the modified GAC that underwent the same modification (HCl-NaOH).

Table 4-19: Adsorption capacities of raw and modified PAC using TGA

| Sample | Adsorption (mg $CO_2$/g AC) | Improvement percentage % |
|---|---|---|
| Raw PAC | 15.04 | - |
| M-PAC | 23.88 | 58.8 |

### 4.7.4 Comparison of the adsorption capacities by different measuring techniques

Table 4.20 and Figure 4.18 display the adsorption capacities of the raw and modified PAC samples using the $CO_2$ incubator, the Fixed-bed column and TGA. The modified PAC examined by the $CO_2$ incubator showed a drastically high value. The table shows the relatively similar values obtained by TGA and fixed-bed column in contrast to the GAC values presented earlier in Table 4.7. This confirms the proposed explanation presented in Section 4.7.2 about the effect of the fineness of PAC on the fixed-bed column results. Therefore, to get an accurate measurement of the adsorption capacity by fixed-bed

column, an inert material with the same fineness as PAC should be examined using the same setup and under the same operation conditions. The difference between the two values might be considered as the actual adsorption capacity of PAC. However, for a comparison purpose only, the modified PAC showed a significantly higher adsorption value than the raw PAC, which emphasises the role that the HCl-NaOH modification plays to enhance the $CO_2$ adsorption.

Table 4-20: $CO_2$ adsorption capacities of modified PAC by the three different techniques

| **Sample** | **$CO_2$ Incubator** | **Fixed-bed column** | **TGA** |
|---|---|---|---|
| | mg $CO_2$/g AC | | |
| Raw PAC | 0 | 17.18 | 15.04 |
| M-PAC | 373 | 24.17 | 23.88 |
| Improvement % | NA | 40.7 | 58.8 |

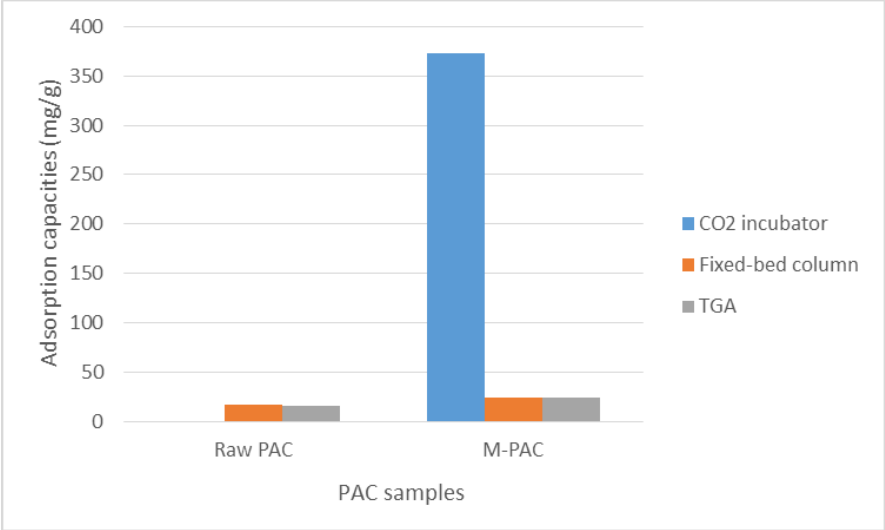


Figure 4-18: $CO_2$ adsorption capacities of raw and M- PAC by the three different techniques

## 4.8 DISCUSSION

This section presents further investigation and discussion on the three techniques of measuring $CO_2$ adsorption capacities. This is followed by a discussion on the effect of the implemented modification on AC samples and the corresponding adsorption capacities.

In sections 4.3.4, 4.5.4 and 4.7.4, a comparison of the results of $CO_2$ adsorption using the three different techniques for the whole set of the modified samples was presented. A detailed discussion in Section 4.3.4 on the potential reasons behind the variations within

the results was provided. Further investigation into the consistency of the results is presented here.

Table 4.21 shows the ratios of the adsorption capacities obtained by (a) the $CO_2$ incubator to those by fixed-bed column, (b) the TGA to the fixed-bed column and (c) the $CO_2$ incubator to the TGA.

Table 4-21: Ratios of adsorption capacities values by different techniques

| Sample | $CO_2$ incubator/ Fixed-bed column | TGA/Fixed-bed column | $CO_2$ incubator/ TGA |
|---|---|---|---|
| Raw | 22.8 | 11.2 | 2.0 |
| | | | |
| 20%NaOH-GAC | 19.1 | 6.1 | 3.1 |
| 10%NaOH-GAC | 25.8 | 6.8 | 3.8 |
| 5%NaOH-GAC | 21.0 | 6.2 | 3.4 |
| | | | |
| 37% HCl-GAC | 17.7 | 6.1 | 2.9 |
| 19% HCl-GAC | 18.2 | 6.7 | 2.7 |
| 13% HCl-GAC | 11.5 | 4.4 | 2.6 |
| | | | |
| 35% $NH_4OH$-GAC | 20.0 | 9.1 | 2.2 |
| 18% $NH_4OH$-GAC | 12.3 | 5.6 | 2.2 |
| 12% $NH_4OH$-GAC | 24.7 | 13.1 | 1.9 |
| | | | |
| 20% $CuSO_4$ -GAC | 15.6 | 6.9 | 2.3 |
| 10% $CuSO_4$ -GAC | 19.6 | 9.0 | 2.2 |
| 5% $CuSO_4$ -GAC | 35.7 | 12.1 | 2.9 |
| | | | |
| HCl-NaOH-GAC | 13.2 | 5.7 | 2.3 |
| HCl-$NH_4OH$-GAC | 15.4 | 5.8 | 2.7 |
| | | | |
| Raw PAC | 0 | 0.9 | 0 |
| HCl-NaOH-PAC | 15.4 | 1.0 | 15.6 |

In order to qualify as systematic findings, the ratios in each column should be equal to or in a limited range. However, the values across the different modification techniques studied varied greatly. In the first column, which presents the ratios of the adsorption capacities by the $CO_2$ incubator to those of the fixed-bed setup, the ratios ranged widely from 11.5 to 35.7. Even within each set of concentrations for one impregnation agent, the ratios differ significantly. This indicates a lower level of consistency in relation to either

the $CO_2$ incubator or the fixed-bed column as measuring techniques for the $CO_2$ adsorption capacities.

The second column shows the ratios between the adsorption capacities obtained by TGA to those obtained by the fixed-bed column. The range of ratios is 4.4 to 13.1 for the M-GAC samples and 0.9 to 1.0 for the M-PAC samples. In spite of the wide range of values, there was some consistency exists within the NaOH set and the second-modified samples. The M-PAC ratios, for example, showed similar values. However, they are not considered as representative samples of the whole examined set of M-GAC and M-PAC since they are only two samples.

In the last column, the ratios of the adsorption capacities when using the $CO_2$ incubator to those obtained by the TGA are presented. The values are in the range of 1.9 to 3.8 for M-GAC. The ratios within each set of concentrations are significantly closer which implies a higher level of consistency in the results. Both the second and the third columns of Table 4.21 show some consistency in the results. This comparison implies that the TGA is the most accurate among the three measuring techniques.

Another approach used to compare the results of the three techniques is to investigate the ratios of the adsorption capacities of each modified sample to that of the raw AC. In Table 4.22, the ratios between modified samples capacities (individually) to the raw sample capacity are presented. If the three techniques were consistent, the values of each row would be the same or within a limited range. The adsorption capacity of each modified sample compared to that of the raw sample measured by any technique should be the same.

Table 4-22: Ratios of adsorption capacities of modified samples to raw samples

| Sample | $(M/R)_{incubator}$ | $(M/R)_{fixed-column}$ | $(M/R)_{TGA}$ |
|---|---|---|---|
| 20%NaOH-GAC | 2.11 | 2.53 | 1.38 |
| 10%NaOH-GAC | 1.78 | 1.57 | 0.96 |
| 5%NaOH-GAC | 1.36 | 1.47 | 0.81 |
| | | | |
| 37% HCl-GAC | 1.53 | 1.98 | 1.08 |

| | | | |
|---|---|---|---|
| 19% HCl-GAC | 1.38 | 1.73 | 1.03 |
| 13% HCl-GAC | 1.33 | 2.64 | 1.04 |
| | | | |
| 35% $NH_4OH$-GAC | 1.16 | 1.32 | 1.07 |
| 18% $NH_4OH$-GAC | 1.07 | 1.98 | 0.98 |
| 12% $NH_4OH$-GAC | 0.93 | 0.86 | 1.01 |
| | | | |
| 20% $CuSO_4$ -GAC | 1.11 | 1.62 | 1.00 |
| 10% $CuSO_4$ -GAC | 0.93 | 1.09 | 0.87 |
| 5% $CuSO_4$ -GAC | 1.11 | 0.71 | 0.77 |
| | | | |
| HCl-NaOH-GAC | 2.09 | 4.43 | 2.24 |
| HCl-$NH_4OH$-GAC | 1.09 | 1.97 | 1.02 |
| | | | |
| HCl-NaOH-PAC | - | 1.41 | 1.59 |

However, overall, the ratios within each row vary greatly. For example, for 20% NaOH M-GAC, the ratio ranges from 1.38 when using TGA, the most accurate technique, to 2.53 when using the fixed-bed column. However, the ratios are almost the same for the 35% $NH_4OH$ pure sample, the 12% $NH_4OH$ modified sample and the 10% $CuSO_4$ modified sample. This demonstrates that the three techniques of assessment do not yield the same level of accuracy; however, they all indicated that the conducted modification increased the $CO_2$ adsorption capacity of both forms of AC.

The second point to address here is the correlation between the adsorption capacities and the texture parameters of modified GAC and PAC. High surface area and high pore volume are essential parameters for $CO_2$ physisorption. The greater the surface area, the more room is available for carbon dioxide molecules to be adsorbed on the surface of the AC. In the current results, the surface areas for all examined samples (raw and modified) are relatively higher than those documented in the literature. This indicates that the observed $CO_2$ adsorption was partially due to the physical adsorption that took place on the AC surface. However, the correlation between surface area and $CO_2$ adsorption capacity of the samples was rather weak. For example, the value of the BET surface area after NaOH modification declined compared to the raw GAC, where there was a considerable increase in the adsorption capacity. This is most probably because of the Na

species that were incorporated during the NaOH modification. The reaction between the Na species and the $CO_2$ increased the adsorption capacity. This reveals that the surface chemistry of the M-AC was the dominant parameter affecting the adsorption capacity in this study. Moreover, the SEM images showed some agglomerated white particles on the surface of the NaOH modified samples (first, second granular and powder AC). This indicated the presence of carbonated sodium areas resulting most probably from the reaction of residual NaOH (after the NaOH treatment) with the surrounding atmosphere, thus, assisting in the total $CO_2$ uptake. Figure 4.19 illustrates the proposed mechanism behind the high adsorption capacity after the HCl-NaOH modification.

A large number of studies have reported the same findings; that surface areas decline combined with higher $CO_2$ capture capacities (Caglayan & Aksoylu 2013; Zhang et al. 2013; Tan et al. 2014; Shim et al. 2001; Zhang et al. 2010). This implies that the $CO_2$ adsorption cannot be only justified by physisorption or controlled by the physical characterisation of the AC. Indeed, it is well documented that the $CO_2$ capacity of AC is controlled by both the textural parameters and the basic functionalities present on the carbon surface (Shafeeyan et al. 2011; Drage et al. 2007; Zhang et al. 2013).

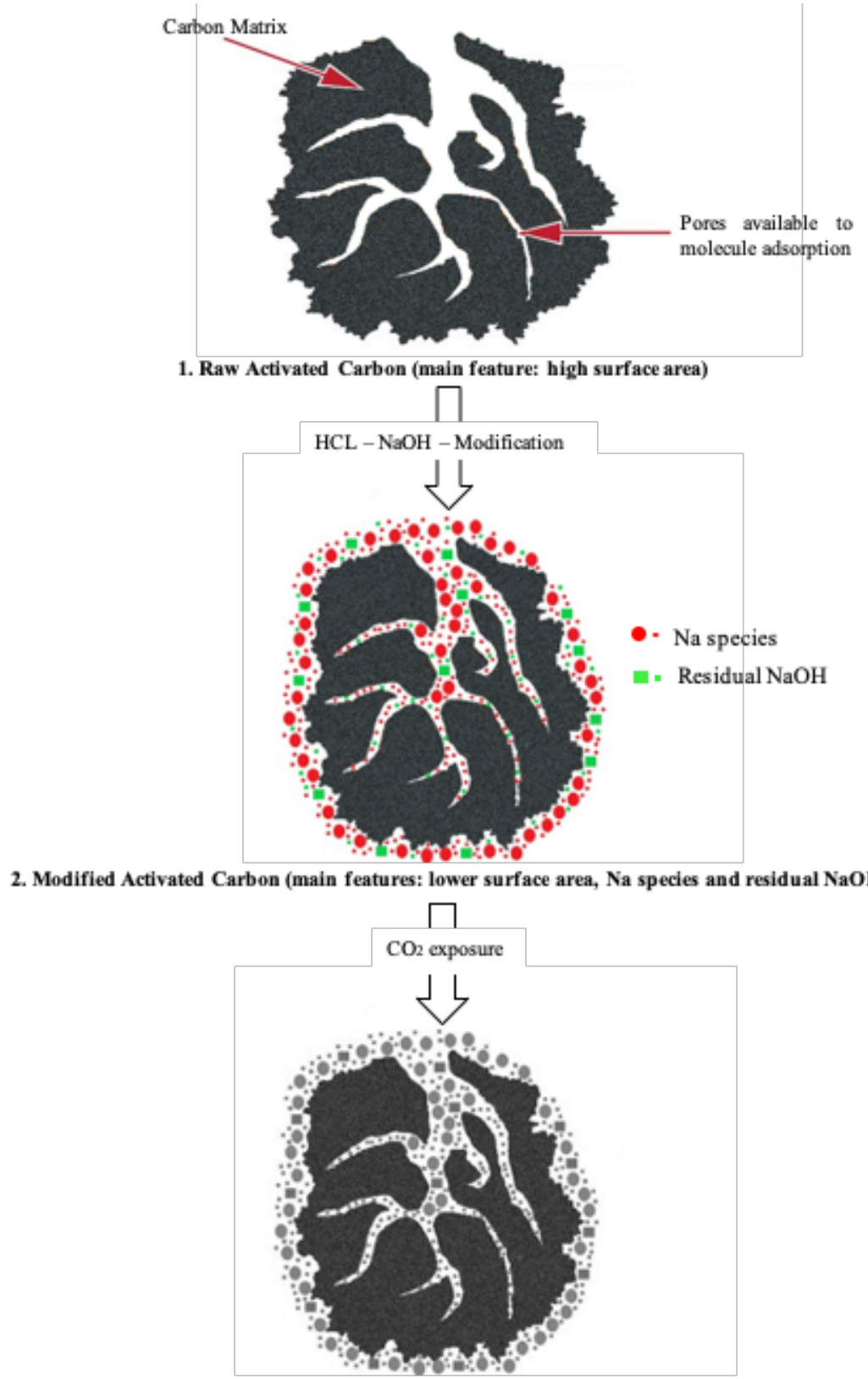


Figure 4-19: Schematic graph showing the adsorption of M-AC

## 4.9 CONCLUSION

This chapter focused on optimising the modification of AC in order to achieve the best modification procedure that maximises the adsorption capacity of AC towards carbon dioxide. An energy-conservative approach was followed through the modification, which involved a technique whereby the AC samples were modified through the impregnation with chemicals without exposing the samples to high temperatures. It is important to note that the modified AC is incorporated later in pervious concrete to enhance its sustainability aspects. Using energy intensive techniques during the AC modification contradicts the purpose of this work, since the $CO_2$ emissions that corresponds to using the high temperature approach may be equivalent or even higher than the $CO_2$ emission being adsorbed later when employed in pervious concrete.

The modification process was conducted in two stages. The first was modification by a single impregnation agent, while the second was modification with two impregnation agents in a sequence. The characterisation of the first and second modified GAC using FTIR, BET and SEM was addressed. This was followed by a presentation and discussion on the $CO_2$ adsorption capacities of the raw and modified granular and powder AC measured using three techniques: the $CO_2$ incubator, the fixed-bed column and TGA. The three techniques employ different operation conditions and resulted in different levels of accuracy. Therefore, there was a great variation in the obtained $CO_2$ adsorption capacities. TGA as a measuring technique focuses on the weight gain due to $CO_2$ adsorption and is believed to be the most accurate technique for measuring the $CO_2$ capacities. However, all the three techniques confirmed that the modifications that were applied to the raw AC increased its affinity towards carbon dioxide. Despite the blocking of AC pores that was noticed in the two-step modification, this approach gave the highest adsorption capacity and; therefore, it was considered as the optimum modification technique in ambient temperatures. Modified granular AC (M-GAC) and modified powder AC (M-PAC) by this technique will be used in the cement-based systems in the next chapter.

# 5 Parametric investigation of modified activated carbon for application in pervious concrete

## 5.1 INTRODUCTION

This chapter details the laboratory work conducted to understand the performance and behaviour of the modified activated carbons developed in Chapter 4 for applications in pervious concrete detailed in Chapter 6. Activated carbon was modified (as described in Chapter 4) using four different techniques to optimise its affinity towards carbon dioxide. As described earlier, the optimum modification approach was modifying the activated carbon with HCl followed by a modification with NaOH under ambient temperature.

In this chapter, the performance of the modified powder activated carbon (M-PAC) as a partial substitution of cement and its influence on the properties of cement pastes and pervious concretes is investigated. Similarly, the performance of modified granular activated carbon (M-GAC) as a partial substitution of fine aggregate and its influence on cement mortars and pervious concrete are also discussed. Table 5.1 presents the tests that were conducted on the different cement-based systems: cement pastes, cement mortars and pervious concrete.

The percentages of substitution (for both cement and fine aggregates) were 0.5%, 1% and 2%. These percentages are within or close to the allowed content of the carbonaceous materials in Portland cement and fine aggregate according to the standards as presented earlier in sections 2.8.5 and 2.8.6. The notations for all the mixes examined in this chapter are presented in Table 5.2.

Table 5-1: Experiments conducted in Chapter 5

| Cement-based systems | Cement substitution by M-PAC | Fine aggregate substitution by M-GAC |
|---|---|---|
| **Cement pastes** | - Standard consistency<br>- Isothermal calorimetry<br>- XRD and TGA | |
| **Cement mortars** | | - Workability (flow table)<br>- UCS |
| **Pervious concrete** | - UCS<br>- Porosity<br>- Density | - UCS<br>- Porosity<br>- Density |

Table 5-2: Notation of all the mixes examined in Chapter 5

| | | control | 0.5% | 1% | 2% |
|---|---|---|---|---|---|
| Modified PAC for cement substitution | Cement pastes | Co-CP | 0.5%M-PAC-CP | 1%M-PAC-CP | 2%M-PAC-CP |
| | Pervious concrete | Co-Con | 0.5%M-PAC-Con | 1%M-PAC-Con | 2%M-PAC-Con |
| | | | | | |
| Modified GAC for fine aggregate substitution | Cement mortars | Co-CM | 0.5%M-GAC-CM | 1%M-GAC-CM | 2%M-GAC-CM |
| | Pervious concrete | Co-Con | 0.5%M-GAC-Con | 1%M-GAC-Con | 2%M-GAC-Con |

## 5.2 PARTIAL SUBSTITUTION OF CEMENT BY MODIFIED POWDER ACTIVATED CARBON

### 5.2.1 Properties of cement pastes with different M-PAC percentages

A number of cement pastes were prepared and cured as outlined in section 3.4.2. Some mixes, such as those used for standard consistence and isothermal calorimetry, were tested directly after mixing. The remaining mixes underwent tests after 28 days of curing for microstructural analysis.

The notation for cement pastes (as illustrated in Table 5.2) is based on the percentage of M-PAC used. They are the control mix (Co-CP), and the three mixes with M-PAC, namely 0.5%M-PAC-CP, 1%M-PAC-CP and 2%M-PAC-CP. The results of these experiments are presented and discussed below.

#### 5.2.1.1 Standard Consistency

Water content is frequently reported as one of the main factors influencing the mechanical and physical properties of cement-based materials. Therefore, water demand for different cement pastes was investigated in this study. The prepared pastes were tested for standard consistency in accordance with BS EN 196-3. For each tested percentage of M-PAC, 5 cement mixes with different water to solids (w/s) ratios (0.28, 0.29, 0.30, 0.31 and 0.32) were prepared and tested using the manual Vicat apparatus. Table 5.3 shows the w/s ratios with the obtained penetration in mm for each percentage

of M-PAC. Water to cement ratios (w/c) are slightly higher than water to solids ratios (w/s) because the higher the percentage of M-PAC added, the lower the proportion of Portland cement in the mixes. The target w/c ratio was set to the paste that achieves 6 mm penetration, since this would achieve similar consistency and workability. Figure 5.1 was plotted in order to calculate the required w/c ratio (corresponding to 6 mm) for each percentage of M-PAC in the cement pastes. The last value of penetration in each percentage set (except the last set) was not considered in the plot. This is because these values are sufficiently similar to the previous small penetration values in each set where the experiments should terminate.

Table 5-3: Penetration values of standard consistency tests on the M-PAC-cement paste mixes tested

| Cement paste mixes | W/S ratio | W/C ratio | Penetration in mm |
|---|---|---|---|
| Co-CP | 0.28 | 0.28 | 14 |
| | 0.29 | 0.29 | 10 |
| | 0.3 | 0.3 | 6 |
| | 0.31 | 0.31 | 2 |
| | 0.32 | 0.32 | 2 |
| 0.5%M-PAC-CP | 0.28 | 0.281 | 15 |
| | 0.29 | 0.291 | 11 |
| | 0.3 | 0.301 | 9 |
| | 0.31 | 0.311 | 3 |
| | 0.32 | 0.321 | 2 |
| 1%M-PAC-CP | 0.28 | 0.283 | 16 |
| | 0.29 | 0.293 | 12 |
| | 0.3 | 0.303 | 10 |
| | 0.31 | 0.313 | 4 |
| | 0.32 | 0.323 | 2 |
| 2%M-PAC-CP | 0.28 | 0.286 | 28 |
| | 0.29 | 0.296 | 18 |
| | 0.3 | 0.306 | 12 |
| | 0.31 | 0.316 | 10 |
| | 0.32 | 0.326 | 3 |

Figure 5.3 shows a strong correlation between the w/c ratio and the corresponding penetration, with $R^2$ being more than 0.95 for all percentages. Unsurprisingly, the higher the water content in the cement paste, the lower the penetration by the Vicat plunger. This is because pastes with a higher w/c ratio demonstrate less stiffness. One key finding from Table 5.3 is that the cement pastes with higher percentages of M-PAC exhibited high

values of penetration at the same water content. This may be explained by the adsorption behaviour of M-PAC to the mixing water of the cement pastes. Modified activated carbon is a highly porous material with a large surface area that has the potential to adsorb water molecules and store them within its pores, leaving the effective w/c ratio lower than the calculated w/c ratio. Therefore, cement pastes with a higher percentage of M-PAC in this work required a greater volume of water to meet the same penetration level. Based on Figure 5.1, the w/c ratios that accomplished 6 mm penetration using the manual Vicat apparatus are presented in Table 5.4.

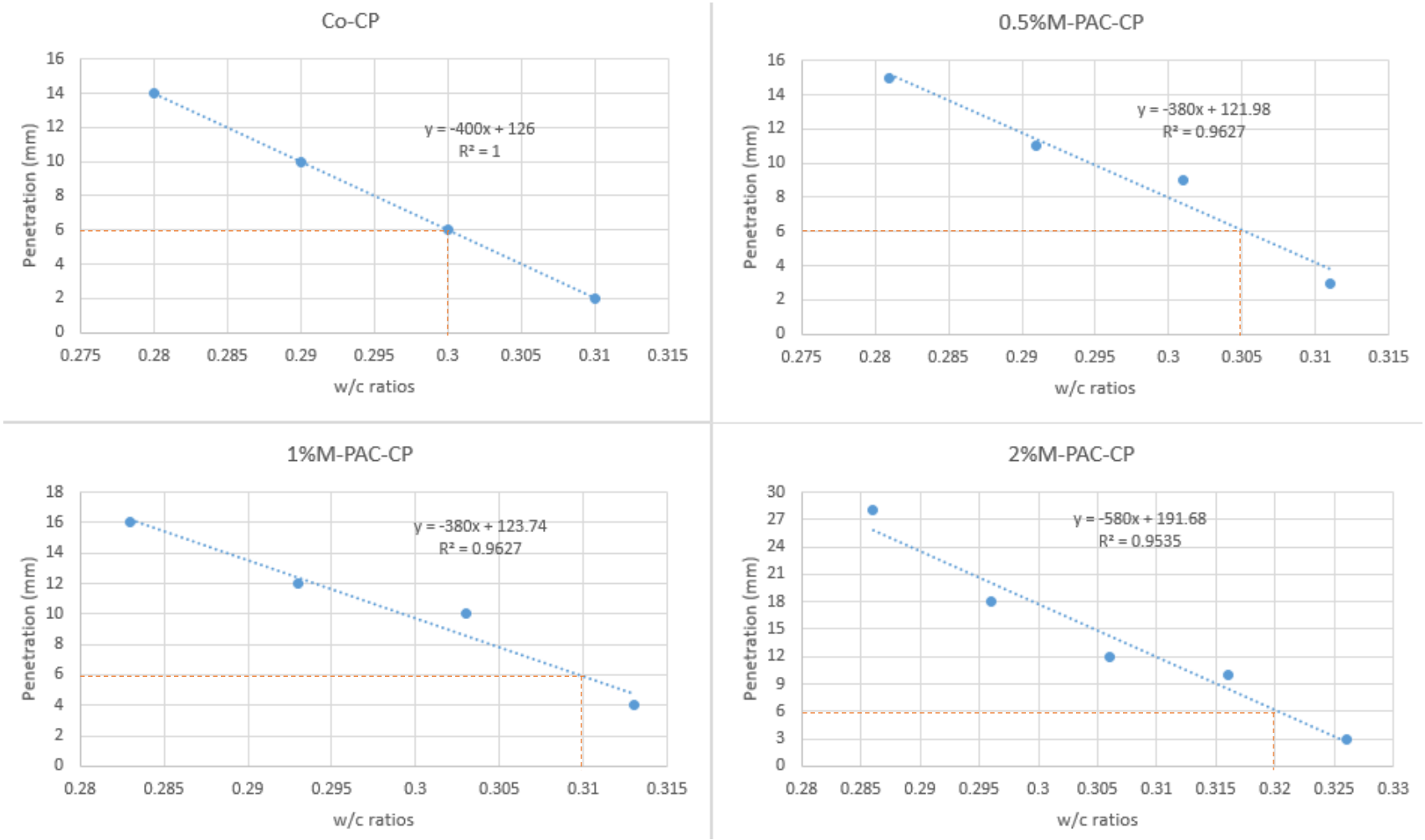


Figure 5-1: Determination of w/c ratios for standard consistency for the various M-PAC-cement paste mixes tested

Table 5-4: W/c ratios for standard consistence M-PAC-cement pastes

| **Cement paste** | Co-CP | 0.5%M-PAC-CP | 1%M-PAC-CP | 2%M-PAC-CP |
|---|---|---|---|---|
| **W/C** | 0.3 | 0.305 | 0.31 | 0.32 |

The water demand for standard consistency was almost directly proportional to the percentage of M-PAC in the mixes, as illustrated in Figure 5.2. The w/c ratio corresponding to the control paste was 0.3. The increase in w/c ratio was 1.7%, 3.3% and 6.7% for 0.5%, 1% and 2%M-PAC-CPs respectively. The standard consistency test reveals that the presence of M-PAC in a cement mix leads to a stiffer paste due to the adsorption of some mixing water by M-PAC. Therefore, more water needs to be added to achieve the same level of workability as in the control sample. The w/c ratios presented in Table 5.4 were used to prepare the cement paste cubes for XRD and TGA analysis.

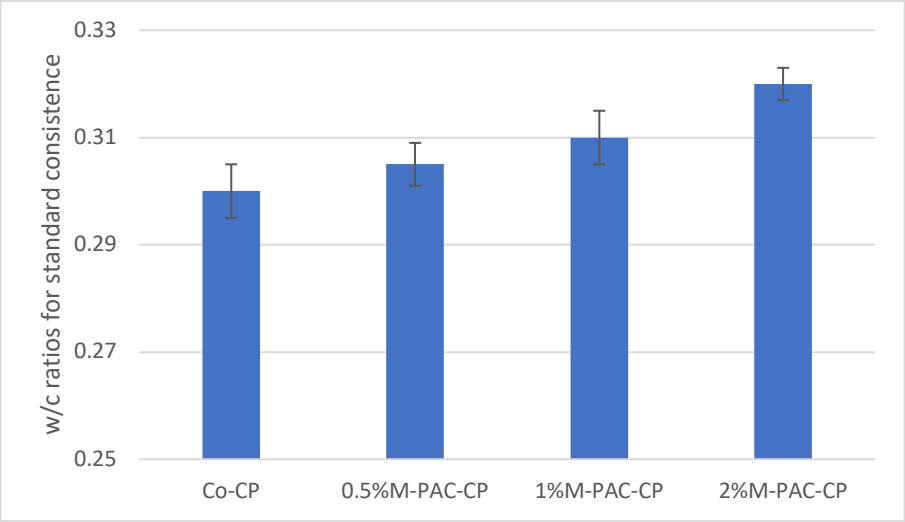


Figure 5-2: Standard consistence w/c ratios of different percentages of M-PAC in the cement paste mixes

A similar performance of adsorption to the mixing water, but by different added materials, has been previously reported by multiple researchers (Hale et al. 2008; Lee & Li 2010; Ganesan et al. 2008). Lee and Li replaced part of the Portland cement with by-products of municipal solid waste incinerators. The water to cement ratio for standard consistency increased from 0.26 to 0.32 at 40% substitution from cement(Lee & Li 2010). Similarly, El-Dakroury and Gasser reported an increase in w/c ratio for standard consistency from 0.28 to 0.6 when 40% of rice rusk ash replaced Portland cement (El-Dakroury & Gasser 2008).

#### 5.2.1.2 Isothermal calorimetry

The influence of partially replacing the Portland cement by M-PAC on the hydration kinetics of cement pastes is investigated in two rounds: fixed w/s ratios and fixed effective w/c ratios as illustrated below.

***Fixed water to solids ratios:***

The water to solids (Portland cement and M-PAC) ratio was held constant at 0.34 in all examined samples. This ratio was chosen to be slightly higher than the ratios demonstrated by the standard consistency test to ease the hand mixing of the samples in one minute before being placed in the isothermal calorimetry instrument. The w/c ratio was variable according to the percentage of M-PAC (therefore, the quantity of Portland cement) in each paste as shown in Table 5.5.

Table 5-5: w/s and w/c ratios for different cement pastes (fixed w/s ratio)

| Cement Paste | W/ solids | Water/ cement | Effective w/c |
|---|---|---|---|
| Con-CP | 0.34 | 0.34 | 0.34 |
| 0.5%M-PAC-CP | 0.34 | 0.3417 | 0.3367 |
| 1%M-PAC-CP | 0.34 | 0.3434 | 0.3333 |
| 2%M-PAC-CP | 0.34 | 0.3469 | 0.3265 |

Power and cumulative energy produced (per gram of cement over 48 hours) was recorded for control and pastes containing different percentages of M-PAC as illustrated in Figure 5.3 (a and b). A summary of the peak power and setting time values is also given in Table 5.6.

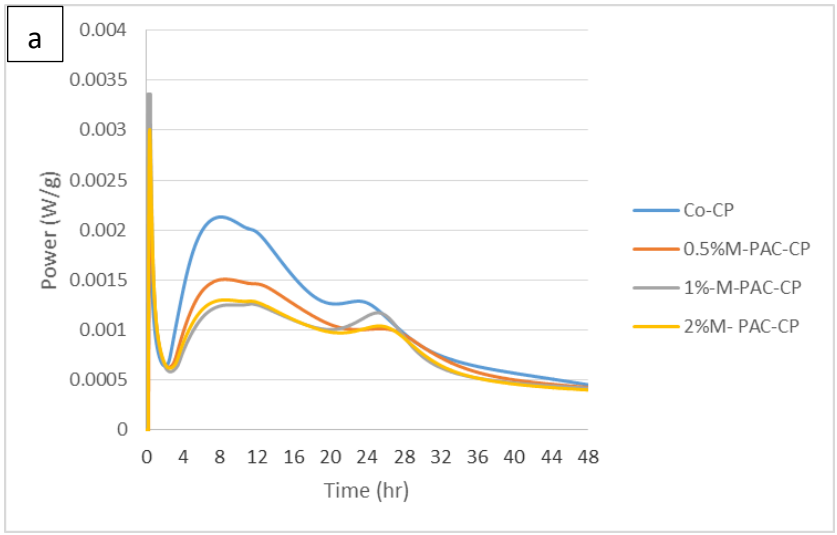


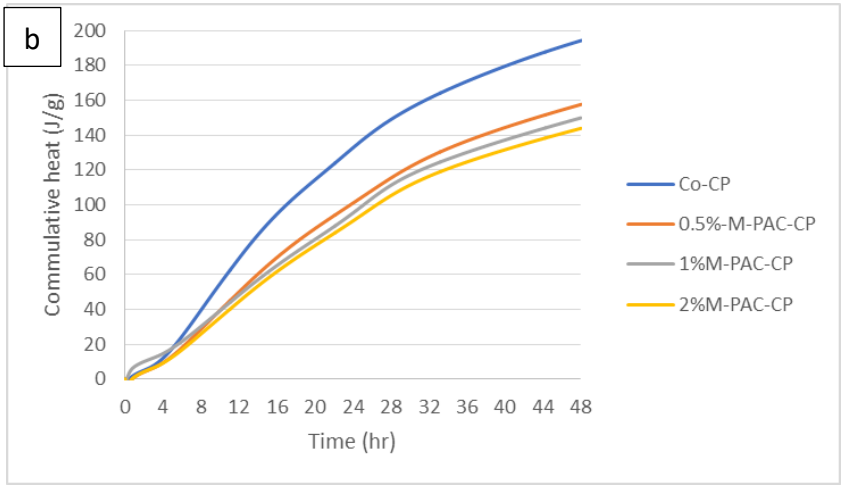


Figure 5-3: Effect of M-PAC addition with fixed w/s ratios on (a) isothermal power and (b) energy production of cement mixes

Table 5-6: Initial setting times and peak power values for cement pastes containing M-PAC (with fixed w/s ratios)

| Cement Paste | Initial time setting (hr) | Peak power (mW/g) |
|---|---|---|
| Control-CP | 3.98 | 1.49 |
| 0.5%M-PAC-CP | 3.81 | 0.677 |
| 1%M-PAC-CP | 4.11 | 0.88 |
| 2%M-PAC-CP | 3.91 | 0.683 |

Two counter-acting effects are expected to arise from the presence of M-PAC in the cement pastes: the 'filler effect' and the 'adsorption effect'. When the M-PAC is considered as a filler in cement pastes, M-PAC provides more space available for the hydration products to form. The M-PAC surface also acts as nucleation sites for the precipitation

and growth of hydration products (Cheung et al. 2011). Moreover, as the w/s ratio is fixed, the w/c ratios are increasing (the greater the percentage of filler, the less Portland cement available, resulting in a higher w/c ratio). This leads to a higher cumulative heat of hydration, because of the higher quantity of water available to hydrate the Portland cement (Berodier & Scrivener 2014; Scrivener et al. 2015).

On the other hand, M-PAC is considered as an adsorbent to the mixing water of the cement pastes. Increasing the percentage of M-PAC in the cement pastes leads to a higher adsorption of the mixing water. This leaves the effective water to cement ratios lower than the actual added mixing water should produce. The lower w/c ratio leads to lower cumulative heat of hydration in the isothermal calorimetry.

To investigate this further, the amount of water absorbed by the M-PAC must be quantified to calculate the effective w/c ratio. Based on a previous study, activated carbon absorbs around 1 $cm^3$ water/g AC (Justo-Reinoso et al. 2018). This indicates that the effective w/c ratios in these experiments are as shown in the last column in Table 5.5, showing that w/c ratios are decreasing with increasing the M-PAC ratio in the cement pastes. Therefore, a lower cumulative heat of hydration for M-PAC-CPs is expected.

With reference to Figure 5.3, it can be seen that incorporation of M-PAC significantly reduced both the peak power and total hydration heat relative to the control mix. The effect increased with increasing the M-PAC replacement percentages. The reduction in cumulative hydration heat might be explained by the adsorption behaviour of M-PAC to the mixing water which resulted in a lower effective w/c ratio available for hydration.

The effect of changing the w/c ratio on the hydration process is well documented (Scrivener et al. 2016; Sharpley 2015; Cheung et al. 2011; Pang et al. 2015; Kirby & Biernacki 2012). Decreasing water content within the cement paste increases the concentration of the ionic species present within the pore solution, promoting dissolution of the anhydrous phases and causing earlier power peaks. However, the increase in water content stimulates nucleation and accelerates cement hydration, thus increasing the cumulative heat of hydration (Scrivener et al. 2016; Shi et al. 2019).

***Fixed effective water to cement ratios:***

During the second round of isothermal calorimetry test, a fixed effective w/c ratio of 0.33 was chosen to isolate the effect of variable w/c as shown in Table 5.7. Power and cumulative energy produced are illustrated in Figure 5.4 (a and b), and a summary of the peak power and setting time values is given in Table 5.8.

Table 5-7: w/s and w/c ratios for different cement pastes (fixed effective w/c)

| Cement Paste | W/ solids | Water/ cement | Effective w/c |
|---|---|---|---|
| Con-CP | 0.33 | 0.33 | 0.33 |
| 0.5%M-PAC-CP | 0.3333 | 0.335 | 0.33 |
| 1%M-PAC-CP | 0.3367 | 0.3401 | 0.33 |
| 2%M-PAC-CP | 0.3434 | 0.3504 | 0.33 |

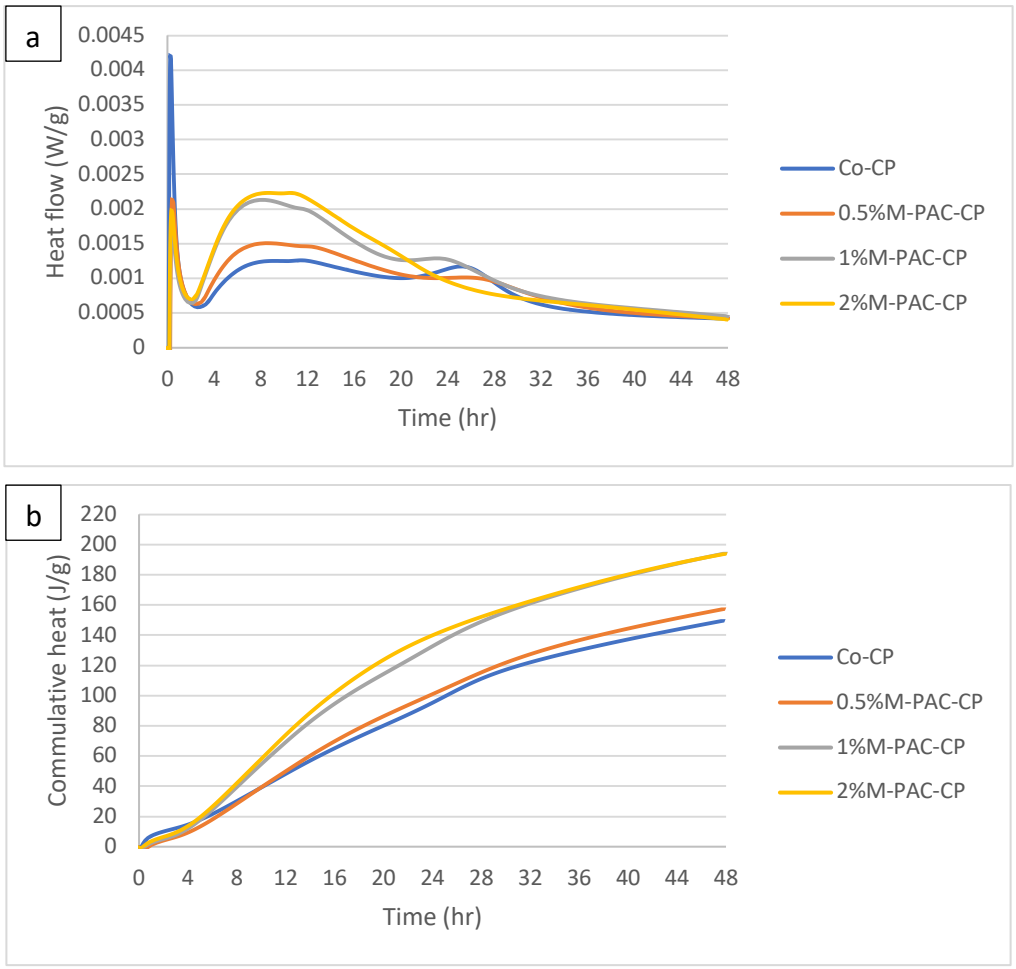


Figure 5-4: Effect of M-PAC addition with fixed effective w/c ratios on (a) isothermal power and (b) energy production of cement mixes

Table 5-8: Initial setting times and peak power values for cement pastes containing M-PAC (with fixed effective w/c ratios)

| Cement Paste | Initial time setting (hr) | Peak power (mW/g) |
|---|---|---|
| Control-CP | 4.02 | 0.81 |
| 0.5%M-PAC-CP | 3.82 | 0.92 |
| 1%M-PAC-CP | 3.43 | 1.14 |
| 2%M-PAC-CP | 3.51 | 1.21 |

From Figure 5.4, it can be seen that incorporation of M-PAC significantly increased both the peak power and total hydration heat compared to the control mix. Moreover, the initial setting time decreased compared to the control paste. The effect increased with increasing the M-PAC replacement percentages. This might be explained by the filler effect due to the physical presence of M-PAC inside the cement pastes, where it allows for two main phenomena. Firstly, relatively more space is available for the formation of the hydration products. Secondly, M-PAC acts as nucleation sites for the hydration products, thus increasing the rate of hydration and decreasing the initial setting time (Berodier & Scrivener 2014; Oey et al. 2013). Moreover, the quantity of mixing water that was absorbed by M-PAC might have desorbed in the cement pastes, increasing the available water, thus enhancing the hydration process. A similar effect was observed by Gupta and his group when 2% biochar (by mass of cement) was added to cement mortars. The authors reported an improvement in reaction kinetics and degree of hydration due to the presence of biochar which acted as sites of heterogeneous nucleation (Gupta et al. 2018).

#### 5.2.1.3 Microstructural analysis

Microstructural analysis was conducted following 28 days of curing to investigate the effect of M-PAC on cement pastes. XRD and TGA tests were conducted on representative samples from the middle part of the cement paste cubes as shown earlier in Figure 3.19.

##### 5.2.1.3.1 XRD analysis

XRD was used to identify the crystalline phases in control and M-PAC-CPs. The XRD spectra of the four samples are shown in Figure 5.5. Overall, the spectra are quite similar, where typical Portland cement hydration products are detected including portlandite (denoted as CH), ettringite (denoted as E), poorly crystallised calcium silicate hydrates (C-S-H, denoted as CSH) and calcite (denoted as C). Moreover, the residual content of

tricalcium silicate ($C_3S$, denoted as TS) and dicalcium silicate ($C_2S$, denoted DS) at (2θ=23, 32.2, 32.6 and 51.7°) and at (2θ=23.4, 39.5°) respectively, were observed in all samples. As can be seen in Figure 5.5, poorly crystallised C-S-H was observed at 2θ = 29.5° with almost the same intensity in all samples. This peak can also be assigned to calcite as a result of the carbonation of calcium hydroxide. The CH peaks (2θ = 18.1°, 34.1° and 47.1°) were very distinct in the spectra of all samples.

Overall, the phases and peak intensities in all tested samples were the same, which implies that incorporation of M-PAC at these percentages does not alter the composition of the hydrated products.

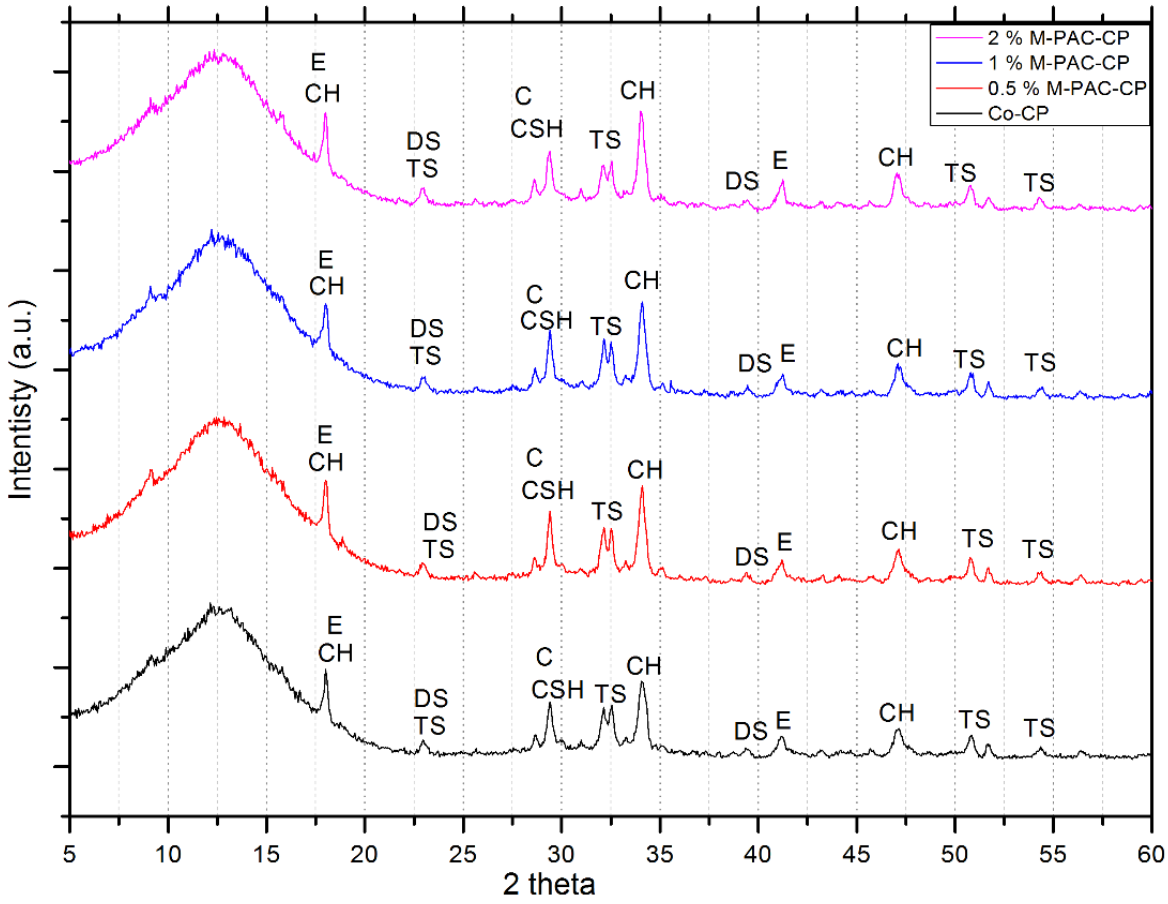


Figure 5-5: XRD spectra for control and M-PAC-cement pastes where (CH is Portlandite, E is Ettringite, C is calcite, CSH is C-S-H, TS is C3S and DS is C2S)

#### 5.2.1.3.2 TGA analysis

TGA was conducted to provide further insight into the hydration products of the control and M-PAC-CPs. The TGA weight loss curves, along with the differential thermogravimetric (DTG) curves, are shown in Figure 5.6 and Figure 5.7. The peak temperatures, temperature ranges and the corresponding weight loss at each step are summarised in Table 5.9.

The peak related to the decomposition of C-S-H at ~90°C was also observed in all samples. Distinct peaks were detected in all samples at ~430°C, due to the dihydroxylation of calcium hydroxide ($Ca(OH)_2$) into calcium oxide and water (Lothenbach et al. 2007). Between 500-800°C, peaks were identified ~650 and ~720°C in all samples. Both peaks arise from the decomposition of calcite ($CaCO_3$) in the cement-based materials (Tabet et al. 2018; Taylor 1997). The total weight loss as presented in Table 5.9 were 21.35%, 22.82%, 23.67% and 24.72% for the control, 0.5%M-PAC, 1%M-PAC and 2%M-PAC-CPs. An increase in weight loss was observed with an increase in the percentage of M-PAC in the cement pastes, occurring mainly in the first zone (30-300°C) and less so in the last zone (500-800°C). Increase in weight loss in the first zone might be attributed to the release of $CO_2$ molecules that were trapped in the activated carbon pores. $CO_2$ is believed to de-attach from activated carbon at temperatures of around 100°C (Zhu et al. 2014; Ello et al. 2013; Ava Heidari et al. 2014). The weight loss in last zone is most probably attributed to the decomposition of calcite. The weight loss increased with an increase in M-PAC percentage. For the 2% M-PAC mix, the weight loss within this zone increased slightly from 5.54% associated with the control sample to 6.62%. This indicates a higher calcite content with a higher percentage of M-PAC. The higher content of calcite in the cement pastes containing M-PAC might be explained as follows: The M-PAC is expected to adsorb $CO_2$ molecules in its pores. Over time the adsorbed $CO_2$ molecules may react with the adjacent cement-hydrate products in the presence of water, forming calcium carbonate. The higher content of M-PAC within the cement paste, the greater the volume of calcium carbonate will be formed.

The last point of notice is the weight loss in the second zone (e. g. 300-500°C), which is attributed to the decomposition of $Ca(OH)_2$. The thermal decomposition of the activated carbon is believed to take place in this zone as well (as will be shown later in Figure 6.14).

However, Table 5.9 reveals almost similar values of weight loss in all the examined samples, which may be explained as follows. The higher the percentage of M-PAC in the cement paste, the higher quantity of $CO_2$ provided by M-PAC to the cement paste. Consequently, the higher carbonation reaction takes place, consuming $Ca(OH)_2$, to form calcite. For each value in this temperature zone, a portion is lost due to the decomposition of $Ca(OH)_2$ and another portion is due to the decomposition of activated carbon. The higher the percentage of M-PAC, the lower the available $Ca(OH)_2$ to decompose, and the higher the portion decomposed due to M-PAC. This is confirmed by the higher content of calcite (the last zone) in the M-PAC-CPs.

Table 5-9: Thermal decomposition of control and M-PAC-CPs by TGA

| Cement Paste | Temperature (°C) | Peak Temperature | Weight loss % | Tot. Weight loss % |
|---|---|---|---|---|
| Co-CP | 30-300 | 101 | 12.54 | 21.35 |
| | 300-500 | 444 | 3.27 | |
| | 500-800 | 695 | 5.54 | |
| | | | | |
| 0.5% M-PAC-CP | 30-300 | 107 | 13.83 | 22.82 |
| | 300-500 | 452 | 3.26 | |
| | 500-800 | 705 | 5.73 | |
| | | | | |
| 1% M-PAC-CP | 30-300 | 104 | 14.38 | 23.67 |
| | 300-500 | 451 | 3.24 | |
| | 500-800 | 701 | 6.05 | |
| | | | | |
| 2% M-PAC-CP | 30-300 | 103 | 14.78 | 24.72 |
| | 300-500 | 457 | 3.32 | |
| | 500-800 | 697 | 6.62 | |

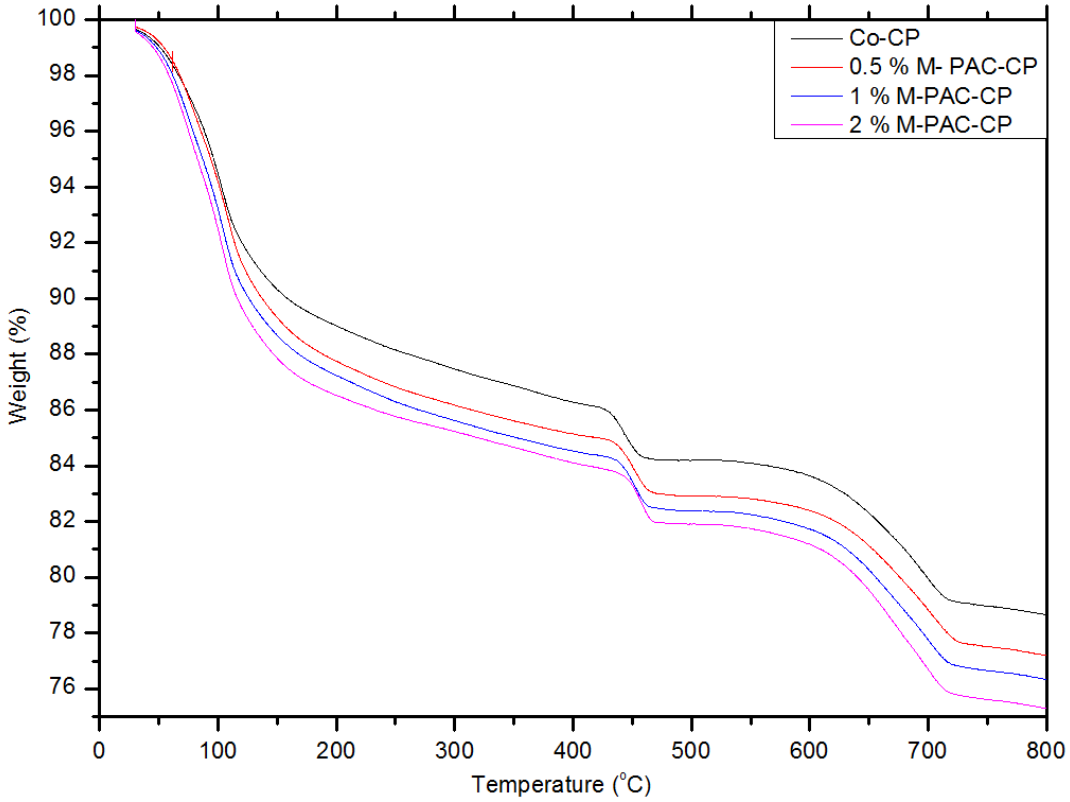


Figure 5-6: TGA curves for control and M-PAC-cement pastes

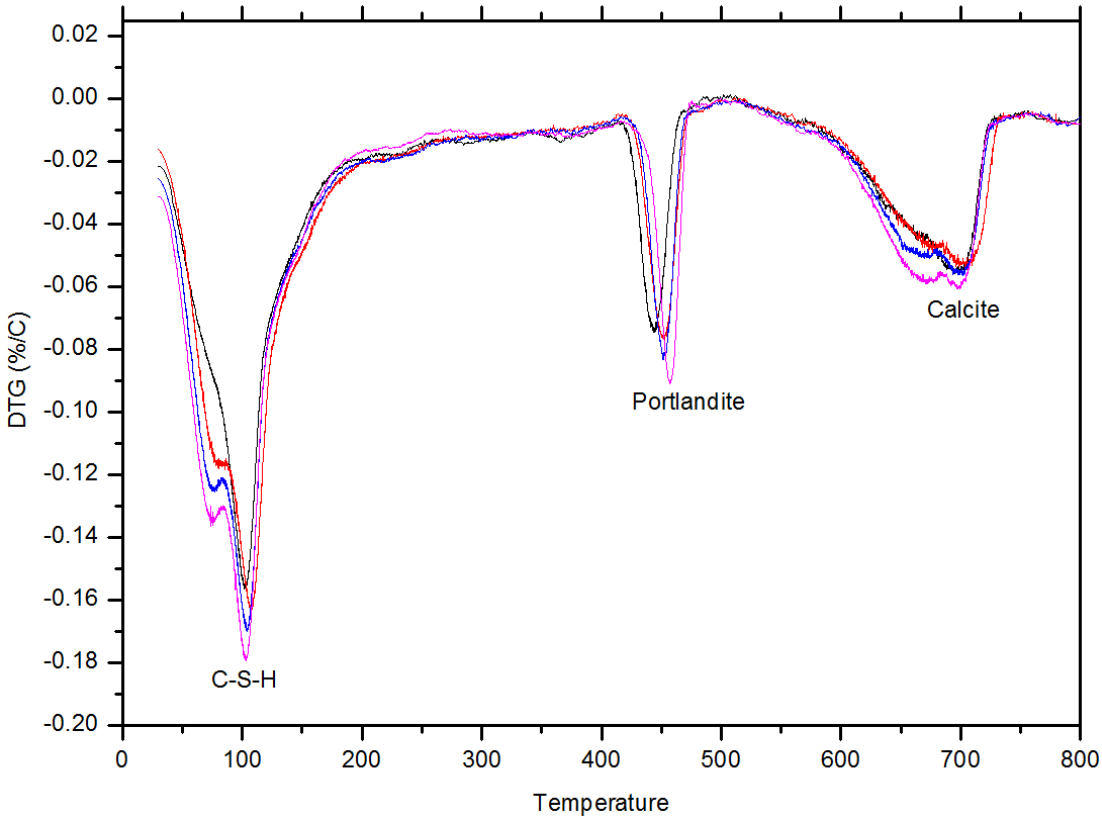


Figure 5-7: DTG curves for control and M-PAC-cement pastes

### 5.2.2 Properties of pervious concrete with different M-PAC percentages

To investigate the effect of different percentages of M-PAC on pervious concrete properties, four pervious concrete mixes were prepared as explained in section 3.4.2 and cured in a water tank for 28 days. These were the control mix, 0.5%M-PAC-Con, 1%M-PAC-Con, 2%M-PAC-Con. The concrete mixes underwent three experiments: unconfined compressive strength, porosity and hardened density.

#### 5.2.2.1 UCS, porosity and hardened density

The UCS test was conducted on four mixes of pervious concrete to examine the effect of M-PAC on pervious concrete. The results are illustrated in Figure 5.8.

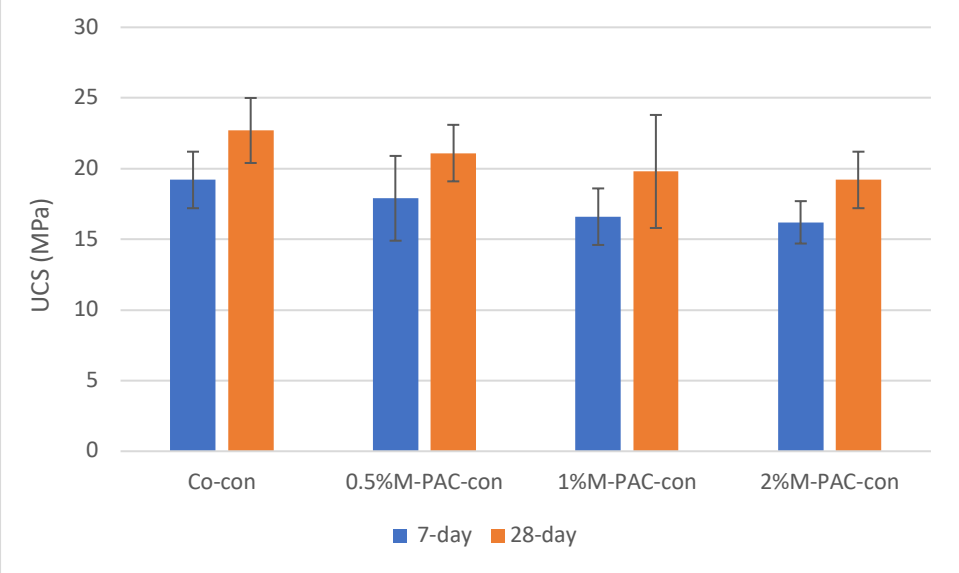


Figure 5-8: UCS at 7- and 28-days M-PAC-con mixes

The UCS of the control concrete was 22.7 MPa at age of 28 days, which was small compared to the traditional type of concrete. UCS of pervious concrete is typically in the range of 3.5 – 28 MPa, which fits with the measured control mix value. Figure 5.8 shows that UCS generally decreases with the addition of M-PAC. The lowest values were 16.2 and 19.2 MPa, for 7 and 28 days respectively, obtained at 2% replacement. These values represent a 15.6 % and 15.4% decrease in UCS, as shown in Table 5.10. However, given that a UCS value of 17 MPa is suitable for a wide range of pervious concrete applications (Tennis et al. 2004), all strength values obtained are acceptable.

The decline in the UCS of the M-PAC-concrete mixes was expected, due to the reduced quantity of Portland cement compared to the control mix. Similar findings were reported by Horgnies and his co-workers, who recorded a 15% decline in UCS after 7 days of curing when 1.5% PAC was incorporated into the concrete mixes. They attributed the decline to the higher water content that was required to achieve the same level of workability of the activated carbon-mixes (Horgnies et al. 2012).

Table 5-10: The decrease in UCS of M-PAC-con mixes

| **Sample** | **Decrease in UCS %** | |
|---|---|---|
| | **7-day** | **28-day** |
| 0.5%M-PAC-Con | 6.8 | 7.0 |
| 1%M-PAC-Con | 13.5 | 12.8 |
| 2%M-PAC-Con | 15.6 | 15.4 |

The porosity of the Co-con was 14.8% and 13.1% at the age of 7 and 28 days respectively. As a type of concrete that is mainly used in pavement, parking lots, and tennis courts etc., a value of higher than 15% is recommended in pervious concrete for rainwater draining requirements. The 28-day porosity of the Co-con was 13.1%, just under the recommended value, which may slightly decrease the volume of water that would be drained through in this concrete mix. Incorporation of M-PAC generally increased the porosity of the pervious concrete samples, as shown in Figure 5.9. This can be explained by the porous nature of M-PAC compared with Portland cement. Activated carbon has significantly higher surface area than Portland cement. As a result, incorporation of such a highly porous material increased the overall porosity. While the porosity of pervious concrete is mainly due to the interconnected network of voids between the coated aggregate, the increased porosity values in M-PAC-con mixes are due to the porosity of M-AC itself, which does not add an actual enhanced value (in terms of drainage requirement) to the porosity of pervious concrete.

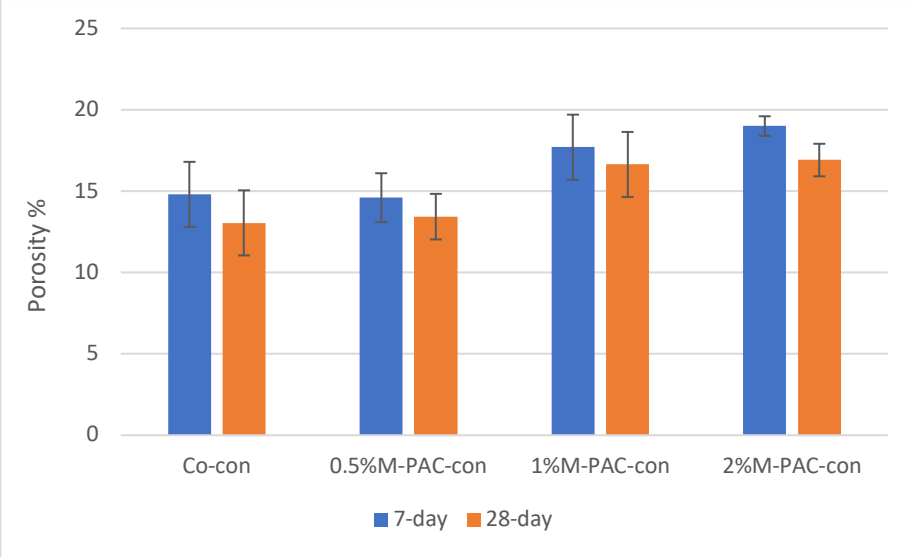


Figure 5-9: Porosity at 7 and 28 days of M-PAC-con mixes

Table 5.11 displays the increase in porosity of M-PAC-pervious concrete mixes compared to the control mix. The increase in porosities at 28-day ranged from ~ 1% to 27%, the latter of which was the maximum value, associated with the 2% PAC mix. A similar increasing porosity trend has been observed by other investigators. Resheidat and his co-workers reported increased porosity of up to 29% when 10% of cement was replaced by powdered charcoal (Resheidat et al. 2002).

Table 5-11: The Increase in porosity of M-PAC-con mixes

| **Sample** | **Increase in porosity %** | |
|---|---|---|
| | **7-day** | **28-day** |
| 0.5%M-PAC-Con | -1.4 | 0.8 |
| 1%M-PAC-Con | 19.5 | 24.9 |
| 2%M-PAC-Con | 28.3 | 26.9 |

The hardened density of the four pervious concrete mixes was investigated after 7 and 28 days of curing. Figure 5.10 illustrates the values for different percentages of M-PAC. The hardened density of the control concrete was 2010 kg/m$^3$ at the age of 28 days, which is in the typical range of pervious concrete densities for pavements (1600-2000 kg/m$^3$). Unsurprisingly the densities of the produced samples slightly decreased with the increasing M-PAC percentage as activated carbon has a lower density than Portland cement. The higher the percentage of the replaced material the lower the corresponding density. Moreover, the reduced quantity of cement decreased the quantity of the hydration products that would have generated and given a denser concrete. However, all the density values were within the typical range of pervious concrete density values, and the overall decrease in density was very low as shown in Table 5.12.

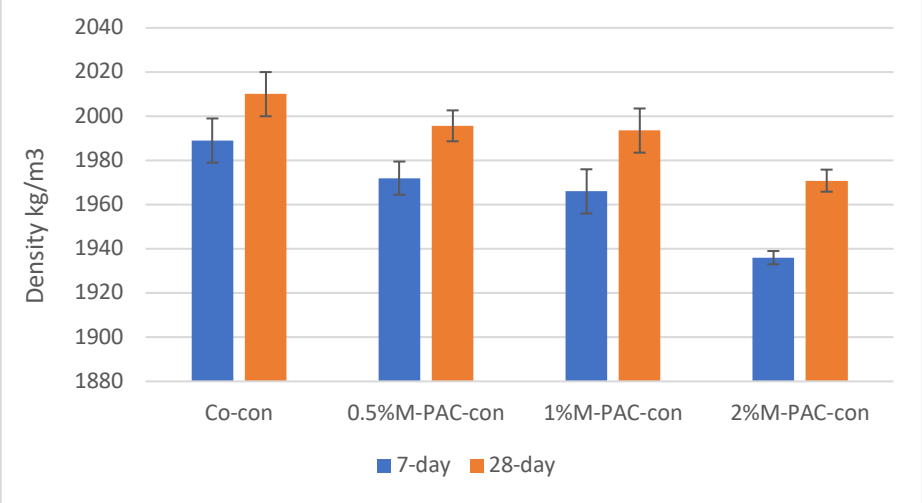


Figure 5-10: Hardened densities at 7 and 28 days of M-PAC-con mixes

Table 5-12: The decrease in hardened densities of M-PAC-con mixes

| **Sample** | **Decrease in density%** | |
|---|---|---|
| | **7-day** | **28-day** |
| 0.5%M-PAC-Con | 0.8 | 0.7 |
| 1%M-PAC-Con | 1.1 | 0.8 |
| 2%M-PAC-Con | 2.7 | 1.9 |

### 5.2.2.2 Summary of the examined properties of M-PAC-pervious concrete

Table 5.13 summarises the properties of pervious concrete mixes with different percentages of M-PAC. Overall, both UCS and hardened density are reduced with increasing proportions of M-PAC, but porosity is increased. The observed changes in the properties of the concrete mixes are most probably due to the inherent characteristics of activated carbon, mainly the high porosity and the lower density. However, the change (increase/decrease) in pervious concrete properties resulted in values that are still acceptable for a wide range of applications such as low traffic pavement, parking lots, structural wall application and base course for streets and roads.

Table 5-13: Summary of the properties of the control and M-PAC-con mixes

| Age | **Sample** | **UCS MPa** | **Porosity %** | **Density kg/m$^3$** |
|---|---|---|---|---|
| 7-day | **Co-Con** | 19.2 | 14.8 | 1989 |
| | 0.5%M-PAC-Con | 17.9 | 14.6 | 1972 |
| | 1%M-PAC-Con | 16.6 | 17.7 | 1966 |
| | 2%M-PAC-Con | 16.2 | 19 | 1936 |
| | | | | |
| 28-day | **Co-Con** | 22.7 | 13.1 | 2010 |
| | 0.5%M-PAC-Con | 21.1 | 13.4 | 1996 |
| | 1%M-PAC-Con | 19.8 | 16.6 | 1994 |
| | 2%M-PAC-Con | 19.2 | 16.9 | 1971 |

Figure 5.11 shows the strength versus porosity of M-PAC concrete. The general trend shows that porosity is inversely proportional to the UCS. The higher the porosity, the greater the number of voids inside the concrete samples, and the lower the UCS. This relationship is well documented (Meininger 1988; ACI 522R 2010; Chopra et al. 2007; Neville 2011; Öz 2018; Tennis et al. 2004). Moreover, the effect of the incorporation of other replaceable materials on the strength and porosity of pervious concrete has been investigated by many researchers. Indeed, Resheidat and his group reported contradictory results to the current findings, where an increase in both porosity and UCS was observed when powder charcoal replaced Portland cement at the range of 2.5 to 10% (Resheidat et al. 2002). While the latter researchers did not provide an explanation for this behaviour, a probable cause for the reported increase in UCS could be the lower effective w/c ratio in the charcoal-mixes as a result of adsorbing mixing water by the charcoal. Figure 5.12 compares the UCS to hardened density of pervious concrete for

different percentages of M-PAC. As presented earlier, the values of both properties decreased with an increase in the percentage of M-PAC.

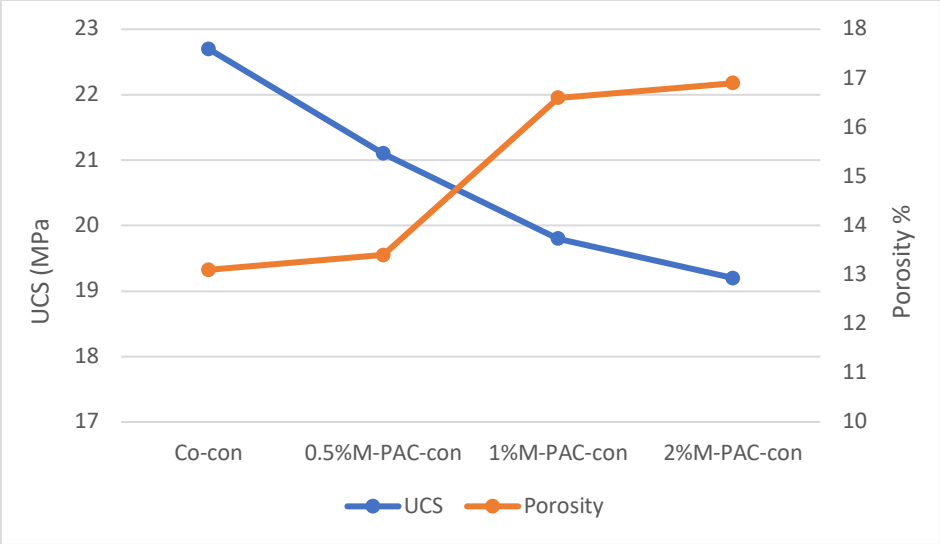


Figure 5-11: The 28-day UCS versus porosity of M-PAC-con

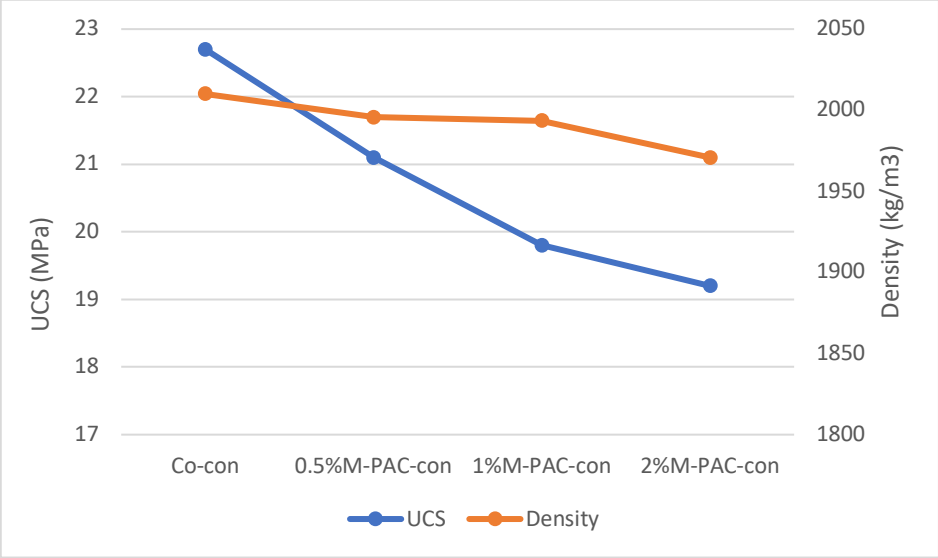


Figure 5-12: The 28-day UCS versus hardened density of M-PAC-con

## 5.3 PARTIAL SUBSTITUTION OF FINE AGGREGATE BY MODIFIED GRANULAR ACTIVATED CARBON

This section outlines modified granular activated carbon (M-GAC) as a partial replacement of fine aggregates in cement mortars and pervious concrete.

### 5.3.1 Properties of cement mortars with different M-GAC percentages

Two sets of cement mortar mixes were prepared as explained in section 3.4.2. The first set of mixes were tested fresh, directly after mixing, to determine the workability of the control and M-GAC-CM using the flow table. The other set was cured for 7, 14 or 28 days before undergoing the UCS test. The notation for cement mortars is based on the percentage of M-GAC inside the cement mixes. They are Co-CM, 0.5%M-GAC-CM, 1%M-GAC-CM and 2%M-GAC-CM.

#### 5.3.1.1 Workability of fresh mortars

To investigate the effect of incorporating different percentages of M-GAC on the flowability of cement mortars, four mixes were prepared with a 0.5 w/c ratio and 2.75 sand/cement ratio and different percentages of M-GAC. The effect of replacing natural sand with 0.5%, 1% or 2% M-GAC on workability was studied through the flow table experiments. Figure 5.13 presents the flow table values for the four tested cement mortars.

As seen from the figure, addition of M-GAC decreased the flow values relative to the control mix, which exhibited a flow table value of 162 mm. This was reduced to 160 mm, 155 mm and 153.8 mm for 0.5% M-GAC-CM, 1% M-GAC-CM and 2% M-GAC-CM respectively. The incorporation of 0.5% M-GAC had negligible influence on the flow table, but this influence increased with increasing percentage of M-GAC. The reduction in flow table values increased from 1.2% for 0.5% M-GAC-CM to 5% for 2% M-GAC-CM.

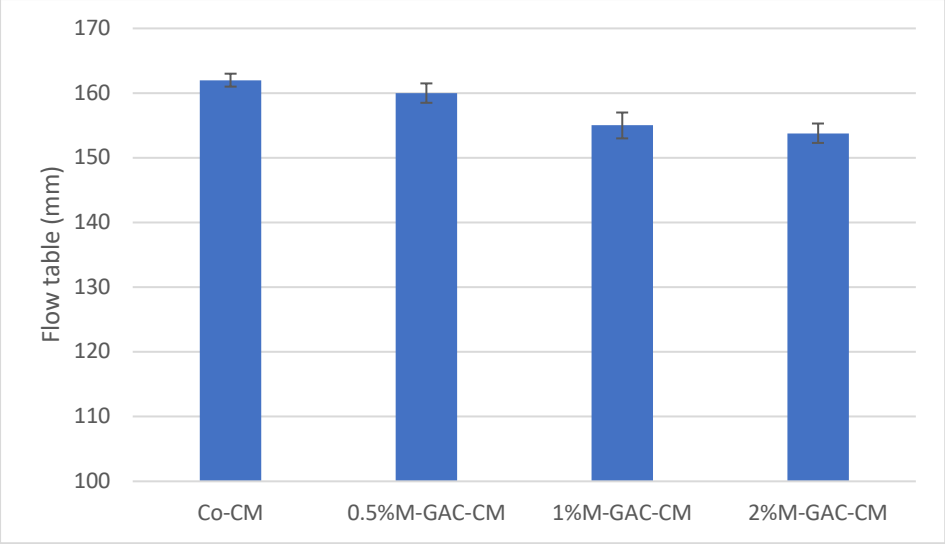


Figure 5-13: Flow table values for control and M-GAC-CMs

A similar trend was observed by Horgnies et al. Incorporation of activated carbon reduced the workability of cement mortars by around 3% when 1.5% activated carbon was added (Horgnies et al. 2012). Similar finding on flowability reduction was also reported by Choi and his group when biochar was incorporated in cement mortars in different percentages (Choi et al. 2012).

There are two possible reasons for the observed decline in the flowability of M-GAC-CMs relative to the control mix. Firstly, activated carbon in any form has a high surface area that enables it to adsorb a variety of materials. In this particular case, M-GAC may adsorb some of the mixing water, resulting in less effective water available for the mix. Water content is a key element in workability of cementitious materials, and reduction of available water produces a stiff mixture with less flowability (Mehta & Monteiro 2006). Secondly, the density of activated carbon is lower than that of natural sand. As modified activated carbon replaces sand by mass, the added volume of M-GAC is larger than the volume of sand that is replaced. The density of natural sand is 2.05 g/cm$^3$, whereas for M-GAC it is 0.54 g/cm$^3$. This result shows that the replacement of sand by the same weight of M-GAC increases the occupied volume by 280%. In accordance with this, the cement quantity available per unit volume of the mix decreases. Cement content is crucial for workability. A higher cement content in the mix leads to more cement paste available to coat the aggregates' surface and fill the voids between them. This reduces the friction between aggregates and smoothens their movement during mixing, thus increasing the

workability of the mix (Taylor 1997). In the M-GAC-CM mixes, the cement content per unit volume was lower than the control mix which resulted reduced workability. However, all the values of the flow table are within 1cm of the control sample. Therefore, the same mix proportions were used for preparing mortar samples for the UCS test.

#### 5.3.1.2 Unconfined compressive strength

The effect of incorporating M-GAC into cement pastes on UCS was investigated. The cement mortars were prepared and tested at certain ages (7, 14 and 28 days) as shown in Figure 5.14. The reported values shown are the average of three cube samples, where the error bars represent the standard deviations.

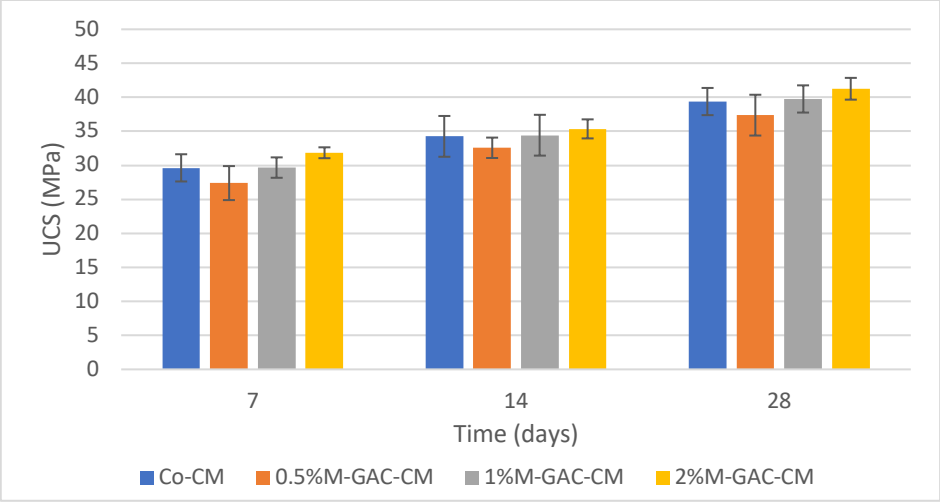


Figure 5-14: UCS of control and M-GAC-CMs at 7, 14 and 28 days of curing

Partial replacement of natural sand with M-GAC slightly changed the UCS of the sand mortars. Apart from the 0.5% M-GAC mix, the UCS increased with increasing M-GAC percentage. Incorporation of 1% or 2% M-GAC slightly improved the early strength of mortars by around 0.13% and 7.5% compared to the control samples, whereas the 0.5% M-GAC strength was 7.6% lower than that of the control mix. A similar trend was observed for samples tested after 14 and 28 days of curing, but with different strength gain ratios. The increase in UCS barely reached 0.5% and 3.2% at 14 days, and 1% and 5% at 28 days, for 1% and 2% M-GAC substitutions respectively.

The increase in strength of the M-GAC mixes could be a consequence of the lower effective w/c ratio. Although all the four mixes had a w/c ratio of 0.5, the adsorption behaviour of

activated carbon may have led to a lower water content and thus to a lower effective w/c ratio. Moreover, the positive strength response might be attributed to an enhanced hydration reaction through an internal curing mechanism provided by the granular activated carbon. With an inter-connected network of voids, activated carbon may act as a supplier of micro-reservoirs that deliver water to the hydration process as needed (Justo-Reinoso et al. 2018). This is because the absorbed water does not bond chemically with carbon so that it would be released during the hydration process (Choi et al. 2012). This mechanism of enhanced curing is consistent with the water desorption behaviour of granular activated carbon considered as a lightweight aggregate by previous researchers (Kosmatka et al. 2002; Ries et al. 2010). However, considering the relatively high standard deviations of the examined samples (shown as the error bars), the UCS values of the concrete samples are noticeably close.

The literature regarding activated carbon substitution in cementitious material is limited. Ersan and his group reported an increase in UCS of more than 10% after 28-days of curing when GAC substituted around 1.7% of sand by mass (Erşan et al. 2015). Similarly, Justo-Reinoso and his group observed an enhancement in UCS of cement mortars containing 1% and 2% GAC as a substitution of natural sand by mass. The maximum strength gain was 10.6% after 28-days of curing when 1% of M-GAC was incorporated as a partial replacement of sand (Justo-Reinoso et al. 2018). A similar trend was observed by Resheidate and his group who reported an increase in UCS for cement mortars that contain 2.5 to 5% charcoal as a partial replacement of Portland cement (Resheidat et al. 2002). Finally, Choi and his group reported an enhancement of 6% in UCS of mortars containing 5% biochar as replacement of Portland cement (Choi et al. 2012).

### 5.3.2 Properties of pervious concrete with different M-GAC percentages

To investigate the performance of modified granular activated carbon as a partial substitution of fine aggregate, four pervious concrete mixes were prepared and cured in a water tank for 28 days. These were the Co-con, 0.5% M-GAC-Con, 1% M-GAC-Con, and 2% M-GAC-Con. The concrete mixes underwent three experiments: UCS, porosity and hardened density.

### 5.3.2.1 UCS, porosity and hardened density

The UCS test was conducted on four mixes of pervious concrete to examine the effect of M-GAC on the UCS. The results are illustrated in Figure 5.15.

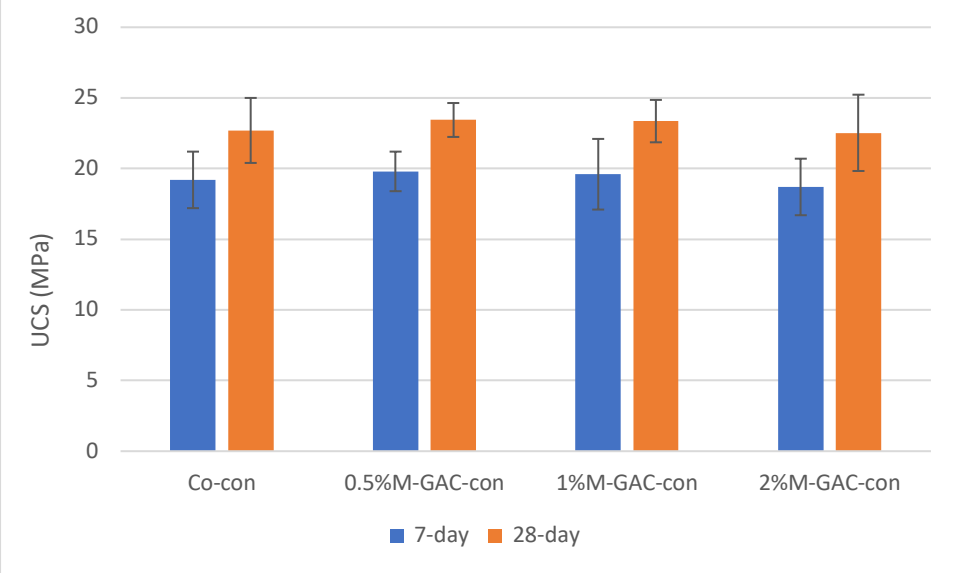


Figure 5-15: UCS at 7 and 28 days of control and M-GAC-con

The 0.5% and 1% M-GAC-con samples demonstrated a slight increase in UCS relative to the control mix, but a slight decline was observed for the 2% M-GAC mix. The mix with the lowest UCS was the 2% M-GAC-Con with 18.7 and 22.5 MPa at 7 and 28 days of curing, constituting a slight decline of 2.6 and 0.7 % from the control mix as presented in Table 5.14.

Table 5-14: Change in the UCS of M-GAC-con mixes

| **Sample** | **Change in UCS %** | |
|---|---|---|
| | **7-day** | **28-day** |
| 0.5%M-GAC-Con | -3.1 | -3.2 |
| 1%M-GAC-Con | -2.1 | -2.9 |
| 2%M-GAC-Con | 2.6 | 0.7 |

The partial substitution of natural sand with M-GAC at a range of up to 1% by mass slightly increased UCS. However, UCS slightly declined when the replacement was 2% by mass. This positive strength response may be attributed to the inherent porous nature of M-GAC, as explained earlier. Granular activated carbon is a porous material that can absorb a quantity of the mixing water and improve cement hydration via an internal curing mechanism. It may act as a micro-reservoir that delivers water when needed during the curing process (Justo-Reinoso et al. 2018). This performance is not provided

by the natural sand since it is chemically and physically inert. However, when the M-GAC replacement was 2%, it appears that internal curing was not sufficient to compensate for the decline in UCS resulting from replacing silica sand grains by a weaker granular activated carbon. Natural sand grains have a higher crushing strength compared to activated carbon. Therefore, the cement strength enhancement obtained by the internal curing effect of modified granular activated carbon can benefit the mix to a certain point, after which it will be contradicted by the strength loss due to differences in the crushing strength of the two materials.

Referring back to section 5.3.1.2 of the UCS values of M-GAC-mortars at 7 and 28 days, it is shown that the effect of incorporating modified granular activated carbon into both cement systems was different. While it had a positive influence on mortars when the ratio was more than 0.5%, the 0.5%M-GAC-Con showed the highest increase in strength. However, taking a possible experimental error into consideration with the 0.5%M-GAC-CM, all UCS values are almost the same or within a limited range.

Regarding porosity, incorporation of M-GAC at all tested percentages increased the porosity of the pervious concrete samples, as shown in Figure 5.16. Similar to M-PAC substitution, this gain in porosity could be explained by the porous nature of M-GAC compared to the replaced natural sand. The 28-day mixes exhibited lower porosity values compared with the early age values at 7 days. This is a consequent result of the continuous hydration of the Portland cement over time, resulting in lower void content inside the samples (Mahoutian et al. 2015). Table 5.15 displays the increase in porosities in M-GAC-con mixes compared to the control mix. The increase in porosities ranged from ~ 6% to 17%, with the highest value observed was associated with the 2% M-GAC-Con at 28-day of curing.

Referring back to section 5.2.2 when M-PAC was used as a partial substitution for cement in pervious concrete, M-PAC-Con samples exhibited a higher porosity than that of the M-GAC-pervious concrete at all replacement ratios. This can be explained by the quantity of added M-PAC to concrete, as it is significantly larger than that of M-GAC despite the percentages remaining the same. In the control concrete mix, Portland cement constitutes around 17% of the dry components while sand constitutes only 5% by mass. The percentages 0.5%, 1% and 2% of modified activated carbon were calculated based on these percentages (17% and 5% for cement and sand respectively). Thus, the

quantities of M-PAC partially replacing Portland cement were higher than that of the M-GAC partially replacing the sand. Consequently, the porosities of M-PAC-con mixes are generally higher than that of M-GAC-con mixes.

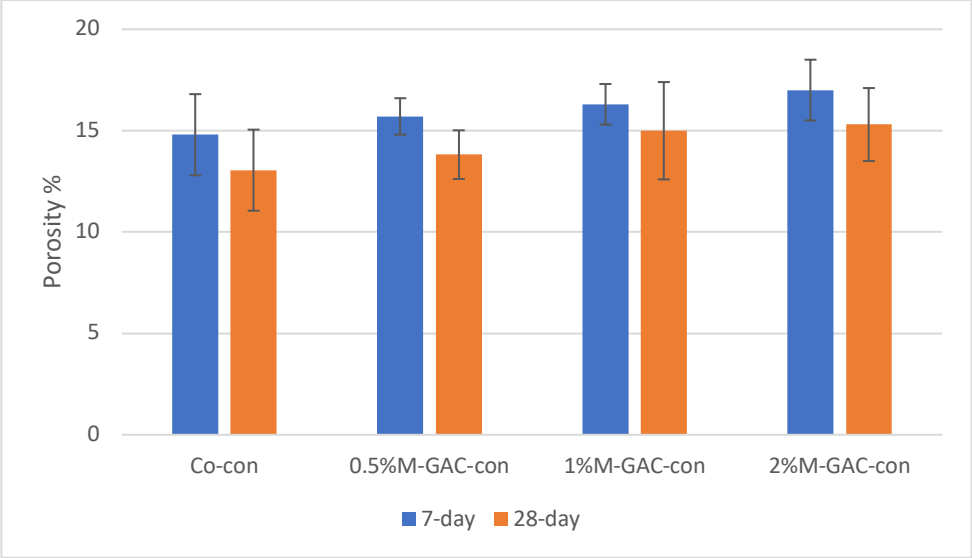


Figure 5-16: Porosity at 7 and 28 days of control and M-GAC-con mixes

Table 5-15: The change in porosity in M-GAC-con mixes

| Sample | Change in porosity % | |
|---|---|---|
| | 7-day | 28-day |
| 0.5%M-GAC-Con | 6.1 | 5.8 |
| 1%M-GAC-Con | 10.1 | 14.9 |
| 2%M-GAC-Con | 14.8 | 17.2 |

The hardened density of the four pervious concrete mixes was also investigated after 7 and 28 days of curing. Figure 5.17 illustrates the values for different percentages of M-GAC. Unsurprisingly, the densities of the produced samples decreased as the M-GAC percentage increased, but increased with time. Granular activated carbon has a lower density than natural sand and thus the replacement resulted in lower density values. The higher the percentage of the replaced material, the lower the resultant density of the concrete. The decrease in density was between 0.6 and 2.7%, as shown in Table 5.16. A similar trend was observed by other investigators. Justo-Reinoso and his co-workers reported a decline in density ranging from ~0.2% to 8% when granular activated carbon was incorporated as a partial replacement of sand in a ratio of 1 to 10% by mass (Justo-Reinoso et al. 2018).

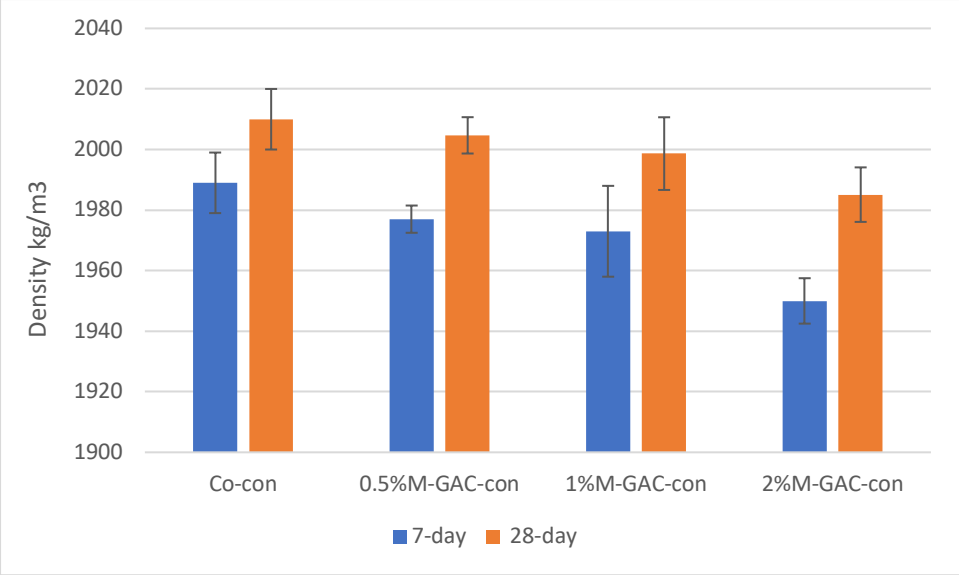


Figure 5-17: Hardened densities of M-GAC-con mixes

Table 5-16: Change in hardened densities of M-GAC-con mixes

| **Sample** | **Decrease in density%** | |
|---|---|---|
| | **7-day** | **28-day** |
| 0.5%M-GAC-Con | 0.6 | 0.3 |
| 1%M-GAC-Con | 0.8 | 0.6 |
| 2%M-GAC-Con | 1.9 | 1.2 |

### 5.3.2.2 Summary of the examined properties of pervious concrete

Table 5.17 summarises the properties of pervious concrete mixes with different percentages of M-GAC. Overall, there is a reduction in hardened density, but an increase in porosity as the percentage of M-GAC increases. The UCS did not show a defined pattern. The observed changes in the properties of the produced concrete mixes is most probably due to the inherent characteristics of activated carbon, mainly the high porosity, the lower density and the weak crushing strength. Based on the obtained properties results, the M-GAC-con mixes are appropriate for any proposed pervious concrete application.

Table 5-17: Summary of the properties of the control and M-GAC-con mixes

| Age | **Sample** | **UCS MPa** | **Porosity %** | **Density kg/m³** |
|---|---|---|---|---|
| 7-day | **Co-Con** | 19.2 | 14.8 | 1989 |
| | 0.5%M-GAC-Con | 19.8 | 15.7 | 1977 |
| | 1%M-GAC-Con | 19.6 | 16.3 | 1973 |
| | 2%M-GAC-Con | 18.7 | 17 | 1950 |
| | | | | |
| 28-day | **Co-Con** | 22.7 | 13.1 | 2010 |
| | 0.5%M-GAC-Con | 23.4 | 13.8 | 2005 |
| | 1%M-GAC-Con | 23.4 | 15.0 | 1999 |
| | 2%M-GAC-Con | 22.5 | 15.3 | 1985 |

Figure 5.18 shows the strength versus porosity of M-GAC concrete, while Figure 5.19 compares the UCS to the hardened density for different percentages of M-GAC. Generally, porosity increased while hardened density decreased with the increase of the M-GAC percentages in pervious concrete. The UCS values showed almost similar values, which might be attributed to the internal hydration provided by the porous M-GAC.

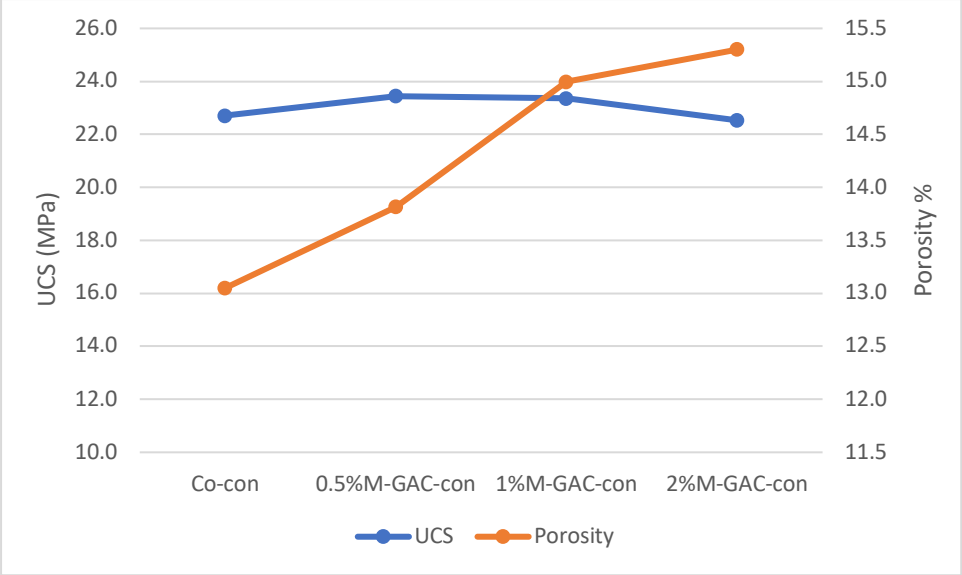


Figure 5-18: The 28-day UCS versus porosity of M-GAC-con

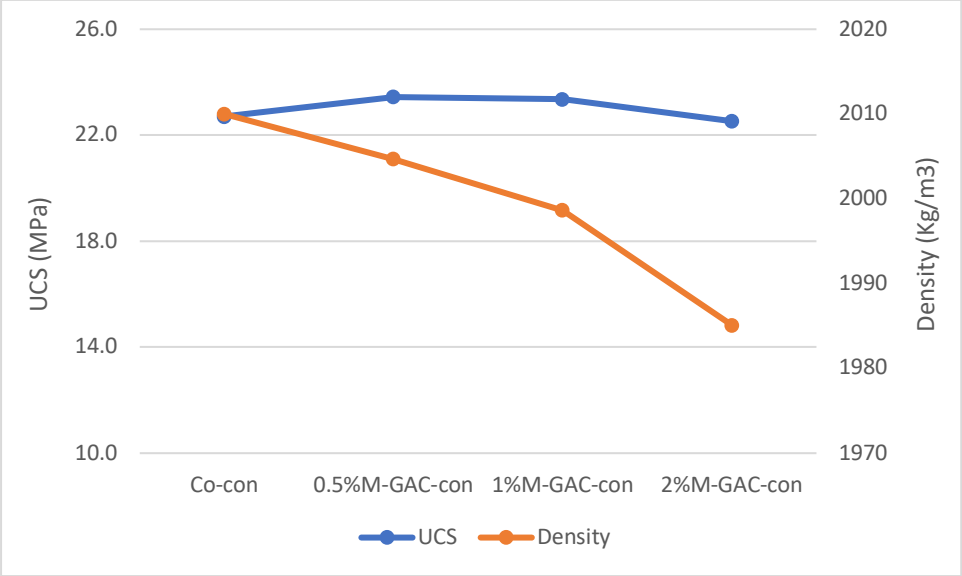


Figure 5-19: The 28-day UCS versus hardened density of M-GAC-con

## 5.4 SUMMARY OF THE PERFORMANCE OF M-AC WITH DIFFERENT PERCENTAGES

The previous sections of this chapter investigated the influence of two types of substitution, M-PAC to partially substitute cement, and M-GAC to partially substitute fine aggregates. This was conducted through three systems of cement-based materials: cement pastes, cement mortars and pervious concrete. Different percentages of modified activated carbon replaced Portland cement (as in cement pastes and pervious concrete) and natural sand (as in cement mortars and pervious concrete). The various mixes underwent several tests as presented and discussed earlier. The next section summarises the main findings of these tests.

### 5.4.1 Summary of the performance of modified activated carbon in cementitious materials

- ***M-PAC as a partial replacement of Portland cement***

The addition of a small percentage of **M-PAC** to cement pastes had two observed influences on their properties. Firstly, addition of M-PAC resulted in the adsorption of mixing water, creating stiff cement pastes compared to control samples prepared with the same w/c ratio as in the standard consistence tests. The adsorption of mixing water by M-PAC resulted in an addition of water in the cement pastes to achieve the same consistency, which consequently resulted in a higher water to cement ratio. This behaviour was also noticed during the isothermal calorimetry test. The presence of M-PAC led to lower effective w/c ratios, and thus a lower cumulative heat of hydration. However, when a fixed effective w/c ratio was applied, the cumulative heat of hydration increased with the increase in M-PAC percentage due to the larger space provided by the M-PAC for hydrates formation.

Secondly, M-PAC substitution resulted in an increase in weight loss (as shown through TGA analysis), potentially as a result of release of $CO_2$ that was trapped inside the incorporated M-PAC. In addition, it was observed through increased calcite content in the M-PAC-cement pastes, compared to the control mix. This indicates that the presence of M-PAC helped in transforming some of the calcium hydroxide to carbonate, by probably providing captured $CO_2$ from the atmosphere to the carbonation reaction.

Based on the results of the properties of the M-PAC-con mixes, it was observed that the lower density of M-PAC combined with its higher porosity compared to cement, resulted in lower-density and higher-porosity mixes. Moreover, higher proportions of M-PAC resulted in lower UCS concrete.

- ***M-GAC as a partial replacement of fine aggregate***

In the experiments that were conducted on cement mortars containing different percentages of **M-GAC**, two main effects were noticeable. The first was similar to the M-PAC adsorption behaviour explained in the previous section. M-GAC has a high surface area that enables it to adsorb part of the mixing water, leaving the effective w/c ratio lower than the actual added value as demonstrated through the flow table test. The second impact observed was a change in the mechanical properties of the M-GAC-mixes compared to the reference mix. The internal curing provided by the high porosity of M-GAC slightly enhanced the UCS of the cement mortars up to a point, after which it did not compensate for the lower strength of activated carbon compared to natural sand. However, for up to 2% of the M-GAC in the cement mortars, the strength values were within an acceptable range compared to the control mix.

The inclusion of M-GAC in pervious concrete as a partial replacement of sand was studied through UCS, porosity and density. Due to the high porosity and lower density of M-GAC, the obtained M-GAC-mixes exhibited higher porosity and lower density results compared to the control mix.

### 5.4.2 Discussion on M-AC percentages

The percentages of M-PAC as a partial replacement of cement in cement pastes and pervious concrete were chosen to be 0.5%, 1% and 2% of Portland cement. The choice of these percentages was inferred by the maximum unburnt carbon quantities in the supplementary cementitious materials as presented and discussed earlier in sections 2.8.5 and 2.8.6.

Similarly, the percentages of M-GAC as a partial replacement of fine aggregate in mortars and pervious concrete were chosen in light of the maximum allowed quantity of carbon content in aggregate. This percentage is between 0.5% and 1% by mass depending on the

importance of the appearance of the concrete (ASTM regulations). Therefore, the percentages of M-GAC were chosen as 0.5%, 1% and 2%.

The influence of both substitutions on the properties of the examined cement-based systems was investigated. Table 5.18 summarises the values of the examined properties along with the change when compared to reference mixes. The change was presented as absolute values to reflect the variations from the reference mixes.

From the table, it can be seen the replacement of cement by M-PAC in cement pastes resulted in a change from the control mixes ranged from ~ 2 to 7% in standard consistency tests and in the range of 11-19% in the initial setting times. The change in the mechanical and physical properties of pervious concrete after M-PAC incorporation ranged from less than 1% (density) up to 27% (porosity).

Regarding M-GAC, the change was almost negligible in cement mortars and the mechanical properties of concrete (less than 5%) but ranged from ~ 6 to 15% in the porosity values of concrete. Although the increase in porosity seems high, the values themselves are within the range of the typical porosity values of pervious concrete, 15 – 35%. The UCS range of values for pervious concrete is 3.5 to 28 MPa, with 17MPa is the typical value for the majority of applications. The 28-day obtained results in the current study are within this range and higher than 17MPa.

Therefore, it can be concluded that even using the highest investigated percentage (2%) of both M-PAC and M-GAC to replace Portland cement and sand respectively, resulted in values within the normal limits of pervious concrete properties. Therefore, these percentages will be selected for further investigation in Chapter 6 to study the effect of the combined substitution of M-PAC and M-GAC on the properties of pervious concrete and on the $CO_2$ sequestration performance of pervious concrete. Choosing higher values would have deviated too far from the specified standards that were used as guidance for selecting the tested percentages.

Table 5-18: Summary of the properties and the variations from control mixes

| M-PAC as a substitution for cement | | | | | M-GAC as a substitution for fine aggregates | | | | |
|---|---|---|---|---|---|---|---|---|---|
| Cement pastes | Standard consistency (w/c ratio) | 0.5%M-PAC-CP | 0.305 | 1.6% | Cement mortars | Flowability (mm) | 0.5%M-GAC-CM | 160 | 1.2% |
| | | 1%M-PAC-CP | 0.31 | 3.3% | | | 1%M-GAC-CM | 155 | 4.3% |
| | | 2%M-PAC-CP | 0.32 | 6.7% | | | 2%M-GAC-CM | 153.8 | 5% |
| | Isothermal calorimetry (I. setting time hr) | 0.5%M-PAC-CP | 3.81 | 11% | | 28-day UCS (MPa) | 0.5%M-GAC-CM | 37.4 | 5% |
| | | 1%M-PAC-CP | 4.11 | 19% | | | 1%M-GAC-CM | 39.8 | 1% |
| | | 2%M-PAC-CP | 3.91 | 14% | | | 2%M-GAC-CM | 41.3 | 4.8% |
| Pervious concrete | 28-day UCS (MPa) | 0.5%M-PAC-Con | 21.1 | 7% | Pervious concrete | 28-day UCS (MPa) | 0.5%M-GAC-Con | 23.4 | 3.2% |
| | | 1%M-PAC-Con | 19.8 | 13% | | | 1%M-GAC-Con | 23.4 | 2.9% |
| | | 2%M-PAC-Con | 19.2 | 15% | | | 2%M-GAC-Con | 22.5 | 0.7% |
| | 28-day porosity % | 0.5%M-PAC-Con | 13.4 | 0.8% | | 28-day porosity % | 0.5%M-GAC-Con | 13.8 | 5.8% |
| | | 1%M-PAC-Con | 16.6 | 25% | | | 1%M-GAC-Con | 15.0 | 14.9% |
| | | 2%M-PAC-Con | 16.9 | 27% | | | 2%M-GAC-Con | 15.3 | 17.2% |
| | 28-day density ($kg/m^3$) | 0.5%M-PAC-Con | 1996 | 0.7% | | 28-day density ($kg/m^3$) | 0.5%M-GAC-Con | 2005 | 0.3% |
| | | 1%M-PAC-Con | 1994 | 0.8% | | | 1%M-GAC-Con | 1999 | 0.6% |
| | | 2%M-PAC-Con | 1971 | 1.9% | | | 2%M-GAC-Con | 1985 | 1.2% |

# 6 Modified activated carbon in pervious concrete: Properties and $CO_2$ sequestration Performance

## 6.1 INTRODUCTION

This chapter presents details of the laboratory work conducted to investigate the modified activated carbon-pervious concrete (M-AC-con). In the previous chapter, modified activated carbons were investigated as a partial substitute of cement and fine aggregate individually. In this chapter, the effect of M-AC as a direct substitution of cement and as a partial replacement for the finer aggregates (sand) on pervious concrete is presented and discussed.

There are three main sections in this chapter. The effect of the combined incorporation of M-PAC and M-GAC on pervious concrete properties (UCS, density, porosity, permeability, workability and carbonation degree) is investigated in the first section. In the second section, the microstructure of M-AC-con is analysed using XRD, TGA and SEM. Finally, the properties of M-AC-con in terms of $CO_2$ sequestration is assessed. The pervious concrete mixes investigated in this chapter are presented in Table 6.1 with the notations and the tests conducted, which will be used throughout this chapter.

Table 6-1: Notation and experiments conducted in Chapter 6

<table>
<tr><th>Section</th><th>Experiments</th><th>Curing</th><th>Notations</th></tr>
<tr><td rowspan="5">First section</td><td>UCS</td><td rowspan="3">28-day of normal curing in a water tank</td><td rowspan="5">• Co-con: Control pervious concrete<br>• M-AC-con: Modified activated carbon-pervious concrete</td></tr>
<tr><td>Permeability</td></tr>
<tr><td>Hardened density</td></tr>
<tr><td>Porosity</td><td rowspan="2">NA</td></tr>
<tr><td>Slump test</td></tr>
<tr><td>Phenolphthalein test</td><td>2 months of elevated $CO_2$ curing</td><td>• C-S5: control concrete at 5 cm depth from cylinder top<br>• C-S10: control concrete at 10 cm depth from cylinder top<br>• M-AC-S5: M-AC concrete at 5 cm depth from cylinder top<br>• M-AC-S10: M-AC concrete at 10 cm depth from cylinder top</td></tr>
<tr><td colspan="4"></td></tr>
<tr><td rowspan="3">Second section</td><td>XRD</td><td rowspan="3">2 months of elevated $CO_2$ curing</td><td rowspan="2">• C-S5: control concrete at 5 cm depth from cylinder top<br>• C-S10: control concrete at 10 cm depth from cylinder top<br>• M-AC-S5: M-AC concrete at 5 cm depth from cylinder top<br>• M-AC-S10: M-AC concrete at 10 cm depth from cylinder top</td></tr>
<tr><td>TGA</td></tr>
<tr><td>SEM</td><td>• Co-con: Control pervious concrete<br>• M-AC-con: Modified activated carbon-pervious concrete</td></tr>
<tr><td colspan="4"></td></tr>
<tr><td>Third section</td><td>$CO_2$ sequestration</td><td>28-day of normal curing in a water tank</td><td>• Co-con: Control pervious concrete<br>• M-AC-con: Modified activated carbon-pervious concrete<br>• Un-AC-con: Unmodified AC-pervious concrete<br>• M-PAC-con: 2%M-PAC-pervious concrete<br>• M-GAC-con: 2%M-GAC-pervious concrete</td></tr>
</table>

## 6.2 PROPERTIES OF M-AC-PERVIOUS CONCRETE

In this section, the properties of the modified activated carbon-pervious concrete (M-AC-con), containing 2%M-PAC and 2%M-GAC, compared to that of the control pervious concrete (Co-con) are presented and discussed. These include UCS, hardened density, porosity, water permeability, workability and $CO_2$ carbonation using phenolphthalein.

### 6.2.1 UCS and hardened density of M-AC-con

To investigate the combined effect of partially substituting both cement and fine aggregate with M-PAC and M-GAC, respectively, on UCS, two concrete mixes were prepared and cured as explained in section 3.2.4 and tested at the age of 7 and 28 days. Figure 6.1 illustrates the results at the two ages.

The UCS of the Co-con was 19.2 and 22.7 MPa at age of 7 and 28 days respectively. The combined incorporation of both forms of M-AC led to a slight reduction in UCS relative to the control samples. Both the control and the M-AC-con exhibited an increase in UCS after 28 days of curing, compared to 7 days, as shown in Figure 6.1. The increase in the UCS over time is an expected result of the generation of hydration products (Scrivener et al. 2016; Sharpley 2015; Hewlett 2004). The percentage of increase over the observed time periods were similar for the control concrete (18.2%) and the M-AC-con (19.1%). Given the comparatively smaller amount of cement in the M-AC-con (due to the M-PAC substitution), the development of strength for the M-AC-con was higher than that of the Co-con. This could be attributed to the internal curing provided by the modified activated carbon, as discussed earlier. Overall, both mixes achieved UCSs that were within the commonly expected values of pervious concrete (3.5 - 28 MPa).

In sections 5.2.2.1 and 5.3.2.1 it was shown that the substitution of cement with 2% M-PAC resulted in a slight reduction in UCS at both ages, whereas negligible change was observed upon substitution of the fine aggregate with 2% M-GAC. The combined incorporation of both forms of M-AC resulted in a UCS value between the two values ($UCS_{M\text{-}PAC}$ and $UCS_{M\text{-}GaC}$). This may indicate the importance of incorporating M-GAC as water-bearing grains to compensate UCS by enhancing the internal hydration although the lower amount of cement available in the M-AC-con.

The UCS results presented here contrast with other studies. Akhtar and Samara (Akhtar & Sarmah 2018) added powder biochar to normal concrete at percentages ranging from 0.1 - 1% of the total volume of concrete. They observed that the early strengths of Biochar-concrete for some ratios were higher than that of the control concrete, whereas the strengths after 28 days were lower (Akhtar & Sarmah 2018). The researchers explained these results as demonstrating higher pozzolanic activity, due to the presence of biochar, in the early stages. They also reported that the filling effect of lower density powder biochar prohibits production of C-S-H, due to higher volume occupation (Akhtar & Sarmah 2018), which contradicts the observations of several researchers about the enhancement in C-S-H development as a result of the filler effect.

The effect of incorporating both forms of M-AC on hardened density was investigated at the age of 7 and 28 days, as shown in Figure 6.2. Both concrete mixes exhibited an increase in hardened density at the age of 28 days compared to 7 days, which is a consequent result of the continuous hydration of the Portland cement over time.

The incorporation of M-AC in both forms decreased the density of pervious concrete from 1989 to 1963 kg/m$^3$ and from 2010 to 1993 kg/m$^3$ at the age of 7 and 28-days, respectively. This is attributed to the lower density of M-AC compared to either natural sand or Portland cement. Compared with the hardened densities of the mixes studied in Chapter 5, the 2% M-PAC-con possessed the lowest density of all mixes. This may be due to the lower density of M-PAC compared to M-GAC and the higher quantity of M-PAC when partially substituted for cement, compared to the quantity of M-GAC that was partially substituted for sand. The hardened density of the M-AC-con which contained both forms of low-density M-AC was surprisingly higher than that of 2%M-PAC-con or 2%M-GAC-con.

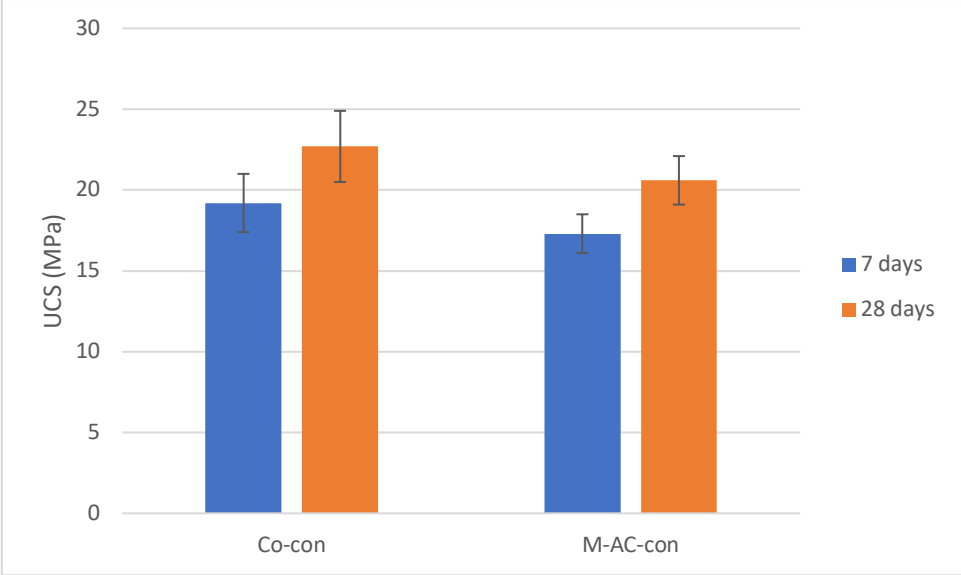


Figure 6-1: UCS for Co-con and M-AC-con at 7 and 28 days

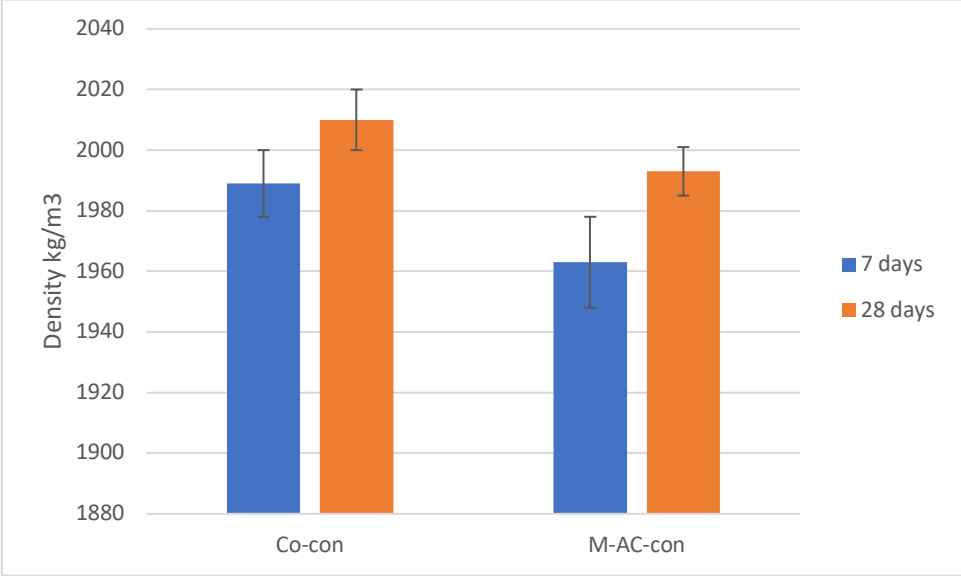


Figure 6-2: Hardened density for Co-con and M-AC-con at 7 and 28 days

### 6.2.2 Porosity and water permeability of M-AC-con

The porosity values of the Co-con and the M-AC-con at the age of 7 and 28 days are presented in Figure 6.3. Generally, a reduction in the porosity was observed with curing age, while inclusion of M-AC resulted in an increase in porosity. Pervious concrete is a porous type of concrete for which the porosity value is typically more than 15%. Co-con exhibited just under 15% porosity at the age of 7 days and around 13% at the age of 28 days. During the continuous hydration process, the porosity of concrete usually declines with time due to the decreasing volume of the voids inside the concrete matrix. The concrete samples that underwent curing for longer durations exhibited lower void volume as a result of the continuous cement hydration which results in filling the hydration products in the air voids, thus reducing the porosity (Mahoutian et al. 2015).

The dual incorporation of M-PAC and M-GAC resulted in porosity values of 18.6% and 16.8% at the age of 7 and 28-days respectively. These constitute an increase in porosity of around 26% and 29% respectively, compared with the control mix at the same ages. The increase in porosity is a direct consequence of the high porosity of M-AC as discussed earlier.

Water permeability is a crucial parameter in pervious concrete. Therefore, the effect of incorporation of both M-PAC and M-GAC on water permeability of the produced mix was investigated at the age of 7 and 28 days. The results are presented in Figure 6.4.

Generally, a slight decrease in permeability was observed following incorporation of M-AC at both ages. At 28 days, the decrease in permeability is highly associated with the decrease in porosity observed earlier. This is a result of strength development and the continuation of the hydration process, resulting in precipitating and filling of the air voids with hydration products (Mahoutian et al. 2015). Moreover, incorporation of M-AC reduced water permeability at both ages compared to the Co-con samples. The substitution or addition of fine materials (e.g. M-AC) generally reduces the permeability of pervious concrete (Maguesvari & Narasimha 2013). In particular, substituting cement with M-PAC, a very fine-grained material compared to Portland cement, could have the effect of filling the voids in the pervious concrete mixes, resulting in concrete with reduced permeability. Overall, pervious concrete mixes should have water permeability values of at least 1mm/sec for infiltration purposes. All mixes maintained this minimum

requirement in spite of the reduction in permeability overall as a result of the addition of M-AC.

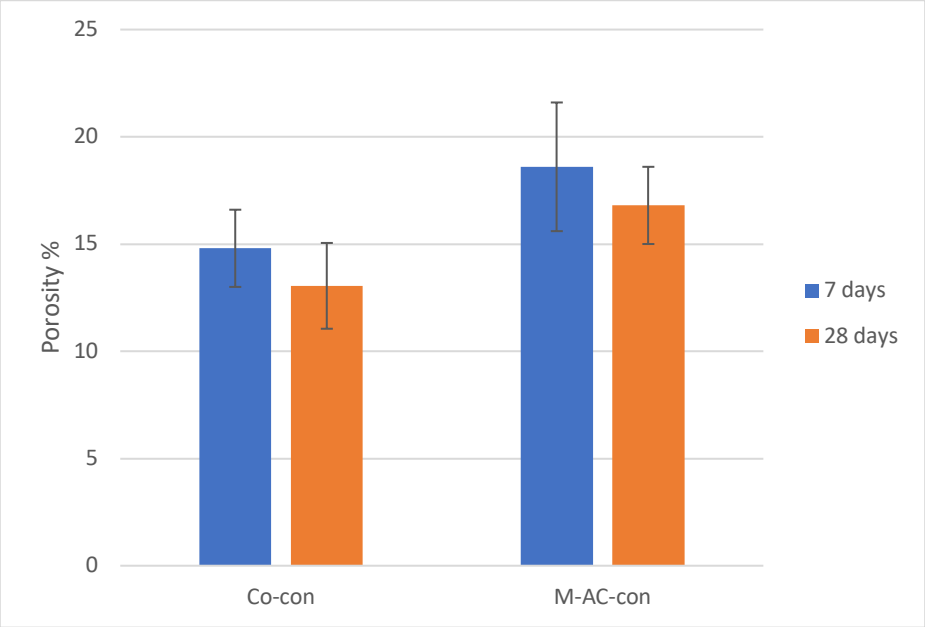


Figure 6-3: Porosity of Co-con and M-AC-con at 7 and 28 days

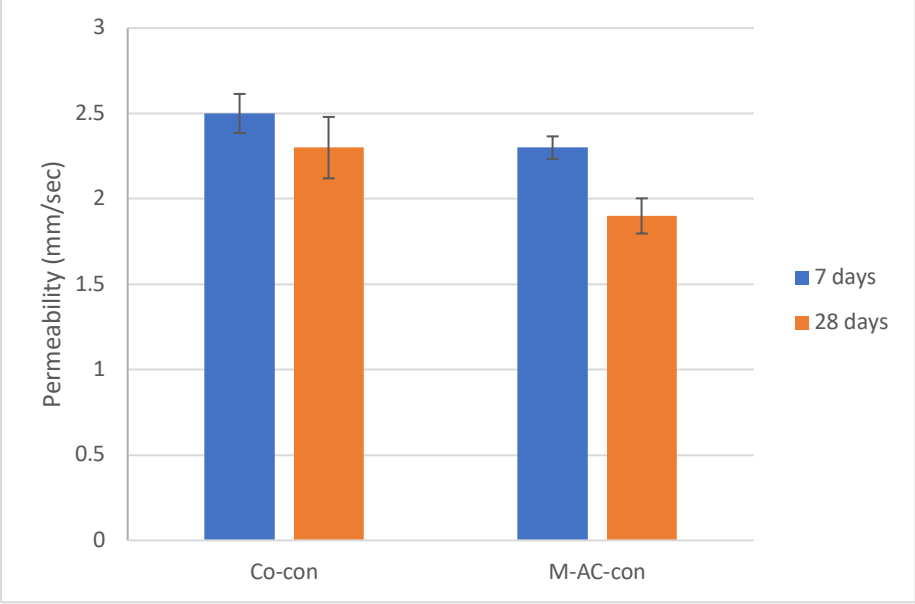


Figure 6-4: Water permeability for Co-con and M-AC-con at 7 and 28 days

Figure 6.5 illustrates the correlation between porosity and permeability. Generally, high porosity leads to higher permeability, but lower strength and density in pervious concrete (Tennis et al. 2004; Huang et al. 2010; Martin et al. 2014; N Neithalath et al. 2010). Figure 6.5 shows that the permeability increased by the increase in porosity value at different ages within the same mix. However, no clear correlation was observed for all the values from both mixes. M-AC may slightly alter pervious concrete properties in two different ways. The first is the increase in the porosity of the produced concrete samples due to the high porosity of M-AC itself, while the second is the partial blocking effect it may have in pervious concrete, thus reducing permeability. On the other hand, porosity showed a strong correlation with UCS and density ($R^2$ ~ 0.68 and 0.81 respectively) as shown in Figure 6.6.

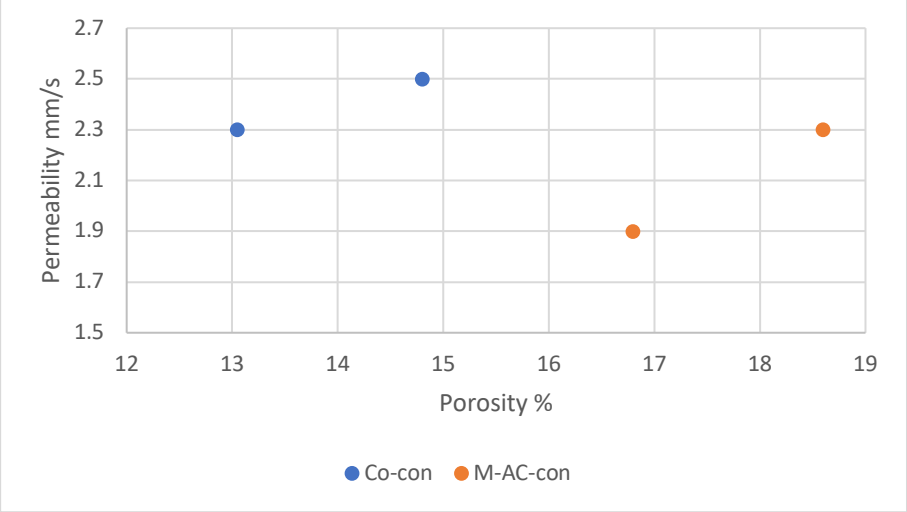


Figure 6-5: Porosity-permeability correlation for Co-con and M-AC-con

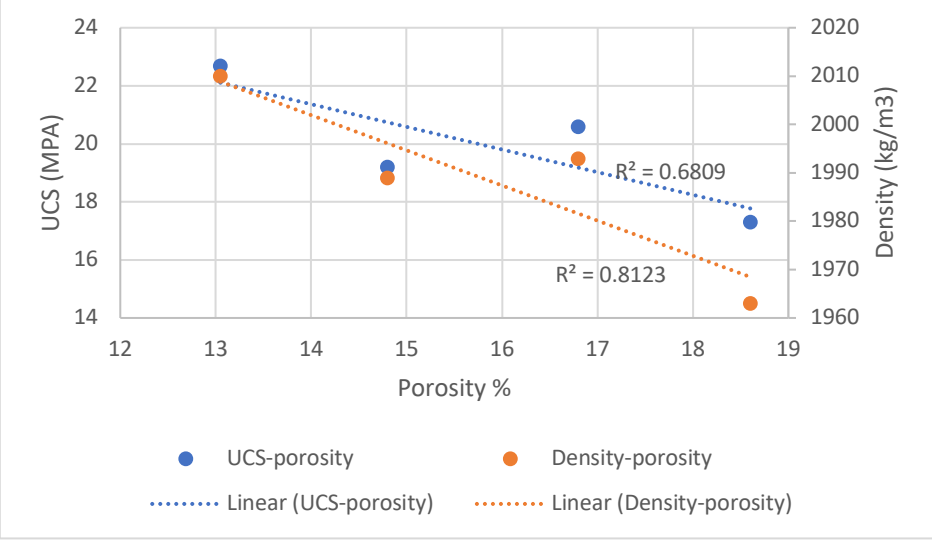


Figure 6-6: Porosity-UCS and porosity-density correlation for Co-con and M-AC-

### 6.2.3 Workability (Slump test)

To evaluate the effect of incorporating both M-AC into the fresh properties of pervious concrete, the slump test was performed following BS EN 12350-2. Figure 6.7 (a and b) shows the slump test for both the control and M-AC-concrete mixes. Both mixes demonstrated no slump at all. Pervious concrete is usually defined as a no-slump concrete. The incorporation of modified activated carbon as a partial replacement of sand and Portland cement did not affect the slump, and therefore the workability of the pervious concrete matrix.

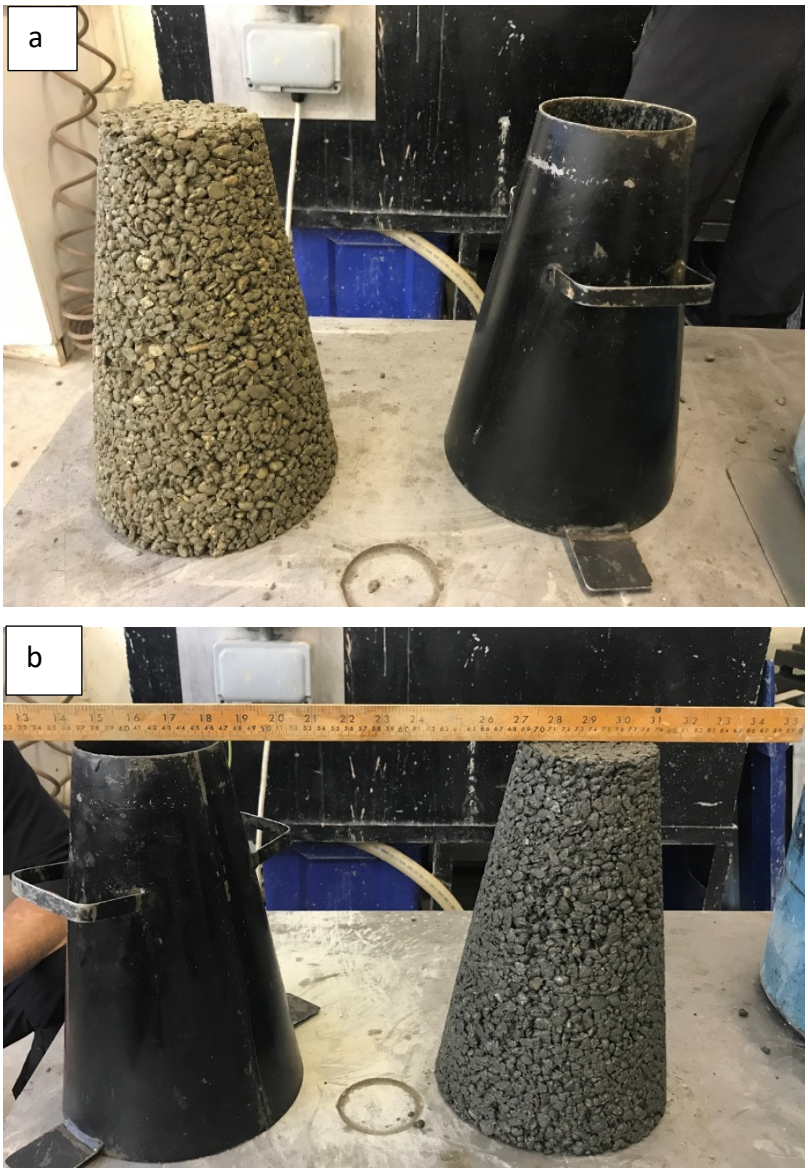


Figure 6-7: Slump test for (a) Co-con (b) M-AC-con

However, it was noticed that the M-AC-concrete required a higher quantity of water than the Co-con to compensate for the mixing water being adsorbed by both the M-PAC and

M-GAC. The determination of water demand for M-AC-con was accomplished through the first set of trial mixes of concrete as explained in section 3.4.1.3. The water to cement ratio increased from 0.35 for the control concrete mix to around 0.36 for the M-PAC and M-GAC concrete mixes and to around 0.37 for the M-AC-con to achieve the same level of workability. Figure 6.8 shows samples of control and M-AC-concrete with the proper amount of water to form a ball in the hand (the ball rolling method) as described by Tennis (Tennis et al. 2004).

Figure 6-8: The rolling ball method to determine the proper amount of water for (a) Co-con (b) M-AC-con

### 6.2.4 Phenolphthalein test for Carbonation

The carbonation test using phenolphthalein was conducted in triplicate on the Co-con and M-AC-con samples as described in section 3.4.3.6. The pervious concrete samples were cured in an incubator for two months in a 20% $CO_2$ environment with 65% relative humidity. On the day of the test, the concrete samples were trimmed longitudinally using an electrical saw, after which Phenolphthalein solution was sprayed directly onto the samples. Figure 6.9 shows the two halves of three samples of Co-con (left) and M-AC-con (right) before and after phenolphthalein application.

Concrete carbonation is a chemical process that takes place between the hydration products and carbon dioxide in the presence of water. Upon application of phenolphthalein, the carbonated area remains colourless, whereas the uncarbonated areas turn pink. Figure 6.9 shows that all samples exhibit carbonation to some extent, but the M-AC-con samples show a slightly increased number of carbonated areas (colourless) than the Co-con samples. Phenolphthalein solution was also applied to the outer surface of the concrete cylinders as shown in Figure 6.9(b). Although the outer surfaces of both samples show higher carbonation than the interior surfaces (Figure 6.9 (c,d and e)) as a direct consequence to their exposure to $CO_2$ in the $CO_2$ incubator, M-AC-con showed a higher number of carbonated spots than Co-con. Therefore, the phenolphthalein test demonstrated the higher calcite content in the M-AC-concrete in comparison to the control concrete. This is confirmed later in this chapter through the microstructural analysis. It was impractical to measure the depth of carbonation in pervious concrete due to its porous nature.


Before applying phenolphthaline


After applying phenolphthaline




Figure 6-9: carbonation test using phenolphthalein for the (left) Co-con and (right) M-AC-con (a)The samples (b)Applying phenolphthalein on the outer surface of the samples (c, d and e)samples before and after applying phenolphthalein

## 6.3 CHARACTERISATION OF THE MODIFIED ACTIVATED CARBON-PERVIOUS CONCRETE

XRD, TGA and SEM analyses were performed on the Co-con and M-AC-con mixes to investigate the effect of the combined incorporation of both M-PAC and M-GAC on the microstructure and hydration products of both mixes. Powder materials were extracted from the pervious concrete cylinders for XRD and TGA tests as described in section 3.4.3.8. The examined powder materials are denoted as (C-S5), (C-S10), (M-AC-S5), (M-AC-S10), where C and M-AC refer to control concrete and M-AC-concrete respectively, and S5 and S10 refers to the depth from where the powder was extracted. The test was conducted at two curing ages; after one month and after two months of accelerated carbonation curing in the $CO_2$ incubator. Small pieces of millimetre size from the crushed concrete cylinders were used for SEM imaging.

### 6.3.1 X-Ray diffraction (XRD)

The results from XRD analysis are combined together in Figure 6.10 and 6.11. Both figures show the main hydration products of both mixes at different depths from the edge, specifically, at depths 5 and 10 cm to compare the level of change in the hydration products with depth. Figure 6.10(a) and (b) show the XRD of the hydration products for both Co-con and M-AC-con respectively at 5 cm from the cylinders edge. Figure (c) and (d) show the same at 10 cm from the cylinder edge. The same arrangement of graphs is followed in Figure 6.11.

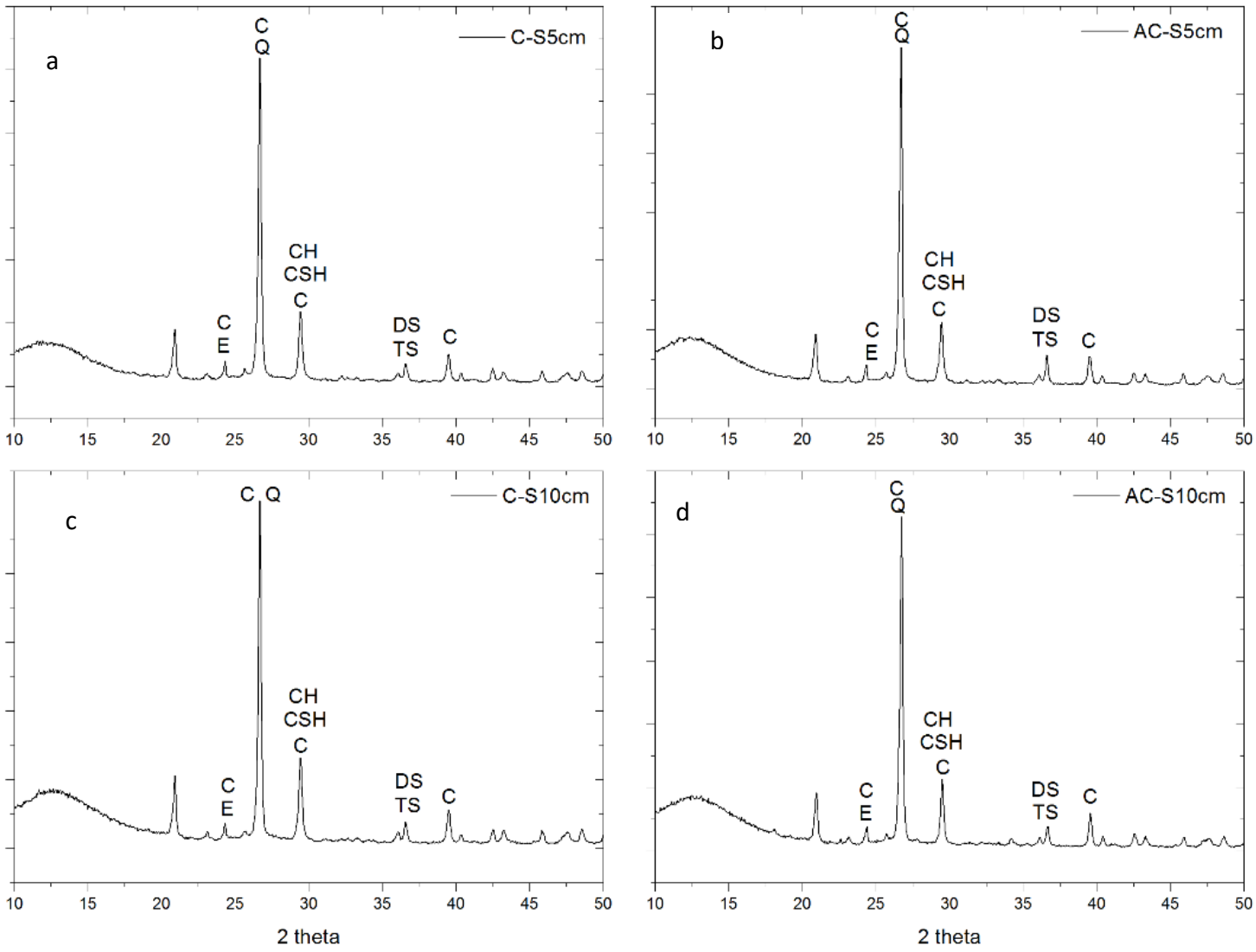


Figure 6-10: XRD for control and M-AC- con after one month of elevated $CO_2$ curing (a&c) Co-con (b&d) M-AC-con

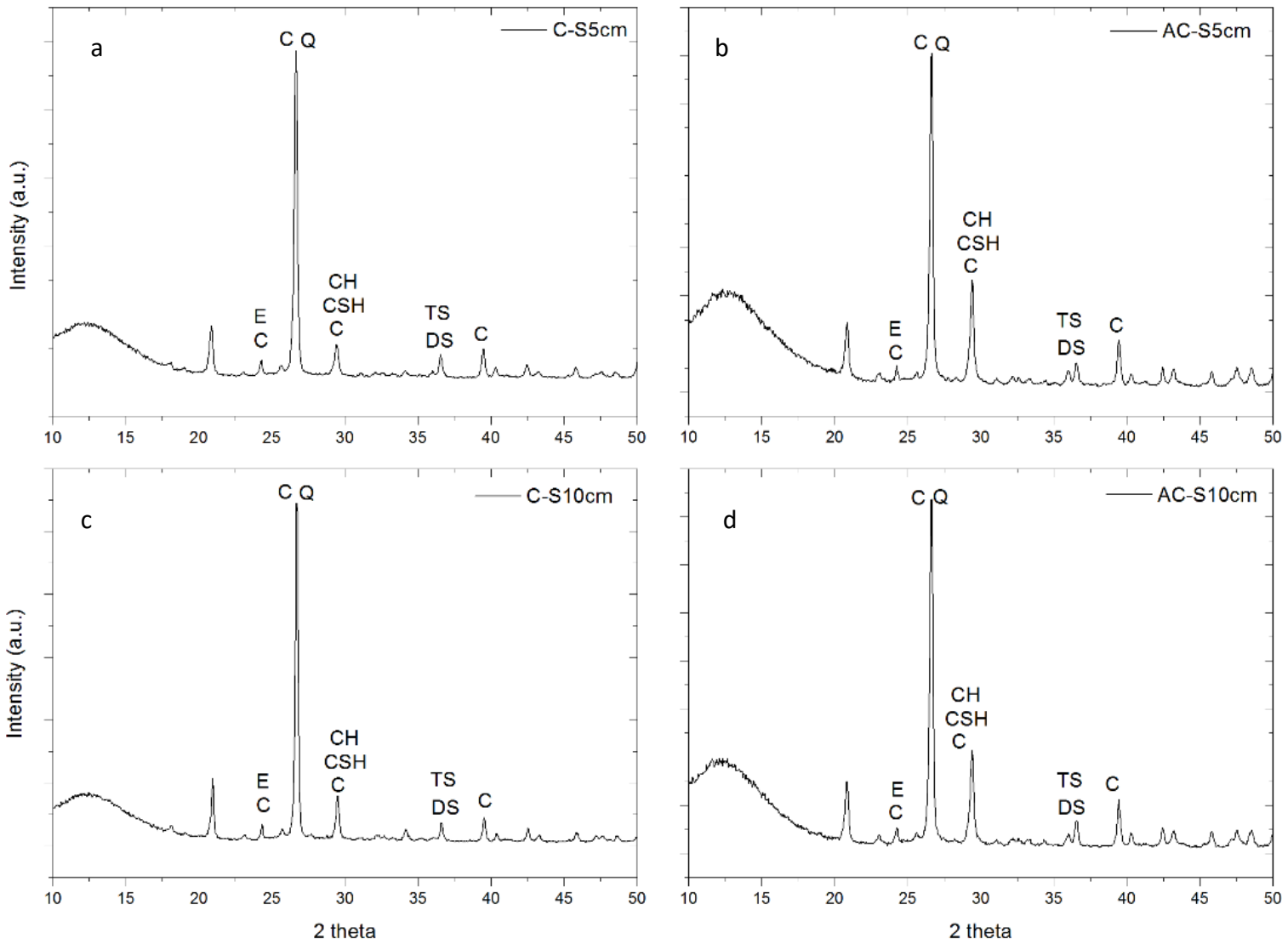


Figure 6-11: XRD for control and M-AC- mixes after two months of elevated $CO_2$ curing (a&c) Co-con (b&d) M-AC-con

Overall, the XRD diffractograms of Figure 6.10 and Figure 6.11 are similar where typical Portland cement hydration products are detected including portlandite (denoted as CH), ettringite (denoted as E), poorly crystallised calcium silicate hydrates (C-S-H, denoted as CSH) and calcite (denoted as C). Also shown in Figure 6.10, the intensity of all the aforementioned hydration products is almost the same. The most distinct peak in all graphs was around 26.5°. This could be attributed to either calcite or quartz. The tested powdered materials were extracted from pervious concrete samples where natural sand is a component of the pervious concrete mix. Quartz is the main mineral in sand, therefore, it was expected to be observed by XRD. Based on the similarity of the spectra in Figure 6.10, the incorporation of M-PAC and M-GAC did not affect the development of the hydration products.

In Figure 6.11 where the powder samples were extracted from pervious concrete after 2 months of elevated $CO_2$ curing, the peaks in M-AC-con graphs (Figure 6.11 b & d) are slightly different from the Co-con sample XRD graphs (Figure 6.11 a & c). One example is the small peaks located around 36°. These peaks which might be residual content of tricalcium silicate (TS) and dicalcium silicate (DS) are slightly more obvious in M-AC-con than the Co-con. Moreover, the peaks at 29.1° are more intense in M-AC-con samples. This peak is most probably attributed to calcite, indicating a higher calcite content in M-AC-con as a result of the presence of M-AC. The 29.1° peak might be also associated to C-S-H gel. In this particular case, the C-S-H content is higher in M-AC- samples, implying a higher developing rate of the hydration products. This might be justified by the internal hydration provided by the M-AC inside concrete. Given the slightly lower UCS of M-AC-con compared to that of the Co-con, this peak is most probably attributed to calcite. The second difference is the peak around 39° which is most probably attributed to calcite. As can be seen from Figure 6.11, this peak is also more explicit in M-AC-con than Co-con sample. This indicates that the presence of M-AC increased the carbonated material inside M-AC-con, which is in agreement with the phenolphthalein test shown earlier. These carbonation products might be referred to calcium carbonates as a direct product of concrete carbonation, and probably sodium carbonates as a result of reacting $CO_2$ with the residual NaOH on the surface of M-AC. Further discussion on the proposed mechanism of calcite formation inside M-AC-con is presented later in section 6.5.

### 6.3.2 Thermogravimetric analysis (TGA)

The results from TGA analysis are shown in Figure 6.12 and Figure 6.13. Both figures show the decomposition of the main hydration products of both mixes at depths 5 and 10 cm at the two different ages of one month and two months after elevated $CO_2$ curing. Three main peaks were observed in all samples in both figures. The peaks at ~100°C are related to the decomposition of C-S-H. Distinct peaks were detected at ~450°C, due to the decomposition of calcium hydroxide into calcium oxide and water (Lothenbach et al. 2007). Between 600-800°C, peaks were identified at ~730°C which are attributed to the decomposition of calcite ($CaCO_3$) in the cement-based materials (Tabet et al. 2018; Taylor 1997). The total weight losses for the Co-con and M-AC-con at a depth of 5 cm and 10 cm from the cylinder top are presented in Table 6.2 for the samples examined after one and two months of elevated $CO_2$ curing.

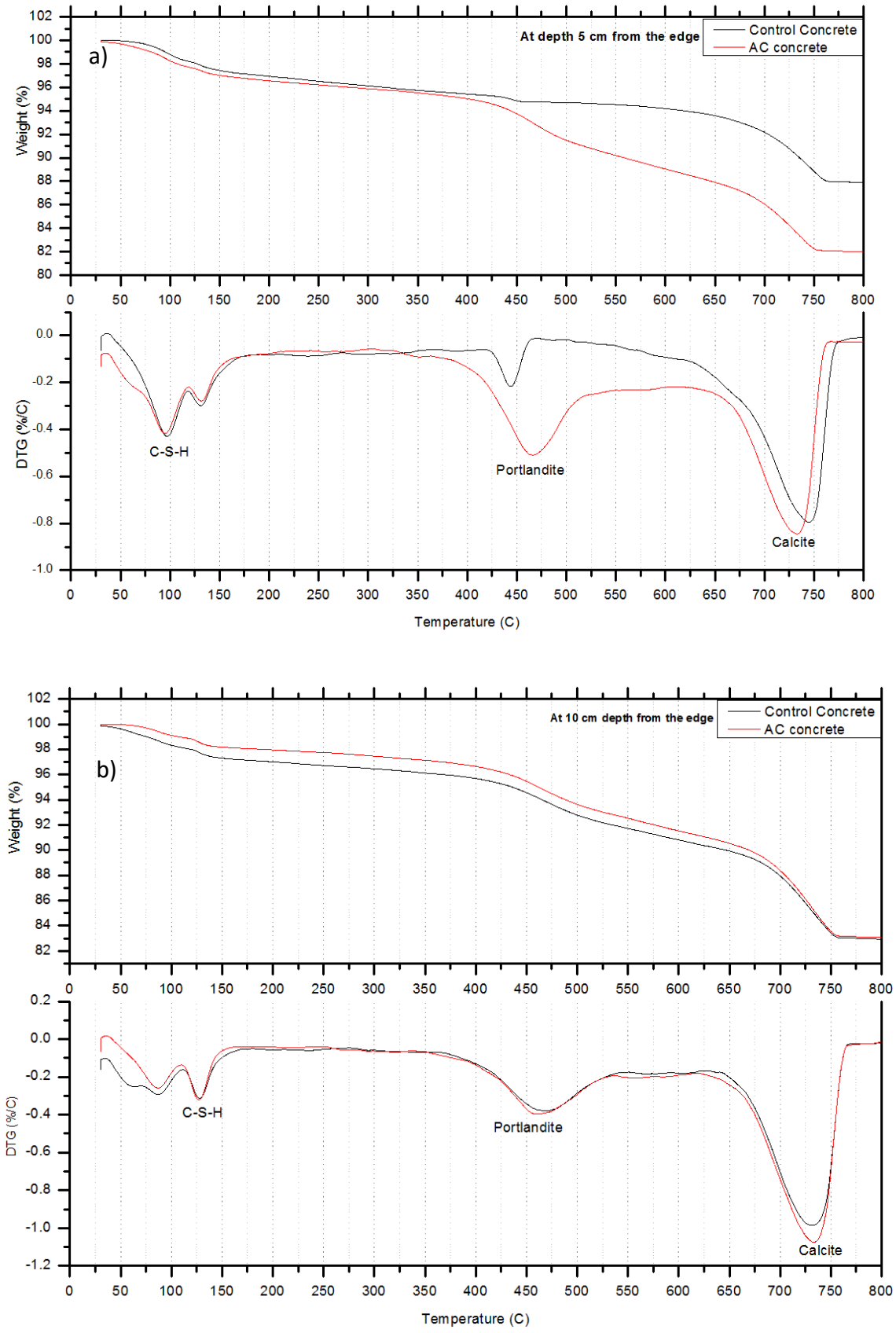


Figure 6-12: TGA and DTG after one month of elevated $CO_2$ curing (a) at 5cm (b) at 10 cm from the edge of the concrete cylinder

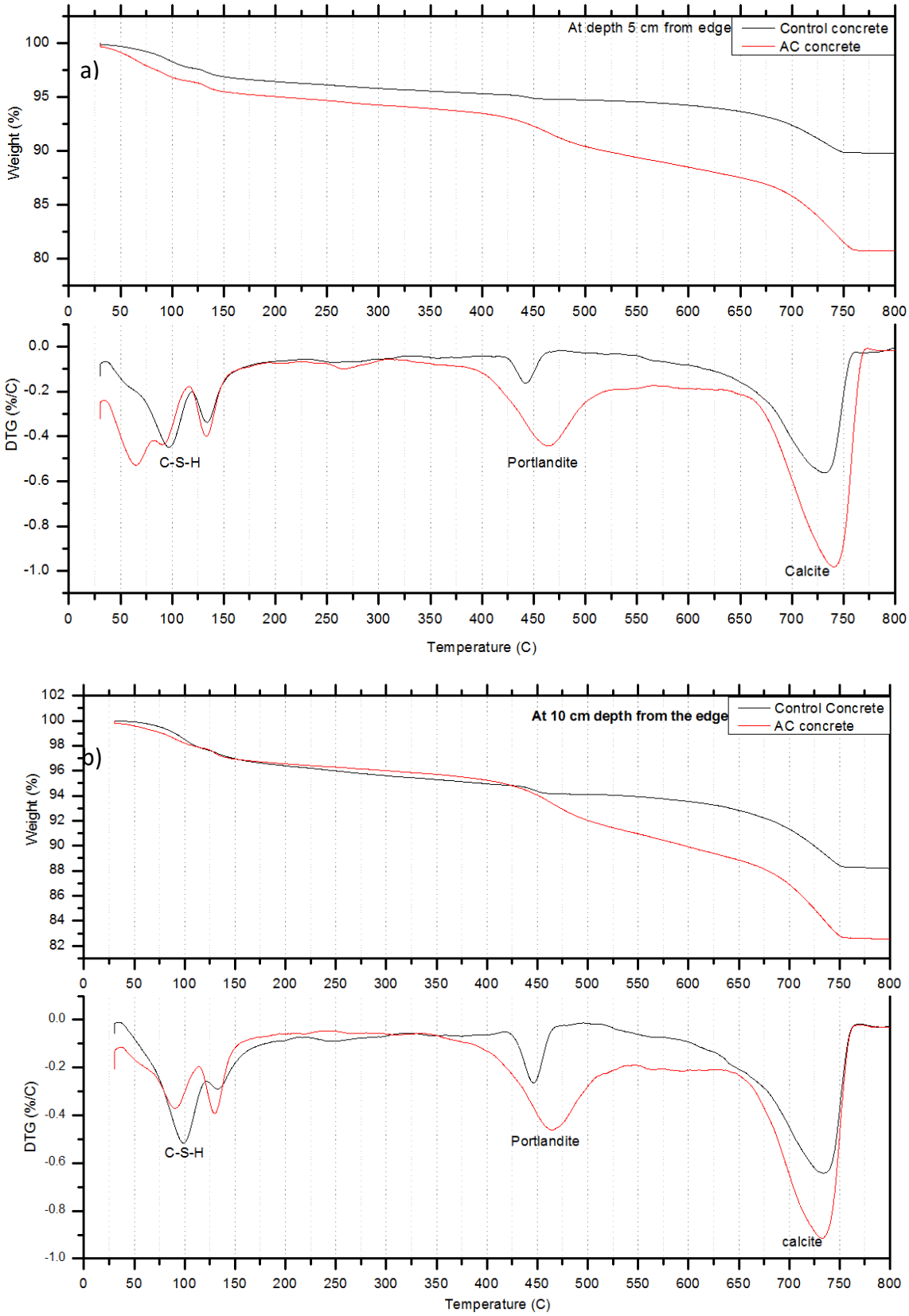


Figure 6-13: TGA and DTG after two months of elevated $CO_2$ curing (a) at 5cm (b) at 10 cm from the edge of the concrete cylinder

Table 6-2: Thermal decomposition, from the TGA of control and M-AC- concrete at one and two months of elevated $CO_2$ curing

| | Cement Paste | Temperature (°C) | Peak Temperature (°C) | Weight Loss % | Tot. Weight loss % |
|---|---|---|---|---|---|
| After 1 Month of $CO_2$ curing | C-S5 | 30-300 | 97 | 3.9 | 12.1 |
| | | 300-500 | 444 | 1.4 | |
| | | 500-800 | 745 | 6.8 | |
| | | | | | |
| | C-S10 | 30-300 | 128 | 3.5 | 17 |
| | | 300-500 | 468 | 3.7 | |
| | | 500-800 | 731 | 9.8 | |
| | | | | | |
| | M-AC-S5 | 30-300 | 95 | 4.1 | 18 |
| | | 300-500 | 466 | 4.4 | |
| | | 500-800 | 733 | 9.5 | |
| | | | | | |
| | M-AC-S10 | 30-300 | 127 | 2.5 | 17 |
| | | 300-500 | 461 | 3.8 | |
| | | 500-800 | 733 | 10.6 | |
| | | | | | |
| After 2 months of $CO_2$ curing | C-S5 | 30-300 | 97 | 4.2 | 10.3 |
| | | 300-500 | 442 | 1.1 | |
| | | 500-800 | 731 | 5.0 | |
| | | | | | |
| | C-S10 | 30-300 | 99 | 4.4 | 11.8 |
| | | 300-500 | 446 | 1.5 | |
| | | 500-800 | 734 | 5.9 | |
| | | | | | |
| | M-AC-S5 | 30-300 | 65 | 5.8 | 19.3 |
| | | 300-500 | 464 | 3.8 | |
| | | 500-800 | 740 | 9.7 | |
| | | | | | |
| | M-AC-S10 | 30-300 | 130 | 4.0 | 17.5 |
| | | 300-500 | 464 | 4.0 | |
| | | 500-800 | 733 | 9.5 | |

The overall shapes of the TGA and DTG graphs of the Co-con and M-AC-con samples are similar. One notable finding is the calcite content in the M-AC-con. For all samples at both ages, the M-AC-con samples showed a higher calcite content than the Co-con. This finding is in in agreement with the XRD spectra and the carbonation test. Both experiments demonstrated a higher carbonated content inside the M-AC-con samples. From the Table, it can be seen that the weight loss in the calcite region for all the examined samples is from 5 to 10.6% of the samples weight, with higher percentages associated with M-AC samples. This implies that the presence of M-AC within pervious concrete help the carbonation reaction to take place, thus, forming more calcite. For example, the weight loss in the M-AC-S5 after 2 months of $CO_2$ curing was 9.7% in the (500-800$^{o}$C) zone compared to 5% in the corresponding control mix. Similarly, the weight loss in M-AC-S10 was 9.5% compare to 5.9% in the control sample. Therefore, the weight loss in M-AC samples is this zone due to the presence of M-AC is 94% and 61% higher than the control sample at 5cm and 10 cm depth respectively. This implies that a significant fraction of the formed calcite in the M-AC concrete is a direct result of the M-AC presence.

Building on this example and these figures, a quantification of the adsorbed $CO_2$ in pervious concrete through carbonation after 2 months of elevated carbonation will be roughly estimated here. Based on the 10 cm depth (as a representative section of the concrete sample), the weight loss in the control and M-AC concrete was 5.9% and 9.5% respectively. This means that each 100 g of the M-AC-cement paste (examined by TGA) contains roughly (9.5-5.9) = 3.6 g calcite that was formed due to M-AC presence. On the other hand, in a typical cube of pervious concrete of the current study, the mass of the cement paste is around 460 g, while the mass of M-AC is 9 g. The 460 g of cement paste contains 16.56 g calcite that was formed due to the presence of M-AC (based on the 3.6g calculated earlier). This means the 9 g M-AC was responsible of fixing 16.56 g calcite within one cube of pervious concrete. Moreover, each percent of $CO_2$ reacts with 1.27 percent of CaO to form 2.27 percent of $CaCO_3$ (Gupta et al. 2017; Abdollahzadeh 2015). This indicates that the 16.56 g of calcite was formed from 7.3 g $CO_2$. This figure can be considered as an estimation value for the adsorbed quantity of $CO_2$ by one cube of pervious concrete after two months of elevated $CO_2$ curing.

As the M-AC-con contained M-PAC and M-GAC, the TGA analysis for both forms of AC under the same temperature was investigated as shown in Figure 6.14. The overall shape of the two samples is similar, where the thermal decomposition took place in two different stages. The first, associated with temperature lower than 100$^{o}$C, could be ascribed to the loss of absorbed water in the M-AC. The thermal decomposition of the organic carbon structure took place in a wide range from around 300 – 600 ˚C (Bazan et al. 2016). The total weight losses for both types of M-AC were more than 90% of the samples original weight. The decomposition of the activated carbon took place almost at the same temperature as Portlandite (temperature range 300 – 500 ˚C). As can be seen from Table 6.2, the weight loss associated with this temperature range is higher in M-AC-con samples than in Co-con samples, which confirms the decomposition of activated carbon in this temperature range.

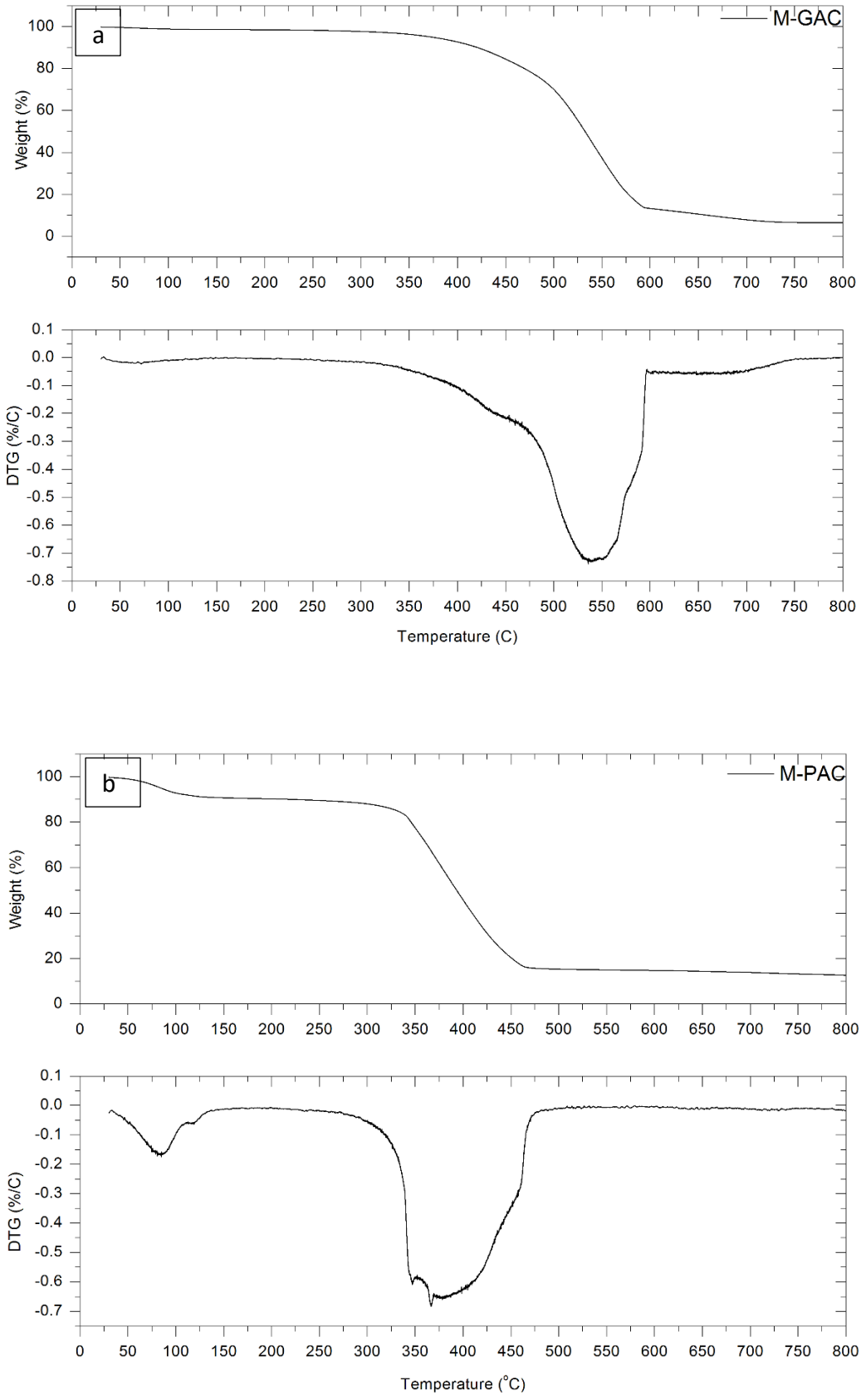


Figure 6-14: TGA and DTG of (a) M-GAC and (b) M-PAC

### 6.3.3 Scanning Electron Microscopy

SEM images from different locations of the Co-con and M-AC-con mixes subjected to accelerated carbonation for two months are shown in Figures 6.15 and 6.16, respectively. Several magnifications were used in each case to provide a better understanding of the microstructure. Typical hydration products were observed in both Figures, including ettringite, portlandite and C-S-H gel. Calcite was also detected at different spots of the two samples. It worth mentioning that SEM technique provides only 2D images of a three-dimensional microstructure, thus, some products such as portlandite with the known hexagonal shape was difficult to detect in a 2D image unless from a certain angle.

Figure 6.15 shows M-AC-con where M-AC was detected in most images, and the hydration products of cement were grown on it. Although both TGA and XRD techniques showed a higher content of calcite in the M-AC-con than control mix, the SEM images showed the presence of calcite in both samples.

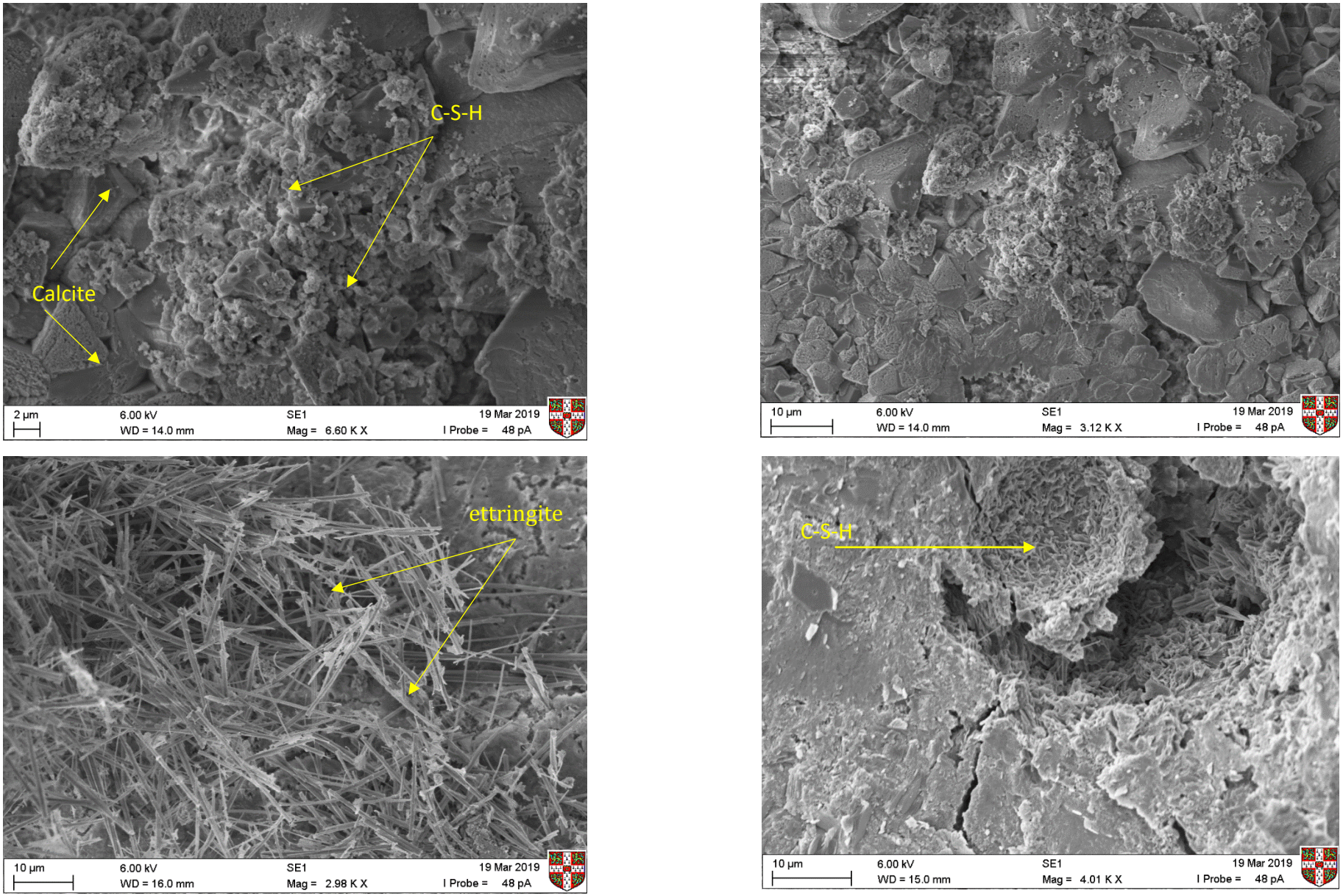


Figure 6-15: SEM images for control concrete (several magnifications at different locations)

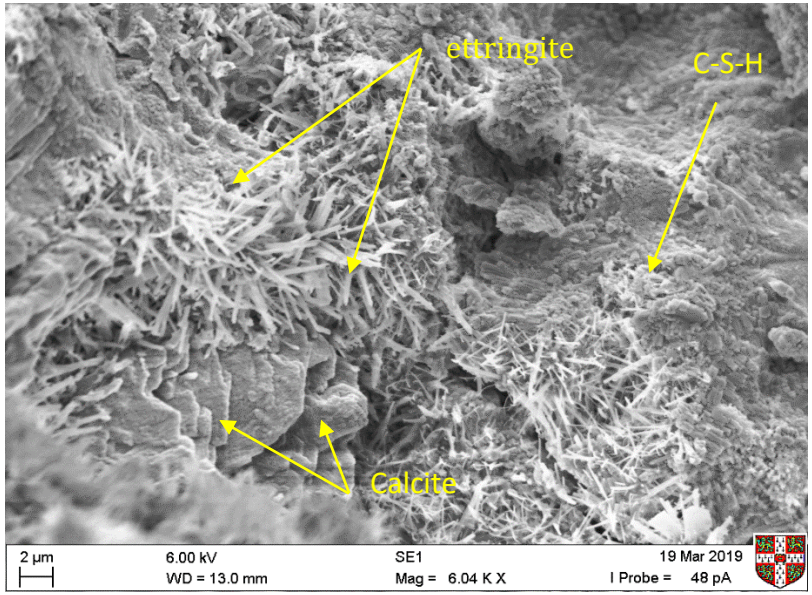


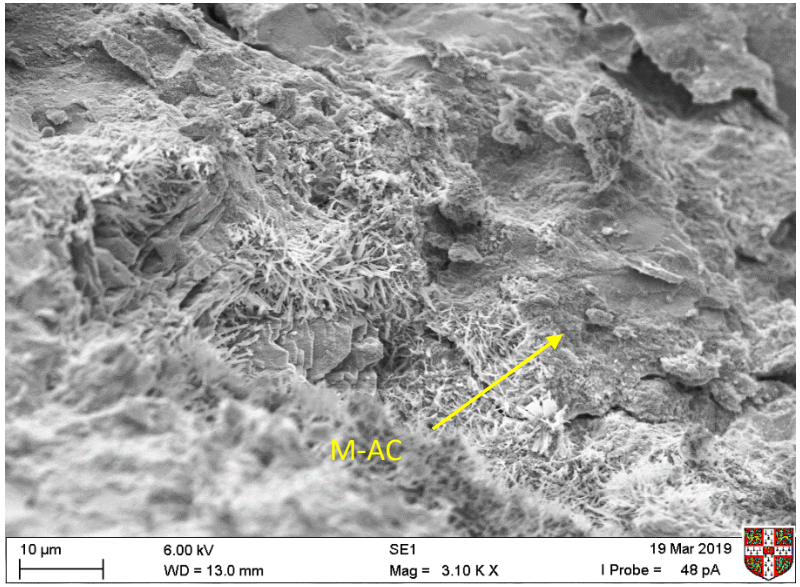


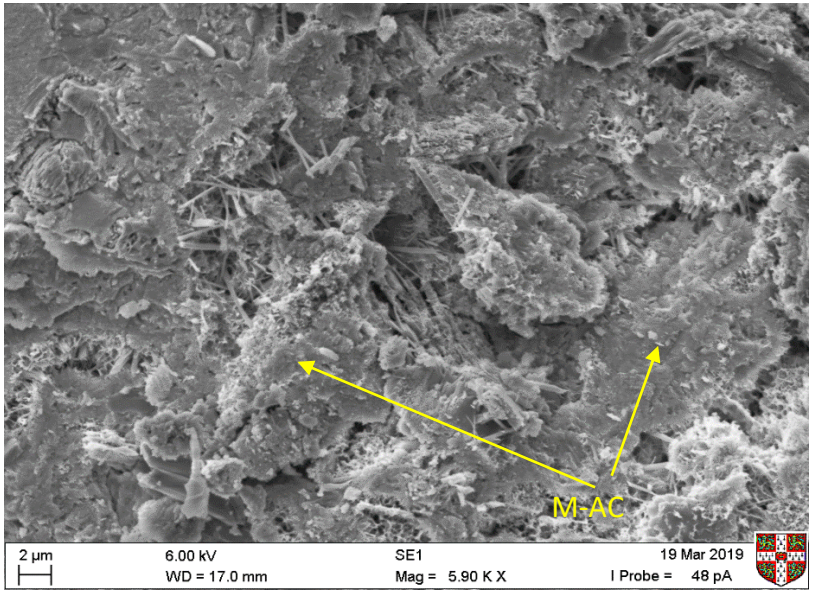


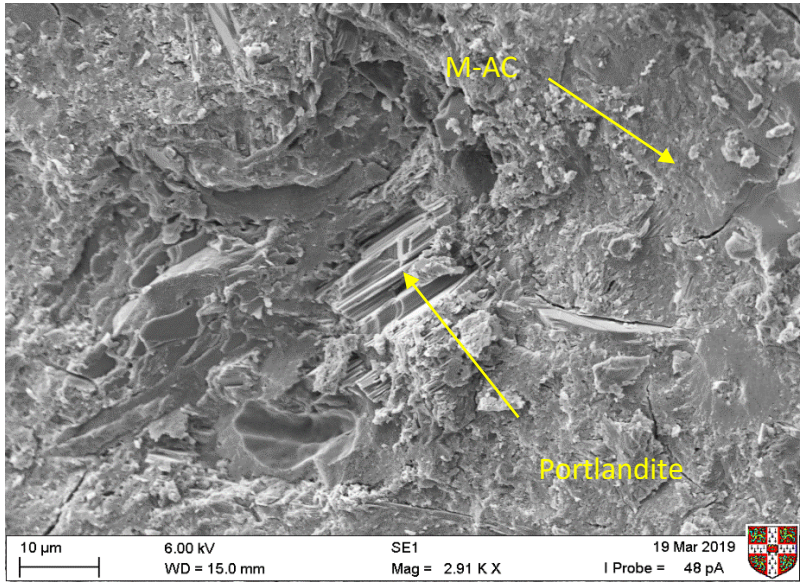


Figure 6-16: SEM images for M-AC concrete (several magnifications at different locations)

## 6.4 $CO_2$ SEQUESTRATION OF M-AC-PERVIOUS CONCRETE

This section investigates the effect of the presence of M-AC within pervious concrete on its $CO_2$ sequestration performance. $CO_2$ sequestration achieved by concrete carbonation is not quantified in this section. Only the sequestration that has been obtained by $CO_2$ adsorption due to the presence of M-AC is addressed and measured.

It also should be highlighted that M-AC-con containing both M-PAC and M-GAC is investigated in this section. However, for reasons of comparison, the sequestration capacity of other samples was also studied as explained in the relevant paragraphs.

### 6.4.1 $CO_2$ sequestration of Co-con and M-AC-con samples

A $CO_2$ sequestration test was conducted on Co-con and M-AC-con samples to determine the quantity of $CO_2$ sequestered by the concrete samples. Each concrete cube was cut in two halves to fit inside the prepared reactor for the sequestration. The dimensions of each half were 10cmx10cmx5cm, and the weight was 1 kg. The $CO_2$ was continuously applied to the system, and the concentration of the gas at the outlet was recorded by the connected $CO_2$ sensor as illustrated in Figure 6.17. The sequestration test was conducted in three rounds as illustrated in the next sections. Figure 6.18 shows the $CO_2$ sequestration results for both the Co-con and M-AC-con samples during the first round of $CO_2$ sequestration tests.

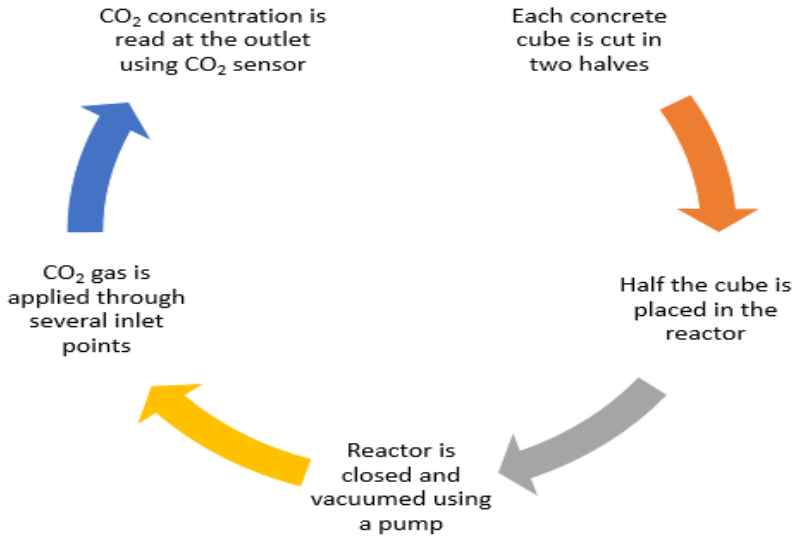


Figure 6-17: The process of producing the $CO_2$ sequestration charts

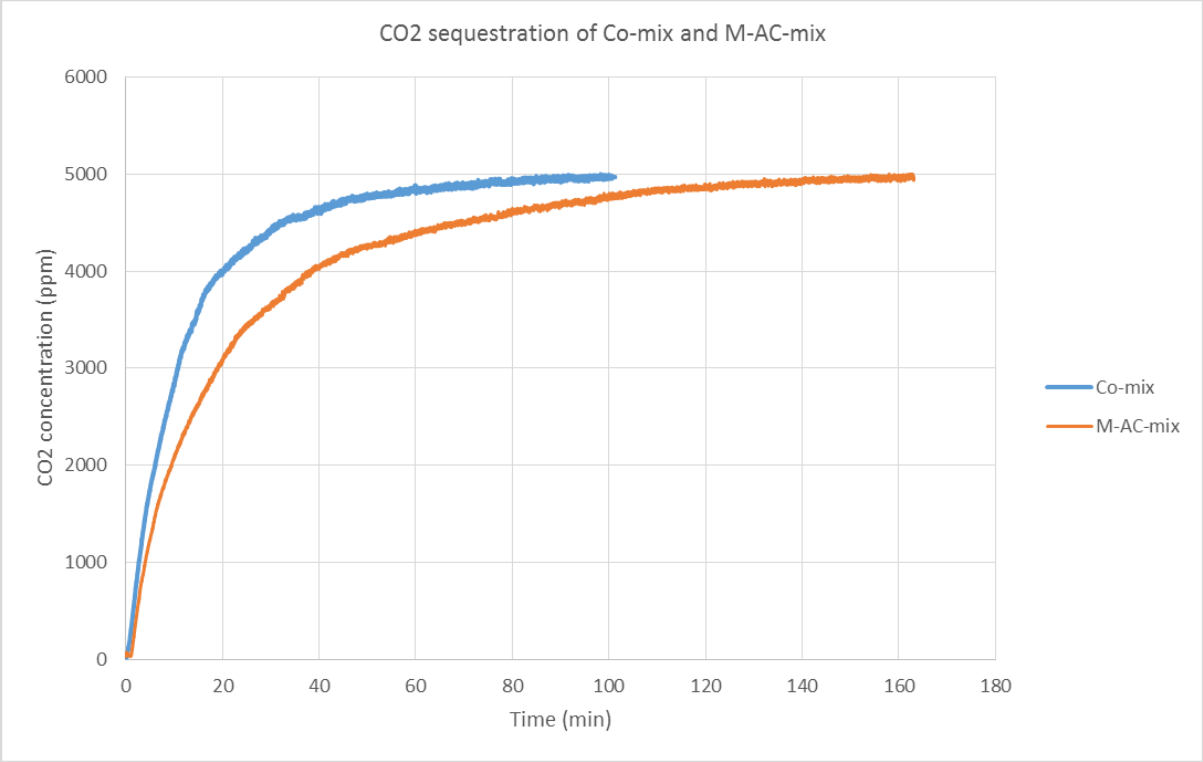


Figure 6-18: Outlet concentrations of $CO_2$ of a reactor containing Co-con and M-AC- con exposed to a continuous flow of 5% $CO_2$ in air

Table 6-3: The $CO_2$ adsorption capacities of Co-con and M-AC-con

| Sample | Adsorption capacity per 1 kg (mg $CO_2$/1 kg concrete) |
|---|---|
| Co-con | 13.73 |
| M-AC-con | 23.04 |

Figure 6.18 shows that the M-AC-con sample required more time than the Co-con sample to reach the initial $CO_2$ concentration (5000 ppm). While the control sample reached the initial concentration after around 100 min, the M-AC sample required more than 160 min. The adsorption capacities for both samples were calculated and presented in Table 6.3. The $CO_2$ adsorption capacity of M-AC-con was 23.04 mg $CO_2$/1 kg concrete, a 68% higher than that of the Co-con. Moreover, the rate of reaching the initial concentration (as shown in Figure 6.18) was slower for the M-AC-con than that of Co-con. This is expected to be due to the adsorption behaviour of the modified activated carbon particles inside the M-AC-con samples which adsorbed $CO_2$ gas molecules injected into the sequestration setup. The Co-con also demonstrated some adsorption behaviour (13.73 mg $CO_2$/1 kg concrete). This could be attributed to one of these two explainations. The first is the consumption of $CO_2$ gas during the carbonation process which takes place between $CO_2$

gas and the hydrated products of concrete. The carbonation reaction is a slow process; therefore, in a case of ~ 3 hours of the test, only very small amount of the outer surface of the concrete samples might have contributed in reaction with $CO_2$, thus consuming some of the $CO_2$ continuously injected to the the reactor setup. The second probable explaination behind the adsorption curve shown by the control samples was inferred by the higher rate of the control sample curve in Figure 6.18. The curve suggests that there was no actual sorption of $CO_2$ by the Co-con, and the adsorption capacity value presented in Table 6.3 is only because the volume of the examined sample was smaller than the volume of the reactor. The tested concrete sample volume was 500 $cm^3$ while the total volume of the reactor was around 4260$cm^3$. Consequantly, the volume of the surrounding space around the sample was 3760 $cm^3$. When $CO_2$ gas was diffused to the reactor, it required time to fill the reactor before discharging out of the setup and being recorded by the $CO_2$ sensor. This explaination justifies the higher rate in control sample curve in Figure 6.18 which may indicate that the $CO_2$ gas quickly reached the initial concentration since no adsorption took place in the reactor.

To investigate which hypothesis is correct, a solid box of the same size (shown in Figure 6.19) was placed in the reactor setup for the $CO_2$ sequestration test. Figure 6.20 shows the results of both the control sample and the solid box. The two curves are notably close to each other which supports the non-adsorption performance of the control concrete. The calculated adsorption capacity for control sample was slightly higher than the solid box (13.73 compared to 12.8 for the solid box), which might be attributed to the high porosity of the pervious concrete. The porosity of the pervious concrete sample provides more space for the $CO_2$ gas to diffuse, thus increasing the volume to be filled before flowing outside the reactor. Based on this explaination, the actual adsorption of M-AC-con would be 23.04 -13.73 = 9.31 mg $CO_2$/g 1 kg concrete.

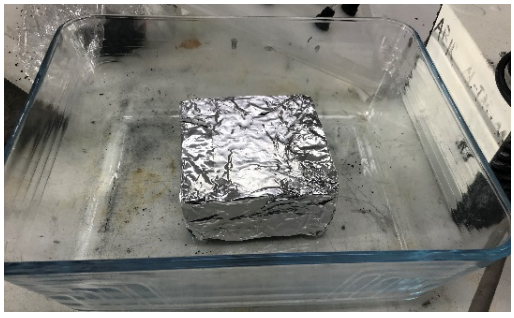

Figure 6-19: A solid box of the same size to be tested in the $CO_2$ sequestration setup

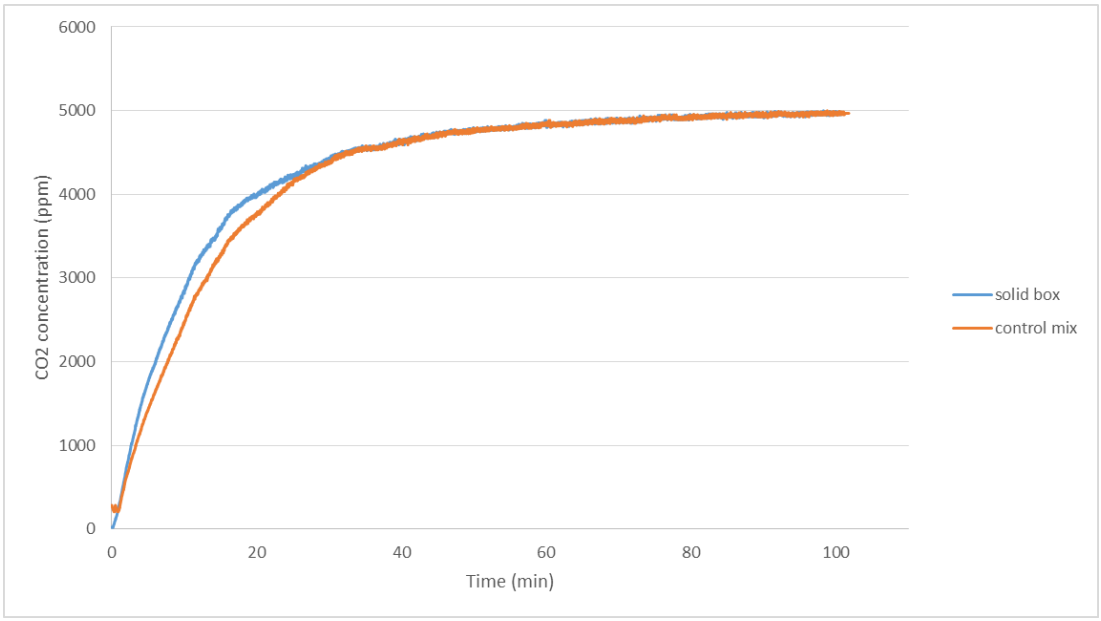


Figure 6-20: Outlet concentrations of $CO_2$ of a reactor containing Co-con and a solid box of the same size

Refering back to the adsorption capacities shown in Table 6.3, it should be highlighted that these figures are measured per sample of concrete not per gram of modified activated carbon. According to the selected percentages of M-AC in pervious concrete (2%M-PAC and 2%M-GAC), there are around 7 g of M-PAC and around 2 g of M-GAC in each cube (10x10x10cm) of M-AC-con (assuming the modified activated carbon to be evenly distributed inside the concrete mix). Given that the cubes were divided into two halves for the test, each tested sample theoretically had a total weight of 4.5 g of M-AC (3.5 g of M-PAC and 1 g of M-GAC). Therefore, the calculated adsorption capacity for each gram of modified activated carbon would be around 9.31/4.5 = 2.07 mg $CO_2$/g M-AC. This figure is significantly lower than the adsorption capacity of HCl-NaOH M-GAC or HCl-NaOH M-PAC provided in Chapter 4 using the $CO_2$ incubator (115 and 373 mg $CO_2$/g), fixed-bed column (8.72 and 24.17 mg $CO_2$/g) and TGA (49.4 and 23.88 mg $CO_2$/g). This might be attributable to one of the following reasons. First is the partial exposure of modified activated carbon grains inside the concrete sample to $CO_2$ in the reactor. Any external grain of M-AC was attached on one side to the cement paste and on the other side to air in the reactor. Only the pores exposed to air would have adsorbed $CO_2$, while the other pores of M-AC did not have access to $CO_2$. The second reason might be that some of the M-AC grains were fully hidden inside the cement paste of the concrete mix (not in any contact with the $CO_2$) and were thus not responsible for any adsorption. The third

reason could be that some (external) M-AC pores were still filled with mixing water so that they did not have the ability to adsorb other molecules. All these reasons (illustrated in Figure 6.21) might be behind the lower capacity of modified activated carbon in this setup. However, compared with the results obtained from the fixed-bed column in Chapter 4 (as both methods of measurement used the $CO_2$ sensor to read the outlet concentrations) the adsorption capacities here are reasonable.

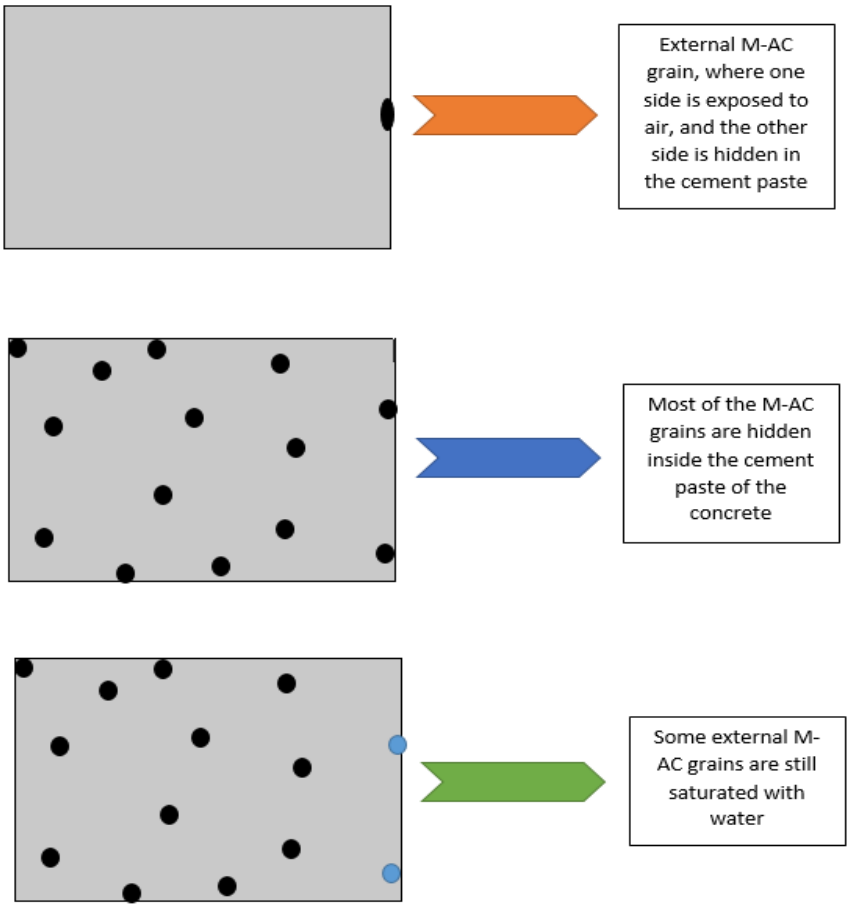


Figure 6-21: The reasons behind the lower adsorption capacity of M-AC in concrete

Moreover, to obtain more insight into the adsorption of M-AC inside the prepared setup for $CO_2$ sequestration, a porous box of the same size (10cmx10cmx5cm) was filled with M-GAC and placed in the centre of the reactor for the sequestration test. The time required for the sensor to reach the initial $CO_2$ concentration was significantly longer than both concrete samples as shown in Figure 6.22. The test terminated after more than 4 hours and the calculated adsorption capacity for this box of M-GAC was 93.3 mg $CO_2$ for the first 260 min of continuous $CO_2$ to the setup. With a weight of around 200 g of modified activated carbon inside the box, the adsorption capacity was around 0.79 mg

$CO_2$/g M-AC which is also considerably lower than the values demonstrated in Chapter 4. However, this value (which is for uncompleted adsorption curve) validates the current values obtained from the M-AC-concrete test. These results suggest that the operation conditions of the current setup are different from the three techniques used in Chapter 4, thus, the obtained results greatly varied. However, for reasons of comparison, these values are acceptable.

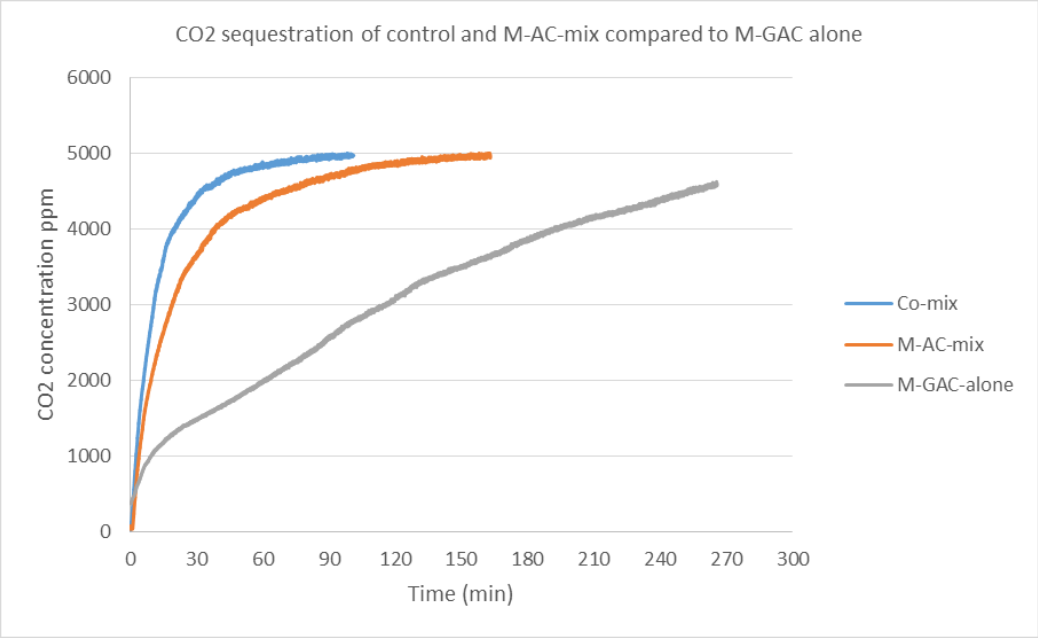


Figure 6-22: Comparing the adsorption capacities of Co-con and M-AC-con to a porous box of M-GAC only

### 6.4.2 Additional $CO_2$ sequestration tests

Two additional investigations were conducted and are explained in this section. The first was to examine the role of M-PAC and M-GAC individually inside the M-AC-concrete mix, while the second investigation was to examine the significance of the AC modification step that activated carbon underwent before being incorporated into the pervious concrete matrix. Therefore, three tests were conducted in the $CO_2$ sequestration setup in two rounds. The first was for samples containing 2%M-PAC compared to samples containing 2%M-GAC, while the second round was for a sample containing both unmodified (2% GAC and 2% PAC) compared with a sample containing (2%M-GAC and 2%M-PAC).

It should be highlighted that the concrete samples for each round were tested on the same day to maintain the same operational conditions. Figure 6.23 shows the differences in

the $CO_2$ sequestration curves for the Co-con, the M-PAC-con, the M-GAC-con and the M-AC-con. The adsorption capacities of the four samples (as calculated using equation 3.1) along with the actual adsorption capacities (after subtracting the value of the control sample) are listed in Table 6.4.

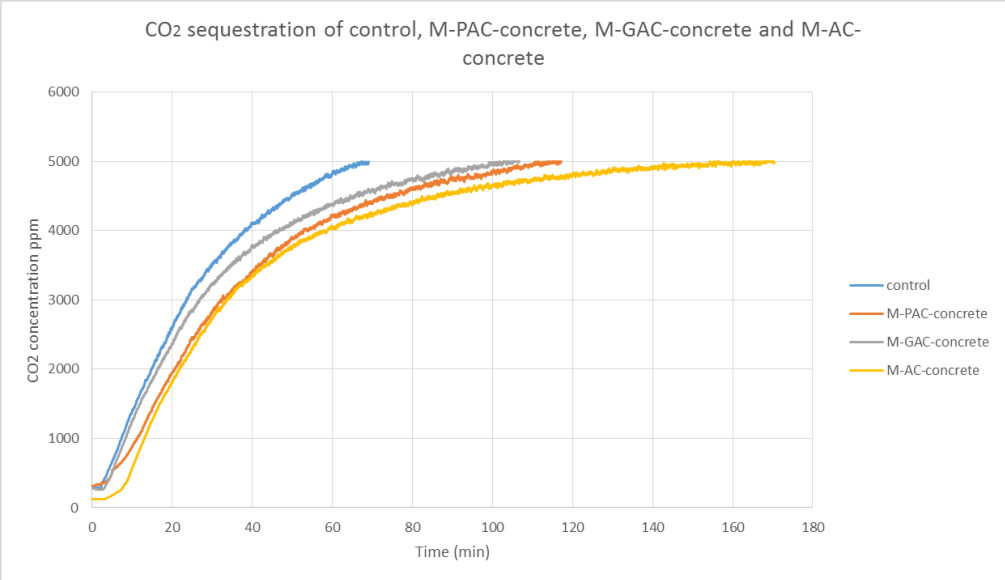


Figure 6-23: Comparing the adsorption capacities of Co-con and M-AC-con to M-PAC-con and M-GAC-con

Table 6-4: The adsorption capacities of control, M-PAC, M-GAC and M-AC-concrete mixes

| Sample | Adsorption capacity per 1 kg (mg $CO_2$/1 kg concrete) | Actual adsorption capacity (mg $CO_2$/1 kg concrete) |
|---|---|---|
| Co-con | 14.5 | 0 |
| M-AC- con | 28.1 | 13.6 |
| 2% M-PAC- con | 23.1 | 8.6 |
| 2% M-GAC- con | 19.9 | 5.4 |

The first aspect of note here is the slight difference between the calculated adsorption capacity of control mix and the M-AC-mix in this round compared with the first round of tests. They are 14.5 and 28.1 compared to 13.73 and 23.04 mg $CO_2$/1 kg concrete for the control and the M-AC-con respectively, which is considered a minor change in terms of adsorption capacities. This change might be explained by the distribution of modified activated carbon inside the concrete cubes. Each sample of concrete should theoretically contain 4.5 grams of modified activated carbon, but it is not necessarily guaranteed. Concrete is a heterogeneous material where the composition of any sample is not exactly the same as the others.

The second aspect of note is that the 2%M-PAC-con demonstrated to have a higher adsorption capacity than the 2%M-GAC-con (8.6 compared to 5.4). This is most probably because of the larger quantity of M-PAC in the M-PAC-con compared to the M-GAC in the GAC-con samples. Combining powder and granular M-AC in one concrete mix increased the adsorption capacity of the final product to 13.6 mg $CO_2$ per sample which is almost the same as the sum of the adsorption capacities of both the M-PAC and M-GAC-sample individually (14 mg $CO_2$). This indicates that the combined incorporation of M-PAC and M-GAC enhanced the final $CO_2$ adsorption capacity of the M-Ac concrete.

The third round of $CO_2$ sequestration compared M-AC-con with unmodified AC- concrete (Un-AC-con) and control concrete as shown in Figure 6.24. The Un-AC-con exhibited less adsorption capacity than the M-AC-con. The calculated adsorption capacity increased by around 20% from 22.6 mg $CO_2$ for the Un-AC-con to 27.3 mg $CO_2$ for the M-AC-con as presented in Table 6.5 (with a suffix of 1). The control concrete sample resulted in an adsorption capacity of 13.6 mg $CO_2$, which was used to obtain the actual adsorption value of the M-AC-con and Un-AC-con. This resulted in 9 and 13.7 mg $CO_2$/1 kg concrete for Un-AC-con and M-AC-con respectively. The other halves of the examined cubes also underwent a $CO_2$ sequestration test. The results are shown in Table 6.5 (with a suffix of 2). These findings show the importance of the modification process that activated carbon underwent before the incorporation into pervious toward a higher $CO_2$ sequestration in pervious concrete.

Table 6-5: The adsorption capacities of Co-con, M-AC-con and Un-AC-con

| Sample | Adsorption capacity per 1 kg concrete (mg $CO_2$/1 kg concrete) | Actual adsorption capacity (mg $CO_2$/1 kg concrete) |
|---|---|---|
| Co-con 1 | 13.6 | 0 |
| M-AC-con 1 | 27.3 | 13.7 |
| Un-AC-con 1 | 22.6 | 9.0 |
| | | |
| Co-con 2 | 12.0 | 0 |
| M-AC-con 2 | 24.3 | 12.3 |
| Un-AC-con 2 | 22.7 | 10.7 |

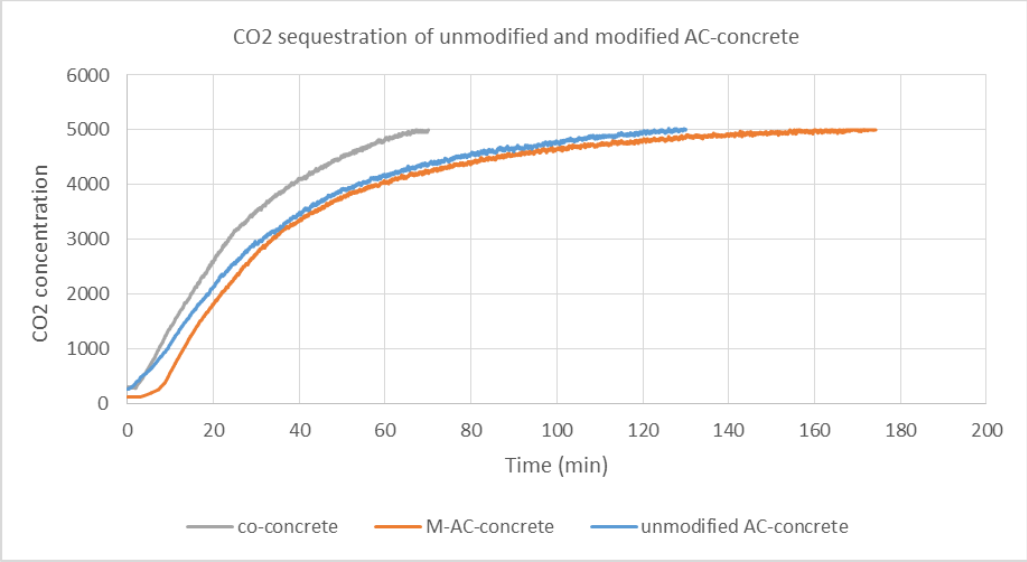


Figure 6-24: Comparing the adsorption capacities of M-AC-con and Un-AC-concrete

### 6.4.3 Summary of the $CO_2$ sequestration results

The $CO_2$ sequestration tests conducted using the $CO_2$ setup prepared in the laboratory gave a general idea about the adsorption behaviour of different concrete samples. The $CO_2$ adsorption values of the M-AC-con are higher than that of the Co-con.

Table 6.6 compares the adsorption capacities of control and M-AC concrete for the three rounds of sequestration. The table shows slight differences among the values of three rounds. The variation in Co-con adsorption capacities could be attributed to the different porosities of the examined samples (samples are not identical). The variation in the adsorption capacities of M-AC-con samples may be due to the uneven distribution of the M-AC particles inside the concrete mix. The average $CO_2$ adsorption of the four examined M-AC-con samples is 12.22 mg/1 kg concrete with a standard deviation of 1.77 mg/1 kg concrete.

Table 6-6: The calculated adsorption capacities of control and M-AC-concrete for the three rounds of the test

| Sample | Cacl./Actual | Adsorption capacity per sample (mg $CO_2$/1 kg concrete) | | | |
|---|---|---|---|---|---|
| | | First round | Second round | Third round | |
| Co-con | Calculated | 13.73 | 14.5 | 13.6 | 12.0 |
| | Actual | 0 | 0 | 0 | 0 |
| M-AC-con | Calculated | 23.04 | 28.1 | 27.3 | 24.3 |
| | Actual | **9.31** | **13.6** | **13.7** | **12.3** |

The values of the adsorption capacities are significantly lower than expected. In addition to the reasons explained earlier in Figure 6.21, the relatively small capacities may be a result of the small quantities of M-AC being incorporated within the pervious concrete matrix. Use of higher percentages of both M-PAC and M-GAC may enable pervious concrete to sequester more $CO_2$, but may also negatively affect the concrete properties, and also would be far from the standard limits for carbon in concrete. Therefore, the added percentages were kept to 2% from either form of activated carbon.

The comparison conducted between the adsorption capacities of M-PAC- concrete and M-GAC concrete reveals that the 2%M-PAC-con adsorbed around 1.5 times the $CO_2$ adsorbed by the 2%M-GAC. This implies that using a concrete mix that contains only M-PAC as a substitution of cement would result in a higher $CO_2$ sequestration than combing M-PAC and M-GAC (e. g. using 4% M-PAC would result in a capacity higher than 2%MPAC and 2%M-GAC in one mix). However, the reduced quantity of cement would have a negative effect on pervious concrete strength.

The modification process of activated carbon increased the adsorption capacities of the M-AC-con compared to the Un-A-con as shown in Figure 6.22. The increased percentage values (based on actual adsorption) were 52% for the first sample and only 15% for the second sample. Given the energy conservative approach that was followed during the modification procedure, these values are acceptable. However, the great variation between the two percentages reveals the non-suitability of this technique to assess the modification process. This is because the quantity of M-AC (or Un-AC) in each sample was not necessarily the same. Moreover, the distribution of AC grains inside the concrete sample (e. g. the quantity of AC grains that were hidden in the cement paste or the grains that participated in the adsorption process) is not the same in each of the examined samples. Therefore, the comparison in this way does not show whether the AC modification positively affected the $CO_2$ sequestration or not.

The last point to address here is that the $CO_2$ sequestration test conducted herein was operating for only a few hours until saturation was attained. However, the key significance of the incorporation is the presence of M-AC itself in pervious concrete as a source of $CO_2$ attraction, which continuously captures, and stores $CO_2$ in pervious concrete as estimated in section 6.3.2 and as will be illustrated in section 6.5. The other key significant is the physical presence of activated carbon inside the pervious concrete.

Therefore, the incorporation of modified activated carbon in pervious concrete is beneficial in three different ways: The direct physical presence of activated carbon in concrete, the $CO_2$ sequestration by the activated carbon itself and lastly the continuous formation of calcite as a result of $CO_2$ capture as described earlier.

## 6.5 GENERAL DISCUSSION AND CONCLUSION

This chapter addressed two principal ideas. The first was investigating the combined effect of two substitutions: cement and fine aggregate, by M-PAC and M-GAC respectively, on the mechanical and physical properties of pervious concrete as well as workability and degree of carbonation. The second was the $CO_2$ sequestration performance of the of resultant M-AC-pervious concrete. It was demonstrated that the incorporation of small percentages (up to 2% each) of M-AC into pervious concrete results in minor changes to the concrete properties, but all properties remained with acceptable ranges for use. However, this small addition could be of great advantage in terms of carbon capture. Apart from the $CO_2$ sequestration effect that was discussed in section 6.4, the presence of activated carbon affects the properties of pervious concrete in two main aspects. The first is the internal hydration provided by the pores of activated carbon. These pores were first filled with water from the mixing water. During the hydration process, these pores work as small reservoirs that supply water to the cement enhancing the hydration. This effect was clearly observed with the increase in the UCS in both cement mortars and pervious concrete when fine aggregate was partially replaced by M-GAC. The second effect is the higher content of calcite in the M-AC-con. This was observed through the phenolphthalein test, when more carbonated spots could be observed in M-AC-con than the Co-con samples. Calcite was also detected by the XRD spectra and the weight loss in TGA curves.

The proposed mechanism for increased calcite might be explained as follows. M-AC, incorporated inside the pervious concrete, sequesters some mixing water inside its pores. During the cement hydration process, M-AC releases this water, thereafter, leaving the M-AC pores empty. M-AC will then be able to capture $CO_2$ molecules and store them in the pores. The availability of stored $CO_2$ molecules next to the hydration products accelerates the carbonation process, thus increasing the content of calcite around the M-AC grains inside the M-AC-concrete. The carbonation reaction that consumed some of the

attached $CO_2$ inside the M-AC pores will leave these pores with a lower quantity of $CO_2$, thus enabling them for further $CO_2$ capture.

It should be highlighted that the grains of M-AC that are on the external edges or are exposed to air (pervious concrete is a porous material) are the only particles that will adsorb $CO_2$. This process is expected to continue over time, thus generating more calcite in the M-AC-concrete. Every time the $CO_2$ molecules are reacting with the hydration products to form calcite, the pores of M-AC will be empty and available for more $CO_2$ capture from the surrounding atmosphere. This cycle could continue until the porous surface of pervious concrete is fully covered with calcite. While this mechanism is highly favourable as a means of $CO_2$ sequestration, care should be given to the resultant decline in porosity over time. Therefore, a higher design porosity value might be chosen to avoid lower porosity values over the long term.

From this mechanism, it could be concluded that $CO_2$ sequestration in M-AC-con takes place in two levels. The first is the traditional concrete carbonation that happens to various types of concrete, but with an enhanced extent in pervious concrete due to the high $CO_2$ diffusion rate provided by the porosity of pervious concrete. The second level is due to the presence of M-AC which continuously adsorbs $CO_2$ and enables more carbonation to take place, thus, sequestering $CO_2$ in calcite form. The two levels lead to a higher $CO_2$ sequestration in this type of concrete. Figure 6.25 illustrates the proposed mechanism for sequestration. While $CO_2$ adsorption by M-AC is a fast process (on the scale of minutes) (Gupta & Kua 2017), the carbonation process itself is a slow process that is governed by the rate of $CO_2$ diffusion and the availability of the right amount of humidity. Therefore, the whole mechanism of $CO_2$ sequestration would be controlled by the progression of concrete carbonation.

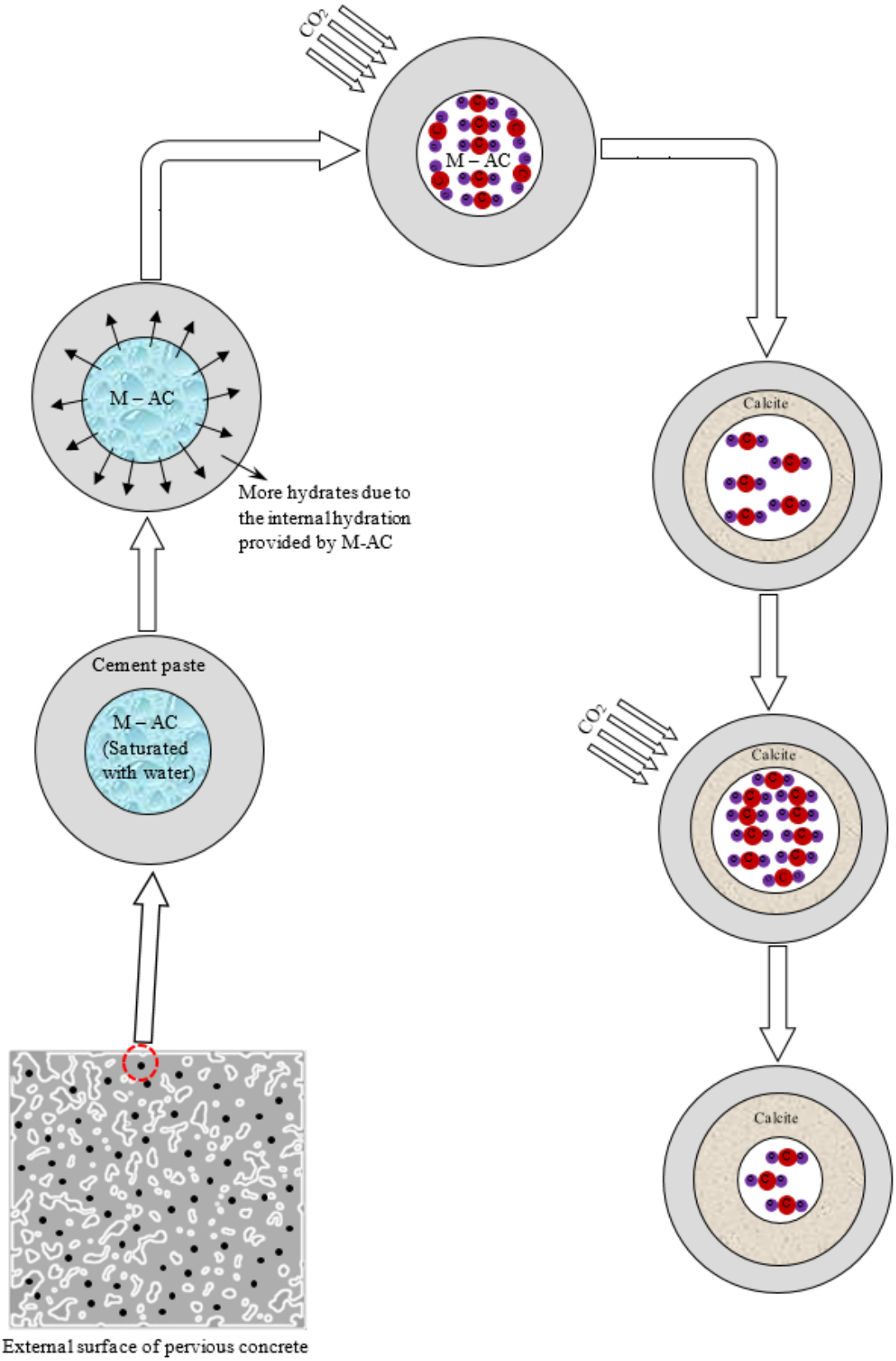


Figure 6-25: The proposed mechanism for $CO_2$ sequestration due to the presence of M-AC in pervious concrete

# 7 Conclusion and Recommendations

This chapter outlines the main findings and conclusions generated from this research, and recommendations for their implementation and further research.

## 7.1 Conclusion

This thesis investigated the potential of modified activated carbon as a partial substitute to Portland-cement based pervious concrete to enhance its $CO_2$ sequestration in order to improve its environmental sustainability. A review of the relevant literature (Chapter 2) highlighted that production of Portland cement, the principal component in most concrete, accounts for ~5 – 7% of total global anthropogenic $CO_2$ emissions, with cement production anticipated to increase to 6 billion tonnes/year by 2050. There are sustainability problems associated with the industry in relation to climate protection, atmospheric emissions, fuel and raw material use. Therefore, several initiatives have been proposed to tackle these issues. These include increasing the efficiency of cement production, utilising alternative raw materials and developing new cement formulations.

Previous research has demonstrated that carbon capture and storage during cement production is a promising technology that could help mitigate climate change. However, it is currently unsuitable for implementation at existing cement plants due to a number of technical and economic barriers. Moreover, most of the currently available technologies focus on capturing, but not storing carbon dioxide, emphasising the need for a specific technology to capture and sequester $CO_2$. Sequestration in cement-based composites may be such a potential strategy. However, $CO_2$ sequestration in cement-based composites through calcium carbonation is known to have several limitations for extensive carbonation potential, such as low porosity and the high density of conventional concrete. Indeed, numerous studies have shown that the extent of carbonation is a function of several variables, such as w/c ratio, cement content, porosity, compaction and curing period. Pervious concrete is a porous concrete that has been developed as a green form of concrete with a wide range of applications. The use of pervious concrete for $CO_2$ sequestration would provide many benefits. A variety of materials have been investigated for $CO_2$ adsorption, including activated carbon, zeolites, silica materials and metal organic frameworks. The aim of this research was to develop

pervious concrete that contains $CO_2$ sorbents as carbon sink materials, in order to maximise its sustainability credentials.

The ideal adsorbent for $CO_2$ capture should meet several requirements, including low-cost raw materials, high $CO_2$ adsorption capacity, high $CO_2$ selectivity and fast kinetics. Among the above-mentioned adsorbents, activated carbon (AC) meets all these requirements. Therefore, AC was selected for investigation in this research. AC can be prepared from a wide range of starting materials such as biomass, coal and industrial by-products, and it has various applications in purifying air, solutions, soil and many chemical products. The literature review showed that AC is produced in two steps: carbonization and activation. While carbonization involves heating the raw material in the absence of oxygen at a temperature around 800$^{o}$C to remove the non-carbon elements, activation can be achieved through either physical activation or chemical oxidation. Moreover, previous studies showed that chemical activation has many advantages compared to physical activation, such as the lower temperature and time required for AC production, and the higher resultant surface area.

The literature on AC production also showed that the final properties of the resulting AC mainly depend on the starting raw material and the activation methodology followed. Moreover, the pore structure and surface chemistry of the produced AC play a significant role in determining its adsorptive properties. Only AC pores that are less than 1.0 nm have been reported to be effective for $CO_2$ capture, because they contribute to the retention of $CO_2$ in the pore wall. In addition, it has been demonstrated that basic functional groups present on the AC surface increases its affinity to $CO_2$. AC is usually modified using different techniques to further enhance its adsorption capacity. Established techniques include heat treatment, impregnation with specific compounds, microwave, plasma and ozone treatment. Following treatment, the types and the amounts of the functional groups are changed. In particular for increasing $CO_2$ adsorption capacity, heating under inert gas removes oxygen functionalities, thus offering AC an alkaline surface. Moreover, ammonia modification was reported as a successful approach to increase the adsorption affinity of AC for $CO_2$. With these modifications, nitrogen functionalities are introduced into activated carbon, offering it a basic surface. Previous studies have shown that treatment with hydroxides increases the alkalinity of the AC surface and provides more functional sites for $CO_2$, thus enhancing its adsorption.

Furthermore, several studies reported that impregnation with metal elements is a promising approach to increasing $CO_2$ uptake, due to the high affinity and chemical reaction between metal oxides and $CO_2$ molecules. From the reviewed studies, it was noticed that the majority of approaches followed for modification are energy intensive processes, which contribute to further $CO_2$ emissions.

The literature also highlighted pervious concrete as a sustainable class of concrete in use since the middle of the nineteenth century. Pervious concrete is considered as one of the Best Management Practices recommended by the Environmental Protection Agency EPA, as it reduces storm water runoff, improves storm water quality and may assist with the recharge groundwater supplies. Previous studies also highlighted that this type of concrete requires special care in designing a mix that meets the required mechanical and drainage properties. Among several approaches, the phase-volume design proposed by ACI was considered as practical. Porosity is the prime characteristic of pervious concrete and all other properties result from it. Porosity is strongly dependent on the volume of cement paste within the mix, the water to cement ratio, the size and gradation of the aggregate and the level of compaction. A porosity of 15% is recommended for a wide range of applications in pervious concrete.

The literature also showed that size, gradation, type of the aggregate and aggregate to cement ratio are known to play a significant role in the mechanical and physical properties of pervious concrete. The decrease in aggregate size has an increasing effect on strength and a decreasing effect on porosity. In general, an aggregate size of 4.75 – 9 mm (No. 8 size), 10% maximum fine aggregate, and aggregate to cement ratios in the range of 4.0 to 4.5 by mass can satisfy both the strength and drainage requirements of pervious concrete. Moreover, previous studies found that the w/c ratio in pervious concrete is usually lower than that of conventional concrete, with a tight range of about 0.27 to 0.35. Optimum water content is essential to prevent materials from crumbling due to lack of water while also preventing the loss of voids because of the excess water.

The literature also showed that AC has been used in multiple studies for different purposes such as adsorbing pollutants and volatile particles. Contradictory findings were reported about the effect of AC presence in cementitious materials. While some researchers claimed an enhancement in mechanical properties, others reported a decline sufficient to adversely affect their usage. Finally, the literature review highlighted that

no specific standards were defined for the maximum quantity of AC in cementitious materials. Most of the studies addressed unburnt carbon as a pollutant to concrete, therefore, limitations for its quantity have been set.

Two different types of AC were used in the study; namely powder and granular, both obtained from Fisher Scientific (UK). AC was modified using different concentrations of chemical solutions. The adsorption capacity of the modified carbon (M-AC) was measured using three techniques. The best M-AC partially replaced cement and fine aggregate in different percentages in two cement-based systems. The performance of the M-AC-pervious concrete compared to the control pervious concrete was studied.

Chapter 4 investigated various modification techniques for the activated carbons. These were modification with different concentrations of NaOH, HCl, $NH_4OH$, and $CuSO_4$. Selected modified samples were then characterised by FTIR, BET and SEM analysis. The adsorption capacity of the M-AC compared with raw carbon was measured using $CO_2$ incubator, fixed-bed column and TGA. It was found that the majority of the M-AC showed higher adsorption capacities than the raw AC (e. g. increase was in the range of ~ 7 to 52 % for $CO_2$ incubator), confirming the role the modification played in changing the surface chemistry of AC, thus boosting its adsorption capacity for $CO_2$. NaOH-modified AC showed the highest $CO_2$ adsorption, as measured by mass uptake, among all the modified samples. The adsorption capacity was around 95, 5 and 30 mg $CO_2$/g AC using $CO_2$ incubator, fixed-bed column and TGA respectively, which constituted 111%, 152% and 37% increase compared to the unmodified AC. This is believed to be due to the Na+ species incorporated on the surface of the activated carbon that easily react with $CO_2$ molecules.

Results also showed that HCl treatment reduced the impurities on the surface of AC, confirmed by SEM images, which enhanced the adsorption capacity of the HCl modified AC by around 97% using fixed-bed column technique. The remaining tested modifying agents did not greatly increase adsorption capacity compared to the raw AC, indicating a poor reaction with $CO_2$. This might be attributed to the modification technique itself which was conducted under ambient temperature contradicting the high temperature approach followed in previous studies.

The FTIR analysis confirmed incorporation of newly developed functional groups (e.g. C≡C, C–N, N–H and O-H) on the surface of the modified AC, explaining the higher

adsorption capacities of modified AC compared to raw AC, and confirming that chemical adsorption was the dominant type of adsorption in the examined samples.

The results also showed that the two-step modification (modification first with HCl, followed by NaOH) achieved a higher adsorption capacity than using a single modification technique. The increase in capacity was measured at 109%, 343% and 123% using $CO_2$ incubator, fixed-bed column and TGA. This emphasised the role of HCl in removing impurities before applying the NaOH. The results also showed that modified powder AC exhibited a higher adsorption capacity than raw powder AC, with an increase of ~ 40% using fixed-bed column and ~ 60% using TGA.

The discussion conducted on the three techniques of measuring the adsorption capacity revealed that TGA is believed to be the highest accuracy technique followed by the fixed-bed column then the $CO_2$ incubator. This is likely because of the desorption step that is conducted in TGA prior to $CO_2$ application. Besides, the TGA adsorption environment is closed and controlled, unlike the open environment of fixed-bed column and $CO_2$ incubator. Moreover, it was found that the adsorption of $CO_2$ by modified activated carbon was a combination of chemical and physical adsorption, but with a higher proportion by the chemical adsorption.

Therefore, Chapter 4 suggested that dual modification with HCl followed by NaOH at ambient temperature is a useful technique for modifying activated carbon in a sustainable manner.

Chapter 5 investigated the performance of the modified activated carbon, both power and granular forms, in three cement-based systems. The modified powder activated carbon (M-PAC) partially substituted cement in cement pastes (CP) and pervious concrete, while the modified granular activated carbon (M-GAC) partially substituted fine aggregate in cement mortars (CM) and pervious concrete. The results showed that inclusion of modified activated carbon into cementitious composites resulted in slight changes to their properties. The main effect was the stiffness of the mix, which required the addition of more water to achieve the same level of workability. The addition of 2% M-PAC increased the w/c ratio from 0.3 to 0.32 to achieve the same consistency.

The results of the isothermal calorimetry test showed that the presence of M-PAC provided more space for the formation of cement hydration products and worked as

nucleation sites, which was confirmed by the 30% increase in the total produced cumulative heat of 2%M-PAC-CPs compared to the control one. In addition, the TGA results showed a higher weight loss in the M-PAC-CPs compared to the control one, especially in the first and the third zones of temperature range (e.g. a 18% and 19% increase in weight loss in the 30-300 and 500-800oC zones). While the first weight loss was probably associated with $CO_2$ release, the remaining weight loss is related to calcite decomposition. This suggested that M-PAC-CPs contained a higher content of calcite than the control mix due to the adsorption behaviour of the incorporated M-PAC within the pastes. Moreover, the presence of M-PAC, with its inherent characteristics (e. g. the high porosity and the low density), affected the mechanical and physical properties of pervious concrete. The UCS and the density declined (e. g. by ~ 15% and 2% respectively at 2% replacement at 28-day) while the porosity increased (e. g. by 27% at 2% replacement at 28-day). However, at all the percentages examined, the change was still within an acceptable range for use of M-PAC concrete in a variety of applications such as low traffic pavement, parking lots, structural walls and base course for streets and roads.

The partial substitution of fine aggregate by M-GAC in cement mortars resulted in a decrease in the flowability of M-GAC-CMs compared to the control CM. This confirmed the adsorption behaviour of M-GAC to mixing water. The reduction in flow table values increased from 1.2% for 0.5% M-GAC-CM to 5% for 2% M-GAC-CM. In addition, the results showed that partial replacement of natural sand with M-GAC slightly enhanced the compressive strength of the mortars (e. g. by 5% for 2%M-GAC at 28-day). This positive strength response might be attributed to an enhanced hydration reaction through an internal curing mechanism provided by the M-GAC. With an inter-connected network of voids, activated carbon may act as a supplier of micro-reservoirs that deliver water to the curing process as needed.

Moreover, the substitution by M-GAC in pervious concrete showed a slight change to the UCS and hardened density, while a more pronounced change in porosity was observed. M-GAC increased the porosity by up to 17%, compared to a maximum increase of 3.2% and 1.2% in UCS and density respectively. The change in the properties of pervious concrete when cement was substituted with M-PAC were more noticeable than the change that resulted from the substitution of fine aggregate with M-GAC. However, even at the highest percentage examined, the properties were still within an acceptable range

for a wide variety of pervious concrete applications including sidewalk and pathways, artificial reefs, greenhouse floors and low traffic pavement. Therefore, Chapter 5 suggests that small replacement of cement or fine aggregate with M-AC did not significantly adversely alter the properties of the examined cementitious composites. Therefore, the maximum examined percentages of both substitutions were used in producing M-AC-pervious concrete mix as detailed in Chapter 6.

Chapter 6 investigated the performance of M-AC pervious concrete that contained both substitutions: cement and fine aggregate. The investigation included the effect on the macro properties of concrete, the microstructural analysis and $CO_2$ sequestration performance. The mechanical and physical property tests showed that M-AC concrete had a higher porosity (e. g. 28%), but a lower compressive strength (e. g. 9%), permeability (e. g. 17%) and hardened density (e. g. 1%) than the control sample after 28 day of curing. Moreover, this substitution resulted in a higher required w/c ratio (e.g. w/c ratio increased from 0.35 to 0.37) to achieve the same level of workability as in the control mix.

The results of the phenolphthalein test showed more carbonated areas in the M-AC-concrete samples than the control concrete. That was confirmed by the TGA and the XRD analysis. The XRD spectra showed peaks at 29.1° and 39 °C that were more intensive in M-AC concrete, indicating higher $CO_2$ adsorption. Moreover, the TGA showed a higher weight loss in M-AC-concrete at the temperature range of 500-800 $^oC$, associated with the decomposition of carbonates. The higher calcite content in M-AC-concrete might be explained as follows: M-AC, incorporated inside the pervious concrete, sequesters some of the mixing water inside its pores. During the hydration process, M-AC supplies this water leaving the M-AC pores empty. The M-AC is then able to capture $CO_2$ molecules and store them in the pores. The availability of attached $CO_2$ molecules next to the hydration products accelerates the carbonation process, thus increasing the content of calcite inside the M-AC-concrete.

Finally, it was found that the M-AC concrete had a higher $CO_2$ sequestration capacity than the control concrete. Sequestration was measured in M-PAC-concrete and M-GAC-concrete, revealing adsorption capacities of 23.1 and 19.9 mg $CO_2$/1 kg concrete respectively, compared to the 14.5 and 28.2 mg $CO_2$/1 kg for control and M-AC concrete respectively. Therefore, 1kg of the M-AC-pervious concrete would contain around 5 g of

activated carbon and hold 12 mg $CO_2$ adsorbed on this activated carbon, while 22 g of carbon would be stored as calcite. This compares with traditional pervious concrete in which 1 kg of it would store 13 g of carbon as calcite. The amount stored in the carbon containing concrete is therefore significantly higher than the traditional pervious concrete.

Furthermore, the comparison between the modified and the unmodified AC inside the pervious concrete showed that M-AC-concrete had a higher adsorption capacity than Un-AC-concrete, however, an extended examination is required to validate the obtained results.

Chapter 6 suggests that the incorporation of both M-PAC and M-GAC is of great advantage to pervious concrete in terms of $CO_2$ sequestration, without significant adverse changes to its properties.

Overall, this study investigated and demonstrated the feasibility of utilising two forms of modified activated carbon in pervious concrete to improve sustainability through $CO_2$ sequestration without detrimental effect on the mechanical and drainage properties.

## 7.2 Recommendations for future research

This thesis demonstrated that the incorporation of modified activated carbon in pervious concrete increases its capacity for $CO_2$ sequestration, representing a method for increasing its environmental sustainability within the construction industry. However further investigations on other adsorbent materials (e.g. zeolites) to enhance the sustainability of cement-based systems are recommended for comparison reasons. In particular, Zeolites, which are mineral sorbents, are known to significantly enhance the mechanical properties of cement. Moreover, it would be beneficial to examine different types of activated carbon, with different grain size or different preparation processes.

As shown in Chapter 4, only four chemical agents were used to modify the activated carbon based on literature recommendations. It would be interesting to explore other chemicals that may have the potential for further increases in $CO_2$ capacity of the modified activated carbon. Furthermore, the measuring techniques that were used to quantify the $CO_2$ demonstrated some degree of inconsistency in the results. Therefore, a more accurate apparatus connected to thermostats, $CO_2$ analysers, gas controlling system

and pressure regulators is recommended for increased accuracy. It is also recommended that further research be undertaken to confirm and provide more details on the mechanism that chemically bonds the $CO_2$ to surface of activated carbon.

In Chapter 5, the influence of M-AC on the properties of three cement-based systems was investigated. All these cement composites are unreinforced, therefore comprehensive research on the effect of modified activated carbon on reinforcement is recommended.

In Chapter 6, $CO_2$ sequestration through the $CO_2$ adsorption by the M-AC was investigated and measured. However, further research to quantify long-term carbonation in pervious concrete, and to provide an estimation of the total $CO_2$ that can be sequestered in M-AC-pervious concrete is recommended. Moreover, it is highly recommended to study the long-term impact of M-AC presence on pervious concrete.

Finally, this work has been carried out under carefully controlled laboratory conditions. Further studies should investigate the M-AC-pervious concrete in situ. Moreover, a feasibility study to evaluate the additional cost of incorporating modified activated carbon in cementitious composites is highly recommended.

## References


Abdollahzadeh, A., 2015. *Characterisation and Performance Evaluation of Reactive Magnesia-Based Pervious Concrete for Application in Green Infrastructure*.

ACI 211, 2002. Guide for Selecting Proportions for No-Slump Concrete Reported by ACI Committee 211. *American Concrete Institute*, 02, pp.1–26.

ACI 522R, 2010. *Report on Pervious Concrete*,

ACI318, 2014. *Building Code Requirements for Structural Concrete (ACI 318-14)*,

Adelodun, A. a., Lim, Y.H. & Jo, Y.M., 2013. Surface oxidation of activated carbon pellets by hydrogen peroxide for preparation of CO2 adsorbent. *Journal of Industrial and Engineering Chemistry*, 20(4), pp.2130–2137.

Agarwal, A., Nanda, B. & Maity, D., 2014. Experimental investigation on chemically treated bamboo reinforced concrete beams and columns. *Computers and Chemical Engineering*, 71, pp.610–617.

Ahmedna, M. et al., 2004. The use of nutshell carbons in drinking water filters for removal of trace metals. *Journal of Chemical Technology and Biotechnology*, 79(10), pp.1092–1097.

AI-khalaf, M.N. & Yousif, H.A., 1986. Compactibility of no-fines concrete. *International Journal of Cement Composites and Lightweight Concrete*, 8(1), pp.45–50.

Akhtar, A. & Sarmah, A.K., 2018. Novel biochar-concrete composites : Manufacturing , characterization and evaluation of the mechanical properties. *Science of the Total Environment*, 616–617, pp.408–416.

Akmil-Başar, C. et al., 2005. Adsorptions of high concentration malachite green by two activated carbons having different porous structures. *Journal of Hazardous Materials*, 127(1–3), pp.73–80.

Al-Akhras, N.M. & Smadi, M.M., 2004. Properties of tire rubber ash mortar. *Cement and Concrete Composites*, 26(7), pp.821–826.

Al-Qodah, Z. & Shawabkah, R., 2009. Production and characterization of granular activated carbon from activated sludge. *Brazilian Journal of Chemical Engineering*, 26(1), pp.127–136.

Al-Tabbaa, A., 2013. 19 - Reactive magnesia cement. In F. Pacheco-Torgal et al., eds. *Eco-Efficient Concrete*. Woodhead Publishing Series in Civil and Structural Engineering. Woodhead Publishing, pp. 523–543.

Alam, M.A. & Naz, S., 2015. Experimental Study on Properties of No-fine Concrete. *International Journal of Informative & Futuristic Research*, 2(10), pp.3687–3694.

Ali, A. et al., 2019. Graphene-based membranes for CO2 separation. *Materials Science for Energy Technologies*, 2(1), pp.83–88.

Aliabdo, A.A., Abd Elmoaty, A.E.M. & Aboshama, A.Y., 2016. Utilization of waste glass powder in the production of cement and concrete. *Construction and Building Materials*, 124, pp.866–877.

Andrew, R.M., 2018. Global CO2 emissions from cement production. *Earth System Science Data*, pp.195–217.

Aranda, M.A.G. & la Torre, A.G. De, 2013. 18 - Sulfoaluminate cement. In F. Pacheco-Torgal et al., eds. *Eco-Efficient Concrete*. Woodhead Publishing Series in Civil and Structural Engineering. Woodhead Publishing, pp. 488–522. Available at: http://www.sciencedirect.com/science/article/pii/B9780857094247500189.

Asadi Zeidabadi, Z. et al., 2018. Synthesis, characterization and evaluation of biochar from

agricultural waste biomass for use in building materials. *Construction and Building Materials*, 181, pp.301–308.
Ashraf, W., 2016. Carbonation of cement-based materials: Challenges and opportunities. *Construction and Building Materials*, 120, pp.558–570.
ASTM-C1679, 2017. *ASTM C1679-14: Standard Practice for Measuring Hydration Kinetics of Hydraulic Cementitious Mixtures Using Isothermal Calorimetry*,
ASTM-C1754, 2015. ASTM C1754/C1754M - Standard Test Method for Density and Void Content of Hardened Pervious Concrete. *Astm*, p.3.
ASTM C33, 2010. ASTM C33-03. , i(C), pp.1–11.
ASTM C618, 2010. *Standard Specification for Coal Fly Ash and Raw or Calcined Natural Pozzolan for Use*,
ASTM Standard C33, 2003. Standard Specification for Concrete Aggregates. *ASTM International*, i(C), p.11.
Athalathil, S. et al., 2013. Characterization and performance of carbonaceous materials obtained from exhausted sludges for the anaerobic biodecolorization of the azo dye Acid Orange II. *Journal of Hazardous Materials*, 267, pp.21–30.
Auta, M. et al., 2013. Fixed-bed column adsorption of carbon dioxide by sodium hydroxide modified activated alumina. *Chemical Engineering Journal*, 233, pp.80–87.
Babu, T.S.R. & Neeraja, D., 2017. A experimental study of natural admixture effect on conventional concrete and high volume class F flyash blended concrete. *Case Studies in Construction Materials*, 6, pp.43–62.
Bae, J.-S. & Su, S., 2013. Macadamia nut shell-derived carbon composites for post combustion CO2 capture. *International Journal of Greenhouse Gas Control*, 19, pp.174–182.
Beltrao-Nunes, A.-P. et al., 2019. CO2 capture by coal ash-derived zeolites- roles of the intrinsic basicity and hydrophilic character. *Journal of Alloys and Compounds*, 778, pp.866–877.
Berodier, E. & Scrivener, K., 2014. Understanding the filler effect on the nucleation and growth of C-S-H. *Journal of the American Ceramic Society*, 97(12), pp.3764–3773.
Bhalla, N. et al., 2018. Monitoring early-age setting of silica fume concrete using wave propagation techniques. *Construction and Building Materials*, 162, pp.802–815.
Bhutta, M.A.R., Tsuruta, K. & Mirza, J., 2012. Evaluation of high-performance porous concrete properties. *Construction and Building Materials*, 31, pp.67–73.
Bilalis, P. et al., 2014. Non-covalent functionalization of carbon nanotubes with polymers. *RSC Advances*, 4(6), pp.2911–2934.
Boehm, H.., 2002. Surface oxides on carbon and their analysis: a critical assessment. *Carbon*, 40(2), pp.145–149.
Boehm, H.P. et al., 1964. Surface Oxides of Carbon. *Angewandte Chemie International Edition In English*, 3(10), pp.669–677.
Boonpoke, A. et al., 2013. Synthesis of activated carbon and MCM-41 from bagasse and rice husk and their carbon dioxide adsorption capacity. *Journal of Sustainable & Environment*, 2, pp.77–81.
Bota, K.B. & Abotsi, G.M.K.D. a-A., 1994. Ammonia - a Reactive Medium for Catalyzed Coal-Gasification. *Fuel*, 73(8), p.1354–1357 ST–Ammonia–a Reactive Medium for Ca.
Bravo, M. & Brito, J., 2012. Concrete made with used tyre aggregate: Durability-related performance. *Journal of Cleaner Production*, 25, pp.42–50.
BS-EN-1015-3, 2004. *Methods of test for mortar for masonry*,

BS-EN-12350-2, 2009. *Testing fresh concrete: Slump-test*, Available at: https://bsol.bsigroup.com/Home.

BS-EN-12690-3, 2009. Testing hardened concrete: Compressive strength. *British Standard*, (August).

BS-EN-196-3, 2016. *BSI Standards Publication Methods of testing cement Part 3 : Determination of setting times and soundness*,

Caglayan, B.S. & Aksoylu, a. E., 2013. CO2 adsorption on chemically modified activated carbon. *Journal of Hazardous Materials*, 252–253, pp.19–28.

Cazorla-Amorós, D. et al., 1996. Selective porosity development by calcium-catalyzed carbon gasification. *Carbon*, 34(7), pp.869–878.

Celis, J. De, Amadeo, N.E. & Cukierman, A.L., 2009. In situ modification of activated carbons developed from a native invasive wood on removal of trace toxic metals from wastewater. , 161, pp.217–223.

CEMBUREAU, 2017. *Activity Report 2017*,

Chen, Z. et al., 2013. Activated carbons and amine-modified materials for carbon dioxide capture — a review. *Frontiers of Environmental Science & Engineering*, 7(3), pp.326–340.

Chen, Z. et al., 2019. Synthesis and applications of three-dimensional graphene network structures. *Materials Today Nano*, 5, p.100027.

Cheung, J. et al., 2011. Impact of admixtures on the hydration kinetics of Portland cement. *Cement and Concrete Research*, 41(12), pp.1289–1309.

Chi, J.M., Huang, R. & Yang, C.C., 2002. Effects of Carbonation on Mechanical Properties and Durability of Concrete Using Accelerated Testing Method. *Science*, 10(1), pp.14–20.

Chindaprasirt, P., Jaturapitakkul, C. & Sinsiri, T., 2007. Effect of fly ash fineness on microstructure of blended cement paste. *Construction and Building Materials*, 21(7), pp.1534–1541.

Chisti, Y., 2008. Biodiesel from microalgae beats bioethanol. *Trends in Biotechnology*, 26(3), pp.126–131.

Choi, S., Drese, J.H. & Jones, C.W., 2009. Adsorbent materials for carbon dioxide capture from large anthropogenic point sources. *ChemSusChem*, 2(9), pp.796–854.

Choi, W.C., Yun, H. Do & Lee, J.Y., 2012. Mechanical Properties of Mortar Containing Bio-Char From Pyrolysis. *Journal of the Korea institute for structural maintenance and inspection*, 16(3), pp.67–74.

Chopda, S. & Chhattani, B., 2015. Mechanical Properties of Pervious Concrete. *International J. Technology*, 5(2), pp.113–117.

Chopra, M., Wanielista, M. & Mulligan, A.M., 2007. *Compressive Strength of Pervious Concrete Pavements*,

Cloete, S. et al., 2019. The Swing Adsorption Reactor Cluster for post-combustion CO2 capture from cement plants. *Journal of Cleaner Production*.

Dali, A., Ibrahem, A.S. & Hadi, A., 2012. General study about activated carbon for adsorption carbon dioxide. *Journal of Purity, Utility Reaction and Environment*, 1(5), pp.236–251.

Dantas, T.L.P. et al., 2011. Carbon dioxide-nitrogen separation through adsorption on activated carbon in a fixed bed. *Chemical Engineering Journal*, 169(1–3), pp.11–19.

Dastgheib, S. a & Karanfil, T., 2004. Adsorption of oxygen by heat-treated granular and fibrous activated carbons. *Journal of colloid and interface science*, 274(1), pp.1–8.

Dastgheib, S. a, Karanfil, T. & Cheng, W., 2004. Tailoring activated carbons for enhanced removal of natural organic matter from natural waters. *Carbon*, 42(3), pp.547–557.

Dave, N. et al., 2009. CO 2 capture by aqueous amines and aqueous ammonia-A Comparison. *Energy Procedia*, 1(1), pp.949–954.
Deja, J., Uliasz-bochenczyk, A. & Mokrzycki, E., 2012. CO2 emissions from Polish cement industry. *International Journal of Greenhouse Gas Control*, 4(4), pp.583–588.
Deng, S. et al., 2014. Superior CO2 adsorption on pine nut shell-derived activated carbons and the effective micropores at different temperatures. *Chemical Engineering Journal*, 253, pp.46–54.
Deng, S.B. et al., 2015. Activated carbons prepared from peanut shell and sunflower seed shell for high CO2 adsorption. *Adsorption-Journal of the International Adsorption Society*, 21(1–2), pp.125–133.
Díaz-Díez, M.A. et al., 2004. Porous texture of activated carbons prepared by phosphoric acid activation of woods. *Applied Surface Science*, 238(1–4 SPEC. ISS.), pp.309–313.
Divsholi, B.S., Lim, T.Y.D. & Teng, S., 2014. Durability Properties and Microstructure of Ground Granulated Blast Furnace Slag Cement Concrete. *International Journal of Concrete Structures and Materials*, 8(2), pp.157–164.
Dong, Q., Huang, B. & Shu, X., 2013. Rubber modified concrete improved by chemically active coating and silane coupling agent. *Construction and Building Materials*, 48, pp.116–123.
Drage, T.C. et al., 2009. Developing activated carbon adsorbents for pre-combustion CO2 capture. *Energy Procedia*, 1(1), pp.599–605.
Drage, T.C. et al., 2007. Preparation of carbon dioxide adsorbents from the chemical activation of urea–formaldehyde and melamine–formaldehyde resins. *Fuel*, 86(1–2), pp.22–31.
Dubois, L. et al., 2017. Study of the Post-combustion CO2 Capture Applied to Conventional and Partial Oxy-fuel Cement Plants. *Energy Procedia*, 114(November 2016), pp.6181–6196.
Dutta, S., 2014. A review on production, storage of hydrogen and its utilization as an energy resource. *Journal of Industrial and Engineering Chemistry*, 20(4), pp.1148–1156.
Ekhlasi, L. et al., 2018. Populus wood biomass-derived graphene for high CO2 capture at atmospheric pressure and estimated cost of production. *Process Safety and Environmental Protection*, 113, pp.97–108.
El-Dakroury, A. & Gasser, M.S., 2008. Rice husk ash (RHA) as cement admixture for immobilization of liquid radioactive waste at different temperatures. *Journal of Nuclear Materials*, 381(3), pp.271–277.
Elango, K.S. & Revathi, V., 2017. Fal-G Binder Pervious Concrete. *Construction and Building Materials*, 140, pp.91–99.
Elchalakani, M., 2015. High strength rubberized concrete containing silica fume for the construction of sustainable road side barriers. *Structures*, 1, pp.20–38.
Eldin, N.N. & Senouci, A.B., 1993. Rubber-Tire Particles as Concrete Aggregate. , 5(4), pp.478–496.
Ello, A.S. et al., 2013. Coconut shell-based microporous carbons for CO2 capture. *Microporous and Mesoporous Materials*, 180, pp.280–283.
Erşan, Y.Ç. et al., 2015. Screening of bacteria and concrete compatible protection materials. *Construction and Building Materials*, 88, pp.196–203.
Flower, D.J.M. & Sanjayan, J.G., 2007. Green house gas emissions due to concrete manufacture. *International Journal of Life Cycle Assessment*, 12(5), pp.282–288.
Francis, A.M., 1965. Early Concrete Buildings in Britain. *Concrete and Constructional*

*Engineering*, 60(2), pp.73–75.
Freeman, E. et al., 1997. Interactions of carbon-containing fly ash with commercial air-entraining admixtures for concrete. *Fuel*, 76(8), pp.761–765.
Fry, M., 2013. Cement, carbon dioxide, and the “necessity” narrative: A case study of Mexico. *Geoforum*, 49, pp.127–138.
G´, M. del M. et al., 2008. Adsorption of Zn ( II ) in aqueous solution by activated carbons prepared from evergreen oak ( Quercus rotundifolia L .). *Journal of Hazardous Materials*, 153, pp.28–36.
Galan, I. et al., 2010. Sequestration of CO2 by Concrete Carbonation. *Environmental science & technology*, 44(8), pp.3181–3186.
Ganesan, K., Rajagopal, K. & Thangavel, K., 2008. Rice husk ash blended cement: Assessment of optimal level of replacement for strength and permeability properties of concrete. *Construction and Building Materials*, 22(8), pp.1675–1683.
Ganesan, N., Bharati Raj, J. & Shashikala, A.P., 2013. Flexural fatigue behavior of self compacting rubberized concrete. *Construction and Building Materials*, 44, pp.7–14.
Ganjian, E., Khorami, M. & Maghsoudi, A.A., 2009. Scrap-tyre-rubber replacement for aggregate and filler in concrete. *Construction and Building Materials*, 23(5), pp.1828–1836.
Gao, Y.M. et al., 1997. Effects of carbon on air entrainment in fly ash concrete: The role of soot and carbon black. *Energy and Fuels*, 11(2), pp.457–462.
García-Lodeiro, I., Fernández-Jiménez, A. & Palomo, A., 2013. 17 - Alkali-activated based concrete. In F. Pacheco-Torgal et al., eds. *Eco-Efficient Concrete*. Woodhead Publishing Series in Civil and Structural Engineering. Woodhead Publishing, pp. 439–487. Available at: http://www.sciencedirect.com/science/article/pii/B9780857094247500177.
Gardarsdottir, S. et al., 2019. Comparison of Technologies for CO2 Capture from Cement Production—Part 2: Cost Analysis. *Energies*, 12(3), p.542.
Geng, Y. et al., 2019. Calculating of CO2 emission factors for Chinese cement production based on inorganic carbon and organic carbon. *Journal of Cleaner Production*, 217, pp.503–509.
Gerbelová, H., Van Der Spek, M. & Schakel, W., 2017. Feasibility Assessment of CO2 Capture Retrofitted to an Existing Cement Plant: Post-combustion vs. Oxy-fuel Combustion Technology. *Energy Procedia*, 114(November 2016), pp.6141–6149.
Gesikiewicz-Puchalska, A. et al., 2017. Improvement of CO2 uptake of activated carbons by treatment with mineral acids. *Chemical Engineering Journal*, 309, pp.159–171.
Gęsikiewicz-Puchalska, A. et al., 2016. Improvement of CO2 uptake of activated carbons by treatment with mineral acids. *Chemical Engineering Journal*.
Gesoğlu, M. et al., 2014a. Abrasion and freezing-thawing resistance of pervious concretes containing waste rubbers. *Construction and Building Materials*, 73, pp.19–24.
Gesoğlu, M. et al., 2014b. Investigating properties of pervious concretes containing waste tire rubbers. *Construction and Building Materials*, 63, pp.206–213.
Gesolu, M. & Güneyisi, E., 2011. Permeability properties of self-compacting rubberized concretes. *Construction and Building Materials*, 25(8), pp.3319–3326.
Ghaedi, M., Ansari, A. & Sahraei, R., 2013. ZnS: Cu nanoparticles loaded on activated carbon as novel adsorbent for kinetic, thermodynamic and isotherm studies of Reactive Orange 12 and Direct yellow 12 adsorption. *Spectrochimica Acta - Part A: Molecular and Biomolecular Spectroscopy*, 114, pp.687–694.
Ghafoori, N. & Dutta, S., 1995a. Building and Nonpavement Applications of No-Fines

Concrete. *Journal of Materials in Civil Engineering*, 7(4), pp.286–289.
Ghafoori, N. & Dutta, S., 1995b. Development of No-Fines Concrete Pavement Applications. *Journal of Transportation Engineering*, 121(3), pp.283–288.
Ghimbeu, C.M. et al., 2014. Controlled synthesis of NiCo nanoalloys embedded in ordered porous carbon by a novel soft-template strategy. *Carbon*, 67, pp.260–272.
Ghosh, A. & Kiran, B., 2017. Carbon Concentration in Algae: Reducing CO2 From Exhaust Gas. *Trends in Biotechnology*, 35(9), pp.806–808.
Gómez-Serrano, V. et al., 2005. Preparation of activated carbons from chestnut wood by phosphoric acid-chemical activation. Study of microporosity and fractal dimension. *Materials Letters*, 59(7), pp.846–853.
González, a. S. et al., 2013. Sustainable biomass-based carbon adsorbents for post-combustion CO2 capture. *Chemical Engineering Journal*, 230, pp.456–465.
Goulias DG, A.A., 1998. Evaluation of rubber-filled concrete and correction between destructive and non-destructive testing results. *Cem Concr Res*, pp.1–5.
Gray, M.. et al., 2004. CO2 capture by amine-enriched fly ash carbon sorbents. *Separation and Purification Technology*, 35(1), pp.31–36.
Groves, G.W. et al., 1991. Progressive Changes in the Structure of Hardened C3S cement pastes due to carbonation. *Journal of American Ceramic Society*, 74(11), pp.2891–2896.
Gupta, S. & Kua, H.W., 2017. Factors Determining the Potential of Biochar As a Carbon Capturing and Sequestering Construction Material: Critical Review. *Journal of Materials in Civil Engineering*, 29(9), p.04017086.
Gupta, S., Kua, H.W. & Low, C.Y., 2018. Use of biochar as carbon sequestering additive in cement mortar. *Cement and Concrete Composites*, 87, pp.110–129.
Gupta, S., Kua, H.W. & Tan Cynthia, S.Y., 2017. Use of biochar-coated polypropylene fibers for carbon sequestration and physical improvement of mortar. *Cement and Concrete Composites*, 83, pp.171–187.
Hägg, M.B. et al., 2017. Pilot Demonstration-reporting on CO2Capture from a Cement Plant Using Hollow Fiber Process. *Energy Procedia*, 114(1876), pp.6150–6165.
Hale, W.M. et al., 2008. Properties of concrete mixtures containing slag cement and fly ash for use in transportation structures. *Construction and Building Materials*, 22(9), pp.1990–2000.
Hao, G.-P. et al., 2010. Rapid Synthesis of Nitrogen-Doped Porous Carbon Monolith for CO 2 Capture. *Advanced Materials*, 22(7), pp.853–857.
Harnisch, J. et al., 2008. Industrial energy efficiency and climate change mitigation. *Energy Efficiency*, 2(2), pp.109–123.
Harrison, A.J., 2005. TECECO ECO-CEMENT MASONRY PRODUCT UPDATE – Carbonation = Sequestration. , 59.
Hassler, J.W., 1951. *Activated carbon*, Chemical Pub. Co.
Hefni, Y., Zaher, Y.A. El & Wahab, M.A., 2018. Influence of activation of fly ash on the mechanical properties of concrete. *Construction and Building Materials*, 172, pp.728–734.
Heidari, A. et al., 2014. Adsorptive removal of CO 2 on highly microporous activated carbons prepared from Eucalyptus camaldulensis wood : Effect of chemical activation. *Journal of the Taiwan Institute of Chemical Engineers*, 45(2), pp.579–588.
Heidari, A. et al., 2014. Evaluation of CO2 adsorption with eucalyptus wood based activated carbon modified by ammonia solution through heat treatment. *Chemical Engineering Journal*, 254, pp.503–513.

Hewlett, P., 2004. *Lea's Chemistry of Cement and Concrete by Peter Hewlett* Fourth edi.,
Hill, R.L. et al., 1997. An examination of fly ash carbon and its interactions with air entraining agent. *Cement and Concrete Research*, 27(2), pp.193–204.
Holmes, N., Browne, A. & Montague, C., 2014. Acoustic properties of concrete panels with crumb rubber as a fine aggregate replacement. *Construction and Building Materials*, 73, pp.195–204.
Horgnies, M., Dubois-Brugger, I. & Gartner, E.M., 2012. NO x de-pollution by hardened concrete and the influence of activated charcoal additions. *Cement and Concrete Research*, 42(10), pp.1348–1355.
Hosseini, S. et al., 2015. Adsorption of carbon dioxide using activated carbon impregnated with Cu promoted by zinc. *Journal of the Taiwan Institute of Chemical Engineers*, 52, pp.109–117.
Hsiu-Mei, C. et al., 2009. Adsorption characteristics of Orange II and Chrysophenine on sludge adsorbent and activated carbon fibers. *Journal of Hazardous Materials*, 161(2–3), pp.1384–1390.
Hsueh, Y.-J. et al., 2013. Ordered porous carbon as the catalyst support for proton-exchange membrane fuel cells. *International Journal of Hydrogen Energy*, 38(25), pp.10998–11003.
Hu, X., Zhang, H. & Sun, Z., 2017. Adsorption of low concentration ceftazidime from aqueous solutions using impregnated activated carbon promoted by Iron, Copper and Aluminum. *Applied Surface Science*, 392, pp.332–341.
Huang, B. et al., 2010. Laboratory evaluation of permeability and strength of polymer-modified pervious concrete. *Construction and Building Materials*, 24(5), pp.818–823.
Ibrahim, A. et al., 2014. Experimental study on Portland cement pervious concrete mechanical and hydrological properties. *Construction and Building Materials*, 50, pp.524–529.
Ioannidou, O. & Zabaniotou, A., 2007. Agricultural residues as precursors for activated carbon production—A review. *Renewable and Sustainable Energy Reviews*, 11(9), pp.1966–2005.
IPCC, 2013. *Climate Change 2013: The Physical Science Basis. Summary for Policymakers*,
Is, H. and & ¸ılUzun, 2010. Preparation and characterization of activated carbons from poplar wood ( Populus L .). , (November 2009), pp.1338–1341.
Islam, G.M.S., Rahman, M.H. & Kazi, N., 2017. Waste glass powder as partial replacement of cement for sustainable concrete practice. *International Journal of Sustainable Built Environment*, 6(1), pp.37–44.
Islam, M.A. et al., 2017. Mesoporous activated carbon prepared from NaOH activation of rattan (Lacosperma secundiflorum) hydrochar for methylene blue removal. *Ecotoxicology and Environmental Safety*, 138(August 2016), pp.279–285.
Jacobsen, S. & Jahren, P., 2001. Binding of CO2 by Carbonation of Norwegian OPC Concrete. , (Nov-7-2000).
Jain, A. et al., 2013. Activated carbons derived from coconut shells as high energy density cathode material for Li-ion capacitors. *Scientific Reports*, 3, pp.1–6.
Jang, J.G. et al., 2016. Review on recent advances in CO2 utilization and sequestration technologies in cement-based materials. *Construction and Building Materials*, 127, pp.762–773.
Jolicoeur, C. et al., 2009. Fly Ash-Carbon Effects on Concrete Air Entrainment : Fundamental Studies on their Origin and Chemical Mitigation. , pp.1–23.

Joo, S.H., Jun, S. & Ryoo, R., 2001. Synthesis of ordered mesoporous carbon molecular sieves CMK-1. *Microporous and Mesoporous Materials*, 44–45, pp.153–158.
Justo-Reinoso, I. et al., 2018. Fine aggregate substitution by granular activated carbon can improve physical and mechanical properties of cement mortars. *Construction and Building Materials*, 164, pp.750–759.
Kabay, N. et al., 2015. Properties of concrete with pumice powder and fly ash as cement replacement materials. *Construction and Building Materials*, 85, pp.1–8.
Kaçan, E. & Kütahyali, C., 2012. Adsorption of strontium from aqueous solution using activated carbon produced from textile sewage sludges. *Journal of Analytical and Applied Pyrolysis*, 97, pp.149–157.
Kamali, M. & Ghahremaninezhad, A., 2015. Effect of glass powders on the mechanical and durability properties of cementitious materials. *Construction and Building Materials*, 98, pp.407–416.
Khatib, Z.K. & Bayomy, F.M., 1999. Rubberized Portland cement concrete. , 11(3), pp.206–213.
Khezami, L. & Capart, R., 2005. Removal of chromium(VI) from aqueous solution by activated carbons: Kinetic and equilibrium studies. *Journal of Hazardous Materials*, 123(1–3), pp.223–231.
Kim, B.J., Cho, K.S. & Park, S.J., 2010. Copper oxide-decorated porous carbons for carbon dioxide adsorption behaviors. *Journal of Colloid and Interface Science*, 342(2), pp.575–578.
Kirby, D.M. & Biernacki, J.J., 2012. The effect of water-to-cement ratio on the hydration kinetics of tricalcium silicate cements: Testing the two-step hydration hypothesis. *Cement and Concrete Research*, 42(8), pp.1147–1156.
Kodasma, R., Fermoso, J. & Sanna, A., 2019. Li-LSX-zeolite evaluation for post-combustion CO2 capture. *Chemical Engineering Journal*, 358, pp.1351–1362.
Konsta-Gdoutos, M.S., 2013. 20 - Nanotechnology for eco-efficient concrete. In F. Pacheco-Torgal et al., eds. *Eco-Efficient Concrete*. Woodhead Publishing Series in Civil and Structural Engineering. Woodhead Publishing, pp. 544–564. Available at: http://www.sciencedirect.com/science/article/pii/B9780857094247500207.
Kosmatka, S., Kerkhoff, B. & C. Panarese, W., 2002. *Design and Control of Concrete Mixtures*,
Krou, N.J. et al., 2013. Mechanisms of NOx entrapment into hydrated cement paste containing activated carbon — Influences of the temperature and carbonation. *Cement and Concrete Research*, 53(x), pp.51–58.
Krou, N.J. et al., 2015. Reactivity of volatile organic compounds with hydrated cement paste containing activated carbon. *Building and Environment*, 87, pp.102–107.
Kumar, B.G.P., Miranda, L.R. & Velan, M., 2005. Adsorption of Bismark Brown dye on activated carbons prepared from rubberwood sawdust (Hevea brasiliensis) using different activation methods. *Journal of Hazardous Materials*, 126(1–3), pp.63–70.
Lagerblad, B., 2005. *Carbon dioxide uptake during concrete life cycle – State of the art*,
Lee, S.-Y. & Park, S.-J., 2014. A review on solid adsorbents for carbon dioxide capture. *Journal of Industrial and Engineering Chemistry*, 23, pp.1–11.
Lee, T.C. & Li, Z.S., 2010. Conditioned MSWI ash-slag-mix as a replacement for cement in cement mortar. *Construction and Building Materials*, 24(6), pp.970–979.
Leung, D.Y.C., Caramanna, G. & Maroto-Valer, M.M., 2014. An overview of current status of carbon dioxide capture and storage technologies. *Renewable and Sustainable Energy Reviews*, 39, pp.426–443.

Li, F. et al., 2010. Adsorption of carbon dioxide by coconut activated carbon modified with Cu/Ce. *Journal of Rare Earths*, 28(SUPPL. 1), pp.334–337.
Li, L., Quinlivan, P. a & Knappe, D.R.U., 2002. Effects of activated carbon surface chemistry and pore structure on the adsorption of organic contaminants from aqueous solution. *Carbon*, 40(12), pp.2085–2100.
Lin, D. et al., 2014. Highly porous carbons with superior performance for CO2 capture through hydrogen-bonding interactions. *RSC Advances*, 4(52), p.27414.
Lin, L. et al., 2017. The visible-light-assisted thermocatalytic methanation of CO2 over Ru/TiO(2-x)Nx. *Applied Catalysis B: Environmental*, 204, pp.440–455.
Ling, T.C. & Nor, H., 2006. Granulated Waste Tyres in Concrete Paving Block. *Proceeding of the 6th Asia-Pasific Structural Engineering and Construction Conference*, (September), pp.65–70.
Liu, C. et al., 2010. Characterization of mesoporous activated carbons prepared by pyrolysis of sewage sludge with pyrolusite. *Bioresource Technology*, 101(3), pp.1097–1101.
Liu, Q. et al., 2017. High-performance removal of methyl mercaptan by nitrogen-rich coconut shell activated carbon. *The Royal Society of Chemistry 2017*, 7, pp.22892–22899.
Lopes, T.R. et al., 2017. Multinuclear magnetic resonance study on the occurrence of phosphorus in activated carbons prepared by chemical activation of lignocellulosic residues from the babassu production. *Journal of Environmental Chemical Engineering*, 5(6), pp.6016–6029.
Lothenbach, B. et al., 2007. Effect of temperature on the pore solution, microstructure and hydration products of Portland cement pastes. *Cement and Concrete Research*, 37(4), pp.483–491.
Lowell, S. et al., 2012. *Characterization of porous solids and powders: surface area, pore size and density*, Springer Science & Business Media.
Lu, C. feng et al., 2018. Effects of micro-environmental climate on the carbonation depth and the pH value in fly ash concrete. *Journal of Cleaner Production*, 181, pp.309–317.
Lua, A.C. & Yang, T., 2004. Effect of activation temperature on the textural and chemical properties of potassium hydroxide activated carbon prepared from pistachio-nut shell. *Journal of Colloid and Interface Science*, 274(2), pp.594–601.
Madani, H., Norouzifar, M.N. & Rostami, J., 2018. The synergistic effect of pumice and silica fume on the durability and mechanical characteristics of eco-friendly concrete. *Construction and Building Materials*, 174, pp.356–368.
Maguesvari, M.U. & Narasimha, V.L., 2013. Studies on Characterization of Pervious Concrete for Pavement Applications. *Procedia - Social and Behavioral Sciences*, 104, pp.198–207.
Mahoutian, M., Lubell, A.S. & Bindiganavile, V.S., 2015. Effect of powdered activated carbon on the air void characteristics of concrete containing fly ash. *Construction and Building Materials*, 80, pp.84–91.
Malhotra, V.M., 1973. *Mechanical properties and freeze-thaw resistance of no-fines concrete*, Ottawa.
Malhotra, V.M., 1976. No-Fines Concrete - Its Properties and Applications. *Journal Proceedings*, 73(11).
Maroto-Valer, M.M., Tang, Z. & Zhang, Y., 2005. CO2capture by activated and impregnated anthracites. *Fuel Processing Technology*, 86(14–15), pp.1487–1502.
Martín, C.F. et al., 2011. Hypercrosslinked organic polymer networks as potential adsorbents for pre-combustion CO2 capture. *Journal of Materials Chemistry*, 21(14),

p.5475.
Martin, M.J. et al., 2003. Activated carbons developed from surplus sewage sludge for the removal of dyes from dilute aqueous solutions. *Chemical Engineering Journal*, 94(3), pp.231–239.
Martin, W.D., Kaye, N.B. & Putman, B.J., 2014. Impact of vertical porosity distribution on the permeability of pervious concrete. *Construction and Building Materials*, 59, pp.78–84.
Mattson, J.S. & Mark, H.B., 1971. *Activated carbon: surface chemistry and adsorption from solution*, M. Dekker.
McGuire, M.J. & Suffet, I.H., 1983. *Treatment of Water by Granular Activated Carbon* M. M. J. & S. I. H., eds., WASHINGTON, D.C.: AMERICAN CHEMICAL SOCIETY.
Mehta, P.K. & Monteiro, P.J.M., 2006. *Concrete: microstructure, properties, and materials*, Available at: http://en.scientificcommons.org/34168511%5Cnhttp://doi.contentdirections.com/mr/mgh_biblio.jsp?doi=10.1036/0071462899.
Meininger, R.C., 1988. No-Fines Pervious Concrete for Paving. *Concrete International*, 10(8), pp.20–27.
Menéndez, J.A. et al., 1996. On the Modification and Characterization of Chemical Surface Properties of Activated Carbon: In the Search of Carbons With Stable Basic Properties. *Langmuir*, 12(18), pp.4404–4410. Available at: http://www.scopus.com/inward/record.url?eid=2-s2.0-0001243462&partnerID=tZOtx3y1.
Miller, S.A., Horvath, A. & Monteiro, P.J.M., 2016. Readily implementable techniques can cut annual CO2 emissions from the production of concrete by over 20%. *Environ. Res. Lett*, 11.
Modak, A. & Jana, S., 2019. Advancement in porous adsorbents for post-combustion CO2 capture. *Microporous and Mesoporous Materials*, 276, pp.107–132.
Modarres, A. et al., 2016. Application of coal waste in sustainable roller compacted concrete pavement-environmental and technical assessment. *International Journal of Pavement Engineering*, 8436, pp.1–14.
Moffatt, E.G., Thomas, M.D.A. & Fahim, A., 2017. Performance of high-volume fly ash concrete in marine environment. *Cement and Concrete Research*, 102(June), pp.127–135.
Mohanty, K., Das, D. & Biswas, M.N., 2005. Adsorption of phenol from aqueous solutions using activated carbons prepared from Tectona grandis sawdust by ZnCl2activation. *Chemical Engineering Journal*, 115(1–2), pp.121–131.
Monahan, A., 1981. *Porous Portland cemente concrete; The State of the Art*,
Montes-Morán, M. a. et al., 2004. On the nature of basic sites on carbon surfaces: an overview. *Carbon*, 42(7), pp.1219–1225.
Morales-Florez, V., Findling, N. & Brunet, F., 2012. Changes on the nanostructure of cementitius calcium silicate hydrates (C-S-H) induced by aqueous carbonation. *Journal of Materials Science*, 47(2), pp.764–771.
Moreno, E.I., 2013. Carbonation coefficients from concrete made with high-absorption limestone aggregate. *Advances in Materials Science and Engineering*, 2013.
Morgan, B.E. & Dumbauld, G.K., 1952. USE OF ACTIVATED CHARCOAL IN CEMENT TO COMBAT EFFECTS OF CONTAMINATION BY DRILLING MUDS. *J. Petroleum Technol. Soc. Petroleum Eng.*, 195, pp.225–233.
Motahari Karein, S.M. et al., 2017. A new approach for application of silica fume in concrete:

Wet granulation. *Construction and Building Materials*, 157, pp.573–581.
Muñiz, J., Herrero, J.E. & Fuertes, a. B., 1998. Treatments to enhance the SO2 capture by activated carbon fibres. *Applied Catalysis B: Environmental*, 18(1–2), pp.171–179.
Murugan, C. & Bajaj, H.C., 2010. Transesterification of propylene carbonate with methanol using Mg-Al-CO3 hydrotalcite as solid base catalyst. *Indian Journal of Chemistry - Section A Inorganic, Physical, Theoretical and Analytical Chemistry*, 49(9), pp.1182–1188.
Naik, T.R. & Kumar, R., 2010. *Global Warming and Cement-based Materials*,
Namazirad, M., 2012. *Investigation into properties of unburned carbon in coal combustion fly ash*. University of Wollongong.
Neithalath, N., 2004. *Development and Characterization of Acoustically Efficient Cementitious Materials*. Purdue University.
Neithalath, N., Bentz, D. & Sumanasoorlya, M., 2010. Predicting the Permeability of Pervious Concrete: Advances in Characterization of Pore Structure and Transport Properties. *Concrete International*, 32(5), pp.35–40.
Neithalath, N., Sumanasooriya, M.S. & Deo, O., 2010. Characterizing pore volume, sizes, and connectivity in pervious concretes for permeability prediction. *Materials Characterization*, 61(8), pp.802–813.
Neville, A.M., 2011. *Properties of Concrete*,
Nguyen, D.H. et al., 2014. A modified method for the design of pervious concrete mix. *Construction and Building Materials*, 73, pp.271–282.
NTPC, 2007. *Fly Ash for Cement Concrete*,
Oey, T. et al., 2013. The filler effect: The influence of filler content and surface area on cementitious reaction rates. *Journal of the American Ceramic Society*, 96(6), pp.1978–1990.
Olajire, A.A., 2018. Synthesis chemistry of metal-organic frameworks for CO2 capture and conversion for sustainable energy future. *Renewable and Sustainable Energy Reviews*, 92, pp.570–607.
Omran, A. & Tagnit-Hamou, A., 2016. Performance of glass-powder concrete in field applications. *Construction and Building Materials*, 109, pp.84–95.
Onuaguluchi, O. & Panesar, D.K., 2014. Hardened properties of concrete mixtures containing pre-coated crumb rubber and silica fume. *Journal of Cleaner Production*, 82, pp.125–131.
Öz, H.Ö., 2018. Properties of pervious concretes partially incorporating acidic pumice as coarse aggregate. *Construction and Building Materials*, 166, pp.601–609.
Pacheco-Torgal, F. & Labrincha, J.A., 2013. 21 - Biotechconcrete: An innovative approach for concrete with enhanced durability. In F. Pacheco-Torgal et al., eds. *Eco-Efficient Concrete*. Woodhead Publishing Series in Civil and Structural Engineering. Woodhead Publishing, pp. 565–576. Available at: http://www.sciencedirect.com/science/article/pii/B9780857094247500219.
Pade, C. & Guimaraes, M., 2007. The CO2 uptake of concrete in a 100 year perspective. *Cement and Concrete Research*, 37(9), pp.1348–1356.
Pang, X., Boul, P. & Jimenez, W.C., 2015. Isothermal calorimetry study of the effect of chloride accelerators on the hydration kinetics of oil well cement. *Construction and Building Materials*, 77, pp.260–269.
Pereira, M.F.R. et al., 2003. Adsorption of dyes on activated carbons: Influence of surface chemical groups. *Carbon*, 41(4), pp.811–821.

Perrin, A. et al., 2004. NaOH activation of anthracites: Effect of temperature on pore textures and methane storage ability. *Carbon*, 42(14), pp.2855–2866.
Pevida, C. et al., 2008. Surface modification of activated carbons for CO2 capture. *Applied Surface Science*, 254(22), pp.7165–7172.
Phung, Q.T. et al., 2015. Effect of limestone fillers on microstructure and permeability due to carbonation of cement pastes under controlled CO2 pressure conditions. *Construction and Building Materials*, 82, pp.376–390.
Pindado, M.Á., Aguado, A. & Josa, A., 1999. Fatigue behavior of polymer-modified porous concretes. *Cement and Concrete Research*, 29(7), pp.1077–1083.
Pinto, A.M., Gonçalves, I.C. & Magalhães, F.D., 2013. Graphene-based materials biocompatibility: A review. *Colloids and Surfaces B: Biointerfaces*, 111, pp.188–202.
Plaza, M.G. et al., 2010. Ammoxidation of carbon materials for CO2 capture. *Applied Surface Science*, 256(22), pp.6843–6849.
Plaza, M.G. et al., 2007. CO2 capture by adsorption with nitrogen enriched carbons. *Fuel*, 86(14 SPEC. ISS.), pp.2204–2212.
Plaza, M.G. et al., 2014. Production of microporous biochars by single-step oxidation: Effect of activation conditions on CO2 capture. *Applied Energy*, 114, pp.551–562.
Plaza, M.G. et al., 2012. Valorisation of spent coffee grounds as CO2 adsorbents for postcombustion capture applications. *Applied Energy*, 99, pp.272–279.
Possan, E. et al., 2017. CO2 uptake potential due to concrete carbonation: A case study. *Case Studies in Construction Materials*, 6, pp.147–161.
Przepiórski, J., Skrodzewicz, M. & Morawski, a. W., 2004. High temperature ammonia treatment of activated carbon for enhancement of CO2 adsorption. *Applied Surface Science*, 225(1–4), pp.235–242.
Qin, W. et al., 2014. Metal-organic framework MIL-101 doped with palladium for toluene adsorption and hydrogen storage. *RSC Advances*, 4(5), pp.2414–2420.
Radosz, M. et al., 2008. Flue-gas carbon capture on carbonaceous sorbents: Toward a low-cost multifunctional carbon filter for "green" energy producers. *Industrial and Engineering Chemistry Research*, 47(10), pp.3783–3794.
Rashidi, A.N., Yusup, S. & Hon, L., 2013. Kinetic Studies on Carbon Dioxide Capture using Activated Carbon. *Energy*, 61, pp.440–446.
Rashidi, N.A. et al., 2014. Experimental and modelling studies of carbon dioxide adsorption by porous biomass derived activated carbon. *Clean Technologies and Environmental Policy*, 16(7), pp.1353–1361.
Rashidi, N.A. & Yusup, S., 2016. An overview of activated carbons utilization for the post-combustion carbon dioxide capture. *Journal of CO2 Utilization*, 13, pp.1–16.
Rege, S.U. & Yang, R.T., 2001. A novel FTIR method for studying mixed gas adsorption at low concentrations: H2O and CO2on NaX zeolite and γ-alumina. *Chemical Engineering Science*, 56(12), pp.3781–3796.
Ren, S., Rong, P. & Yu, Q., 2018. Preparations, properties and applications of graphene in functional devices: A concise review. *Ceramics International*, 44(11), pp.11940–11955.
Resheidat, M., Al-Araji, N. & Ghanma, M., 2002. EFFECT OF CHARCOAL ON THE POROSITY AND THE PROPERTIES OF CONCRETE. In *Innovations and Developments In Concrete Materials And Construction*. pp. 615–624. Available at: https://www.icevirtuallibrary.com/doi/abs/10.1680/iadicmac.31791.0059.
Rezagholilou, A., Papadakis, V.G. & Nikraz, H., 2017. Rate of carbonation in cement modified base course material. *Construction and Building Materials*, 150, pp.646–652.

Ries, J.P. et al., 2010. Guide for Structural Lightweight-Aggregate Concrete Reported by ACI Committee 213. , pp.1–38.
Rozada, F. et al., 2003. Dye adsorption by sewage sludge-based activated carbons in batch and fixed-bed systems. *Bioresource Technology*, 87(3), pp.221–230.
Rozada, F. et al., 2005. Producing adsorbents from sewage sludge and discarded tyres: Characterization and utilization for the removal of pollutants from water. *Chemical Engineering Journal*, 114(1–3), pp.161–169.
Sahu, D. et al., 2013. Hydrogen Adsorption on Zn-BDC, Cr-BDC, Ni-DABCO, and Mg-DOBDC Metal–Organic Frameworks. *Journal of Chemical & Engineering Data*, 58(11), pp.3096–3101.
Sahu, J.N., Acharya, J. & Meikap, B.C., 2010. Bioresource Technology Optimization of production conditions for activated carbons from Tamarind wood by zinc chloride using response surface methodology. *Bioresource Technology*, 101(6), pp.1974–1982.
Sanjuán, M.Á. et al., 2018. Effect of curing time on granulated blast-furnace slag cement mortars carbonation. *Cement and Concrete Composites*, 90(February), pp.257–265.
Satayeva, A.R. et al., 2018. Investigation of rice husk derived activated carbon for removal of nitrate contamination from water. *Science of the Total Environment*, 630, pp.1237–1245.
Savova, D. et al., 2001. Biomass conversion to carbon adsorbents and gas. *Biomass and Bioenergy*, 21(2), pp.133–142.
Sayari, A., Belmabkhout, Y. & Serna-Guerrero, R., 2011. Flue gas treatment via CO2 adsorption. *Chemical Engineering Journal*, 171(3), pp.760–774.
Schaefer, V. et al., 2006. *Mix design development for pervious concrete in cold weather climates*,
Schaefer, V.R. & Kevern, J.T., 2011. *An Integrated Study of Pervious Concrete Mixture Design for Wearing Course Applications An Integrated Study of Pervious Concrete Mixture Design for Wearing*,
Schneider, M. et al., 2011. Sustainable cement production-present and future. *Cement and Concrete Research*, 41(7), pp.642–650.
Scrivener, K., Snellings, R. & Lothenbach, B., 2016. *A practical guide to microstructural analysis of cementitious materials*, Crc Press.
Scrivener, K.L., Juilland, P. & Monteiro, P.J.M., 2015. Advances in understanding hydration of Portland cement. *Cement and Concrete Research*, 78, pp.38–56.
Sevelsted, T.F. & Skibsted, J., 2015. Carbonation of C-S-H and C-A-S-H samples studied by C, Al and Si MAS NMR spectroscopy. *Cement and Concrete Research*, 71, pp.56–65.
Sevilla, M., Valle-Vigón, P. & Fuertes, A.B., 2011. N-Doped Polypyrrole-Based Porous Carbons for CO 2 Capture. *Advanced Functional Materials*, 21(14), pp.2781–2787.
Shafeeyan, M.S. et al., 2010. A review on surface modification of activated carbon for carbon dioxide adsorption. *Journal of Analytical and Applied Pyrolysis*, 89(2), pp.143–151.
Shafeeyan, M.S. et al., 2011. Ammonia modification of activated carbon to enhance carbon dioxide adsorption: Effect of pre-oxidation. *Applied Surface Science*, 257(9), pp.3936–3942.
Shafeeyan, M.S., Wan Daud, W.M.A. & Shamiri, A., 2014. A review of mathematical modeling of fixed-bed columns for carbon dioxide adsorption. *Chemical Engineering Research and Design*, 92(5), pp.961–988.
Shao, Y., Mirza, M.S. & Wu, X., 2006. CO2 sequestration using calcium-silicate concrete.

*Canadian Journal of Civil Engineering*, 33(6), pp.776–784.
Shao, Y., Zhou, X. & Monkman, S., 2006. A New CO2 Sequestration Process via Concrete Products Production. *EIC Climate Change Technology Conference,*.
Sharpley, I., 2015. The Effect of Hydration on the Microstructural Properties of Individual Phases of Ordinary Portland Cement. , (April).
Shen, W., Li, Z. & Liu, Y., 2008. Surface Chemical Functional Groups Modification of Porous Carbon. *Recent Patents on Chemical Engineeringe*, 1(1), pp.27–40.
Shi, H. et al., 2019. Properties of Portland cement paste blended with coral sand powder. *Construction and Building Materials*, 203, pp.662–669.
Shim, J.W., Park, S.J. & Ryu, S.K., 2001. Effect of modification with HNO3 and NaOH on metal adsorption by pitch-based activated carbon fibers. *Carbon*, 39(11), pp.1635–1642.
Short, A. & Kinniburgh, W., 1963. *Lightweight concrete*, London: C.R. Books Ltd. [usw].
Siddique, R. & Naik, T.R., 2004. Properties of concrete containing scrap-tire rubber - An overview. *Waste Management*, 24(6), pp.563–569.
Sircar, S., Golden, T.C. & Rao, M.B., 1996. Activated carbon for gas separation and storage. *Carbon*, 34(1), pp.1–12.
Siriwardane, R. V et al., 2001. Adsorption of CO 2 on Molecular Sieves and Activated Carbon. , pp.279–284.
Smith, A.T. et al., 2019. Synthesis, properties, and applications of graphene oxide/reduced graphene oxide and their nanocomposites. *Nano Materials Science*.
Snoeyink, V.L. & Weber, W.J., 1966. The Surface Chemistry of Active Carbon.
Socrates, G., 2004. *Infrared and Raman characteristic group frequencies*,
Somy, A. et al., 2009. Adsorption of carbon dioxide using impregnated activated carbon promoted by Zinc. *International Journal of Greenhouse Gas Control*, 3(3), pp.249–254.
Son, K.S., Hajirasouliha, I. & Pilakoutas, K., 2011. Strength and deformability of waste tire rubber-filled reinforced concrete columns. *Constar Build Mater*.
Son, S.-J. et al., 2005. Development of carbon dioxide adsorbents using carbon materials prepared from coconut shell. *Korean Journal of Chemical Engineering*, 22(2), pp.291–297.
Sooraj VM, 2013. Effect of Palm Oil Fuel Ash (POFA) on Strength Properties of Concrete. *International Journal of Scientific and Research Publications*, 3(6), pp.2250–3153.
Spigarelli, B.P. & Kawatra, S.K., 2013. Opportunities and challenges in carbon dioxide capture. *Journal of CO2 Utilization*, 1, pp.69–87.
Sreńscek-Nazzal, J. et al., 2016. Modification of Commercial Activated Carbons for CO 2 Adsorption. *Acta Physica Polonica A*, 129(3), pp.394–401.
Stöhr, B., Boehm, H.P. & Schlögl, R., 1991. Enhancement of the catalytic activity of activated carbons in oxidation reactions by thermal treatment with ammonia or hydrogen cyanide and observation of a superoxide species as a possible intermediate. *Carbon*, 29(6), pp.707–720.
Su, H. et al., 2015. Properties of concrete prepared with waste tyre rubber particles of uniform and varying sizes. *Journal of Cleaner Production*, 91, pp.288–296.
Sulapha, P., Wong, S. & Wee, T., 2003. Carbonation of concrete containing mineral admixtures. *J Mater Civil Eng*, 15(April), pp.134–143.
Suleiman, M. et al., 2006. Effect of compaction energy on pervious concrete properties. *Concrete Technology Forum-Focus on Pervious Concrete, National Ready Mix Concrete Association*, (April 2014), pp.1–8.
Tabet, W.E. et al., 2018. Characterization of Hydration Products' Formation and Strength

Development in Cement-Stabilized Kaolinite Using TG and XRD. *Journal of Materials in Civil Engineering*, 30(10), p.04018261.
Talukdar, S. et al., 2012. Carbonation in concrete infrastructure in the context of global climate change: Part 2 - Canadian urban simulations. *Cement and Concrete Composites*, 34(8), pp.931–935.
Tamai, H., Nagoya, H. & Shiono, T., 2006. Adsorption of methyl mercaptan on surface modified activated carbon. *Journal of Colloid and Interface Science*, 300(2), pp.814–817.
Tan, G. et al., 2016. Sorption of mercury (II) and atrazine by biochar, modified biochars and biochar based activated carbon in aqueous solution. *Bioresource Technology*, 211, pp.727–735.
Tan, Y.L. et al., 2014. Adsorption of carbon dioxide by sodium hydroxide-modified granular coconut shell activated carbon in a fixed bed. *Energy*, 77, pp.926–931.
TANG, Z. et al., 2013. Preparation of nanoporous carbons with hierarchical pore structure for CO2 capture. *New Carbon Materials*, 28(1), pp.55–60.
Taylor, H.F.W., 1997. *Cement chemistry* Second edi.,
Tennis, P.D., Leming, M.L. & Akers, D.J., 2004. *Pervious Concrete Pavements*,
Thomas, B.S. et al., 2015. Performance of high strength rubberized concrete in aggressive environment. *Construction and Building Materials*, 83, pp.320–326.
Thomas, B.S. et al., 2014. Strength, abrasion and permeation characteristics of cement concrete containing discarded rubber fine aggregates. *Construction and Building Materials*, 59, pp.204–212.
Thomas, B.S. & Gupta, R.C., 2016. A comprehensive review on the applications of waste tire rubber in cement concrete. *Renewable and Sustainable Energy Reviews*, 54, pp.1323–1333.
Tikalsky, P.J. et al., 2002. *Use of Fly Ash in Concrete*,
Tošić, N. et al., 2018. Long-term behaviour of reinforced beams made with natural or recycled aggregate concrete and high-volume fly ash concrete. *Construction and Building Materials*, 176, pp.344–358.
Tseng, H.H. et al., 2003. Catalytic removal of SO2, NO and HCl from incineration flue gas over activated carbon-supported metal oxides. *Carbon*, 41(5), pp.1079–1085.
UN, 1992. *United Nations Framework Convention on Climate Change (UN FCCC)*,
UNEP, 2016. *Eco-efficient cement: Potential, economically viable solutions for a low CO2, cement-based materials industry*,
Unluer, C., 2012. *Enhancing the Carbonation of Reactive Magnesia Cement-Based Porous Blocks*. University of Cambridge.
USGS, 2018. *Mineral commodity summaries*,
Usman, H.D. et al., 2012. Modification of Activated Carbon for Enhancement of Gas Contaminant Removal : A Review. *UMT 11th International Annual Symposium on Sustainability Science and Management*, (July), pp.1336–1342.
Vargas, D.P. et al., 2013. Chemical modification of activated carbon monoliths for CO2 adsorption. *Journal of Thermal Analysis and Calorimetry*, 114(3), pp.1039–1047.
Vegas, I. et al., 2006. Obtaining a pozzolanic addition from the controlled calcination of paper mill sludge. *Materiales de Construcción*, 56, pp.49–60.
Verian, K.P. & Behnood, A., 2018. Effects of deicers on the performance of concrete pavements containing air-cooled blast furnace slag and supplementary cementitious materials. *Cement and Concrete Composites*, 90, pp.27–41.

Villain, G., Thiery, M. & Platret, G., 2007. Measurement methods of carbonation profiles in concrete: Thermogravimetry, chemical analysis and gammadensimetry. *Cement and Concrete Research*, 37(8), pp.1182–1192.
Vu, M.T. et al., 2018. Removal of ammonium from groundwater using NaOH-treated activated carbon derived from corncob wastes: Batch and column experiments. *Journal of Cleaner Production*, 180, pp.560–570.
Wang, H. et al., 2013. Graphene-based materials: Fabrication, characterization and application for the decontamination of wastewater and wastegas and hydrogen storage/generation. *Advances in Colloid and Interface Science*, 195–196, pp.19–40.
Wang, J. et al., 2006. Modification of activated carbon fiber by loading metals and their performance on SO2removal. *Chinese Journal of Chemical Engineering*, 14(4), pp.478–485.
Wang, J. & Kaskel, S., 2012. KOH activation of carbon-based materials for energy storage. *Journal of Materials Chemistry*, 22(45), p.23710.
Wang, P. et al., 2015. Removal of chlorpyrifos from waste water by wheat straw-derived biochar synthesized through oxygen-limited method. *RSC Advances*, 5(89), pp.72572–72578.
Wang, Q. et al., 2011. CO2 capture by solid adsorbents and their applications: Current status and new trends. *Energy and Environmental Science*, 4(1), pp.42–55.
Wang, X., Zhu, N. & Yin, B., 2008. Preparation of sludge-based activated carbon and its application in dye wastewater treatment. *Journal of Hazardous Materials*, 153(1–2), pp.22–27.
WBCSD, 2009a. *Cement Technology Roadmap 2009 Carbon emissions reductions up to 2050*,
WBCSD, 2012. *The Cement Sustainability Initiative*,
WBCSD, 2009b. *The Cement Sustainability Initiative*,
WBCSD, 2002. *Toward a Sustainable Cement Industry*,
Wei, J. et al., 2013. A controllable synthesis of rich nitrogen-doped ordered mesoporous carbon for CO2 capture and supercapacitors. *Advanced Functional Materials*, 23(18), pp.2322–2328.
Wilcox, J. et al., 2014. Advancing Adsorption and Membrane Separation Processes for the Gigaton Carbon Capture Challenge. *Annual Review of Chemical and Biomolecular Engineering*, 5(1), pp.479–505.
Wu, H. et al., 2016. Experimental investigation on freeze-thaw durability of Portland cement pervious concrete (PCPC). *Construction and Building Materials*, 117, pp.63–71.
Xiong, Z. et al., 2013. Influence of NH3/CO2 Modification on the Characteristic of Biochar and the CO2 Capture. *Bioenergy Research*, 6, pp.1147–1153.
Yahia, A. & Kabagire, K.D., 2014. New approach to proportion pervious concrete. *Construction and Building Materials*, 62, pp.38–46.
Yang, J. & Jiang, G., 2003. Experimental study on properties of pervious concrete pavement materials. *Cement and Concrete Research*, 33(3), pp.381–386.
Yang, K.-H. et al., 2015. Effect of supplementary cementitious materials on reduction of CO2 emissions from concrete. *Journal of Cleaner Production*, 103, pp.774–783.
Yap, S.P. et al., 2018. Characterization of pervious concrete with blended natural aggregate and recycled concrete aggregates. *Journal of Cleaner Production*, 181, pp.155–165.
Yong, Z., Mata, V. & Rodrigues, A.E., 2002. Adsorption of carbon dioxide at high temperature—a review. *Separation and Purification Technology*, 26(2), pp.195–205.
Yong, Z.O.U. & Mata, V.G., 2001. Adsorption of Carbon Dioxide on Chemically Modified High

Surface Area Carbon-Based Adsorbents at High Temperature. *Adsorption*, pp.41–50.
Youssf, O. et al., 2014. An experimental investigation of crumb rubber concrete confined by fibre reinforced polymer tubes. *Construction and Building Materials*, 53, pp.522–532.
Yu, C.-H., 2012. A Review of CO2 Capture by Absorption and Adsorption. *Aerosol and Air Quality Research*, pp.745–769.
Yung, W.H., Yung, L.C. & Hua, L.H., 2013. A study of the durability properties of waste tire rubber applied to self-compacting concrete. *Construction and Building Materials*, 41, pp.665–672.
Zaetang, Y. et al., 2016. Properties of pervious concrete containing recycled concrete block aggregate and recycled concrete aggregate. *Construction and Building Materials*, 111, pp.15–21.
Zhang, C. et al., 2013. CO2 capture with activated carbon grafted by nitrogenous functional groups. *Energy and Fuels*, 27(8), pp.4818–4823.
Zhang, D. & Luo, R., 2018. Modifying the BET model for accurately determining specific surface area and surface energy components of aggregates. *Construction and Building Materials*, 175, pp.653–663.
Zhang, F.S., Nriagu, J.O. & Itoh, H., 2005. Mercury removal from water using activated carbons derived from organic sewage sludge. *Water Research*, 39(2–3), pp.389–395.
Zhang, R., Tu, B. & Zhao, D., 2007. Synthesis of mesoporous carbon frameworks with graphitic walls by secondary hard template method. In D. Zhao et al., eds. *Recent Progress in Mesostructured Materials*. Studies in Surface Science and Catalysis. Elsevier, pp. 373–376.
Zhang, Z. et al., 2010. Enhancement of CO2 adsorption on high surface area activated carbon modified by N2, H2 and ammonia. *Chemical Engineering Journal*, 160(2), pp.571–577.
Zhang, Z. et al., 2017. Waste is a Misplayed Resource: Synthesis of Zeolites from Fly Ash for CO2 Capture. *Energy Procedia*, 114, pp.2537–2544.
Zheng, M., Chen, S. & Wang, B., 2012. Mix design method for permeable base of porous concrete. *International Journal of Pavement Research and Technology*, 5(2), pp.102–107.
Zhi, Y. & Liu, J., 2016. Surface modification of activated carbon for enhanced adsorption of perfluoroalkyl acids from aqueous solutions. *Chemosphere*, 144, pp.1224–1232.
Zhong, R. & Wille, K., 2016. Compression response of normal and high strength pervious concrete. *Construction and Building Materials*, 109, pp.177–187.
Zhou, F. et al., 2019. Ultrathin, ethylenediamine-functionalized graphene oxide membranes on hollow fibers for CO2 capture. *Journal of Membrane Science*, 573, pp.184–191.
Zhou, Q. et al., 2007. Concretes and Fly Ashes from a Full-Scale , Mercury Control Trial.
Zhu, X.-L. et al., 2014. Activated carbon produced from paulownia sawdust for high-performance CO2 sorbents. *Chinese Chemical Letters*, 25(6), pp.929–932.
Zuo, S., 2010. Effects of the heating history of impregnated lignocellulosic material on pore development during phosphoric acid activation. *Carbon*, 48(11), pp.3293–3295.